ISBN ISBN 978-82-471-1662-3 (printed ver.)
ISBN ISBN 978-82-471-1663-0 (electronic ver.)
ISSN 1503-8181

Doctoral theses at NTNU, 2009:137

Lingyun Shang

Evaluation of fracture parameters for notched multi-layered structures

NTNU
Norwegian University of
Science and Technology

Lingyun Shang

Doctoral Thesis

NTNU
Norwegian University of
Science and Technology

Thesis for the degree of
philosophiae doctor

Faculty of Engineering Science and Technology
Department of Structural Engineering

Doctoral theses at NTNU, 2009:137

NTNU

Lingyun Shang

Evaluation of fracture parameters for notched multi-layered structures

Thesis for the degree of philosophiae doctor

Trondheim, May 2009

Norwegian University of
Science and Technology
Faculty of Engineering Science and Technology
Department of Structural Engineering

NTNU
Norwegian University of
Science and Technology

NTNU
Norwegian University of Science and Technology

Thesis for the degree of philosophiae doctor

Faculty of Engineering Science and Technology
Department of Structural Engineering

ISBN ISBN 978-82-471-1662-3 (printed ver.)
ISBN ISBN 978-82-471-1663-0 (electronic ver.)
ISSN 1503-8181

Doctoral Theses at NTNU, 2009:137

Printed by Tapir Uttrykk

Evaluation of fracture parameters for notched multi-layered structures

Lingyun Shang

NTNU

Innovation and Creativity

Norwegian University of Science and Technology
Faculty of Engineering Science and Technology
Department of Structural Engineering
Trondheim, Norway

Preface

The doctoral thesis is submitted to the Norwegian University of Science and Technology (NTNU) for implementing the degree of philosophiae doctor.

The research work has been carried out at the Department of Structural Engineering, NTNU and supported by the Faculty of Engineering Science and Technology, NTNU, Trondheim. It has been my great fortune to be guided by my supervisor Professor Bjørn Skallerud and by my co-supervisor Professor Zhiliang Zhang, and surrounded by inspirational colleagues over the last few years.

Abstract

For the last three decades, the field of MEMS (Micro-Electro-Mechanical Systems) has emerged to a technology with significant potential. Re-entrant sharp corners or notches have increasingly appeared in MEMS fabrication and packaging. Due to the stress concentration and/or elastic mismatch at re-entrant corner, the initiation of failure at sharp corner or at free edges in multi-material systems often occurs. Hence, how to characterize the singular stress fields and the interface strength at these failure sites becomes very important.

This dissertation consists of six chapters and three papers. The background of this problem is presented in Chapter 1. In Chapter 2, MEMS technology and useful online resources are provided. Anisotropic elasticity theory including Stroh formalism is briefly addressed in Chapter 3. The focus of Chapter 4 is on distinction of notch mechanics from classical fracture mechanics. Chapter 5 gives an overview of the three appended papers. Conclusions of this study are summarized in Chapter 6 along with recommendations for future work.

Finally, three papers are appended investigating various aspects of multi-layered notched problem. The specific structures we have studied are popular in MEMS. The H-integral approach, as a tool to derive stress intensity factors for notches and cracks, has been performed in all the papers. This path independent contour integral method is based on a combination of Betti's law, Stroh's formalism, finite element results and asymptotic analysis with a complementary field. Plane strain conditions are assumed in all modeling. Linear elastic finite element analyses are performed with ABAQUS (Finite element code). A good agreement between numerical predictions obtained from the H-integral method and the detailed FE results has been achieved, showing the applicability of this approach.

Paper I focuses on the fracture behavior of two types of triple stacks specimens with a sharp corner. Standardized numerical formulae of the dimensionless stress intensity factor are proposed for two typical specimens, and the dependence of geometry is analyzed. The effect of glass thickness on stress intensity is explored for anodic-bonded Si-Glass-Si triple stacks. Distinct failure criteria for sharp notches have been qualified and three different approaches have been compared and quantified. The influencing factors and uncertainties for their applicability of critical stress intensity factors have also been discussed. Furthermore, the deviation between a fine mesh and a coarse mesh has been quantified.

Paper II investigates the weak singularity problem at free edges in multi-layered structural components. In Paper II, the effects of elastic constants of various material combinations on the weak singularity at free edges are analyzed. Using the H-integral approach, the effects of elastic mismatch parameters, the bond area and the thickness of the thin metal layer on the stress intensity

factor are quantified. The relationship between the valid range of the K-dominated field and the thin-film thickness is then demonstrated. Besides, the competition of crack initiation between the free edge interface (180º opening angle) and a 90º notch interface in a generic specimen is investigated, in order to find out which is the prevailing failure mode. Comparison between isotropic Si and anisotropic Si substrate is also illustrated.

Paper III concentrates on a general notch problem and presents the computational procedure for obtaining the stress intensity factor in a flow chart. Three critical issues are addressed to clear up some confusion in the notch mechanics: the interpretation of the eigenvalue equation, the definition of stress intensity factors, and the effect of the outer contour location on H-integral evaluations.

Acknowledgements

It has been great fortunate for me to work at NTNU for the last several years. I wish to thank my supervisor Prof. Bjørn Skallerud for his continuous inspiration, good concern and insightful comments. Both his rigorous scientific approach and his humanistic care impressed me greatly. His caring and thoughtfulness lighten up the dark winter sky. I particularly would like to thank my co-supervisor Prof. Zhiliang Zhang for his guidance, inspiration, and constructive discussion. Both his enthusiasm of scientific research and his open mind about exotic culture are highly appreciated.

Furthermore, my grateful thanks are due to Espen Berg, Sune Pettersen and Victorien Prot for not only their valuable discussion on simulations, programs, Matlab scripts but also their profound friendship. Thank Jun Liu for his kind help on modelling and for useful discussion about Fracture mechanics. Specially, I am truly grateful to Aase Reyes and Sumita Dey for their Norwegian cultural interpretation and everlasting friendship as well as to Jianying He and Micol Pezzotta for their constant stimulations.

My acknowledgements are also attributed to the Department of Structural Engineering, Faculty of Engineering Science and Technology for their financial support.

Besides, I wish to thank Tor Myhre, Bente Lehovd, Are Torstensen and Tor Skjelby from Veritas management team for their encouragement and support at the end of my PhD thesis writing, so that I could have flexible working hours and time-offs.

Special recognitions are given to my husband, Zheng, for his patience and understanding, and my daughter, Qianwen, for her smiling faces.

At last but not least, I would like to thank my parents, my colleagues and friends, particularly those who I haven't mentioned by name, together with our department secretaries for their enduring and helpful support.

Content

CHAPTER 1

Introduction

1.1 Motivations

The strong growth of MEMS (Micro-Electro-Mechanical Systems) market, particularly over the past 10 years, has brought out many excitements and challenges to the technology development. Sharp corners or notches have inevitably emerged in microsystem fabrication and packaging. The failure often occurs at sharp corners or at free edges in multi-material systems (Fig. 1) as a result of the stress concentration and/or the elastic mismatch. Therefore, it is essential to characterize the singular stress fields around the notch tip and to ensure the capacity and stability of structural components.

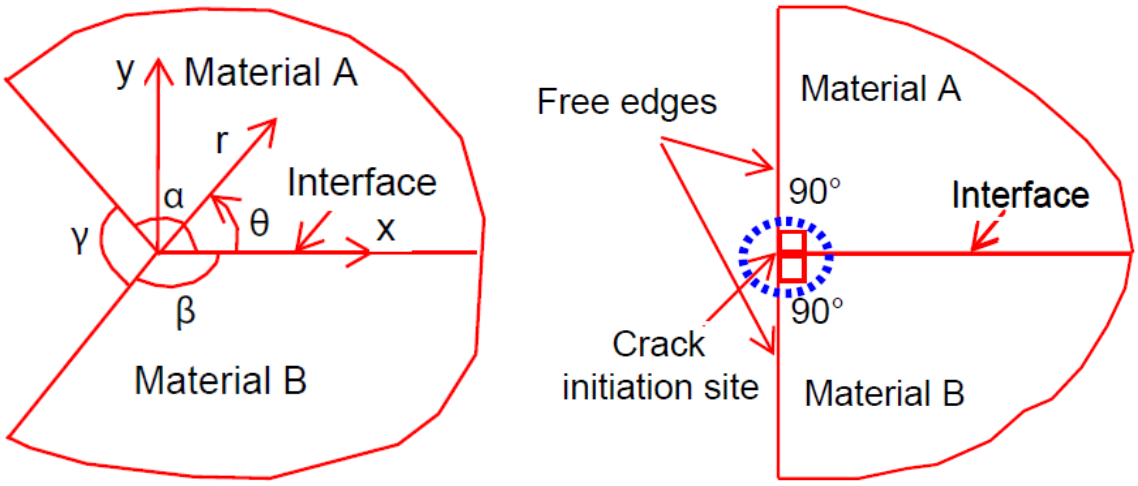

Fig. 1 Schematic plot of a sharp corner and an free edge in a bi-material system.

In terms of strength, the interfaces in the multi-layered component are usually the weakest. The interface failure in the processing and in service sometimes results in critical malfunction of the

devices. Accordingly, it is necessary to evaluate the interface strength between different materials. It is well known that the interface stress fields around the notch tip are of the form $K_m^n r^{\lambda_m - 1} (m = 1, 2, \cdots N)$ where N is the number of eigenvalues available from the characteristic equation. Superscript n indicates the notch for the sake of distinction from the stress intensity factor K_m in classical fracture mechanics, r is the radial distance from the notch corner and $\lambda_m - 1$ is the order of the stress singularity. The stress field is singular for $0 < \mathrm{Re}(\lambda_m) < 1$ where $\mathrm{Re}(\lambda_m)$ is the real part of λ_m, depending on the material elastic properties and notch geometries. The intensity of the singular stress state near an interface corner is characterized by the magnitude of K_m^n which depends on the edge geometry, the elastic constants and the remote loading modes. Therefore, the knowledge of both K_m^n and λ_m are needed to fully describe the stresses and displacements in the vicinity of the notch tip. The near-tip fields are presented and developed for a general corner (e.g., Barnett and Kirchner, 1997; Carpenter, 1984a; 1984b; Labossiere and Dunn, 1999; Walsh, 1976; Sinclair et al., 1984; Munz and Yang, 1993; Munz et al., 1993; Yang and Chao, 1992; Reedy, 1993) and for an edge interface (e.g., Akisanya, 1997; Akisanya and Fleck, 1997; Banks-Sills, 1997; Fett, 1994; Qian and Akisanya, 1999a). The stresses at the edge interface including singular and constant terms under thermal loading are examined in the literature (e.g., Munz et al., 1993; Qian and Akisanya, 1998; Munz and Yang, 1992). The order of the stress singularity, $\lambda_m - 1$, near the interface corner has been extensively studied for isotropic materials (e.g., Bogy and Wang, 1971; Carpenter, 1984a; 1984b; Dempsey and Sinclair, 1979; 1981; Hein and Erdogan, 1971; Williams, 1952; Yang and Munz, 1997; Hutchinson and Suo, 1992; England, 1971; Theocaris, 1974; Kelly et al., 1992; Paggi and Carpinteri, 2008) and anisotropic materials (e.g., Barroso et al., 2003; Kuo and Bogy, 1974; Yosibash and Szabo, 1995; Szabo and Yosibash, 1996; Ting, 1996; 1997; Labossiere and Dunn, 1999; Chen and Nisitani, 1993).

In particular, the magnitude of the stress intensity factor is generally determined by either an extrapolation method or a path-independent integral approach. The former method involves the matching of the asymptotic displacements along the notch flanks (e.g., Reedy, 1993; Su et al., 2003) or the stresses (e.g., Munz et al., 1993; Munz and Yang, 1992; Su et al., 2003) along the interface to the corresponding finite element results. Relatively fine meshes close to the notch tip are required to capture the effects of the singularity. In the latter approach, the H-integral combined with finite element solutions is used to calculate the stress intensity factor for a general corner. The H-integral approach for cracked isotropic solids, pioneered by Stern et al. (e.g., Hong and Stern, 1978; Stern et al., 1976; Stern and Soni, 1975; Stern and Soni, 1976a; 1976b; Stern, 1979) and Snyder and Cruse (1975), was extended by Carpenter (1984a), Sinclair et al. (1984; 1985) and Babuska and Miller (1984) to notched solids in isotropic media where both mode I and mode II loading were taken into account. This was further extended to an isotropic bimaterial notched body by Carpenter and Byers (1987) and Banks-Sills (1997), and applied by Labossiere and Dunn (1999) to a general sharp notch with anisotropic materials. The effect of higher order terms ($\lambda_m > 1$) on the stress state near the interface corner of a bi-material joint is demonstrated by Qian and Akisanya (1999b). The accuracy of the extrapolation method is subject to numerical error introduced to the nodal displacements or stresses close to the interface corner. By contrast, the path-independent integral method utilizes the stresses and displacements away from the notch tip, and therefore the accuracy doesn't depend critically on the mesh density near the interface corner. Qian and Akisanya (1998) found that the values of K for a sandwiched scarf joint using the extrapolation method are lower by about 15-25% than those obtained by the path-independent integral method. However, few researchers addressed weak singularity problems at free edges.

Kitamura et al. (2002; 2003; 2007) explored the free edge effect on singular stress fields and evaluated the fracture strength at the interface edge through delamination tests. Xu et al. (2004) conducted an integrated experimental and numerical investigation for removing or reducing the free-edge stress singularities in dissimilar material joints by alternatively using a convex joint design.

Due to its significant electrical, mechanical, optical and thermal properties, single crystal silicon is of interest to electronics industry and has important industrial applications in the fabrication of semiconductors. As we know, single crystal silicon is a slightly anisotropic material. Owing to its anisotropy, an issue is arisen whether it is necessary to conduct anisotropic stress analysis or isotropic stress analysis. Chen et al. (2000) performed 2D (two-dimensional) axisymmetric and 3D (three-dimensional) FEA simulations for SCS (Shear-compression specimen) biaxial flexure specimen. Results indicated that they could justify using 2D isotropic analysis with Young's modulus E = 170 GPa and Possion's ratio v = 0.1 for SCS to model the stress state in the biaxial flexure specimens.

Fracture resistance of structural components with stress concentration at sharp notches or at free edges can be evaluated by different failure criteria. Note that a traditional yield criterion is not applicable to correlate with failure because typically the failure load measured from tests depends on specimen geometry, size and type of remote loading. It is interesting to investigate the failure criterion. The failure initiation criterion at interface corners has been discussed in many studies (e.g., Stern et al., 1976; Sinclair, 1985; Carpenter and Byers, 1987; Munz and Yang, 1993; Yang and Munz, 1997; Carpenter, 1995; Labossiere and Dunn, 1998; Dunn et al., 2000; Reedy and Guess, 2002; Qian, 2001; Wang et al., 2002). Mainly two different failure criteria have been proposed to predict the failure initiation at sharp notches (Fig. 13) or wedge corners (e.g., Luo and Subbarayan, 2007). One is based on the assumption of "small scale yielding" near the corner. The failure occurs when the dominating stress intensity factor reaches a critical value (e.g., Hutchinson, 1990; Yin, 1999; Reedy and Guess, 1993). Alternatively, failure occurs when the function of comparable stress intensity factors, for example in the $K_I - K_{II}$ space in case of mixed-mode deformation, reaches a critical value (e.g., Labossiere et al., 2002). In the other approach, failure starts at the notch corner when the strain energy density at a point ahead of the notch reaches a critical value (e.g., Sih and Ho, 1991). Although the units of the strain energy density is independent of the wedge angle, the evaluation of the strain energy requires knowledge of both the order of the stress singularity and the stress intensity factor, since the stresses as well as the strains rely on these two parameters. Hence, a single parameter to correlate fracture initiation at sharp notches is promising, similar to the concept of yield stress. Additionally, key factors affecting the magnitude of critical stress intensity have also been discussed by some others (e.g., Beadle et al., 1985; Henning et al., 2004; Shang et al., 2008).

1.2 Objectives and scope

The objective of this work is to investigate a re-entrant corner/notch or free edge in multi-layered structures and evaluate the corresponding fracture parameters.

Over the last 20 years, notch mechanics and analysis of an interface between two elastically dissimilar materials has been an active research field. For multimaterial media, the situation becomes complicated as the mixed-mode deformation generally occurs. With this, the asymptotic elastic fields depend on the radial position, the elastic mismatch and the interface corner geometry. Due to the high stresses at sharp notch corners, the crack often starts at the interfaces in the multi-

layered component and then results in malfunction of the MEMS devices. Similar to the concept of yield stress, we strive to propose a fracture initiation criterion used for the notch components. Our goal is to develop a method for crack initiation analysis at interface corners or at free edges. A convenient computational procedure to obtain the stress intensity factor for a general notch problem is necessary. Key factors influencing the fracture parameter along with the feasibility and limitations of the methods derived are then discussed.

Because of the complexity of MEMS structures, two different interface corners may exist simultaneously in one multi-layered structure. The question of prevailing failure mode in multi-layered structural components is addressed.

To facilitate engineering application, standardized numerical formulae for varying material combinations in a notched body are proposed.

Furthermore, on account of its excellent performance, single crystal silicon is at the heart of the electronics industry. Single crystal silicon is, however, a slightly anisotropic material. The importance of material anisotropy to evaluate the fracture parameter when combined with diverse materials is investigated.

1.3 Outline

The framework of this dissertation is outlined herein. As stated above, the motivation, objective and scope of the study have been introduced. Chapter 2 is intended for a review of MEMS technology. It contains the definition of MEMS or Microsystems, a presentation of silicon properties, brief descriptions of processes in micromachining, a prospect of future potential markets and a list of useful online resources. In Chapter 3, an overview of anisotropic elasticity theory is given. The stiffness transformation between one crystallographic system and global coordinate system is briefly presented. The development and the advantages of Stroh's formalism compared with Lekhnitskii's formalism are addressed. Two eigenvalue problems are also highlighted. We dedicate Chapter 4 to present why notch mechanics is used for solving the crack initiation problem for an interface corner, instead of strength theories, classical fracture mechanics and interface fracture mechanics. Furthermore, two important parameters, λ and K are discussed, describing the singular stress field around a notch tip. The concept of H-integral is introduced and the method for obtaining the stress intensity factor has been provided. Chapter 5 is a summary of three appended papers. Paper I and Paper II address the different notch angle problems. 54.74° notch is the focus of Paper I, the main concern of Paper II is then the free edge (180º opening angle) and a 90° notch. Parameters influencing the stress intensity factors have been extensively studied in both papers. Dimensionless stress intensity factors in different deformation modes are analyzed. Three different approaches to obtain the stress intensity factors are compared. Analysis of the competition of crack initiation between a free edge interface and a 90° notch interface has been explored. Related mechanical aspects, such as anisotropy of the silicon material, mesh refinement, load misalignment, plastic deformations in the ductile material, the extent of K-dominated field, varying failure criteria have been discussed. The appendix is a supplement to Paper II. It is shown that the material dependence of the dimensionless stress intensity factor can be normalized. Paper III addresses three puzzling issues emerging often in the notch mechanics: mathematical interpretation of the eigen-equation, definitions of stress intensity factors and the effect of the contour selection. Chapter 6 presents concluding remarks and recommendations for future work.

CHAPTER 2

Microsystems and MEMS

This Chapter is a summary of Microsystems and MEMS. More detailed information on this topic can be found in textbooks (e.g., Senturia, 2003; Maluf and Williams, 2004; Madou, 1997; Mohamed, 2002; Trimmer, 1997) and literature (e.g., Enikov, 2006; Mounier and Eloy, 2007; Mehregany, 1993; Liu, 2001; Yole Development, 2006; Starman, 2006).

2.1 What are Microsystems and MEMS?

Microsystems or Microsystems technology (MST) used in Europe, Micro-electro-mechanical Systems (MEMS acronym) used in the United States and elsewhere is an equivalent term describing the technology, for example, see Fig. 2. MEMS is simultaneously a toolbox/portfolio of techniques and processes to design and create miniature systems, a physical product often specialized and unique to a final application, and a methodology of making sensors, actuators with computation and communication to locally control physical parameters at the microscale, yet causing effects at much larger scales. Enikov (2006) also stated that MEMS was coined to describe a sub-millimeter integrated electro-mechanical system that contains both electrical and mechanical components with sizes in the range of 1 μm to 1 mm and is fabricated in a massively parallel manner through photolithography. With the advance of exposure systems, the lowest size limit is constantly being broken until 30-100nm range nowadays. Fig. 3 illustrates the size definition of MEMS in comparison with other commonly known structures and technologies. Compared with macroscopic products, the success of MEMS is not simply reducing the size scale, but implementing its functions at low cost, low power, and with high performance, and great integration. It is making possible the realization of complete systems-on-a-chip.

Although the term MEMS was proposed until the early 1980s, MEMS elements were present even in the early days of the IC (Integrated Circuit) industry. The first devices composing of both electronic elements and mechanical component were a resonant gate (RGT) field effect transistor invented by Nathanson and Wickstrom (1965) of Westinghouse Research Laboratories and a pressure sensor based on the piezoresitive effect of Si in 1960s but demonstrated by Kurtz and Goodman (1974) later.

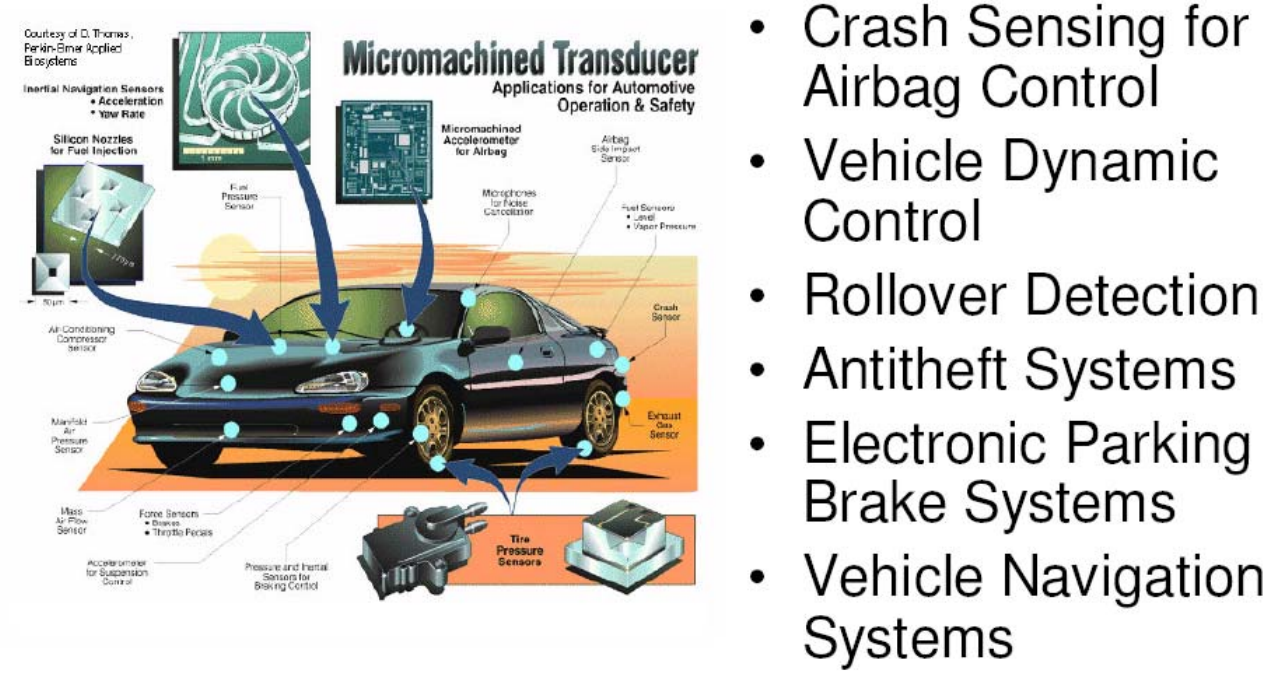

Fig. 2 An example for MEMS applications

(Starman, 2006; Liu, 2001; coutesy of Dr. Thomas Perkin-Elmer)

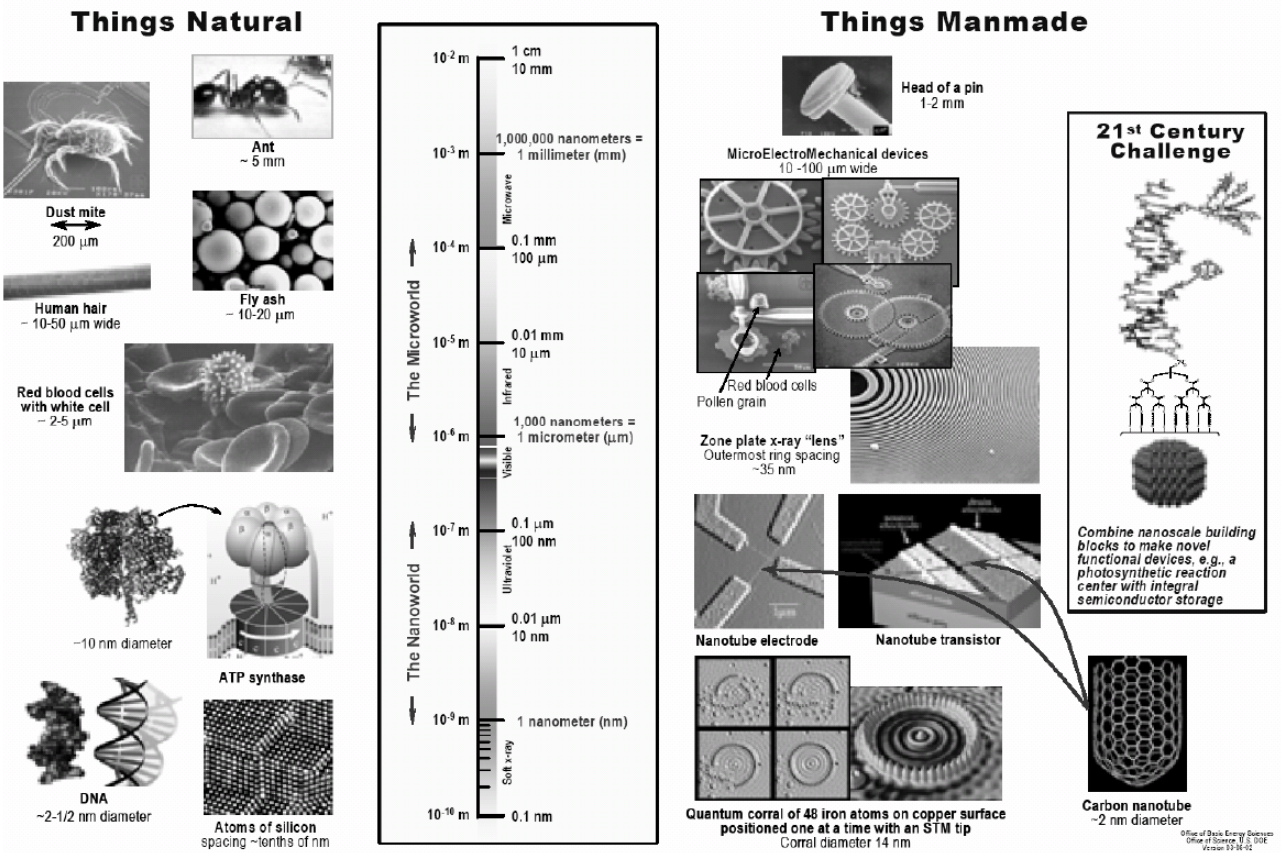

Fig. 3 The scale of Micro devices *(Liu, 2001)*

2.2 Silicon and its crystallographic structure

Due to its economical manufacturing processes and its significant electrical and mechanical advantages, silicon, which is a Group IV element, is the most popular substrate material for the electronic integrated circuit industry and micro-electro-mechanical systems. Visualization of crystallographic planes is a key to understand the dependence of material properties on crystal orientation and the effects of plane-selective etch solutions, see Fig. 4. Silicon has a diamond-cubic crystal structure. The illustration on the left in Fig. 4 shows an interior atom bound to one corner atom and three face-center atoms. For clarity, atoms at the corner of the cubic unit cell are shaded, those in the center of the faces are white, and those interior atoms that are displaced by ¼ of the body diagonal from either a face or corner atom are shaded back. Since every atom is identical, they have the exact same bonding structure and local environment. The principal axes are defined as the three major coordinate axes of the cube. By using Miller indices (Ashcroft and Merimin, 1976), specific planes and directions within the crystal are designated with respect to the principal axes. Miller indices (Fig. 5) are a special notation for cubic crystals in materials science. That is, three integers are encompassed with various punctuation marks. Brackets specify the directions, for instance [100] which is a vector in the +x direction. Carets indicate groups of directions with equivalent properties, e.g., <100>, which covers the $[100] = +x$, $[\bar{1}00] = -x$, $[010] = +y$, $[0\bar{1}0] = -y$, $[001] = +z$, $[00\bar{1}] = -z$ directions. Parentheses specify a plane that is perpendicular to a direction with the same numbers, for example, (110) is a plane perpendicular to the [110] vector. All equivalent crystallographic planes are specified by braces; e.g., Ashcroft and Merimin (1976) represents the four equivalent crystallographic planes $(111) = (\bar{1}\,\bar{1}\,\bar{1})$, $(\bar{1}11) = (1\,\bar{1}\,\bar{1})$, $(1\,\bar{1}1) = (\bar{1}1\,\bar{1})$, and $(11\,\bar{1}) = (\bar{1}\,\bar{1}1)$. For a simple cubic crystal, the +x, -x, +y, -y, +z, and –z directions are all equivalent.

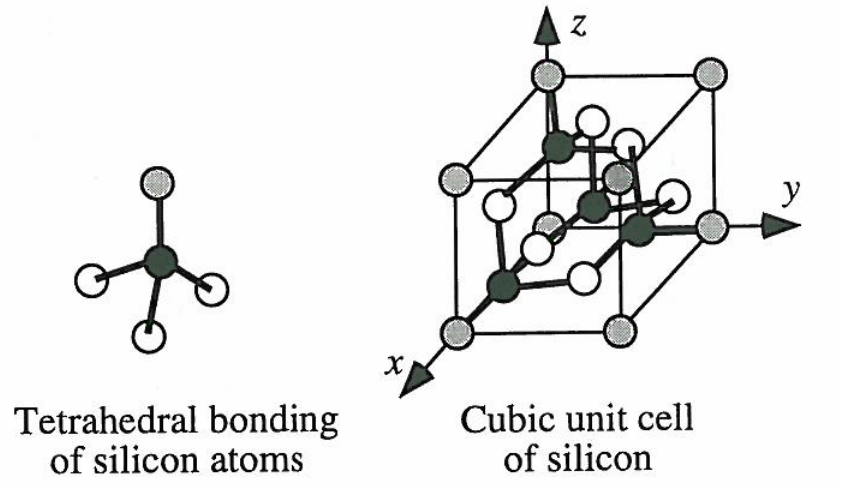

Fig. 4 Crystal structure in single crystal silicon *(Senturia, 2003).*

.

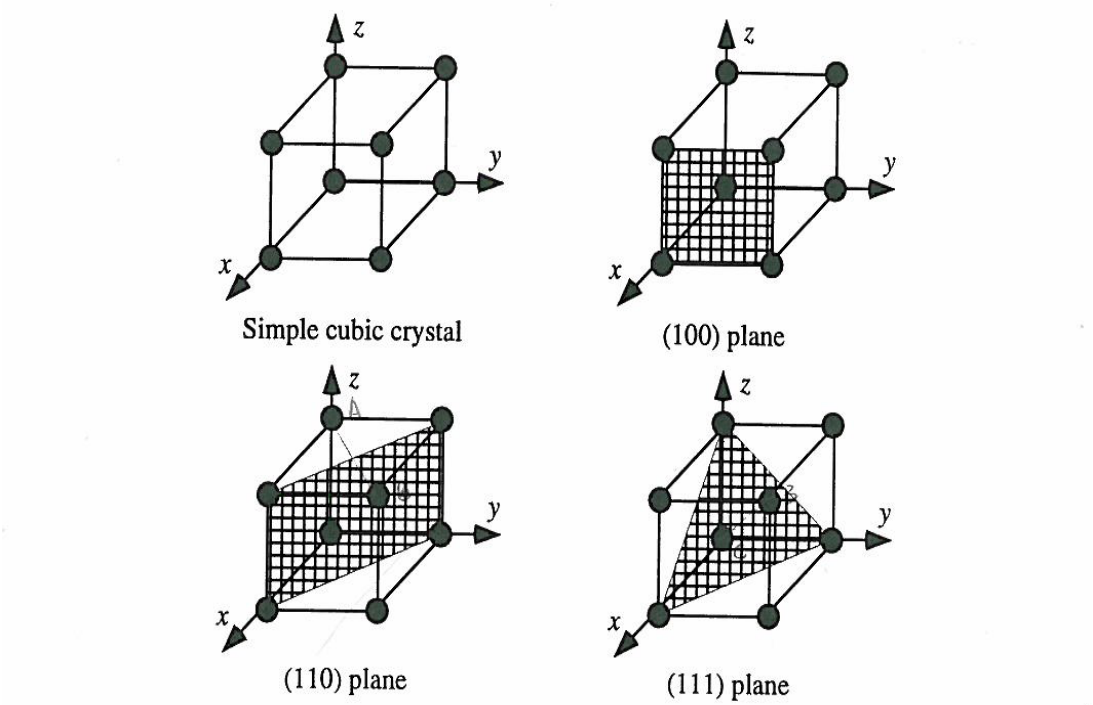

Fig. 5 Illustration of crystallographic planes and their Miller indices for a simple cubic crystal. *(Senturia, 2003)*

The fact that silicon can be anisotropically etched by certain etchants is partly attributed to the detailed bond structure of the atoms that are revealed in different surface planes. Note that a (111) oriented surface has the highest density of atoms per unit area. Vector algebra illustrates that the angles between {100} and {111} plane are 54.7° or 125.3°, and the angles between {100} and {110} planes are 45° or 90°. Similarly, {111} and {110} planes can intersect with each other at 35.3°, 90°, or 144.7°.

Wafers are also characterized by their doping level, p-type or n-type. Doping refers to the process by which impurities are intentionally added to modify the electrical conductivity and conductivity type. Note that introduction of Group III atoms (e.g., boron) produces p-type material, while introduction of Group V atoms (e.g. phosphorus and arsenic) produce n-type material.

Furthermore, crystalline silicon is a hard and brittle material deforming elastically until it reaches its yield strength, at which point it breaks. Its tensile yield strength is 7GPa. Its Young's modulus is dependent on crystal orientation, being 130.2 GPa in <111> directions and 168.9 GPa in <110> directions which near that of steel (Mason, 1958; Wortman and Evans, 1965).

The surface of silicon oxidizes immediately upon exposure to the oxygen in air (referred to as native oxide). The oxide thickness self-limits at a few nanometers at room temperature. As silicon dioxide is very inert, it acts as a protective layer that prevents chemical reactions with the underlying silicon.

2.3 MEMS micromachining technology (Microfabrication)

Micromachining is a key fabrication technology for solid state sensors and actuators, as well as microelectromechanical systems (MEMS). The reasons for employing micromachining are that this technology can minimize energy and materials use in manufacturing, improve reproducibility (batch fabrication), integrate with electronics, improve accuracy and reliability, and display cost and performance advantages. The birth of the first micromachined components dates back many decades, but many MEMS fabrication borrowed from the Integrated Circuit (IC) industry, such as lithographic tools, in addition to a few specialized processes developed specifically for silicon micromachining, e.g., wafer bonding, anisotropic chemical wet etching, deep reactive ion etching, sacrificial etching, and critical-point drying. Note that the distinct differences of micromachining from conventional machining are due to its batch process and its miniature dimension on the order of micrometers. Systematic descriptions for MEMS micromachining technology are addressed in other references (Senturia, 2003; Maluf and Williams, 2004).

Micromachining can be classified as bulk and surface micromachining, see Fig. 6. Both are based on silicon IC technology. Surface micromachining refers to a fabrication process that removes sacrificial layers from beneath thin-film structures, leaving free-standing mechanical structures. This process generates mechanical structures on the surface of the substrate. By comparison, bulk micromachining was developed between 1970 and 1980 for fabrication of three dimensional structures. As opposed to surface structure formation, it refers to a process of forming structures in the bulk of the substrate. Bulk micromachining of silicon uses wet and dry etching techniques in conjunction with etch masks and etch stops to sculpt micromechanical devices from the silicon substrate.

In terms of the fabrication processes, silicon micromachining can be also classified as material deposition, pattering, and etching techniques. Among those, lithography plays a significant role in the delineation of precise patterns. Fig. 7 illustrates the basic process flow in micromachining: layers are deposited; photoresist is lithographically patterned and then used as a mask to etch the underlying materials. The process is repeated until completion of the microstructure.

Although silicon remains the popular material for micro-electro-mechanical systems, a vast range of materials has been used for microsystems such as glass, ceramics, polymers and group III and V elements, as well as a variety of metals including titanium and tungsten.

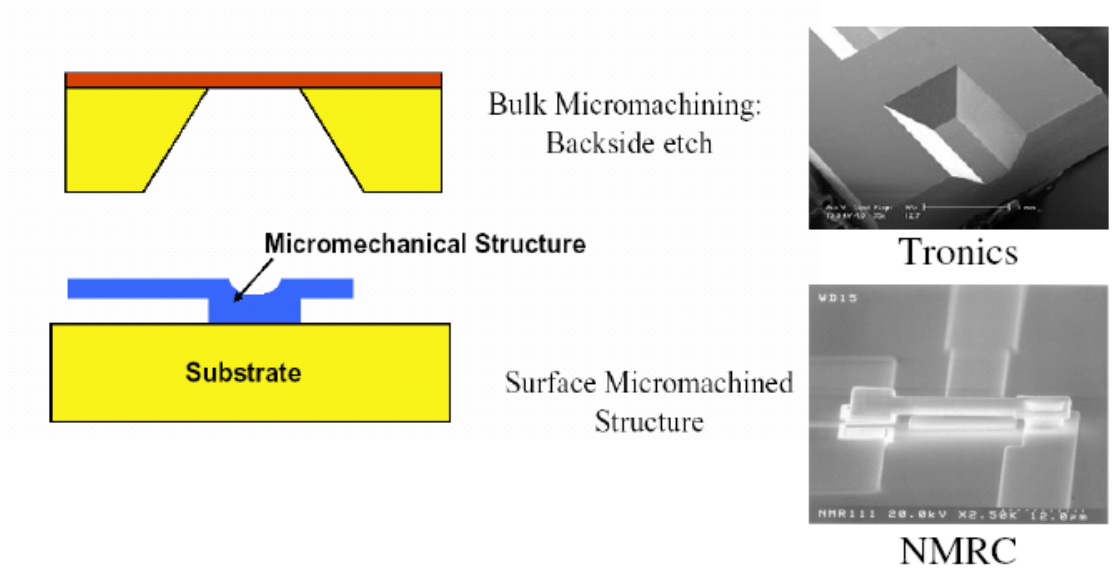

Fig. 6 Bulk micromachining and surface micromachining *(Liu, 2001)*

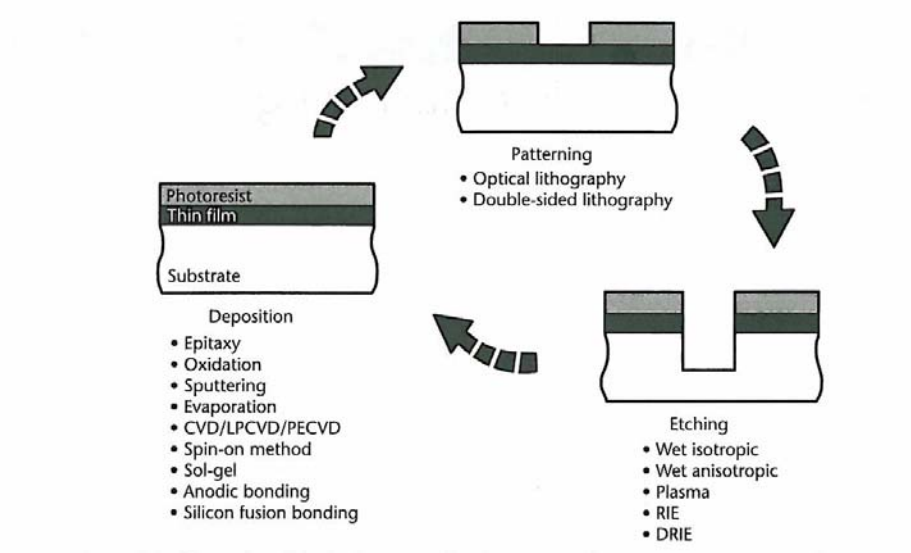

Fig. 7 Illustration of the basic process flow in micromachining *(Maluf and Williams, 2004)*.

2.3.1 Deposition

Epitaxy, oxidation, sputtering, evaporation, chemical vapor deposition, and spin-on method are common techniques used to deposit uniform layers of semiconductors, metals, insulators, and polymers (Maluf and Williams, 2004). Specially, only wafer bonding is addressed here. Wafer bonding is a method for firmly joining two wafers to create a stacked wafer layer. Wafer bonding is used both in MEMS devices fabrication and in device packaging. Three main types of wafer bonding processes, direct wafer bonding, anodic bonding, and bonding with an intermediate layer, are presented below.

Direct wafer bonding

Direct wafer bonding, also known as silicon fusion bonding, is a process capable of securely joining two silicon substrates at high temperature, on the order of 1000°C. Silicon direct bonding can be performed between two bare single-crystal silicon surfaces or polished polysilicon. One or both surfaces may have thermal or other smooth silicon dioxide or silicon nitride on them. Starting with the cleaning and hydration of the surfaces, the bond surfaces are then carefully brought into contact and held together by Van Der Waals forces (Tong and Gosele, 1999). An anneal at 800°C to 1100°C for a few hours promotes and strengthens the bond with respect to the reaction

$$\text{Si-O-H}\cdots\text{H-O-Si} \rightarrow \text{Si-O-Si}+\text{H}_2\text{O} \quad (1)$$

Anodic bonding

Anodic bonding (Fig. 8), also known as field-assisted bonding or Mallory® bonding, is a simple method of bonding a sodium-containing glass substrate (e.g., Corning Pyrex 7740® an 7070, Schott 8330 and 8329) to conductors such as silicon or metal. This bonding method is first introduced by Wallis and Pomerantz (1969) and has been commonly used in the manufacturing of a variety of sensors as it provides a rigid support to the silicon that mechanically isolates it from packaging stress.

The dominant mechanism of formation of anodic bonds between glasses and metals is electrochemical, i.e., the mobility of sodium ions in the glass makes oxidization of the silicon surface into the glass network to form permanent Si-O bonds.

The bonding is performed at an elevated temperature between 200°C -500°C either in vacuum, air, or in an inert gas environment. An electrical field, 500 to 1500V, is applied with the anode on the conductor and the cathode on the glass. The mobile positive ions (mostly Na^+) in the glass causes to migrate away from the silicon glass interface toward the cathode, leaving behind the negatively charged oxygen ions in the glass close to the glass/conductor interface. The electrostatic attraction pulls the glass and conductor together with a pressure high enough to initiate a surface reaction and eventually form a chemical bond.

The surfaces need to be sufficiently smooth and the thermal expansion coefficients of the two materials should be matched within 2ppm (parts per million) /°C, since a larger mismatch will lead to bond failure upon cooling of the stack (Enikov, 2006). Hence, one of the important successful characters in bonding silicon to glass is their similar thermal property, for instance, Corning Pyrex® 7740 has a coefficient of thermal expansion of 3.2×10^{-6}/°C; silicon's coefficient is 2.6×10^{-6}/°C at room temperature but rising to 3.8×10^{-6}/°C at 300°C. Note that silicon dioxide on the silicon surface should be removed before bonding, as a thin 100nm layer is sufficient to disturb the current flow and the bond. Usually, several nanometers up to 20nm of natural silicon oxide will be grown on the silicon to form a good bond to glass.

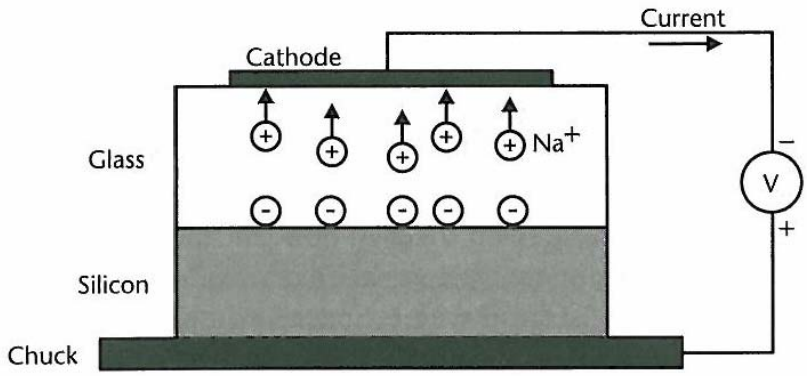

Fig. 8 Illustration of anodic bonding between glass and silicon *(Maluf and Williams, 2004)*.

Bonding with an intermediate layer

As we know, adhesives or solders are often used to bond and laminate bulk structural elements together. In particular, detailed techniques about thin-film anodic bonding are presented in Ref. (e.g., Shang et al., 2008; Visser, 2002). Note that thin-film anodic bonding, was invented by Brooks and Donovan (1972) as a promising sealing technique for highly structured wafers combining the advantages of direct wafer bonding and anodic bonding. The relatively low process temerature, typically ranging from 250 to 450 ºC, and the relaxed requirements for surface roughness, are achieved by introducing a thin-sodium borosilicate glass film. The advantages of direct wafer bonding of two silicon wafers, the perfect match of thermal expansion coefficients and modulus of elasticity, are approached by choosing a thin glass film.

An alternative "adhesive" method is thermocompression bonding. This method has been developed to bond 3 inch borosilicate sputter coated silicon wafers to silicon wafers coated either with aluminium, silicon dioxide, polysilicon or silicon nitride. The bondings were performed with applying moderate pressure to the two wafers at a temperature between 300 and 400 ºC. The bond strengths of the different samples bonded with these methods are all in the region 5-25 MPa (Nese and Hanneborg, 1993).

2.3.2 Pattern

MEMS devices and integrated circuits are formed by defining patterns in the various layers created by wafer-level process steps. The desired pattern is photographically transferred from an optical plate to a photosensitive film coating the wafer. Most MEMS devices and systems are made by using lithography-based microfabrication in combination with micromachining techniques.

Lithography (Fig. 9) is the technique of transferring the pattern on the mask to a layer of radiation sensitive material (photoresist) which is subsequently used as a protective mask against etching. The key feature of LIGA is its ability to produce high-aspect-ratio structures. The radiation used may be optical, X-ray, electron beam (e-beam), or ion beam.

Three sequential steps for lithography are:

- Fabrication of masks (or pattern generation)
- Optical exposure to print an image of the mask onto the photoresist.
- Immersion in an aqueous developer solution to dissolve the exposed photoresist and render visible the latent image.

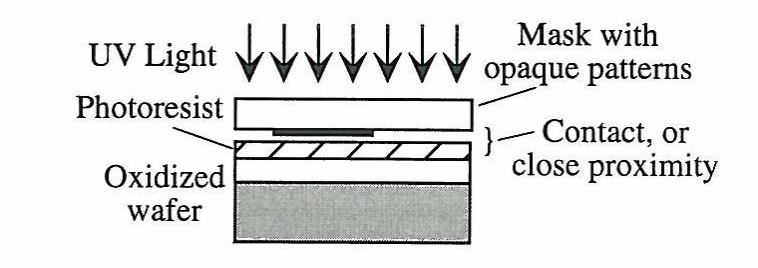

Fig. 9 Illustration of contact or proximity photolithography *(Senturia, 2003)*.

2.3.3 Etching

Etching is used for delineating patterns, removing surface damage, cleaning the surface to remove contamination, and fabricating three-dimensional structures. Both wet chemical etching and dry etching are utilized to selectively remove material. The commonly used etching methods are isotropic wet (chemical) etching, anisotropic wet etching, vapor etching, plasma etching or plasma-assisted etching, deep reactive ion etching (DRIE). Note that deep etching of silicon lies at the core of bulk micromachining. Bulk micromachining of silicon by anisotropic etching has been extensively reviewed (Petersen, 1982).

The selectivity of the etchant for the desired material is important, e.g., HF etches silicon dioxide, but etches silicon nitride slowly. When etching a single crystal, certain etchants exhibit orientation-dependent etch rates. That is, atoms in {111} planes are “more tightly bound” to the rest of the crystal. It has observed experimentally is that the anisotropic etchants of silicon etch the (100) and (110) crystal planes significantly faster than the (111) crystal planes, e.g., the {110} planes are etched in KOH about twice as rapidly as {100} planes, while {111} planes are etched at a rate about 100 times slower than for {100} planes (Seidel et al., 1990).

Fig. 10 demonstrates the basic concepts of bulk micromachining by anisotropic etching of a (100) silicon substrate, e.g., a (100) silicon substrate etching proceeds along the (100) planes while it is practically stopped along the (111) planes. Since the (111) planes make a 54.7° angle with the (100) planes, the slanted walls are induced. Due to the slanted (111) planes, the size of the etch mask opening determines the final etch result (e.g., a hole or a cavity). If the etch mask openings are rectangular (or square) and the sides are aligned with the [110] direction (i.e., the direction of the intersection line between (100) and (111) planes), no undercutting of the etch mask feature takes place, assuming the etch rate of the (111) planes is negligible. Furthermore, the illustration of Fig. 10 is explained as follows: (a) the bottom plan view of an anisotropic etched wafer showing the fabrication of cavities, diaphragms and holes; (b) the top plan view of an anisotropically etched wafer showing the fabrication of a cantilever beam using the etch stop layers; (c) the cross section, A-A', showing the hole, diaphragm and cavity of (a); (d) the cross section, B-B', showing the cantilever beam of (b).

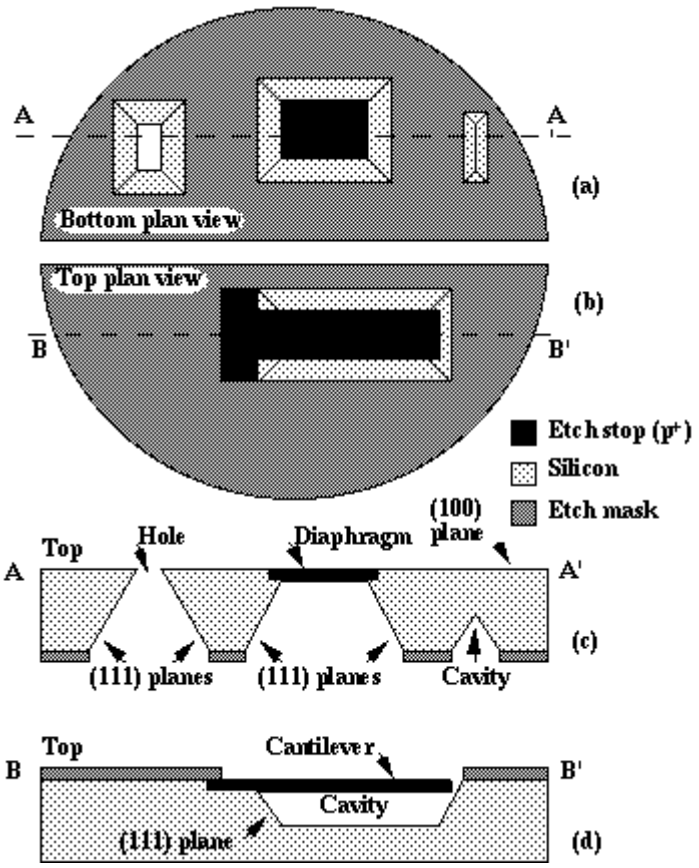

Fig. 10 A schematic drawing of the basic concepts of bulk micromachining by anisotropic etching of a (100) silicon substrate *(Mehregany, 1993; Bhat, 2007)*

2.4 Markets for Microsystems and MEMS

Since the demonstration of the first micromachined accelerometer in 1979 at Stanford University (Roylance and Angell, 1979), MEMS devices have been widely used in the industry over the past several decades. Silicon pressure sensor, accelerometers, gyroscopes, microphones, inject print heads, high-resolution digital displays and micro-fuel cells have been leading consumer applications in the present markets. New applications include tire pressure sensing, RF (Radio Frequency) MEMS, fiber optical components, MOEMS (Micro-opto-electromechanical systems), energy harvesting systems, MEMS based oscillators and fluid management and process in devices for chemical microanalysis, medical diagnostics, and drug delivery.

As an emerging technology with significant future potential, MEMS is subjected to a rising level of excitement and publicity. Fig. 11 shows the market for the different MEMS devices. Fig. 12 shows the MEMS regional production sites revenues breakdown in 2005. At Yole, it predicts that the MEMS market will be 9.7B$ in 2010 and 18 B$ in 2015 (Mounier and Eloy, 2007).

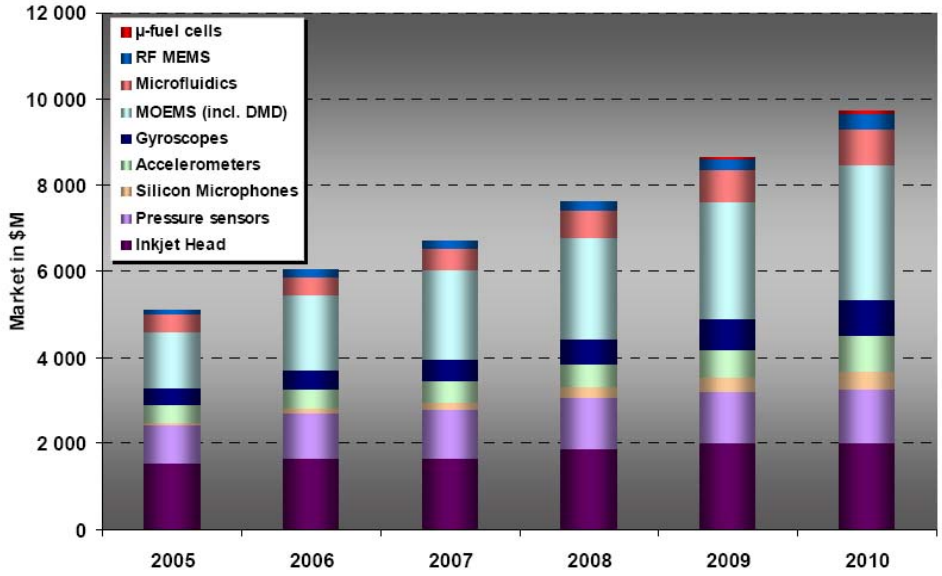

Fig. 11 Global MEMS market 2005-2010 for first-level packaged devices *(Yole Development, 2006)*

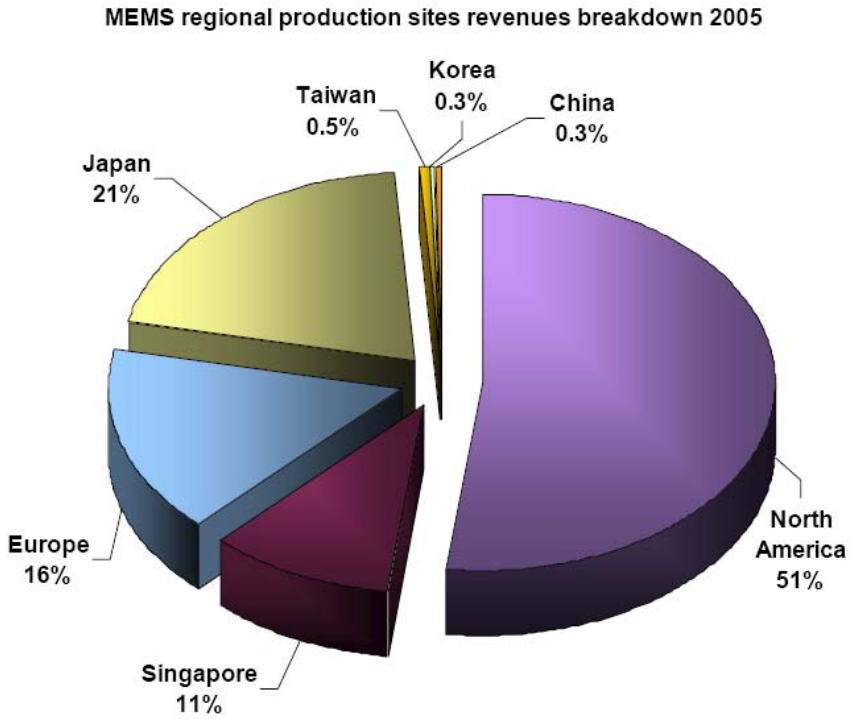

Fig. 12 MEMS regional production sites revenues breakdown in 2005 *(Mounier and Eloy, 2007)*

In a word, Micro-electro-mechanical structures and systems are miniature devices that enable the operation of complex systems. They exist today in many environments, especially automotive, IT, consumer, aerospace and medical. Their potential for a wide range of future applications is real and the MEMS market will continuously grow.

2.5 Journals, conferences and websites in MEMS

Table. 1
List of Journals/Magazines, Conferences and online resources in MEMS

List	Information resources
Journal and Magazines	Journal of Micromechanical Systems (JMEMS)
	Journal of Micromechanics and Microengineering (JMM)
	Sensors and Actuators (A: Physical, B: Chemical & C: Materials)
	Sensors Magazine
	Micronews (Yole Development)
	Micromachine Devices
	MST News
	Micro/Nano Newsletter
	Small Times Magazine
	IEEE Electron Device Letters
	Journal of the Electrochemical Society
	Journal of the Vacuum Society
Conferences	International Conference on Solid-State Sensors, Actuators and Microsystems (Transducers), held on odd years
	Solid-State Sensor and Actuator Workshop (Hilton-Head), held on even years
	MicroElectroMechanical Systems Workshop (MEMS), IEEE
	International Society for Optical Engineering (SPIE)
	Micro Total Analysis Systems (μTAS)
	European Microelectronics and Packaging Conference
	Micromachining and Micropackaging of Transducers
Online Resources	MEMSnet www.memsnet.org
	Yole Development http://www.yole.fr/
	MEMS Industry Group™ www.memsindustrygroup.org
	MEMS Exchange www.mems-exchange.org
	Silicon-Based MEMS site at Sandia National Laboratories http://mems.sandia.gov/
	IEEE Xplore http://ieeexplore.ieee.org/Xplore/dynhome.jsp
	United States Patent and Trademark office http://www.uspto.gov/
	DARPA www.darpa.mil

	Microfabrica http://www.microfabrica.com/
	trimmer.net ™site http://www.trimmer.net/
	Center for Integrated Systems (Stanford University) http://www-cis.stanford.edu/
	IDA Mems.ida.org
	MEMSSCAP http://www.memscap.com/
	Small Times http://www.smalltimes.com/
	The MOSIS Services http://www.mosis.com//
	NEXUS www.nexus-mems.com
	AIST-MITI www.aist.go.jp
	NIST www.atp.nist.gov
	Berkeley Sensor & Actuator Center http://www-bsac.eecs.berkeley.edu/
	ATIP www.atip.org
	VDI/VDE-IT www.mstonline.de
	Danny Banks' MEMS book http://www.dbanks.demon.co.uk/ueng/index.html

CHAPTER 3

Anisotropic Elasticity

3.1 Linear anisotropic elastic materials

For small displacements, it is a consequence of Hooke's law that the stresses are proportional to the strains. In a fixed rectangular coordinate system $x_i \ (i = 1,\ 2,\ 3)$, let u_i, σ_{ij}, and ε_{ij} be the displacement, stress, and strain, respectively. Strain is acquired by differentiating the displacement, u_i, with respect to position and the strain-displacement relations is

$$\varepsilon_{ij} = \frac{1}{2}\left(u_{i,j} + u_{j,i}\right) \tag{2}$$

in which a comma stands for partial differentiation.

The constitutive equations that relate the stress and strain for an anisotropic solid can be expressed in tensor form as:

$$\sigma_{ij} = C_{ijkl}\varepsilon_{kl} \quad \text{or} \quad \varepsilon_{ij} = S_{ijkl}\sigma_{kl} \tag{3}$$

where C_{ijkl} and S_{ijkl} are, respectively, the elastic stiffnesses and compliances. They possess the full symmetry and satisfy the requirement that the strain energy is positive. The elastic stiffness tensor, C_{ijkl}, is a fourth-order tensor that in its most general form contains 36 elastic constants. The stiffness constants satisfy the following symmetry conditions:

$$C_{ijkl} = C_{jikl} = C_{klij} = C_{ijlk} \tag{4}$$

In this case, a linear anisotropic elastic material can have as many as 21 independent elastic constants. Additional material symmetries can further reduce the number of independent constants to a minimum of two, for a material that has an infinite number of symmetry planes. These materials are designated as isotropic materials, and the two independent elastic constants are often presented as the Young's modulus and the Poisson ratio. On the other hand, cubic materials have nine planes of symmetry. Three planes of symmetry have normals on the three coordinate axes and six planes of symmetry are planes at an angle 45° to the coordinate axes. The number of independent elastic constants is three for cubic materials.

In the absence of body forces, the state of equilibrium can be expressed as:

$$\sigma_{ij,j} = 0 \tag{5}$$

in which the stress, σ_{ij}, is a second-order tensor. Insertion of (2) into $(3)_1$, and then into (5) yields

$$\sigma_{ij} = C_{ijkl} u_{k,l} \tag{6}$$

$$C_{ijkl} u_{k,lj} = 0 \tag{7}$$

According to the contracted notation (e.g., Christensen, 1979; Lekhnitskii, 1950; Voigt, 1910; Jones, 1975; Cowin et al., 1992), the ordinary elastic constants $C_{\alpha\beta}$ are determined from the stiffness by replacing 11 by 1, 22 by 2, 33 by 3, 23 by 4, 13 by 5, 12 by 6. As a result, the stress-strain law (3) can be stated as

$$\begin{Bmatrix} \sigma_1 \\ \sigma_2 \\ \sigma_3 \\ \sigma_4 \\ \sigma_5 \\ \sigma_6 \end{Bmatrix} = \begin{bmatrix} C_{11} & C_{12} & C_{13} & C_{14} & C_{15} & C_{16} \\ & C_{22} & C_{23} & C_{24} & C_{25} & C_{26} \\ & & C_{33} & C_{34} & C_{35} & C_{36} \\ & & & C_{44} & C_{45} & C_{46} \\ & & & & C_{55} & C_{56} \\ & & & & & C_{66} \end{bmatrix} \begin{Bmatrix} \varepsilon_1 \\ \varepsilon_2 \\ \varepsilon_3 \\ \varepsilon_4 \\ \varepsilon_5 \\ \varepsilon_6 \end{Bmatrix} \tag{8}$$

i.e.,

$$\sigma_\alpha = C_{\alpha\beta} \varepsilon_\beta, \; C_{\alpha\beta} = C_{\beta\alpha} \tag{9}$$

Note that engineering strains are used throughout this thesis.

For isotropic material, the stiffness can be presented as

$$C_{\alpha\beta} = \begin{bmatrix} \chi+2\mu & \chi & \chi & 0 & 0 & 0 \\ & \chi+2\mu & \chi & 0 & 0 & 0 \\ & & \chi+2\mu & 0 & 0 & 0 \\ & & & \mu & 0 & 0 \\ & & & & \mu & 0 \\ & & & & & \mu \end{bmatrix} \tag{10}$$

In the above, χ and μ are called Lamé constants (μ is also donated as the shear modulus), expressed by $\chi = \dfrac{E\nu}{(1+\nu)(1-2\nu)}$ and $\mu = \dfrac{E}{2(1+\nu)}$ with E being Young's modulus and ν being Poisson's ratio.

Consider anisotropic elastostatics, two-dimensional deformations of anisotropic elastic bodies are addressed in this thesis. Main deformation modes are hence briefly presented in the following. For two-dimensional deformations for which the displacement $u_i \; (i = 1,\ 2,\ 3)$ depends only on x_1 and x_2, the equations of equilibrium Eq. (7) is written explicitly as

$$C_{i1k1} u_{k,11} + C_{i2k2} u_{k,22} + (C_{i1k2} + C_{i2k1}) u_{k,12} = 0 \tag{11}$$

which provides three differential equations for the three displacement components u_1, u_2 and u_3. In general, the in-plane and anti-plane deformation may be coupled for anisotropic solids, e.g., in-plane loading gives rise to anti-plane displacements and vice versa. In certain cases, however, the in-plane and anti-plane deformations are decoupled. This situation occurs when $C_{14} = C_{15} = C_{24} = C_{25} = C_{34} = C_{35} = C_{46} = C_{56} = 0$ as described by Ting (1996). If the anti-plane displacement u_3 can be uncoupled from the in-plane displacements u_1 and u_2, we may consider

anti-plane deformations and in-plane deformations separately. The deformations due to in-plane displacement are plane strain deformations. For the plane strain deformations

$$u_1 = u_1(x_1, x_2),\ u_2 = u_2(x_1, x_2),\ u_3 = 0 \tag{12}$$

The third equation is satisfied if the material meets

$$C_{14} = C_{15} = C_{24} = C_{25} = C_{46} = C_{56} = 0 \tag{13}$$

For the anti-plane deformations

$$u_1 = u_2 = 0,\ u_3 = u(x_1, x_2) \tag{14}$$

Note that imposing the conditions (13) can induce the first two equations in (14) to vanish identically. Hence, an anisotropic elastic material that can sustain a plane strain deformation can also maintain an anti-plane deformation.

On the other hand, when in-plane and anti-plane deformation are coupled for a very general anisotropic elastic body, all three displacement components have to be considered simultaneously even though they depend only on x_1 and x_2. Such a deformation is called a generalized plane strain deformation, i.e., $u_3 \neq 0,\ \varepsilon_{13} \neq 0,\ \varepsilon_{23} \neq 0$ but $\varepsilon_{33} = 0$.

3.2 Stiffness transformation between a crystallographic coordinate system and a global coordinate system

In order to derive some of the required relations between the elastic constants in one crystallographic system and the elastic constants in another system, rotated with respect to the first, a brief presentation of transformation theory is given in this section. This can be used to determine the elastic constants in a system of coordinates, different from the crystallographic axis system. The detailed description can be found in (e.g., Chadwick and Smith, 1977).

The importance of the constitutive equation in tensor equations (3) lies in the fact that it provides a ready method for transforming the elastic constants from one system of axes to another system by means of the tensor transformation equations

$$C'_{ijkl} = \frac{\partial x'_i}{\partial x_m}\frac{\partial x'_j}{\partial x_n}\frac{\partial x'_k}{\partial x_o}\frac{\partial x'_l}{\partial x_p} C_{mnop} \tag{15}$$

A simple form with the reduced index symbols is shown in Eq. (16) for calculating the result of the indicated operation above.

$$
C'_{ijkl} = C'_{\alpha\beta} =
\begin{array}{cccccc}
 & & & \dfrac{\partial x'_i}{\partial x_2}\dfrac{\partial x'_j}{\partial x_3} & \dfrac{\partial x'_i}{\partial x_1}\dfrac{\partial x'_j}{\partial x_3} & \dfrac{\partial x'_i}{\partial x_1}\dfrac{\partial x'_j}{\partial x_2} \\
 & & & + & + & + \\
\dfrac{\partial x'_i}{\partial x_1}\dfrac{\partial x'_j}{\partial x_1} & \dfrac{\partial x'_i}{\partial x_2}\dfrac{\partial x'_j}{\partial x_2} & \dfrac{\partial x'_i}{\partial x_3}\dfrac{\partial x'_j}{\partial x_3} & \dfrac{\partial x'_i}{\partial x_3}\dfrac{\partial x'_j}{\partial x_2} & \dfrac{\partial x'_i}{\partial x_3}\dfrac{\partial x'_j}{\partial x_1} & \dfrac{\partial x'_i}{\partial x_2}\dfrac{\partial x'_j}{\partial x_1} \\
C_{11} & C_{12} & C_{13} & C_{14} & C_{15} & C_{16} \\
C_{21} & C_{22} & C_{23} & C_{24} & C_{25} & C_{26} \\
C_{31} & C_{32} & C_{33} & C_{34} & C_{35} & C_{36} \\
C_{41} & C_{42} & C_{43} & C_{44} & C_{45} & C_{46} \\
C_{51} & C_{52} & C_{53} & C_{54} & C_{55} & C_{56} \\
C_{61} & C_{62} & C_{63} & C_{64} & C_{65} & C_{66}
\end{array}
\begin{array}{c}
\dfrac{\partial x'_k}{\partial x_1}\dfrac{\partial x'_l}{\partial x_1} \\
\dfrac{\partial x'_k}{\partial x_2}\dfrac{\partial x'_l}{\partial x_2} \\
\dfrac{\partial x'_k}{\partial x_3}\dfrac{\partial x'_l}{\partial x_3} \\
\dfrac{\partial x'_k}{\partial x_2}\dfrac{\partial x'_l}{\partial x_3} + \dfrac{\partial x'_k}{\partial x_3}\dfrac{\partial x'_l}{\partial x_2} \\
\dfrac{\partial x'_k}{\partial x_1}\dfrac{\partial x'_l}{\partial x_3} + \dfrac{\partial x'_k}{\partial x_3}\dfrac{\partial x'_l}{\partial x_1} \\
\dfrac{\partial x'_k}{\partial x_1}\dfrac{\partial x'_l}{\partial x_2} + \dfrac{\partial x'_k}{\partial x_2}\dfrac{\partial x'_l}{\partial x_1}
\end{array}
\tag{16}
$$

This relation is a general solution to solve the case $C_{ij} \neq C_{ji}$, as emerging for magnetostrictive, electrostrictive, or photoelastic tensors. As far as an elastic tensor, $C_{ij} = C_{ji}$, is concerned, the direction cosines are related to the partial derivatives appearing in (16) as in Eq. (17).

$$
\begin{array}{cccc}
 & x_1 & x_2 & x_3 \\
x'_1 & \dfrac{\partial x'_1}{\partial x_1} = l_1; & \dfrac{\partial x'_1}{\partial x_2} = m_1; & \dfrac{\partial x'_1}{\partial x_3} = n_1; \\
x'_2 & \dfrac{\partial x'_2}{\partial x_1} = l_2; & \dfrac{\partial x'_2}{\partial x_2} = m_2; & \dfrac{\partial x'_2}{\partial x_3} = n_2; \\
x'_3 & \dfrac{\partial x'_3}{\partial x_1} = l_3; & \dfrac{\partial x'_3}{\partial x_2} = m_3; & \dfrac{\partial x'_3}{\partial x_3} = n_3; \\
 & x'_1 & x'_2 & x'_3 \\
x_1 & \dfrac{\partial x_1}{\partial x'_1} = l_1; & \dfrac{\partial x_1}{\partial x'_2} = m_1; & \dfrac{\partial x_1}{\partial x'_3} = n_1; \\
x_2 & \dfrac{\partial x_2}{\partial x'_1} = l_2; & \dfrac{\partial x_2}{\partial x'_2} = m_2; & \dfrac{\partial x_2}{\partial x'_3} = n_2; \\
x_3 & \dfrac{\partial x_3}{\partial x'_1} = l_3; & \dfrac{\partial x_3}{\partial x'_2} = m_3; & \dfrac{\partial x_3}{\partial x'_3} = n_3;
\end{array}
\tag{17}
$$

If the elastic stiffness matrix in the crystallographic axis system is $\mathbf{C}$, the transformed stiffness matrix in the other system of coordinates will be $\mathbf{E} = \mathbf{DCD}^{\mathrm{T}}$. That is, by introducing the direction cosines from Eq. (17), the six possible row multiplying factors are

$$\mathbf{D} = \begin{bmatrix} l_1^2 & m_1^2 & n_1^2 & 2m_1n_1 & 2n_1l_1 & 2l_1m_1 \\ l_2^2 & m_2^2 & n_2^2 & 2m_2n_2 & 2n_2l_2 & 2l_2m_2 \\ l_3^2 & m_3^2 & n_3^2 & 2m_3n_3 & 2n_3l_3 & 2l_3m_3 \\ l_2l_3 & m_2m_3 & n_2n_3 & m_2n_3+n_2m_3 & l_2n_3+n_2l_3 & l_2m_3+m_2l_3 \\ l_3l_1 & m_3m_1 & n_3n_1 & m_3n_1+n_3m_1 & l_3n_1+n_3l_1 & l_3m_1+m_3l_1 \\ l_1l_2 & m_1m_2 & n_1n_2 & m_1n_2+n_1m_2 & l_1n_2+n_1l_2 & l_1m_2+m_1l_2 \end{bmatrix} \tag{18}$$

The corresponding column multipliers are

$$\mathbf{D}^{\mathrm{T}} = \begin{bmatrix} l_1^2 & l_2^2 & l_3^2 & l_2l_3 & l_1l_3 & l_1l_2 \\ m_1^2 & m_2^2 & m_3^2 & m_2m_3 & m_1m_3 & m_1m_2 \\ n_1^2 & n_2^2 & n_3^2 & n_2n_3 & n_1n_3 & n_1n_2 \\ 2m_1n_1 & 2m_2m_2 & 2m_3n_3 & m_2n_3+n_2m_3 & m_1n_3+n_1m_3 & m_1n_2+n_1m_2 \\ 2n_1l_1 & 2n_2l_2 & 2l_3n_3 & l_2n_3+n_2l_3 & l_1n_3+n_1l_3 & l_1n_2+n_1l_2 \\ 2l_1m_1 & 2l_2m_2 & 2l_3m_3 & l_2m_3+m_2l_3 & l_1m_2+m_1l_2 & l_1m_2+m_1l_2 \end{bmatrix} \tag{19}$$

3.3 The Stroh formalism

Basic formulations for representing displacement and stress fields in an anisotropic body under plane deformation have been developed in two entirely different ways by Lekhnitskii (1950) and Eshelby et al. (1953). Lekhnitskii (1950) introduced the complex potentials for stress to treat generalized plane deformation problems. Using the compatibility equations, he derived a set of coupled elliptic partial differential equations for the complex potentials, to obtain the general representation for solutions. On the other hand, Eshelby et al. (1953) presented a more elegant formalism, based on the Navier-Cauchy equations. Following the work of Eshelby, Stroh (1958; and 1962) subsequently developed a powerful formalism for treating a certain class of two-dimensional problems involving dislocations, line forces and steady state waves in anisotropic elastic solids (including the surface waves, Stonely waves, and waves in layered composites). The formalism is well-known in the physics and materials science community.

The advantages of Stroh's formalism are also widely recognized. Unlike the two-dimensional anisotropic solutions developed by Green and Zerna (1954) which are restricted to plane strain deformations and hence to monoclinic materials which posses a symmetry plane at $x_3 = 0$, the Stroh formalism can apply to general anisotropic elastic materials for which all three displacement components are necessarily coupled. Besides, unlike the Lekhnitskii's formalism (1950; 1957), which breaks down for orthotropic materials (Ting and Chou, 1982) and requires a special treatment (Wang and Choi, 1982), the Stroh formalism has no such restrictions. Note that the Lekhnitskii's formalism begins with the stresses and assumes that stresses depend only x_1 and x_2. It is thus a compliance-based formalism. By contrast, the Stroh formalism starts with the displacements and assumes that displacments depend only x_1 and x_2. Hence, it is a stiffness-based formalism. According to the Lekhnitskii formalism, the stress is expressed in terms of a pair of stress functions such that the equilibrium equations are satisfied identically, and through the

compatibility conditions a system of high order differential equations for the stress functions is derived to determine the solution. In the Stroh formalism the general solution is expressed with respect to the eigenvectors and analytic functions of complex variables, and the matrix identities derived from the eigen relations are useful in simplifying or interpreting the results.

Suo (1990) showed that these two formulations derived in very different ways are equivalent to each other. This was further taken for granted that Barnett and Kirchner (1997) gave a formal proof of the equivalence of the sextic equations in the two formalisms (Tarn, 2002). An excellent review on the Stroh formalism can be found in the paper of Chadwick and Smith (1977), see also Ting (1996; 2000). It should be noted that the Stroh formalism does not allow anti-plane deformations associated with extension, torsion and bending (Tarn, 2002).

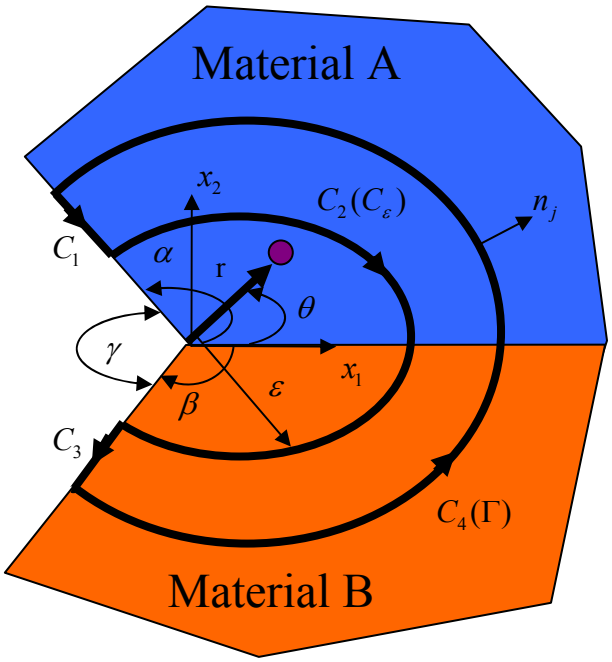

Fig. 13 Schematic plot of a closed integration contour around a general corner in dissimilar materials where $C = C_1 + C_2 + C_3 + C_4, C_2 = C_\varepsilon, C_4 = \Gamma$

The Stroh's formalism for anisotropic elasticity is outlined below. The first eigenvalue problem is set up and the method for solving six complex eigenvalues p_α is also presented here. In two-dimensional anisotropic elastostatics, the general displacements **u** in the material $M\,(M = A, B)$ around the interface corner can be expressed by

$$\mathbf{u} = \sum_{\alpha=1}^{3} \left[\mathbf{a}_\alpha f_\alpha(z_\alpha) + \overline{\mathbf{a}}_\alpha f_{\alpha+3}(\overline{z}_\alpha) \right] \tag{20}$$

As Stroh's formalism is based on the assumption that two-dimensional deformations $u_i\ (i = 1,\ 2,\ 3)$ depend only x_1 and x_2, a general solution for u_i depends on one composite variable that is linear combination of x_1 and x_2. Without loss of generality, we choose the coefficient of x_1 in the linear combination to be unity and $z_\alpha = x_1 + p_\alpha x_2$. Furthermore, f_α are arbitrary functions of the arguments z_α, where z_α is the complex variable. f_α depend on the geometry, radial distance from the interface corner and material elastic parameters. The six

complex eigenvalues p_α satisfy $p_{\alpha+3} = \overline{p}_\alpha$ and are the solutions of a quadratic eigenvalue problem (22).

Differentiating equation (20) twice with respect to x_1 and x_2, we get

$$\begin{aligned} u_{k,l} &= (\delta_{l1} + \delta_{l2} p) a_k f'(z) \\ u_{k,lj} &= (\delta_{l1} + \delta_{l2} p)(\delta_{j1} + \delta_{j2} p) a_k f''(z) \end{aligned} \tag{21}$$

The prime denotes differentiation with argument z and δ_{li} is the Kronecker delta. Insertion of (21) into the stress-strain law $\sigma_{ij} = C_{ijkl} u_{k,l}$ and then into the static equilibrium equations $\sigma_{ij,j} = 0$, results in the eigenvalue equations written in matrix form as:

$$\left\{ \mathbf{Q} + p(\mathbf{R} + \mathbf{R}^{\mathrm{T}}) + p^2 \mathbf{T} \right\} \mathbf{a} = \mathbf{0} \tag{22}$$

in which

$$Q_{ik} = C_{i1k1},\ R_{ik} = C_{i1k2},\ T_{ik} = C_{i2k2} \tag{23}$$

Equation (22) is the characteristic equation of anisotropic materials and p is the material eigenvalues of the anisotropic material. For a non-trivial solution of $\mathbf{a}$, the characteristic equation must be zero, i.e. $\det\left|\mathbf{Q} + p(\mathbf{R} + \mathbf{R}^{\mathrm{T}}) + p^2 \mathbf{T}\right| = 0$, which leads to six roots for the eigenvalue p. In matrix form and with Voigt's notation, we have

$$\mathbf{Q} = \begin{bmatrix} C_{11} & C_{16} & C_{15} \\ C_{16} & C_{66} & C_{56} \\ C_{15} & C_{56} & C_{55} \end{bmatrix},\ \mathbf{T} = \begin{bmatrix} C_{66} & C_{26} & C_{46} \\ C_{26} & C_{22} & C_{24} \\ C_{46} & C_{24} & C_{44} \end{bmatrix} \text{ and } \mathbf{R} = \begin{bmatrix} C_{16} & C_{12} & C_{14} \\ C_{66} & C_{26} & C_{46} \\ C_{56} & C_{25} & C_{45} \end{bmatrix} \tag{24}$$

$$\begin{bmatrix} C_{11} + 2pC_{16} + p^2 C_{66} & C_{16} + p(C_{12} + C_{66}) + p^2 C_{26} & C_{15} + p(C_{14} + C_{56}) + p^2 C_{46} \\ & C_{66} + 2pC_{26} + p^2 C_{22} & C_{56} + p(C_{46} + C_{25}) + p^2 C_{24} \\ \textit{symmetric} & & C_{55} + 2pC_{45} + p^2 C_{44} \end{bmatrix} \mathbf{a} = \mathbf{0} \tag{25}$$

In the special case of isotropic elasticity

$$\mathbf{Q} = \begin{bmatrix} \chi + 2\mu & 0 & 0 \\ 0 & \mu & 0 \\ 0 & 0 & \mu \end{bmatrix},\ \mathbf{T} = \begin{bmatrix} \mu & 0 & 0 \\ 0 & \chi + 2\mu & 0 \\ 0 & 0 & \mu \end{bmatrix},\ \mathbf{R} = \begin{bmatrix} 0 & \chi & 0 \\ \mu & 0 & 0 \\ 0 & 0 & 0 \end{bmatrix} \tag{26}$$

where the Lamé constants are denoted by $\chi = \dfrac{E\nu}{(1+\nu)(1-2\nu)}$ and $\mu = \dfrac{E}{2(1+\nu)}$ with E being Young's modulus and ν being Poisson's ratio.

Furthermore, the stress function $\boldsymbol{\phi}$ in the material $M\,(M = A, B)$ around the interface corner can be represented as

$$\boldsymbol{\phi} = \sum_{\alpha=1}^{3} \left[\mathbf{b}_\alpha f_\alpha(z_\alpha) + \overline{\mathbf{b}}_\alpha f_{\alpha+3}(\overline{z}_\alpha) \right] \tag{27}$$

In most applications the arbitrary functions f_α appearing in (20) and (27) are of the same functional form. We may then have

$$f_\alpha(z_\alpha) = f(z_\alpha) q_\alpha,\ f_{\alpha+3}(\overline{z}_\alpha) = \overline{f}(\overline{z}_\alpha) \overline{q}_\alpha, \text{ where } \alpha = 1, 2, 3 \tag{28}$$

q_α are arbitrary complex constants. The second equation of (28) helps to obtain the real form solutions for $\mathbf{u}$ and $\boldsymbol{\phi}$. Equations (20) and (27) can thus be written as

$$\mathbf{u} = 2\,\mathrm{Re}\left\{ \mathbf{A} \left\langle f(z_*) \right\rangle \mathbf{q} \right\} \tag{29}$$

$$\boldsymbol{\phi} = 2\,\mathrm{Re}\left\{\mathbf{B}\left\langle f\left(z_*\right)\right\rangle \mathbf{q}\right\} \tag{30}$$

where Re stands for the real part, **A** and **B** are 3 × 3 complex matrices defined by

$$\mathbf{A} = [\mathbf{a}_1,\ \mathbf{a}_2,\ \mathbf{a}_3],\ \mathbf{B} = [\mathbf{b}_1,\ \mathbf{b}_2,\ \mathbf{b}_3] \tag{31}$$

and $\left\langle f\left(z_*\right)\right\rangle$ is the diagonal matrix

$$\left\langle f\left(z_*\right)\right\rangle = \mathrm{diag}\left[f\left(z_1\right), f\left(z_2\right), f\left(z_3\right)\right] \tag{32}$$

The stresses can be further expressed in accordance with the stress function $\boldsymbol{\phi}$ as

$$\mathbf{t} = \frac{d}{dr}\boldsymbol{\phi} \quad \text{or} \quad \sigma_{k1} = -\frac{\partial \varphi_k}{\partial x_2} = -pb_k f'\left(z\right),\ \sigma_{k2} = \frac{\partial \varphi_k}{\partial x_1} = b_k f'\left(z\right) \tag{33}$$

Inserting Eq. $(21)_1$ into the constitutive equation $\sigma_{ij} = C_{ijkl}u_{k,l}$ and then making use of Eq. (23), we get σ_{ij} :

$$\begin{aligned} \sigma_{i1} &= \left(Q_{ik} + pR_{ik}\right)a_k f'\left(z\right) \\ \sigma_{i2} &= \left(R_{ki} + pT_{ik}\right)a_k f'\left(z\right) \end{aligned} \tag{34}$$

Comparing Eq. (33) with Eq. (34), the relation between **a** and **b** yields:

$$\mathbf{b} = \left(\mathbf{R}^{\mathrm{T}} + p\mathbf{T}\right)\mathbf{a} = -\frac{1}{p}\left(\mathbf{Q} + p\mathbf{R}\right)\mathbf{a} \tag{35}$$

This equation distinguishes the Stroh formalism from others in that the vectors $\mathbf{a}_\alpha$ and $\mathbf{b}_\alpha$ for different α are related. Note that **a** and **b** are termed as the Stroh eigenvectors, satisfying $\mathbf{a}_{\alpha+3} = \overline{\mathbf{a}}_\alpha$ and $\mathbf{b}_{\alpha+3} = \overline{\mathbf{b}}_\alpha$, related through the matrices **Q**, **R** and **T** described in Eq. (24). Without loss of generality, the imaginary part of p_α is taken to be positive. Overbars of p_α, z_α, **a**, **b** denote the complex conjugates.

With this, the above quadratic eigenvalue problem can be recast as a conventional six-dimensional linear eigenvalue problem

$$\begin{aligned} &\begin{bmatrix} \mathbf{N}_1 & \mathbf{N}_2 \\ \mathbf{N}_3 & \mathbf{N}_1^T \end{bmatrix}\begin{Bmatrix} \mathbf{a} \\ \mathbf{b} \end{Bmatrix} = p\begin{Bmatrix} \mathbf{a} \\ \mathbf{b} \end{Bmatrix} \\ &\Rightarrow \mathbf{N}\boldsymbol{\eta} = p\boldsymbol{\eta},\ \ \boldsymbol{\eta} = \begin{Bmatrix} \mathbf{a} \\ \mathbf{b} \end{Bmatrix} \end{aligned} \tag{36}$$

In the above, $\mathbf{N}_1 = -\mathbf{T}^{-1}\mathbf{R}^{\mathrm{T}}$, $\mathbf{N}_2 = \mathbf{T}^{-1}$ and $\mathbf{N}_3 = -\mathbf{Q} + \mathbf{R}\mathbf{T}^{-1}\mathbf{R}^{\mathrm{T}}$. Until now, the first eigenvalue problem is solved by using the characteristic equation (36) for the complex eigenvalue p. Note that $\mathbf{N}_2$ and $\mathbf{N}_3$ are symmetric and that $\mathbf{N}_2$ is positive definite and $-\mathbf{N}_3$ is positive semi-definite. The 6 × 6 matrix **N** is the fundamental elasticity matrix first introduced by Ingebrigtsen and Tonning (1969). It should be also noted that $\mathbf{N}_3$ has the dimensions of stress, $\mathbf{N}_2$ has the dimension of compliance and $\mathbf{N}_1$ is dimensionless. Eshelby et al. (1953) stated that since p cannot be real if the strain energy is to be positive, we have three pairs of complex conjugates for p as well as for $\boldsymbol{\eta}$. If p_α and $\boldsymbol{\eta}_\alpha\left(\alpha = 1, 2, \cdots, 6\right)$ are the eigenvalues and eigenvectors, we let

$$\left.\begin{aligned} p_{\alpha+3} &= \overline{p}_\alpha,\ \ \mathrm{Im}\, p_\alpha > 0 \\ \boldsymbol{\eta}_{\alpha+3} &= \overline{\boldsymbol{\eta}}_\alpha \end{aligned}\right\}\ \alpha = 1, 2, 3 \tag{37}$$

where Im denotes the imaginary part.

The Stroh eigenvectors are determined up to an arbitrary constant. They are normalized as

$$\mathbf{a}_\alpha = \frac{\hat{\mathbf{a}}_\alpha}{\sqrt{2\hat{\mathbf{a}}_\alpha^{\mathrm{T}}\hat{\mathbf{b}}_\alpha}} \text{ and } \mathbf{b}_\alpha = \frac{\hat{\mathbf{b}}_\alpha}{\sqrt{2\hat{\mathbf{a}}_\alpha^{\mathrm{T}}\hat{\mathbf{b}}_\alpha}},\ \alpha = 1,2,3 \tag{38}$$

in which $\hat{\mathbf{a}}_\alpha$ and $\hat{\mathbf{b}}_\alpha$ are the non-normalized eigenvectors, i.e. those that would be produced by a standard eigensolver.

The physical meanings of p**, a, b** have been explored by Ting (1996). Since the eigenvalues p_α and the eigenvectors $\mathbf{a}_\alpha$ and $\mathbf{b}_\alpha$ depend only on the elastic stiffnesses C_{ijkl}, they can be regarded as material constants in despite of their complex values. For general anisotropic elastic materials, there are three polarization planes (the planes $\mathbf{a_1}$, $\mathbf{a_2}$, $\mathbf{a_3}$) for the displacement **u** and three polarization planes (the planes $\mathbf{b_1}$, $\mathbf{b_2}$, $\mathbf{b_3}$) for the surface traction **t**. The displacement associated with $\mathbf{a_3}$ is the anti-plane displacement and the stresses associated with $\mathbf{b}_3$ are the anti-plane stresses. Additionally, the displacement associated with $\mathbf{a_1}$, $\mathbf{a_2}$ is the in-plane displacement and the stresses associated with $\mathbf{b_1}$, $\mathbf{b_2}$ are the in-plane stresses. Although no physical meanings for the complex eigenvalues p_α have been found, it is shown that p_α are solely responsible for the locations of the image singularities for Green's functions for half-spaces, bi-materials, and elliptic inclusions.

3.4 Asymptotic analysis

Asymptotic analysis of the singular stress field at the vertex of re-entrant corners involves two eigenvalue problems. One is material related as stated in Sec 3.3, the other is geometry related, as presented in this section.

It is well known from Williams (1952) that the eigen-equation in a notched/cracked body for an isotropic material (i.e. $\alpha = \beta$ in Fig. 13) can be represented by Eq. (39) where plus sign and minus sign are associated with the opening mode (mode I) and sliding mode (mode II), respectively

$$\lambda \sin(2\pi - \gamma) \pm \sin(\lambda(2\pi - \gamma)) = 0 \tag{39}$$

The stress singularity depends only on the notch angle γ regardless of material. For a crack, $\alpha = \beta = \pi$, Eq. (39) simplifies to $\sin 2\pi\lambda^{\mathrm{I}} = \sin 2\pi\lambda^{\mathrm{II}} = 0$ and the stress singularity is $-½$; for a free edge, $\alpha = \beta = \pi/2$, the stress singularity disappears.

Furthermore, the characteristic equation of the stress singularity for a general re-entrant corner bonding two dissimilar isotropic materials with two arbitrarily oriented traction free surfaces at $\theta = \alpha$ and $\theta = -\beta$ is expressed by Carpenter (1984a)

$$\det \begin{vmatrix} \cos(2\lambda\beta) - \cos(2\lambda\alpha) & -\sin(2\lambda\beta) - \sin(2\lambda\alpha) \\ \quad + \lambda\cos(2\beta) - \lambda\cos(2\alpha) & \quad + \lambda\sin(2\beta) + \lambda\sin(2\alpha) \\ \text{----------} & \text{----------} \\ \sin(2\lambda\beta) + \sin(2\lambda\alpha) & \cos(2\lambda\beta) - \cos(2\lambda\alpha) \\ \quad + \lambda\sin(2\beta) + \lambda\sin(2\alpha) & \quad - \lambda\cos(2\beta) + \lambda\cos(2\alpha) \end{vmatrix} = 0 \tag{40}$$

For a general anisotropic bi-material system, the formalisms to solve λ are briefly and explicitly presented below. Meanwhile, the singular stress fields around the notch tip are also

shown. Recall the displacement and the stress functions near a sharp notch in an anisotropic solid expressed in Eqs. (20) and (27), note that $f_\alpha(z_\alpha)$ is the arbitrary function of z_α and often have the form of z_α^λ. As suggested by Ting (1996; 1997), Labossiere and Dunn (1999), we choose $f(z_\alpha)$ as

$$f_\alpha(z_\alpha)=\frac{1}{\lambda}z_\alpha^\lambda q_\alpha \quad \text{and} \quad f_{\alpha+3}(\bar{z}_\alpha)=\frac{1}{\lambda}\bar{z}_\alpha^\lambda h_\alpha \tag{41}$$

where q_α and h_α are the unknown complex constants and will be determined by Eq. (46) once λ is obtained. Using the expression $z_\alpha = x_1 + p_\alpha x_2 = r\xi_\alpha(\theta) = r(\cos\theta + p_\alpha \sin\theta)$, the displacements and tractions in a plane polar coordinate system originated at the notch tip are derived

$$\begin{aligned}\mathbf{u}^M &= \frac{1}{\lambda}r^\lambda \sum_{\alpha=1}^{3}\left[\xi_\alpha^M(\theta)^\lambda \mathbf{a}_\alpha q_\alpha + \bar{\xi}_\alpha^M(\theta)^\lambda \bar{\mathbf{a}}_\alpha h_\alpha\right]\\ \mathbf{t}^M &= \frac{\lambda}{r}\boldsymbol{\phi} = r^{\lambda-1}\sum_{\alpha=1}^{3}\left[\xi_\alpha^M(\theta)^\lambda \mathbf{b}_\alpha q_\alpha + \bar{\xi}_\alpha^M(\theta)^\lambda \bar{\mathbf{b}}_\alpha h_\alpha\right]\end{aligned} \tag{42}$$

where superscript M indicates material A or B. The second eigenvalue problem can be solved using the boundary conditions for the interface notch problem, see Fig. 13.

The traction-free boundary conditions on the notch flanks ($\theta=\alpha,\ \theta=-\beta$) and the continuity conditions of the stresses and displacements along the interface ($\theta=0$) result in the following boundary condition equations

$$\mathbf{t}^A(\alpha)=0,\ \mathbf{t}^B(-\beta)=0,\ \mathbf{t}^A(0)=\mathbf{t}^B(0),\ \mathbf{u}^A(0)=\mathbf{u}^B(0) \tag{43}$$

Substituting Eq. (42) into Eq. (43), a group of 12 linear equations in the 12 unknown coefficients q_α^M, h_α^M $(M=A,B;\alpha=1,2,3)$ is deduced.

$$\begin{aligned}&\sum_{\alpha=1}^{3}\xi_\alpha^A(\alpha)^\lambda \mathbf{b}_\alpha^A q_\alpha^A + \sum_{\alpha=1}^{3}\bar{\xi}_\alpha^A(\alpha)^\lambda \bar{\mathbf{b}}_\alpha^A h_\alpha^A = 0\\ &\sum_{\alpha=1}^{3}\xi_\alpha^B(-\beta)^\lambda \mathbf{b}_\alpha^B q_\alpha^B + \sum_{\alpha=1}^{3}\bar{\xi}_\alpha^B(-\beta)^\lambda \bar{\mathbf{b}}_\alpha^B h_\alpha^B = 0\\ &\sum_{\alpha=1}^{3}\xi_\alpha^A(0)^\lambda \mathbf{b}_\alpha^A q_\alpha^A + \sum_{\alpha=1}^{3}\bar{\xi}_\alpha^A(0)^\lambda \bar{\mathbf{b}}_\alpha^A h_\alpha^A - \sum_{\alpha=1}^{3}\xi_\alpha^B(0)^\lambda \mathbf{b}_\alpha^B q_\alpha^B - \sum_{\alpha=1}^{3}\bar{\xi}_\alpha^B(0)^\lambda \bar{\mathbf{b}}_\alpha^B h_\alpha^B = 0\\ &\sum_{\alpha=1}^{3}\xi_\alpha^A(0)^\lambda \mathbf{a}_\alpha^A q_\alpha^A + \sum_{\alpha=1}^{3}\bar{\xi}_\alpha^A(0)^\lambda \bar{\mathbf{a}}_\alpha^A h_\alpha^A - \sum_{\alpha=1}^{3}\xi_\alpha^B(0)^\lambda \mathbf{a}_\alpha^B q_\alpha^B - \sum_{\alpha=1}^{3}\bar{\xi}_\alpha^B(0)^\lambda \bar{\mathbf{a}}_\alpha^B h_\alpha^B = 0\end{aligned} \tag{44}$$

Using Eq. $(44)_1$ and $(44)_2$, we can express $\mathbf{h}^A$ in terms of $\mathbf{q}^A$ and $\mathbf{q}^B$ in terms of $\mathbf{h}^B$, respectively. A non-trivial solution exists only if the determinant of the coefficient matrix vanishes. This occurs when the eigenvalue, λ, satisfies the following equation which is dependent on the stiffness matrix, C_{ijkl}:

$$\begin{bmatrix}\mathbf{b}^A\left(\mathbf{B}^A\right)^{-1} - \bar{\mathbf{b}}^A\left(\bar{\mathbf{B}}^A\right)^{-1} & \left(\mathbf{b}^B\left(\mathbf{B}^B\right)^{-1} - \bar{\mathbf{b}}^B\left(\bar{\mathbf{B}}^B\right)^{-1}\right)\\ \mathbf{a}^A\left(\mathbf{B}^A\right)^{-1} - \bar{\mathbf{a}}^A\left(\bar{\mathbf{B}}^A\right)^{-1} & \left(\mathbf{a}^B\left(\mathbf{B}^B\right)^{-1} - \bar{\mathbf{a}}^B\left(\bar{\mathbf{B}}^B\right)^{-1}\right)\end{bmatrix}\begin{Bmatrix}\mathbf{B}^A\mathbf{q}^A\\ \bar{\mathbf{B}}^B\mathbf{h}^B\end{Bmatrix} = \mathbf{0} \tag{45}$$

which results in six simultaneous eigenvalue equations with six unknowns q_α^A, h_α^B $(\alpha=1,2,3)$

$$\mathbf{K}(\lambda)\ \ \mathbf{D}(\lambda)=\mathbf{0},\ \ \det\mathbf{K}(\lambda)=0 \tag{46}$$

In the above equations, $\mathbf{a}^M = \left[\mathbf{a}_1^M, \mathbf{a}_2^M, \mathbf{a}_3^M\right]$, $\mathbf{b}^M = \left[\mathbf{b}_1^M, \mathbf{b}_2^M, \mathbf{b}_3^M\right]$, $\mathbf{B}^A = \left[\xi_1^A(\alpha)^\lambda \mathbf{b}_1^A,\ \xi_2^A(\alpha)^\lambda \mathbf{b}_2^A,\ \xi_3^A(\alpha)^\lambda \mathbf{b}_3^A\right]$, $\mathbf{B}^B = \left[\xi_1^B(-\beta)^\lambda \mathbf{b}_1^B,\ \xi_2^B(-\beta)^\lambda \mathbf{b}_2^B,\ \xi_3^B(-\beta)^\lambda \mathbf{b}_3^B\right]$, $\mathbf{D} = \left[\mathbf{B}^A\mathbf{q}^A,\ \overline{\mathbf{B}}^B\mathbf{h}^B\right]^{\mathrm{T}}$, $\mathbf{q}^M = \left[q_1^M, q_2^M, q_3^M\right]^{\mathrm{T}}$, $\mathbf{h}^M = \left[h_1^M, h_2^M, h_3^M\right]^{\mathrm{T}}$ $(M = A, B)$

When the in-plane and anti-plane deformation are decoupled, the equation (44) can be rewritten in matrix notation as:

$$\begin{aligned} \boldsymbol{\kappa}^{\mathrm{IP}}\mathbf{q}^{\mathrm{IP}} &= \mathbf{O}^{\mathrm{IP}} \\ \boldsymbol{\kappa}^{\mathrm{AP}}\mathbf{q}^{\mathrm{AP}} &= \mathbf{O}^{\mathrm{AP}} \end{aligned} \tag{47}$$

where $\mathbf{q}^{\mathrm{IP}} = \left[q_1\ q_2\ h_1\ h_2\right]^{\mathrm{T}}$, $\mathbf{q}^{\mathrm{AP}} = \left[q_3\ h_3\right]^{\mathrm{T}}$, the matrix $\mathbf{O}^{\mathrm{IP}}$ is a 4×1 null matrix, and $\mathbf{O}^{\mathrm{AP}}$ is a 2×1 null matrix. The superscript IP denotes in-plane terms, and AP denotes anti-plane terms.

Equation (47) is the characteristic equation for the eigenvalues λ of the anisotropic notched body. The values of λ can be obtained by solving the roots of the determinant of $\boldsymbol{\kappa}^{\mathrm{IP}}$ or $\boldsymbol{\kappa}^{\mathrm{AP}}$. Once the value of λ has been computed from the characteristic equation (46) or (47), the eigenvectors **q, h** can only be solved up to an arbitrary constant multiplier. Then the stress intensity factor for a sharp notch, wedge corner or a crack, can be computed using the path independent H-integral approach (e.g., Labossiere and Dunn, 1999; Shang et al., 2008; 2009). If the real part of λ is smaller than one, then the stress field near $r = 0$ has generally the $r^{\lambda-1}$ type singularity. Eigenvalues are thus called singular eigenvalues. The roots of the characteristic equation with the real parts smaller or equal to zero are ignored since the associated eigensolution requires infinite strain energy (Yin, 1999). In the particular case of a crack ($\gamma = 0$) with an isotropic or anisotropic homogeneous material, the well-known result, $\lambda = ½$ is obtained. In the case of an edge notch $(\gamma = \pi, \alpha = \pi/2)$ with a homogeneous isotropic or anisotropic material, $\lambda = 1$ is yielded and the stress singularity disappears.

CHAPTER 4

Notch Mechanics and Fracture Mechanics

Why should we use notch mechanics to solve the crack intiation problem for an interface corner? Because traditional failure theories for brittle materials are inapplicable to notch problem. Strength theories are not appropriate as the elastic fields at the interface corner often exhibit singular behavior, similar to the stress field ahead of a crack. Both classical fracture mechanics approaches and interface fracture mechanics, are not applicable since no precrack exists in a notched body.

Note that K_m is used herein to indicate the stress intensity factor in classical fracture mechanics, while K_m^n is the intensity of notch stress field with respect to eigenvalues $\lambda_m \ (m=1,2,\cdots N)$ where N is the number of eigenvalues available from the characteristic equation. K_m^n are functions of the thermomechanical loading, material properties and the geometry.

The general configuration for a notch/wedge/crack geometry in dissimilar anisotropic materials is addressed here, see Fig. 13. Such a situation usually induces mixed-mode deformations and the stress fields are no longer symmetric and/or anti-symmetric. The stresses and displacements in the vicinity of the interface corner are often obtained using complex variable methods or the Airy's stress function approach. Using either of these methods, the asymptotic fields near the interface corner can be expressed as

$$\begin{aligned} \sigma_{ij}^M &= \sum_{m=1}^{N} K_m^n r^{\lambda_m - 1} f_{ij}^{mM}(\theta, \lambda_m) + \sigma_{ij0}^M(\theta) \\ u_i^M &= \sum_{m=1}^{N} K_m^n r^{\lambda_m} g_i^{mM}(\theta, \lambda_m) + u_{i0}^M(\theta) \end{aligned} \tag{48}$$

where $\lambda_m \ (m=1,2,\cdots N)$ are the eigenvalues of the problem. Superscript M indicates material A or B which is elastic, homogeneous, isotropic or anisotropic. $\sigma_{ij0}^M(\theta)$ denotes the constant stress field ($\mathrm{Re}(\lambda_m)=1$) independent of the radial distance from the notch corner and $u_{i0}^M(\theta)$ is the associated displacement field near the interface corner. These constant terms which can be determined analytically, are finite for thermal loading and/or surface tractions on the notch flanks but vanish for remote mechanical loading. Besides, the remaining stress term is comprised of

several stress fields of the form $K_m^n r^{\lambda_m - 1}$. When two or more stress fields of the form $K_m^n r^{\lambda_m - 1}$ exist near the notch corner, one pair of K_m^n and $\lambda_m - 1$ describes one stress field, and the total stresses are determined by superposing contributions from all the stress fields. There are an infinite number of values λ_m which satisfy the eigenvalue equations. Both the stress intensity factor and the stress singularity may be real positive, real negative or complex, but in most circumstances, they are real constants (e.g., Banks-Sills and Sherer, 2002; Qian and Akisanya, 1999a). Although not explicitly shown in Eq. (48), there are certain special combinations of elastic properties and notch angles that can also generate logarithmic singularities, as described in Sec 4.2.1. In this study, the power-logarithmic singularity is not considered. Moreover, only positive λ_m are admissible in order to ensure finite displacements at the notch tip. $f_{ij}^{mM}\left(\theta, \lambda_m\right)$ is a function describing the angular profile of the stress field in conjunction with material elastic properties and the opening angle. Note that $f_{ij}^{mM}\left(\theta, \lambda_m\right)$ is non-dimensional but $g_i^{mM}\left(\theta, \lambda_m\right)$ has the unit of $(\text{length})^2(\text{force})^{-1}$. They are determined analytically while the eigenvalues $\lambda_m \left(m = 1, 2, \cdots, N\right)$ for a given notch geometry are obtained by solving a characteristic equation. The closed-form expression for these functions will be briefly described below. More details can be found in references such as Stroh (1958); Ting (1996); Labossiere and Dunn (1999); and Shang et al. (2008; 2009).

Consider a linear elastic body with a re-entrant corner subjected to remote in-plane mechanical loading, see Fig. 13. Without loss of generality, we focus on two singular terms, i.e. $0 < \lambda_1 \le \lambda_2 < 1$, considering the higher order terms ($\lambda_m > 1$) to be insignificant. The singular stress and displacement field around the notch tip can be reduced as follows:

$$\begin{aligned} \sigma_{ij}^M(r,\theta) &= K_1^n r^{\lambda_1 - 1} f_{ij}^{1M}\left(\theta, \lambda_1\right) + K_2^n r^{\lambda_2 - 1} f_{ij}^{2M}\left(\theta, \lambda_2\right) \\ u_i^M(r,\theta) &= K_1^n r^{\lambda_1} g_i^{1M}\left(\theta, \lambda_1\right) + K_2^n r^{\lambda_2} g_i^{2M}\left(\theta, \lambda_2\right) \end{aligned} \tag{49}$$

r and θ are the polar coordinates with an origin at the notch tip. For the homogeneous isotropic case, $\lambda_1 = \lambda_2 = ½$, corresponding to the definition by Williams (1952) and Hong and Stern (1978).

4.1. Classical fracture mechanics

It is well known that the stress fields near the tip of a crack in a linear elastic material exhibit a square-root singularity. The amplitudes of the singular stress fields are characterized by the stress intensity factors K_m (SIFs). In linear elastic fracture mechanics, the SIFs are usually used as the quantitative parameters describing the amplitude of singular stress fields for elastic cracked bodies.

Analytical solutions of SIFs are limited to a few idealized cases. For practical problems involving finite geometries and complex loadings, numerical methods such as finite element methods or boundary element methods must be employed to extract the SIFs. Alternatively, SIFs can be calculated by the path-independent *J*-integral, proposed by Rice (1968). With this, the data far from the crack tip are used and higher accuracy can be achieved. Nevertheless, the *J*-integral approach is not applicable for mixed-mode problems since the integral value gives only the sum of SIFs. Instead, an energy method via the path-independent contour integrals can be utilized to obtain SIF corresponding to each fracture mode. By using this method, the interaction energy between the elastic state of interest and an auxiliary state is examined and the appropriate auxiliary states should be chosen. The concept of this method was discussed by Chen and Shield (1977).

Stern et al. (1976) and Yau et al. (1980) have applied this approach for isotropic homogeneous materials. Hong and Stern (1978) and Sih and Asaro (1988) have also used the method for interfacial crack problems with isotropic bi-materials. In the works of Stern et al. (1976) and Hong and Stern (1978), Betti's reciprocal work theorem was used to obtain SIFs by integrating displacements and tractions in the problem of interest and those in the particular auxiliary fields. Yau et al. (1980) and Sih and Asaro (1988) gave line integrals for SIFs based on the interaction energy release rate. Sih and Asaro (1988) have employed the singular fields for isotropic bi-material interfacial cracks as the auxiliary state in their analysis. Both types of integrals are limited to contours enclosing only one crack tip. Wu (1989) further derived path-independent integrals for a crack in a homogeneous anisotropic medium. The basic concept used in Wu (1989) is that the energy release rate associated with a crack tip is a quadratic in SIFs which characterize the square-root singular stress field at the crack tip. In addition, the new integrals are utilized to determine the stress intensity factors due to a body force and a dislocation for a finite crack in an infinite anisotropic body.

4.2. Notch mechanics

The presence of V-notches in an elastic body may induce stress singularities at the tips within the context of small strain elasticity theory. Fracture is often initiated in the highly-stressed regions near the notch tips. It is thus important to determine the near-tip fields accurately to assess the reliability and integrity of notched body. With given notch angle and materials, and boundary conditions on the notch faces, the structure of the singular fields can be determined by asymptotic analysis to within multiplicative constants (Ting and Chou, 1981; Wu and Chang, 1993). The complete singular stress field is derived by Wu and Chang (1993) for an infinite wedge in the presence of body forces or dislocations. For bodies with finite dimensions, for which analytic solutions are generally not available, near-tip stresses can only be determined by numerical methods.

Due to the singular nature of the stress field, i.e., the stress approaches infinity near the notch tip, it is usually difficult to accurately compute stresses near notch tips using regular boundary element or finite element methods. Several techniques have been proposed to overcome the difficulty. For example, eigenfunction expansion method (Gross and Mendelson, 1972), path-independent integral in the case of a crack (Wu, 1989), a combination of eigenfunction expansion method and standard boundary element method treated for isotropic plates (Barone and Robinson, 1972), and a combination of eigenfunction expansion method and boundary integral equation (Wu and Chen, 1996) extended to anisotropic notched bodies and traction problems. Complete fields near the tip of a V-notch in an anisotropic body are also derived in (Wu and Chen, 1996).

4.2.1. Eigenvalue λ describing the order of the notch tip stress singularity

Note that λ may be real or complex, depending upon the relative elastic properties of the materials, the wedge angles as well as the edge loads. The eigen-equation may yield an infinite number of possible solutions for the eigenvalue λ. Only positive solutions are admissible in order to ensure finite displacements, i.e., $\lambda \geq 0$. Since we are concerned with the singular stress field surrounding the notch tip, then in the limit as $r \to 0$, the dominant stress field terms come from $\lambda < 1$.

Certain situations yield stress singularities of the form $O(r^{-\lambda}\ln r)$ as $r \to 0$. Power-logarithmic singularities have been extensively reviewed in (Song, 2005). When the eigenvalues change from real to complex at some opening angles of a composite material wedge, multiple eigenvalues corresponding to the same independent eigenfunction may occur. The power series solution breaks down at these critical angles and exhibits very low numerical accuracy for a specific range of opening angles around the critical values. The analytical solution of such a special case includes terms with not only power functions but also logarithmic functions of the radial coordinate. The power-logarithmic stress singularities have been identified by Dempsey and Sinclair (1979; 1981) for multi-material wedges subjected to homogeneous boundary conditions on the surfaces forming the wedge vertex. Dempsey (1995) examined the eigenvalues in the asymptotic solutions for isotropic composite wedges under homogeneous boundary conditions. It has been pointed out that the power-logarithmic function is more singular than the power function at the vertex and particular cases in which the logarithmic singularities occur are identified. Also, Pageau et al. (1996) have investigated the power-logarithmic stress singularities. Joseph and Zhang (1998) have reviewed the studies on power-logarithmic stress singularities for multiple material wedge. Angular variations of the displacement and stress fields are presented in (Joseph and Zhang, 1998; Gadi et al., 2000) for wedges comprised of isotropic materials. Conditions for such behavior are described by Ting (1996) for anisotropic bimaterials. Bogy and Wang (1971) determined how the order of the singularity in the stress field at the corner depends on the material constants and corner angle for two materially dissimilar isotropic, homogeneous, elastic wedges. Furthermore, additional logarithmic singularities can be induced by inhomogeneous boundary conditions on the surfaces forming the wedge vertex and by body forces (Timoshenko and Goodier, 1970; Chen, 1996). A related problem is a wedge under a concentrated couple studied by Sternberg and Koiter (1958). Dempsey (1981) obtained a solution including a power-logarithmic stress term for a single material wedge at its critical angle. The solution, however, can still be very large at an angle very close to the critical value. Ting (1985) has provided a continuous solution as the vertex angle passes to the critical angle. Sinclair (1998; 1999a; 1999b) has extended Ting's (1985) technique to solve several commonly occurred cases in single material wedges. Gadi et al. (2000) have investigated the thermally induced stresses in a composite wedge and presented cases with triple eigenvalues, which results in the square of the logarithmic function of the radial coordinate. These analytical methods require the determination of the critical angles as the first step of an analysis.

4.2.2. H-integral approach

The H-integral approach, as a tool to derive stress intensity factors for notches and cracks, is based on a combination of finite element results, Betti's law, and asymptotic analysis with a complementary field. This approach gains its popularity by the fact of avoiding time-consuming mesh refinement near the singularity, easy performance of parametric analyses and excellent numerous accuracy.

First of all, we will briefly introduce Betti's reciprocal law (Sokolnikoff, 1956). If you have a linear elastic body in equilibrium subject to two different sets of forces with corresponding displacements, we will get the following equation called Betti's law, see Fig. 14.

$$\sum^{n} F_i^* u_i = \sum^{n} F_i \, u_i^* \tag{50}$$

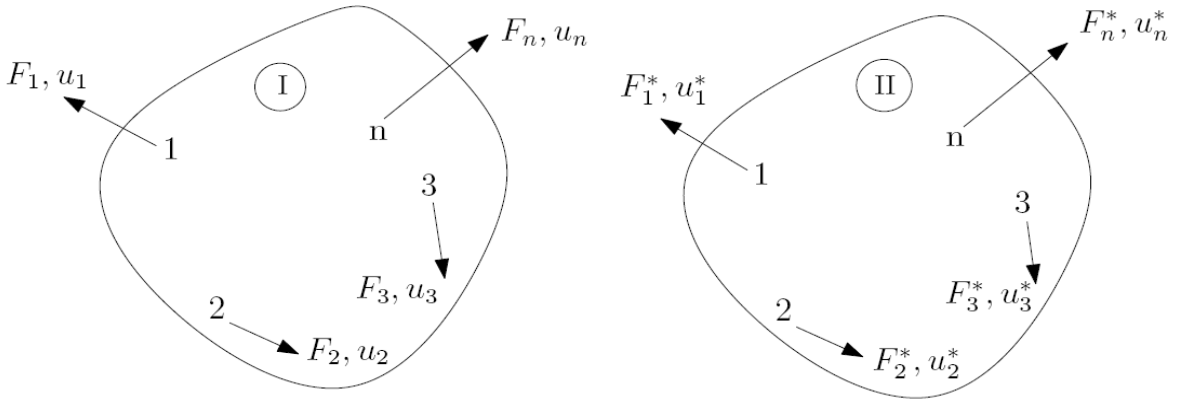

Fig. 14 Two systems in Betti's law

If we apply the Betti's law to the linear elastic planar notched body particularly with closed contour $C = C_1 + C_2 + C_3 + C_4$ around a re-entrant corner excluding the stress singularity in a planar linear elastic body, as shown in Fig. 15, and two systems are replaced with two fields: actual field and complementary field (singular field), the Betti's reciprocal law in the absence of any body force can be stated as

$$\oint_C \left(\sigma_{ij} u_i^* - \sigma_{ij}^* u_i \right) n_j ds = 0 \quad where \; C = C_1 + C_2 + C_3 + C_4 \tag{51}$$

and where $(i, j) = (r, \theta)$ are the plane polar coordinates centered at the interface corner, n_j is the outward unit normal to the counterclockwise closed contour C, ds is an infinitesimal line segment of C. σ_{ij}, u_i are the notch corner stress and displacement fields in terms of eigenvalue $\lambda_m (\lambda_m \neq 1)$ and stress intensity factor K_m^n. σ_{ij}^*, u_i^* are complementary singular stresses and displacements satisfying the same boundary conditions as (σ_{ij}, u_i) but with respect to an associated eigenvalue λ_m^* and stress intensity factor K_m^{n*}. Note that the employed complementary field has no physical significance here.

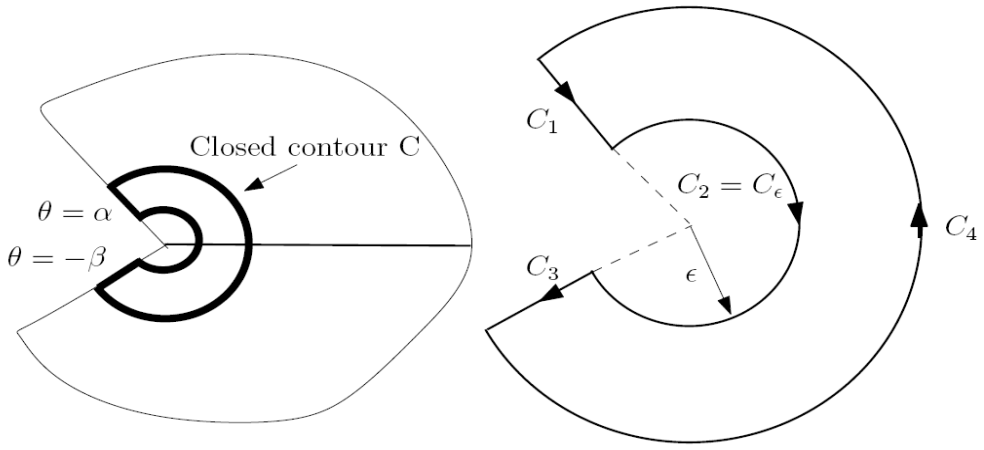

Fig. 15. Illustration of the closed contour around a re-entrant corner

Szabo and Babuska (1988) and Wu and Chang (1993) showed that if λ_m is an eigenvalue for the given material properties and notch geometry, $\lambda_m^* = -\lambda_m$ is also the eigenvalue for the same problem. Hence, the near-tip stress and displacement fields corresponding to the eigenvalue λ_m^* can be taken as the complementary fields. According to Eq. (49), they are described by

$$\begin{aligned}\sigma_{ij}^{M^*}(r,\theta) &= K_1^{n^*} r^{-\lambda_1 - 1} f_{ij}^{1M^*}\left(\theta, -\lambda_1\right) + K_2^{n^*} r^{-\lambda_2 - 1} f_{ij}^{2M^*}\left(\theta, -\lambda_2\right) \\ u_i^{M^*}(r,\theta) &= K_1^{n^*} r^{-\lambda_1} g_i^{1M^*}\left(\theta, -\lambda_1\right) + K_2^{n^*} r^{-\lambda_2} g_i^{2M^*}\left(\theta, -\lambda_2\right)\end{aligned} \tag{52}$$

Since the integration in (51) vanishes along the traction free surfaces C_1 and C_3 . i.e., $\sigma_{ij} n_j = \sigma_{ij}^* n_j = 0$, see Fig. 13, it reduces to

$$-\int_{C_2} \left(\sigma_{ij} u_i^* - \sigma_{ij}^* u_i\right) n_j ds = \int_{C_4} \left(\sigma_{ij} u_i^* - \sigma_{ij}^* u_i\right) n_j ds \tag{53}$$

On the left-hand side of Eq. (53), the contour integral is simplified to either one coefficient proportional to the stress intensity factor or a linear combination of K_1^n and K_2^n for an arbitrarily small radius ε (Stern and Soni, 1976b)

$$I_\varepsilon = -\int_{C_2} \left(\sigma_{ij} u_i^* - \sigma_{ij}^* u_i\right) n_j ds = e_1 K_1^n + e_2 K_2^n \tag{54}$$

where e_1 , e_2 are constants. The unstarred stresses and displacements along C_2 were taken from the asymptotic analysis, Eq. (49), while the starred stresses and displacements were employed from the complementary singular field, Eq. (52).

Accordingly, only the outer contour C_4 is involved in the numerical integration for determining the desired stress intensity factors. The H-integral is defined as

$$H = \int_{C_4} \left(\sigma_{ij} u_i^* - \sigma_{ij}^* u_i\right) n_j ds = \int_{\Gamma} \left(\sigma_{ij} u_i^* - \sigma_{ij}^* u_i\right) n_j ds \tag{55}$$

and in polar coordinates, the above equation becomes

$$H = \int_{-\beta}^{\alpha} \left(\sigma_{rr} u_r^* + \sigma_{r\theta} u_\theta^* - \sigma_{rr}^* u_r - \sigma_{r\theta}^* u_\theta\right) r d\theta \tag{56}$$

In Eq. (55), Γ can be any contour within the planar linear elastic body commencing on the lower notch flank and terminating on the upper. The unstarred fields (σ_{ij}, u_i) are obtained from the finite element calculations while the starred fields (σ_{ij}^*, u_i^*) are taken from the complementary singular field satisfying the same boundary conditions as those for (σ_{ij}, u_i). Sinclair (1985) also presents how the integral (54) yields the mode I intensity factor for a mixed-mode problem in an isotropic material. This is basically because the complementary fields in the mode I integral are symmetric so that when they are multiplied by any anti-symmetric fields, including the singular mode II field, then integrated, no contribution results, i. e., the only nontrivial contributions to H_I must come from the symmetric part of σ_{ij} , u_i . Analogously, H_{II} may be shown to pick off only K_{II} in mixed-mode problems.

For a general corner (Fig. 13), we can define the respective stress intensity factors by

$$K_1^n = \lim_{\theta=0, r\to 0} \frac{\sigma_{\theta\theta}(r,\theta)}{r^{\lambda_1 - 1}},\ K_2^n = \lim_{\theta=0, r\to 0} \frac{\tau_{r\theta}(r,\theta)}{r^{\lambda_2 - 1}} \tag{57}$$

where $\sigma_{\theta\theta}$, $\tau_{r\theta}$ are the normal and shear component in the θ direction of the stress field, respectively. λ_1, λ_2 are the eigenvalues stemming from the corresponding eigen-equation (46).

The different stress intensity factors K_1^n and K_2^n corresponding to the individual eigenvalues λ_1 and λ_2 can be evaluated simultaneously (Carpenter and Byers, 1987). Alternatively, it can be attained independently as described here. Since the eigenvectors $\mathbf{q}^M$, $\mathbf{h}^M$ in Eq. (45) for each eigenvalue are determined only up to an arbitrary constant, we normalize the stress fields such that $\sigma_{\theta\theta}(r,\theta=0)=K_1^n r^{\lambda_1-1}, \tau_{r\theta}(r,\theta=0)=K_2^n r^{\lambda_2-1}$. Similarly, for the complementary field: $\sigma_{\theta\theta}^*(r,\theta=0)=K_1^{n*} r^{-\lambda_1-1}$, $\tau_{r\theta}^*(r,\theta=0)=K_2^{n*} r^{-\lambda_2-1}$. Note that the complementary field must satisfy the equilibrium equations and traction-free conditions on the notch flanks so that the integral along the inner contour C_ε yields the desired stress intensity factor. Moreover, the complementary solution is chosen with eigenvalue $\lambda_m^*=-\lambda_m$ to eliminate the dependence of the integrand on the r-coordinate. With all these conditions, the magnitudes of $K_m^{n*}(m=1,2)$ are determined so that the resulting inner contour integral identically produces K^n , either $K_1^n(e_1=1,\ e_2=0)$ or $K_2^n(e_1=0,\ e_2=1)$. The choice of $K_m^{n*}(m=1,2)$ is also described by Banks-Sills and Sherer (2002) and Zhang and Mikkola (1992).

As indicated in some other studies (e.g., Carpenter, 1984a; 1984b; Stern et al., 1976; Labossiere and Dunn, 1998; 1999), inaccuracy of the stress intensity factor can be induced by the numerical approximations (Gauss points or nodes, idealization) made in the finite element calculations and by the numerical integration schemes (programming details) adopted to calculate the H-integral. It can be improved by generating a reasonable finite element mesh, averaging results obtained along various contours and choosing a contour with a reasonable number of integration points, sufficiently far from the notch tip where the numerical results are generally smooth. Furthermore, the acquisition of complementary stress intensity factors K_m^{n*} on actual integration paths may also provide an alternative check for accuracy of compuational procedures.

CHAPTER 5

Summary of Appended Papers

Fracture of anodic-bonded silicon-thin film glass-silicon triple stacks

Shang LY, Zhang ZL and Skallerud B.
Engineering Fracture Mechanics; 2008; ***75****(5):1064-82.*

Two types of silicon-thin film glass-silicon (Si-Glass-Si) triple stacks specimens with a sharp corner are examined. Three approaches including displacement approach, stress approach and H-integral approach are presented and compared. The applicability of the H-integral approach is quantified and the different failure criteria have been discussed. The effect of glass thickness on the stress intensity factor has been studied and proved that the glass thickness is an important geometrical quantity affecting the stress intensity factors for triple stacks with a thick glass layer. Mesh refinement and the influencing factors on critical stress intensity have also been addressed.

Evaluation of fracture mechanics parameters for free edges in multi-layered structures with weak singularities

Shang LY, Zhang ZL and Skallerud B.
International Journal of Solids and Structures; 2009; ***46****(5):1134-48.*

The edge stress intensity factor in multi-layered structural components with weak singularities is investigated in detail. The dependence of stress singularity on elastic mismatch parameters of various material combinations is analyzed and illustrated. The effects of elastic mismatch, bond area and metal layer thickness on the stress intensity factor have been quantified. Standardized numerical formulae of the dimensionless stress intensity factor have been derived to guide the engineering application. Moreover, the analysis of the competition for crack initiation between a free edge interface and a 90º notch interface in the chosen specimen has been explored and the question of prevailing failure mode in multi-layered structural components has been addressed. Also, plastic deformations in the ductile material, anisotropy of the silicon substrate and different failure criterions have been discussed.

Comments on the evaluation of the stress intensity factor for a general re-entrant corner in anisotropic bi-materials

Shang LY, Zhang ZL and Skallerud B.
Engineering Fracture Mechanics; accepted, DOI: 10.1016/j.engfracmech.2009.01.012.

The computational procedure to obtain the stress intensity factor is illustrated in a flow chart. Three puzzling issues emerging often in the notch mechanics are addressed. Eigen-equation with regard to the stress singularity is interpreted from a mathematical viewpoint and the detailed calculation of eigenvalues for the corner problem has been presented. The different definitions of stress intensity factors is explained in a historical perspective and the stress intensity factor with respect to the shear stress component has been addressed by means of example calculation. Additionally, the effect of contour selection is further discussed and some suggestions are made for improving accuracy of results.

Other articles:

Crack initiation at thin-film edges with weak singularity

Shang LY, Zhang ZL and Skallerud B.
Proceedings of 17th European Conference on Fracture (ECF), 2-5, Sep, 2008, Brno, Czech Republic.

Fracture initiation for anodic-bonded triple stacks

Shang LY, Zhang ZL and Skallerud B.
Proceedings of the 20th Nordic Seminar on Computational Mechanics (NSCM), 23-24, Nov, 2007, Göthenburg, Sweden.

CHAPTER 6

Conclusions and Further Work

6.1 Concluding Remarks

To conclude, we have looked deeply into the analysis of a sharp re-entrant corner and a free edge in multi-layered structure without pre-existing crack. Singular near-tip stress fields and fracture parameters to correlate crack initiation have been extensively studied.

An efficient computational procedure to obtain stress intensity factors around multimaterial interface corners can be realized by the path-independent H-integral. The stress intensity factors are obtained for a wide range of material and geometry parameters. For the interface corner problem considered in Paper I and II, the stress intensity factors obtained from the H-integral approach show excellent agreement with those obtained from the asymptotic solutions by finite element calculations of displacements along the notch flanks or of stresses along the interface. The deviation of the displacement approach and the stress approach from the H-integral method is typically less than 5%.

Furthermore, the influencing factors of the stress intensity factors have been investigated, including not only the interface corner geometry, the thickness of intermediate layer, and material elastic constants, but also the interface strength resulting in diverse failure modes. Different failure criteria for notch problems have been addressed in Paper I and Paper II, such as strength approach, interfacial mechanics method, strain energy method. The feasibility and accuracy of H-integral method has also been explored.

The effects of elastic mismatch, bond area and metal layer thickness on the stress intensity factor have been quantified in Paper I and II for the various aspects of the notch problem. The proposed approach is favorable from an engineering point of view, due to the fact that such situations occur very frequently in composite structural elements and it can be used as a supplement for a preliminary design of new MEMS components. On the other hand, the effect of intermediate glass thickness in triple stacks on the stress intensity factor has been presented in Paper I. It has been found that the mode 1 stress intensity factor increases with glass thickness but basically decreases for mode 2 loading as the glass thickness increases. It also turns out that the glass thickness is an important geometrical quantity affecting the stress intensity factors for triple stacks with a thick glass layer.

The accuracy and stability of the results obtained from H-integral approach have been discussed. In Paper I, it has been found that relatively course meshes can be used in the H-integral approach. But it should be pointed out that the smallest mesh size is restricted by geometric conditions around the notch tip, such as glass thickness, etching depth and so on. The effect of contour selection is further explored in Paper III. It has been suggested that the selection of outer contour location should be neither be very close to the notch tip which is disturbed by material nonlinearities and geometric irregularities nor be far away from the interface corner which is affected by far-field loading and boundaries. Plastic deformation in the ductile material has been explored in paper II. The existence of the K-dominated field with respect to the applicability of the H-integral approach has been studied. The extent of the singular field is assessed by comparing the asymptotic solution to the detailed finite element analysis of the stress fields. It is observed that the valid range of the K-field is strongly influenced by the thin-film thickness.

Besides, the analysis of the competition for crack initiation between a free edge interface and a 90º notch interface in the chosen specimen has been presented in Paper II. Due to the possibility to shift the crack initiation site between two different notch interfaces, sufficient attention has been paid to this issue. It has been found out that the stress field is proportional to $\frac{Y}{r^{1-\lambda}}$.The fracture competition between different interfaces is governed by the set (K or Y, λ, fracture resistance) of the corresponding notch, respectively.

Standardized numerical formulae for varying material combinations in a notched bi-material system are proposed from a design engineer's perspective. The average solution proposed in Appendix may be a favorable alternative to provide application guidance for engineers.

Comparison between isotropic Si and anisotropic Si substrate is also illustrated in Paper II. Anisotropy of the Si substrate has a significant influence on the stress intensity factor when combined with an Au or Al metal layer but not with a Cu layer for free edge bi-material problems.

The different definitions of stress intensity factors are further explained in Paper III from a historical perspective and the stress intensity factor with respect to the shear stress component has been calculated for a sample. The analysis shows that the definition according to Eq. (57) provides the most accurate results. Moreover, eigen-equation with regard to the stress singularity is interpreted in Paper III from a mathematical viewpoint and the detailed calculation of eigenvalues for the corner problem has been presented.

6.2 Recommendations for future work

Some recommendations for future work are summarized in the following.

- The methodology and computational procedure presented herein to obtain stress intensity factors around multimaterial interface corners open up for integration of this with commercial finite element codes in a user-friendly option.
- A notched body subjected to remote forces in dissimilar materials generally results in the mixed-mode deformations. The problem of finding the appropriate mixed-mode failure criterion for interface corners is still open. If mode 1 stress singularity is not dominating, i.e., more than one comparable deformation modes exist, the evaluation of the interface strength is challenging, The proposal of the dimensionless stress intensity factor has removed the effect of interface geometry, such as bond width, intermediate layer thickness, but not the notch angles. A unified failure criterion applicable for different angles may be further explored.

- Our study is a continuum problem. It can be used for macroscopic notch problems although it is hard to find sharp notches in macroscopic world. On the other hand, sharp notches in the microscopic domain can be obtained. However, the size effect and limitations (e.g., the effect of the non-sharp notch root, the effect of plastic zone and material nonlinearities) for applying the method presented in this thesis to nanoscales are worthy of further investigations.
- Very few experimental data for the real MEMS components are available, specifically for corrosive and high temperature environment. Hence, more comprehensive test programs are required.
- The main focus of the MEMS industry is on the electrical and material functionalities rather than the mechanical properties. More focus on mechanical aspects can help the industry to understand the failure mechanisms and reduce the failure rates in manufacturing MEMS products.
- When different notch interfaces exist in a multi-layered structural component, the question of shifting the crack initiation site between two interfaces and which interface will fail first are still pending.
- Due to its specific crystallographic structure, anisotropy of the single crystal silicon may have a significant influence on the stress intensity factor at interface corners. This effect should be quantified for guidance of application.
- The thin intermediate layers grown between the silicon substrate and the steel cantilever are not considered in the present study. We assume that the interface is perfectly bonded with no relative displacements between each other. The validity of this assumption should be studied further (e.g., Carpenter, 1984a; 1984b; Stern et al., 1976; Labossiere and Dunn, 1998; 1999).
- The awareness of the anisotropic elasticity and the notch mechanics is still low in the engineering field. An advanced fracture mechanics course may be introduced to a master's program for engineering graduates.

Reference List

Akisanya, A. R., (1997). On the singular stress field near the edge of bonded joints. Journal of Strain Analysis for Engineering Design 32**,** 301-311.

Akisanya, A. R., Fleck, N. A., (1997). Interfacial cracking from the free-edge of a long bi-material strip. International Journal of Solids and Structures 34**,** 1645-1665.

Ashcroft, N. W., Merimin, N. D., (1976). Solid State Physics. PA: Saunders College, Philadelphia.

Babuska, I., Miller, A., (1984). The Post-Processing Approach in the Finite-Element Method .2. the Calculation of Stress Intensity Factors. International Journal for Numerical Methods in Engineering 20**,** 1111-1129.

Banks-Sills, L., (1997). A conservative integral for determining stress intensity factors of a bimaterial strip. International Journal of Fracture 86**,** 385-398.

Banks-Sills, L., Sherer, A., (2002). A conservative integral for determining stress intensity factors of a bimaterial notch. International Journal of Fracture 115**,** 1-26.

Barnett, D. M., Kirchner, H. O. K., (1997). A proof of the equivalence of the Stroh and Lekhnitskii sextic equations for plane anisotropic elastostatics. Philosophical Magazine A-Physics of Condensed Matter Structure Defects and Mechanical Properties 76**,** 231-239.

Barone, M. R., Robinson, A. R., (1972). Determination of elastic stresses at notches and corners by integral equations. International Journal of Solids and Structures 8**,** 1319-1338.

Barroso, A., Mantic, V., Paris, F., (2003). Singularity analysis of anisotropic multimaterial corners. International Journal of Fracture 119**,** 1-23.

Beadle, W. E., Tsai, J. C. C., Plummer, R. D., (1985). Quick Reference Manual for Silicon Integrated Circuit Technology. Wiley, New York.

Bhat, K. N., (2007). Silicon micromachined pressure sensors. Journal of the Indian Institute of Science 87**,** 115-131.

Bogy, D. B., Wang, K. C., (1971). Stress Singularities at Interface Corners in Bonded Dissimilar Materials. International Journal of Solids and Structures 7**,** 993-1005.

Brooks, A. D., Hardesty, C. A., Donovan, R. P., (1972). Low-Temperature Electrostatic Silicon-To-Silicon Seals Using Sputtered Borosilicate Glass. Journal of the Electrochemical Society 119**,** 545-546.

Carpenter, W. C., (1984a). Calculation of Fracture-Mechanics Parameters for A General Corner. International Journal of Fracture 24**,** 45-58.

Carpenter, W. C., (1984b). Mode I and Mode II stress intensity factors for plates with cracks of finite opening. International Journal of Fracture 26**,** 201-214.

Carpenter, W. C., (1995). Insensitivity of the reciprocal work contour integral method to higher order eigenvectors. International Journal of Fracture 73**,** 93-108.

Carpenter, W. C., Byers, C., (1987). A Path Independent Integral for Computing Stress Intensities for V-Notched Cracks in A Bi-Material. International Journal of Fracture 35**,** 245-268.

Chadwick, P., Smith, G. D., (1977). Foundations of the theory of surface waves in anisotropic elastic materials. Advances in Applied Mechanics 17**,** 303-376.

Chen, D. H., (1996). Logarithmic singular stress field in a semi-infinite plate consisting of two edge-bonded wedges subjected to surface tractions. International Journal of Fracture 75**,** 357-378.

Chen, D. H., Nisitani, H., (1993). Singular Stress-Field Near the Corner of Jointed Dissimilar Materials. Journal of Applied Mechanics-Transactions of the ASME 60**,** 607-613.

Chen, F. H. K., Shield, R. T., (1977). Conservation Laws in Elasticity of J-Integral Type. Zeitschrift fur Angewandte Mathematik und Physik 28**,** 1-22.

Chen, K. S., Ayon, A., Spearing, S. M., (2000). Controlling and testing the fracture strength of silicon on the mesoscale. Journal of the American Ceramic Society 83**,** 1476-1484.

Christensen, R. M., (1979). Mechanics of Composite Materials. Wiley, New York.

Cowin, S. C., Mehrabadi, M. M., adegh, A. M., (1992). "Kelvin's formulation of the anisotropic Hook's law" in Modern Theory of Anisotropic Elasticity and Applications. SIAM Proceedings Series, SIAM 340-356.

Dempsey, J. P., (1981). The Wedge Subjected to Tractions - A Paradox Resolved. Journal of Elasticity 11**,** 1-10.

Dempsey, J. P., (1995). Power-Logarithmic Stress Singularities at Bi-Material Corners and Interface Cracks. Journal of Adhesion Science and Technology 9**,** 253-265.

Dempsey, J. P., Sinclair, G. B., (1979). On the Stress Singularities in the Plane Elasticity of the Composite Wedge. Journal of Elasticity 9**,** 373-391.

Dempsey, J. P., Sinclair, G. B., (1981). On the Singular Behavior at the Vertex of a Bimaterial Wedge. Journal of Elasticity 11**,** 317-327.

Dunn, M. L., Cunningham, S. J., Labossiere, P. E. W., (2000). Initiation toughness of silicon/glass anodic bonds. Acta Materialia 48**,** 735-744.

England, A. H., (1971). On Stress Singularities in Linear Elasticity. International Journal of Engineering Science 9**,** 571-585.

Enikov, E. T., (2006). Introduction to Micro-systems and to the techniques for their fabrication. Microsystems Mechanical Design, CISM (International Centre For Mechanical Sciences) Courses and Lectures. Springer, Udine, Italy.

Eshelby, J. D., Read, W. T., Shockley, W., (1953). Anisotropic Elasticity with Applications to Dislocation Theory. Acta Metallurgica 1**,** 251-259.

Fett, T., (1994). Determination of Stresses in A Plate Strip of Bonded Dissimilar Materials. Engineering Fracture Mechanics 47**,** 547-557.

Gadi, K. S., Joseph, P. F., Zhang, N. S., Kaya, A. C., (2000). Thermally induced logarithmic stress singularities in a composite wedge and other anomalies. Engineering Fracture Mechanics 65**,** 645-664.

Green, A. E., Zerna, W., (1954). Theoretical Elasticity. Oxford University Press, New York.

Gross, B., Mendelson, A., (1972). Plane Elastostatic Analysis of V-Notched Plates. International Journal of Fracture Mechanics 8**,** 267-276.

Hein, V. L., Erdogan, F., (1971). Stress Singularities in a Two Material Wedge. International Journal of Fracture Mechanics 7**,** 317-330.

Henning, A. K., Patel, S., elser, M., ozad, B. A., (2004). Factors affecting silicon membrane burst strength. Proceeding of SPIE - The International Society for Optical Engineering (Conference of Reliability, Testing, and Characterization of MEMS/MOEMS III) 5343**,** 145-153.

Hong, C. C., Stern, M., (1978). Computation of Stress Intensity Factors in Dissimilar Materials. Journal of Elasticity 8**,** 21-34.

Hutchinson, J. W., (1990). Mixed mode fracture mechanics of interfaces. Metal-Ceramic Interfaces, Acta-Scripta Metalurgica Proceedings Series 4**,** 295-306.

Hutchinson, J. W., Suo, Z., (1992). Mixed-Mode Cracking in Layered Materials. Advances in Applied Mechanics, Vol 29 29**,** 63-191.

Ingebrigtsen, K. A., Tonning, A., (1969). Elastic surface waves in crystal. Physical Review 184**,** 942-951.

Jones, R. M., (1975). Mechanics of Composite Materials. McGrawHill, New York.

Joseph, P. F., Zhang, N. S., (1998). Multiple root solutions, wedge paradoxes and singular stress states that are not variable-separable. Composites Science and Technology 58**,** 1839-1859.

Kelly, P. A., Hills, D. A., Nowell, D., (1992). The Design of Joints Between Elastically Dissimilar Components (with Special Reference to Ceramic Metal Joints). Journal of Strain Analysis for Engineering Design 27**,** 15-20.

Kitamura, T., Hirakata, H., Itsuji, T., (2003). Effect of residual stress on delamination from interface edge between nano-films. Engineering Fracture Mechanics 70**,** 2089-2101.

Kitamura, T., Hirakata, H., Van Truong, D., (2007). Initiation of interface crack at free edge between thin films with weak stress singularity. Thin Solid Films 515**,** 3005-3010.

Kitamura, T., Shibutani, T., Ueno, T., (2002). Crack initiation at free edge of interface between thin films in advanced LSI. Engineering Fracture Mechanics 69**,** 1289-1299.

Kuo, M. C., Bogy, D. B., (1974). Plane Solutions for Displacement and Traction-Displacement Problems for Anisotropic Elastic Wedges. Journal of Applied Mechanics-Transactions of the Asme 41**,** 197-202.

Kurtz, A. D., Goodman, S. J., (1974). Apparatus and method for interconnecting leads in a high temperature pressure transducer. Patent (3800264), U.S.

Labossiere, P. E. W., Dunn, M. L., (1998). Calculation of stress intensities at sharp notches in anisotropic media. Engineering Fracture Mechanics 61**,** 635-654.

Labossiere, P. E. W., Dunn, M. L., (1999). Stress intensities at interface corners in anisotropic bimaterials. Engineering Fracture Mechanics 62**,** 555-575.

Labossiere, P. E. W., Dunn, M. L., Cunningham, S. J., (2002). Application of bimaterial interface corner failure mechanics to silicon/glass anodic bonds. Journal of the Mechanics and Physics of Solids 50**,** 405-433.

Lekhnitskii, S. G., (1950). Theory of elasticiy of an anisotropic body (in Russian), [Theory of elasticiy of an anisotropic elastic body, Holden-day, San Francisco (in English, 1963), and Mir Publishers, Moscow (in English, 1981)]. Gostekhizdat, Moscow.

Lekhnitskii, S. G., (1957). Anisotropic Plates. Gostekhizdat, Moscow (in Russian).

Liu, C. H., (2001). Micro-Electro-Mechanical Systems. Mechanical Engineering Department Seminar, National Chiao Tung University.

Luo, Y. P., Subbarayan, G., (2007). A study of multiple singularities in multi-material wedges and their use in analysis of microelectronic interconnect structures. Engineering Fracture Mechanics 74**,** 416-430.

Madou, M., (1997). Fundamentals of Microfabrication. CRC press, New York.

Maluf, N., Williams, K., (2004). An introduction to Microelectromechanical systems engineering. Artech House, Boston, London.

Mason, W. P., (1958). Physical Acoustics and the Properties of Solids. Van Nostrand, New York.

Mehregany, M., (1993). Microelectromechanical Systems. IEEE Circuits and Devices Magazine 9**,** 14-22.

Mohamed, G. E. H. E., (2002). The MEMS Handbook: MEMS, introduction and fundamentals. CRC press, Baco Raton.

Mounier, E., Eloy, J. C., (2007). New Emerging MEMS Applications. Proc.of SPIE (Micromachining Technology for Micro-Optics and Nano-Optics V and Microfabrication Process Technology XII) 6462.

Munz, D., Fett, T., Yang, Y. Y., (1993). The Regular Stress Term in Bonded Dissimilar Materials After A Change in Temperature. Engineering Fracture Mechanics 44**,** 185-194.

Munz, D., Yang, Y. Y., (1992). Stress Singularities at the Interface in Bonded Dissimilar Materials Under Mechanical and Thermal Loading. Journal of Applied Mechanics-Transactions of the Asme 59**,** 857-861.

Munz, D., Yang, Y. Y., (1993). Stresses Near the Edge of Bonded Dissimilar Materials Described by 2 Stress Intensity Factors. International Journal of Fracture 60**,** 169-177.

Nathanson, H. C., WICKSTRO.RA, (1965). A Resonant Gate Surface Transistor with High-Q Bandpass Properties. IEEE Transactions on Electron Devices ED12**,** 507.

Nese, M., Hanneborg, A., (1993). Anodic Bonding of Silicon to Silicon-Wafers Coated with Aluminum, Silicon-Oxide, Polysilicon Or Silicon-Nitride. Sensors and Actuators A-Physical 37-8**,** 61-67.

Pageau, S. S., Gadi, K. S., Biggers, S. B., Joseph, P. F., (1996). Standardized complex and logarithmic eigensolutions for n-material wedges and junctions. International Journal of Fracture 77**,** 51-76.

Paggi, M., Carpinteri, A., (2008). On the stress-singularities at multi-material interfaces and related analogies with fluid dynamics and diffusion. ASME Applied Mechanics Reviews 61**,** 1-22.

Petersen, K. E., (1982). Silicon As A Mechanical Material. Proceedings of the IEEE 70**,** 420-457.

Qian, Z. Q., (2001). On the evaluation of wedge corner stress intensity factors of bi-material joints with surface tractions. Computers & Structures 79**,** 53-64.

Qian, Z. Q., Akisanya, A. R., (1998). Analysis of free-edge stress and displacement fields in scarf joints subjected to a uniform change in temperature. Fatigue & Fracture of Engineering Materials & Structures 21**,** 687-703.

Qian, Z. Q., Akisanya, A. R., (1999a). An investigation of the stress singularity near the free edge of scarf joints. European Journal of Mechanics A-Solids 18**,** 443-463.

Qian, Z. Q., Akisanya, A. R., (1999b). Wedge corner stress behaviour of bonded dissimilar materials. Theoretical and Applied Fracture Mechanics 32**,** 209-222.

Reedy, E. D., (1993). Asymptotic Interface Corner Solutions for Butt Tensile Joints. International Journal of Solids and Structures 30**,** 767-777.

Reedy, E. D., Guess, T. R., (1993). Comparison of Butt Tensile-Strength Data with Interface Corner Stress Intensity Factor Prediction. International Journal of Solids and Structures 30**,** 2929-2936.

Reedy, E. D., Guess, T. R., (2002). Nucleation and propagation of an edge crack in a uniformly cooled epoxy/glass bimaterial. International Journal of Solids and Structures 39**,** 325-340.

Rice, J. R., (1968). A Path Independent Integral and Approximate Analysis of Strain Concentration by Notches and Cracks. Journal of Applied Mechanics 35**,** 379-386.

Roylance, L. M., Angell, J. B., (1979). Batch-Fabricated Silicon Accelerometer. IEEE Transactions on Electron Devices 26**,** 1911-1917.

Seidel, H., Csepregi, L., Heuberger, A., Baumgartel, H., (1990). Anisotropic Etching of Crystalline Silicon in Alkaline-Solutions .1. Orientation Dependence and Behavior of Passivation Layers. Journal of the Electrochemical Society 137**,** 3612-3626.

Senturia, S. D., (2003). Microsystem design. Kluwer Academic Publishers, Boston, the U.S.

Shang, L. Y., Zhang, Z. L., Skallerud, B., (2008). Fracture of anodic-bonded silicon-thin film glass-silicon triple stacks. Engineering Fracture Mechanics 75**,** 1064-1082.

Shang, L. Y., Zhang, Z. L., Skallerud, B., (2009). Evaluation of fracture mechanics parameters for free edges in multi-layered structures with weak singularities. International Journal of Solids and Structures 46**,** 1134-1148.

Shih, C. F., Asaro, R. J., (1988). Elastic-Plastic Analysis of Cracks on Bimaterial Interfaces .1. Small-Scale Yielding. Journal of Applied Mechanics-Transactions of the Asme 55**,** 299-316.

Sih, G. C., Ho, J. W., (1991). Sharp Notch Fracture Strength Characterized by Critical Energy Density. Theoretical and Applied Fracture Mechanics 16**,** 179-214.

Sinclair, G. B., (1985). A Remark on the Determination of Mode-I and Mode-II Stress Intensity Factors for Sharp Re-Entrant Corners. International Journal of Fracture 27**,** R81-R85.

Sinclair, G. B., (1998). Further paradoxes in generalized Levy problems. Journal of Elasticity 50**,** 253-259.

Sinclair, G. B., (1999a). A note on the removal of further breakdowns in classical solutions of Laplace's equation on sectorial regions. Journal of Elasticity 56**,** 247-252.

Sinclair, G. B., (1999b). Logarithmic stress singularities resulting from various boundary conditions in angular corners of plates in extension. Journal of Applied Mechanics-Transactions of the ASME 66**,** 556-560.

Sinclair, G. B., Okajima, M., Griffin, J. H., (1984). Path Independent Integrals for Computing Stress Intensity Factors at Sharp Notches in Elastic Plates. International Journal for Numerical Methods in Engineering 20**,** 999-1008.

Snyder, M. D., Cruse, T. A., (1975). Boundary-Integral Equation Analysis of Cracked Anisotropic Plates. International Journal of Fracture 11**,** 315-328.

Sokolnikoff, I. S., (1956). Mathematical Theory of Elasticity. McGraw Hill, New York.

Song, C. M., (2005). Evaluation of power-logarithmic singularities, T-stresses and higher order terms of in-plane singular stress fields at cracks and multi-material corners. Engineering Fracture Mechanics 72**,** 1498-1530.

Starman, L., (2006). Micro-Electro-Mechanical Systems (MEMS). Online resources.

Stern, M., (1979). Numerical-Calculation of Thermally Induced Stress Intensity Factors. Journal of Elasticity 9**,** 91-95.

Stern, M., Becker, E. B., Dunham, R. S., (1976). Contour Integral Computation of Mixed-Mode Stress Intensity Factors. International Journal of Fracture 12**,** 359-368.

Stern, M., Soni, M. L., (1975). The calculation of stress intensity factors in anisotropic materials by a contour integral method. Computational Fracture Mechanics, ASME 2nd National Congress on Pressure Vessels and Piping, San Francisco.

Stern, M., Soni, M. L., (1976a). Computation of Stress Intensities at Fixed-Free Corners. International Journal of Solids and Structures 12**,** 331-337.

Stern, M., Soni, M. L., (1976b). On the Computation of Stress Intensities at Fixed-Free Corners. International Journal of Solids and Structures 12**,** 331-337.

Sternberg, E., Koiter, W., (1958). The wedge under a concentrated couple: a paradox in the two-dimensional theory of elasticity. ASME Journal of Applied Mechanics 4**,** 575-581.

Stroh, A. N., (1958). Dislocations and Cracks in Anisotropic Elasticity. Philosophical Magazine 3**,** 625-646.

Stroh, A. N., (1962). Steady State Problems in Anisotropic Elasticity. Journal of Mathematics and Physics 41**,** 77-103.

Su, B. Z., Lee, Y. C., Dunn, M. L., (2003). Die cracking at solder (NO-PNO) joints on brittle (GaAs) chips: Fracture correlation using critical bimaterial interface corner stress intensities. Journal of Electronic Packaging 125**,** 369-377.

Suo, Z., (1990). Singularities, Interfaces and Cracks in Dissimilar Anisotropic Media. Proceedings of the Royal Society of London A427**,** 331-358.

Szabo, B. A., Babuska, I., (1988). Computation of the amplitude of stress singular terms for cracks and re-entrant corners. San Antonio, TX, United States.

Szabo, B. A., Yosibash, Z., (1996). Numerical analysis of singularities in two dimensions .2. Computation of generalized flux/stress intensity factors. International Journal for Numerical Methods in Engineering 39**,** 409-434.

Tarn, J. Q., (2002). A state space formalism for anisotropic elasticity. Part I: Rectilinear anisotropy. International Journal of Solids and Structures 39**,** 5143-5155.

Theocaris, P. S., (1974). The order of singularity at a multi-wedge corner in a composite strip. International Journal of Engineering Science 12**,** 102-120.

Timoshenko, S. P., Goodier, J. N., (1970). Theory of elasticity. McGraw-Hill Inc., New York.

Ting, T. C. T., (1985). Elastic Wedge Subjected to Antiplane Shear Tractions - A Paradox Explained. Quarterly Journal of Mechanics and Applied Mathematics 38**,** 245-255.

Ting, T. C. T., (1996). Anisotropic Elasticity: Theory and Applications. Oxford University Press, New York.

Ting, T. C. T., (1997). Stress Singularities at the Tip of Interfaces in Polycrystals. Damage and Failure of Interfaces, Rossmanith (ed.) 75-82.

Ting, T. C. T., (2000). Recent developments in anisotropic elasticity. International Journal of Solids and Structures 37**,** 401-409.

Ting, T. C. T., Chou, S. C., (1981). Edge Singularities in Anisotropic Composites. International Journal of Solids and Structures 17**,** 1057-1068.

Ting, T. C. T., Chou, S. C., (1982). Stress singularities in laminated composites. Proceedings of the second USA-USSR Symposium (Conference of Fracture of Composite Materials) 265-277.

Tong, Q. Y., Gosele, U. M., (1999). Semiconductor Wafer Bonding. Wiley, New York, pp. 49-72.

Trimmer, M., (1997). Micromechanics and MEMS. IEEE Press, New York.

Visser, M. M., (2002). Wafer bonding for MEMS. Ph.D Thesis, University of Oslo.

Voigt, W., (1910). Lehrbuch der Kristallphysik (Textbook of. Crystal Physics). Teubner, Leipzig.

Wallis, G., Pomerantz, D. I., (1969). Field Assisted Glass-Metal Sealing. Journal of Applied Physics 40**,** 3946-3949.

Walsh, P. F., (1976). Crack Initiation in Plain Concrete. Magazine of Concrete Research 28**,** 37-41.

Wang, S. S., Choi, I., (1982). Boundary-Layer Effects in Composite Laminates .1. Free-Edge Stress Singularities. Journal of Applied Mechanics-Transactions of the Asme 49**,** 541-548.

Wang, X. S., Deng, Y. H., Li, Y. Q., (2002). An experimental investigation of failure behavior of conducting polythiophene coating films. Journal of Materials Science 37**,** 4743-4748.

Williams, M. L., (1952). Stress Singularities Resulting from Various Boundary Conditions in Angular Corners of Plates in Extension. Journal of Applied Mechanics-Transactions of the ASME 19**,** 526-528.

Wortman, J. J., Evans, R. A., (1965). Young's Modulus, Shear Modulus, and Poisson's Ratio in Silicon and Germanium. Journal of Applied Physics 36**,** 153-156.

Wu, K. C., (1989). Representations of stress intensity factors by path-independent integrals. Journal of applied mechanics 56**,** 780-785.

Wu, K. C., Chang, F. T., (1993). Near-Tip Fields in A Notched Body with Dislocations and Body Forces. Journal of Applied Mechanics-Transactions of the ASME 60**,** 936-941.

Wu, K. C., Chen, C. T., (1996). Stress analysis of anisotropic elastic V-notched bodies. International Journal of Solids and Structures 33**,** 2403-2416.

Xu, L. R., Sengupta, S., (2004). Dissimilar material joints with and without free-edge stress singularities: Part II. An integrated numerical analysis. Experimental Mechanics 44**,** 616-621.

Yang, S. R., Chao, Y. J., (1992). Asymptotic Deformation and Stress-Fields at the Tip of A Sharp Notch in An Elastic Plastic Material. International Journal of Fracture 54**,** 211-224.

Yang, Y. Y., Munz, D., (1997). Stress singularities in a dissimilar materials joint with edge tractions under mechanical and thermal loadings. International Journal of Solids and Structures 34**,** 1199-1216.

Yau, J. F., Wang, S. S., Corten, H. T., (1980). A Mixed-Mode Crack Analysis of Isotropic Solids Using Conservation-Laws of Elasticity. Journal of Applied Mechanics-Transactions of the ASME 47**,** 335-341.

Yin, W. L., (1999). Mixed mode stress singularities in anisotropic composites. Thick Composites for Load Bearing Structures, ASME, AMD 235**,** 33-45.

Yole Development, (2006). Status of the MEMS Industry 2006. Lyon, France.

Yosibash, Z., Szabo, B., (1995). Numerical-Analysis of Singularities in 2-Dimensions .1. Computation of Eigenpairs. International Journal for Numerical Methods in Engineering 38**,** 2055-2082.

Zhang, Z. L., Mikkola, T. P. J., (1992). A Simple Path-Independent Integral for Calculating Mixed-Mode Stress Intensity Factors. Fatigue & Fracture of Engineering Materials & Structures 15**,** 1041-1049.

PAPER I

Fracture of anodic-bonded silicon-thin film glass-silicon triple stacks
Shang LY, Zhang ZL and Skallerud B.
*Engineering Fracture Mechanics 2008;**75**(5):1064-82.*

Fracture of anodic-bonded silicon-thin film glass-silicon triple stacks

L. Y. Shang, Z. L. Zhang[1] and B. Skallerud

Department of Structural Engineering, Norwegian University of Science and Technology (NTNU), Trondheim, Norway

Abstract

In this study we focus on the fracture behavior of two types silicon-thin film glass-silicon (Si-Glass-Si) triple stacks specimens with a sharp corner. We determine the notch stress intensity factor K^n for both specimens using a combination of the Williams eigenfunction expansion method, Stroh's sextic formalism, finite element analysis, and the path-independent H-integral. Empirical solutions of dimensionless stress intensity factors are proposed for two typical specimens, and the dependence of geometry is analyzed. Furthermore, the effect of glass thickness on stress intensity is explored for anodic-bonded Si-Glass-Si triple stacks. We discuss the feasibility of using a critical value of K^n to correlate the failure results for both specimens with various bond area and glass thickness.

Keywords: MEMS reliability, interface fracture, wafer bonds, notch mechanics, path-independent integral

1. Introduction

Wafer-to-wafer bonding is critical in the production of Micro-Electro-Mechanical Systems (MEMS). Among the different types of wafer bonding, the anodic bonding plays an important role especially for silicon wafers. Anodic bonding (also called field-assisted thermal bonding, electrostatic bonding, etc), a technique for sealing glass and silicon wafers, was presented by Wallis and Pomerantz (1969). The advantage of anodic bonding for MEMS is that the low temperature provides a metalization layer that does not degrade due to temperature effects. Anodic bonding is a commercially available technique. However, thin-film anodic bonding, invented by Brooks and Donovan (1972), is not yet industrialized. Si-Glass-Si triple stacks with free edges and corners are also common in wafer-level vacuum packaging of microelectronic devices and microsensors. A thin layer of glass is either electron beam evaporated or sputtered onto a silicon wafer. Another silicon wafer is then bonded onto the glass film. Detailed techniques can be found in Ref. (Visser, 2002). All published results indicate that a certain minimum critical thickness of the glass layer is required to ensure good bonding, otherwise, it will decrease the bond strength or even result in failure. The minimum thickness of the glass film depends on the concentration of alkali ions in the glass, and the typical minimum thickness is $2\,\mu m$ (Quenzer et al., 2001). In contrast to sputtering, evaporation can contain many more sodium ions in the glass layer and the anodic bonding can be performed at lower temperature and voltage in the bonding process (Choi et al., 1997). An advantage with thin-film anodic bonding, as compared to anodic bonding, is that problems caused by different thermal expansion coefficients and Young's modulus of the glass and the silicon are reduced. Additionally, two highly patterned silicon wafers can be bonded together with thin-film anodic bonding. The disadvantage with the technique is that the process has not been studied and optimized to the same degree as the well known anodic bonding process.

[1] Corresponding author: e-mail: Zhiliang.zhang@ntnu.no

In linear elastic fracture mechanics, the use of a critical stress intensity factor K_C to predict brittle fracture of cracked solids is widely accepted. The feasibility of using the single parameter K (or a function of two parameters in mixed-mode cases) is due to the universal nature of the singular stress field surrounding a crack tip as shown by Williams (1952). In a number of MEMS components, sharp re-entrant corners or notches are introduced, usually to facilitate fabrication. Over the last 20 years, notch mechanics and analysis of an interface between two elastically dissimilar materials have been an active research field. As we know, the near-tip singular stress field in a notched body is characterized by the form $\sigma_{ij} = K_I^n r^{\lambda_I - 1} f_{ij}^I(\theta) + K_{II}^n r^{\lambda_{II} - 1} f_{ij}^{II}(\theta)$. The stress singularity $\lambda - 1$ for various single and multiple-phase notch geometries in both isotropic (e.g., Bogy and Wang, 1971; Dempsey and Sinclair, 1979; Dunn et al., 1997b; Dunn et al., 1997a; Dempsey and Sinclair, 1981; Hein and Erdogan, 1971) and anisotropic (e.g., Cho et al., 1992; Pageau et al., 1995; Suwito et al., 1999; Suwito et al., 1998; Wu and Chen, 1996; Dunn et al., 2000; Ting, 1997; Ting and Chou, 1981) media has been studied. For multimaterial media, the situation becomes complicated as in mixed-mode deformation the asymptotic elastic fields depend on radial position, elastic mismatch and interface corner geometry. Accordingly, the mode I and mode II fields are usually not symmetric with the notch bisector as they are for the isotropic homogeneous case. An efficient computational procedure to obtain stress intensity factors around multimaterial interface corners can be realized by the path-independent H-integral. The interested readers can confer the review of Hutchinson and Suo (1992), and Labossiere and Dunn (1999) for more details. Despite some extensive studies related to anisotropic materials and bimaterial media, few studies focused on the three-material interface notch problems. This gives motivation of our work.

In this paper, we extend the H-integral approach to compute stress intensity factors at interface corners of thin-film anodic-bonded Si-Glass-Si triple stacks. Two types of specimens, named MESA and FRAME, with different bond area and various glass thickness are considered. We apply this approach to the mixed-mode I and II loading. The stress intensity factors obtained from the H-integral approach are in good agreement with those obtained by matching the asymptotic solutions with detailed finite element analysis. Empirical solutions of dimensionless stress intensity factors are established to facilitate engineering application. Furthermore, the effect of glass thickness on the stress intensity is studied for triple stacks. The magnitude of critical stress intensity factor for thin-film Si-Glass-Si triple stacks is determined from tests. Finally, mesh effect and some uncertainties are discussed.

2. Asymptotic analysis of interface notch tip fields with anisotropic elastic materials

The asymptotic analysis of anisotropic elastic fields at the bimaterial interface corner is briefly presented. The asymptotic analysis solves two eigenvalue problems obtained by Stroh's sextic formalism (e.g., Labossiere and Dunn, 1999; Stroh, 1958; Ting, 1996) and the eigenfunction expansion method of Williams (1952).

2.1 First eigenvalue problem - Stroh's sextic formalism

According to Stroh, when two-dimensional deformations depend only on x_1 and x_2, the displacement $\mathbf{u}$ and stress function $\boldsymbol{\varphi}$ of an anisotropic elastic solid in a fixed rectangular coordinate system can be generally expressed as:

$$\mathbf{u} = \sum_{\alpha=1}^{3}\left[\mathbf{a}_\alpha f_\alpha(z_\alpha) + \bar{\mathbf{a}}_\alpha f_{\alpha+3}(\bar{z}_\alpha)\right] \tag{1}$$

$$\boldsymbol{\varphi} = \sum_{\alpha=1}^{3}\left[\mathbf{b}_\alpha f_\alpha(z_\alpha) + \bar{\mathbf{b}}_\alpha f_{\alpha+3}(\bar{z}_\alpha)\right] \tag{2}$$

Here f_α are arbitrary functions of their arguments z_α depending on the geometry and loading, $z_\alpha = x_1 + p_\alpha x_2$ is the complex variable. The six complex eigenvalues p_α satisfy $p_{\alpha+3} = \bar{p}_\alpha$ and are the solutions of the quadratic eigenvalue problem (4). In addition, **a** and **b** are the Stroh eigenvectors and satisfy $\mathbf{a}_{\alpha+3} = \bar{\mathbf{a}}_\alpha$ and $\mathbf{b}_{\alpha+3} = \bar{\mathbf{b}}_\alpha$ related through the matrix **Q**, **R** and **T** described later. p_α, $\mathbf{a}_\alpha$ and $\mathbf{b}_\alpha$ depend only on the elastic stiffnesses C_{ijkl}. Without loss of generality, the imaginary part of p_α is taken to be positive. Overbar of $p, z, \mathbf{a}, \mathbf{b}$ denotes the complex conjugate.

In terms of the stress-strain laws $\sigma_{ij} = C_{ijkl}u_{k,l}$ and using Eq. (1), the equilibrium equations $C_{ijkl}u_{k,lj} = 0$ can be written:

$$C_{ijkl}(\delta_{l1} + \delta_{l2}p)(\delta_{j1} + \delta_{j2}p)a_k = 0 \tag{3}$$

in which a comma denotes differentiation and δ_{li} is the Kronecker delta. The above equation can be written in matrix form as:

$$\left\{\mathbf{Q} + p(\mathbf{R} + \mathbf{R}^{\mathrm{T}}) + p^2\mathbf{T}\right\}\mathbf{a} = \mathbf{0} \tag{4}$$

where $Q_{ik} = C_{i1k1}$, $R_{ik} = C_{i1k2}$ and $T_{ik} = C_{i2k2}$. For a non-trivial solution of **a**, we must have $\det\left|\mathbf{Q} + p(\mathbf{R} + \mathbf{R}^{\mathrm{T}}) + p^2\mathbf{T}\right| = \mathbf{0}$, which results in six roots for the eigenvalue *p*. In matrix forms and with Voigt's notation,

$$\mathbf{Q} = \begin{bmatrix} C_{11} & C_{16} & C_{15} \\ C_{16} & C_{66} & C_{56} \\ C_{15} & C_{56} & C_{55} \end{bmatrix},\ \mathbf{T} = \begin{bmatrix} C_{66} & C_{26} & C_{46} \\ C_{26} & C_{22} & C_{24} \\ C_{46} & C_{24} & C_{44} \end{bmatrix} \text{ and } \mathbf{R} = \begin{bmatrix} C_{16} & C_{12} & C_{14} \\ C_{66} & C_{26} & C_{46} \\ C_{56} & C_{25} & C_{45} \end{bmatrix} \tag{5}$$

$$\begin{bmatrix} C_{11} + 2pC_{16} + p^2C_{66} & C_{16} + p(C_{12} + C_{66}) + p^2C_{26} & C_{15} + p(C_{14} + C_{56}) + p^2C_{46} \\ & C_{66} + 2pC_{26} + p^2C_{22} & C_{56} + p(C_{46} + C_{25}) + p^2C_{24} \\ \textit{symmetric} & & C_{55} + 2pC_{45} + p^2C_{44} \end{bmatrix}\mathbf{a} = \mathbf{0} \tag{6}$$

Differentiating Eq. (1) and then inserting into constitutive equation, we can obtain σ_{ij}:

$$\sigma_{i1} = \left(Q_{ik} + pR_{ik}\right)a_k f'(z)$$
$$\sigma_{i2} = \left(R_{ki} + pT_{ik}\right)a_k f'(z) \tag{7}$$

Making use of Eq. (2), the relation between **a** and **b** can be written:

$$\mathbf{b} = \left(\mathbf{R}^{\mathrm{T}} + p\mathbf{T}\right)\mathbf{a} = -\frac{1}{p}\left(\mathbf{Q} + p\mathbf{R}\right)\mathbf{a} \tag{8}$$

The above quadratic eigenvalue problem (three dimensional) can be recast as a conventional six-dimensional linear eigenvalue problem

$$\begin{bmatrix} \mathbf{N}_1 & \mathbf{N}_2 \\ \mathbf{N}_3 & \mathbf{N}_1^T \end{bmatrix} \begin{Bmatrix} \mathbf{a} \\ \mathbf{b} \end{Bmatrix} = p \begin{Bmatrix} \mathbf{a} \\ \mathbf{b} \end{Bmatrix}$$
$$\Rightarrow \mathbf{N}\eta = p\eta, \quad \eta = \begin{Bmatrix} \mathbf{a} \\ \mathbf{b} \end{Bmatrix} \tag{9}$$

where $\mathbf{N}_1 = -\mathbf{T}^{-1}\mathbf{R}^{\mathrm{T}}$, $\mathbf{N}_2 = \mathbf{T}^{-1}$ and $\mathbf{N}_3 = -\mathbf{Q} + \mathbf{R}\mathbf{T}^{-1}\mathbf{R}^{\mathrm{T}}$. Since p cannot be real if the strain energy is to be positive (Eshelby et al., 1953), we have three pairs of complex conjugates for p as well as for η. If p_α and $\eta_\alpha \left(\alpha = 1, 2, \cdots, 6\right)$ are the eigenvalues and eigenvectors, we let

$$\left.\begin{aligned} p_{\alpha+3} &= \overline{p}_\alpha, \ \operatorname{Im} p_\alpha > 0 \\ \eta_{\alpha+3} &= \overline{\eta}_\alpha \end{aligned}\right\} \ \alpha = 1, 2, 3 \tag{10}$$

where Im denotes the imaginary part.

The Stroh eigenvectors are determined up to an arbitrary constant. They are normalized as:

$$\mathbf{a}_\alpha = \frac{\hat{\mathbf{a}}_\alpha}{\sqrt{2\hat{\mathbf{a}}_\alpha^{\mathrm{T}}\hat{\mathbf{b}}_\alpha}} \ \text{ and } \ \mathbf{b}_\alpha = \frac{\hat{\mathbf{b}}_\alpha}{\sqrt{2\hat{\mathbf{a}}_\alpha^{\mathrm{T}}\hat{\mathbf{b}}_\alpha}} \tag{11}$$

where $\hat{\mathbf{a}}_\alpha$ and $\hat{\mathbf{b}}_\alpha$ are the non-normalized eigenvectors, i.e. those that would be produced by a standard eigensolver; $\mathbf{a}_\alpha$ and $\mathbf{b}_\alpha$ represent the direction of the displacement $\mathbf{u}_\alpha$ and traction $\mathbf{t}_\alpha$, respectively .

2.2 Second eigenvalue problem – notch tip stress singularity

A stress singularity exists at sharp notches/crack tips. The degree of stress singularity is obtained from solving the second eigenvalue problem.

The traction $\mathbf{t}$ at any material point (r, θ) along the radial line from the notch tip can be written

$$\mathbf{t} = \frac{d}{dr}\boldsymbol{\phi} \ \text{ or } \ \sigma_{k1} = -\frac{\partial \varphi_k}{\partial x_2}, \ \sigma_{k2} = \frac{\partial \varphi_k}{\partial x_1} \tag{12}$$

where $\boldsymbol{\phi}$ is the stress function given by Eq. (2) and r is the radial distance measured from the notch tip.

By choosing $f\left(z_\alpha\right)$ (e.g., Ting, 1997; Labossiere and Dunn, 1999; Ting, 1996) as

$$f_\alpha\left(z_\alpha\right) = \frac{1}{\lambda} z_\alpha^\lambda q_\alpha \ \text{ and } \ f_{\alpha+3}\left(\overline{z}_\alpha\right) = \frac{1}{\lambda}\overline{z}_\alpha^\lambda h_\alpha \tag{13}$$

where q_α and h_α are the unknown complex constants and will be determined by Eq. (19) once λ is obtained. Using the expression $z_\alpha = x_1 + p_\alpha x_2 = r\xi_\alpha(\theta) = r(\cos\theta + p_\alpha \sin\theta)$, the displacement and traction functions can be written

$$\mathbf{u}^M = \frac{1}{\lambda} r^\lambda \sum_{\alpha=1}^{3} \left[\xi_\alpha^M \left(\theta\right)^\lambda \mathbf{a}_\alpha q_\alpha + \overline{\xi}_\alpha^M \left(\theta\right)^\lambda \overline{\mathbf{a}}_\alpha h_\alpha \right]$$
$$\mathbf{t}^M = \frac{\lambda}{r}\boldsymbol{\phi} = r^{\lambda-1} \sum_{\alpha=1}^{3} \left[\xi_\alpha^M \left(\theta\right)^\lambda \mathbf{b}_\alpha q_\alpha + \overline{\xi}_\alpha^M \left(\theta\right)^\lambda \overline{\mathbf{b}}_\alpha h_\alpha \right] \tag{14}$$

where superscript M indicates material A or B. The second eigenvalue problem can be

solved by using the boundary conditions for the interface notch problem, see Fig. 1. There are four sets of boundary conditions:

$$\begin{aligned}
&\mathbf{t}^A(\alpha)=0\ , \qquad \sum_{\alpha=1}^{3}\xi_\alpha^A(\alpha)^\lambda\,\mathbf{b}_\alpha^A q_\alpha^A+\sum_{\alpha=1}^{3}\overline{\xi}_\alpha^A(\alpha)^\lambda\,\overline{\mathbf{b}}_\alpha^A h_\alpha^A=0\\
&\mathbf{t}^B(-\beta)=0\ , \qquad \sum_{\alpha=1}^{3}\xi_\alpha^B(-\beta)^\lambda\,\mathbf{b}_\alpha^B q_\alpha^B+\sum_{\alpha=1}^{3}\overline{\xi}_\alpha^B(-\beta)^\lambda\,\overline{\mathbf{b}}_\alpha^B h_\alpha^B=0\\
&\mathbf{t}^A(0)=\mathbf{t}^B(0)\ , \ \sum_{\alpha=1}^{3}\xi_\alpha^A(0)^\lambda\,\mathbf{b}_\alpha^A q_\alpha^A+\sum_{\alpha=1}^{3}\overline{\xi}_\alpha^A(0)^\lambda\,\overline{\mathbf{b}}_\alpha^A h_\alpha^A-\sum_{\alpha=1}^{3}\xi_\alpha^B(0)^\lambda\,\mathbf{b}_\alpha^B q_\alpha^B-\sum_{\alpha=1}^{3}\overline{\xi}_\alpha^B(0)^\lambda\,\overline{\mathbf{b}}_\alpha^B h_\alpha^B=0\\
&\mathbf{u}^A(0)=\mathbf{u}^B(0)\ , \sum_{\alpha=1}^{3}\xi_\alpha^A(0)^\lambda\,\mathbf{a}_\alpha^A q_\alpha^A+\sum_{\alpha=1}^{3}\overline{\xi}_\alpha^A(0)^\lambda\,\overline{\mathbf{a}}_\alpha^A h_\alpha^A-\sum_{\alpha=1}^{3}\xi_\alpha^B(0)^\lambda\,\mathbf{a}_\alpha^B q_\alpha^B-\sum_{\alpha=1}^{3}\overline{\xi}_\alpha^B(0)^\lambda\,\overline{\mathbf{a}}_\alpha^B h_\alpha^B=0
\end{aligned} \tag{15}$$

The equations above can be rewritten as

$$\begin{aligned}
&\mathbf{B}^A\mathbf{q}^A+\overline{\mathbf{B}}^A\mathbf{h}^A=\mathbf{0}\\
&\mathbf{B}^B\mathbf{q}^B+\overline{\mathbf{B}}^B\mathbf{h}^B=\mathbf{0}\\
&\mathbf{b}^A\mathbf{q}^A+\overline{\mathbf{b}}^A\mathbf{h}^A-\mathbf{b}^B\mathbf{q}^B-\overline{\mathbf{b}}^B\mathbf{h}^B=\mathbf{0}\\
&\mathbf{a}^A\mathbf{q}^A+\overline{\mathbf{a}}^A\mathbf{h}^A-\mathbf{a}^B\mathbf{q}^B-\overline{\mathbf{a}}^B\mathbf{h}^B=\mathbf{0}
\end{aligned} \tag{16}$$

where

$\mathbf{B}^A=\left[\xi_1^A(\alpha)^\lambda\,\mathbf{b}_1^A,\ \xi_2^A(\alpha)^\lambda\,\mathbf{b}_2^A,\ \xi_3^A(\alpha)^\lambda\,\mathbf{b}_3^A\right]$, $\mathbf{B}^B=\left[\xi_1^B(-\beta)^\lambda\,\mathbf{b}_1^B,\ \xi_2^B(-\beta)^\lambda\,\mathbf{b}_2^B,\ \xi_3^B(-\beta)^\lambda\,\mathbf{b}_3^B\right]$,

$\mathbf{a}^M=\left[\mathbf{a}_1^M,\mathbf{a}_2^M,\mathbf{a}_3^M\right]$, $\mathbf{b}^M=\left[\mathbf{b}_1^M,\mathbf{b}_2^M,\mathbf{b}_3^M\right]$, , $\mathbf{q}^M=\left[q_1^M,q_2^M,q_3^M\right]^{\mathrm{T}}$, $\mathbf{h}^M=\left[h_1^M,h_2^M,h_3^M\right]^{\mathrm{T}}$

$(M=A,B)$

From the first two equations, we have

$$\begin{aligned}
&\mathbf{h}^A=-\left(\overline{\mathbf{B}}^A\right)^{-1}\mathbf{B}^A\mathbf{q}^A\\
&\mathbf{q}^B=-\left(\mathbf{B}^B\right)^{-1}\overline{\mathbf{B}}^B\mathbf{h}^B
\end{aligned} \tag{17}$$

By substituting Eq. (17) into the last two equations of Eq. (16), we get

$$\begin{bmatrix}
\mathbf{b}^A\left(\mathbf{B}^A\right)^{-1}-\overline{\mathbf{b}}^A\left(\overline{\mathbf{B}}^A\right)^{-1} & \left(\mathbf{b}^B\left(\mathbf{B}^B\right)^{-1}-\overline{\mathbf{b}}^B\left(\overline{\mathbf{B}}^B\right)^{-1}\right)\\
\mathbf{a}^A\left(\mathbf{B}^A\right)^{-1}-\overline{\mathbf{a}}^A\left(\overline{\mathbf{B}}^A\right)^{-1} & \left(\mathbf{a}^B\left(\mathbf{B}^B\right)^{-1}-\overline{\mathbf{a}}^B\left(\overline{\mathbf{B}}^B\right)^{-1}\right)
\end{bmatrix}
\begin{Bmatrix}\mathbf{B}^A\mathbf{q}^A\\ \overline{\mathbf{B}}^B\mathbf{h}^B\end{Bmatrix}=0 \tag{18}$$

that results in 6 simultaneous eigenvalue equations

$$\mathbf{K}(\lambda)\ \mathbf{D}=0 \tag{19}$$

where $\mathbf{D}=\left[\mathbf{B}^A\mathbf{q}^A,\ \overline{\mathbf{B}}^B\mathbf{h}^B\right]^{\mathrm{T}}$. For the single crystal silicon and glass material considered in this study, $\mathbf{K}$, can be partitioned into in-plane and anti-plane deformations.

$$\mathbf{K}=\begin{bmatrix}\mathbf{K}_{\mathrm{IP}} & \mathbf{0}\\ \mathbf{0} & \mathbf{K}_{\mathrm{AP}}\end{bmatrix} \tag{20}$$

In order to obtain a non-trivial solution, we get the characteristic equation for λ

$$\det\left[\mathbf{K}(\lambda)\right]=0 \tag{21}$$

3. H-integral approach

A path-independent H-integral approach for calculation of the stress intensity factor at sharp notches (e.g., Labossiere and Dunn, 1999) is briefly presented here. The main advantage of this method is that the stress intensity factor can be obtained by a contour integral around the notch tip with only tractions and displacements required.

Considering the configuration of a bimaterial interface corner shown in Fig. 1, the upper and lower notch faces are at $\theta = \alpha$ and $\theta = -\beta$ and the notch angle is γ, where angle θ is measured from the interface. For anisotropic materials, their elastic stiffnesses can be transformed with respect to the $x_1 - x_2$ axes (Mason, 1958). The notch faces are traction-free and the notched body is loaded at remote boundaries by tractions or displacements.

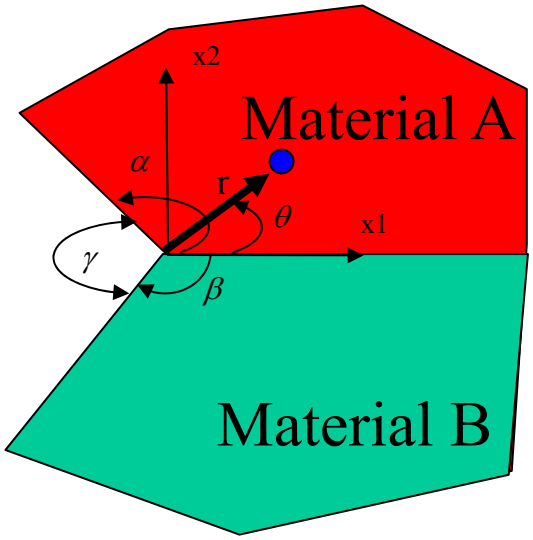

Fig. 1. Configuration of bimaterial interface corner

In this paper we study only the in-plane fields and real eigenvalues λ_I and λ_{II} solved by (21). With normalizations of the mode I fields by $\sigma_{22}(\theta = 0) = K_I^n r^{\lambda_I - 1}$ and of the mode II fields by $\sigma_{12}(\theta = 0) = K_{II}^n r^{\lambda_{II} - 1}$, the in-plane asymptotic singular fields near the notch tip can be expressed as:

$$\sigma_{ij}^M(r,\theta) = K_I^n r^{\lambda_I - 1} f_{ij}^{IM}(\theta) + K_{II}^n r^{\lambda_{II} - 1} f_{ij}^{IIM}(\theta)$$
$$u_i^M(r,\theta) = K_I^n r^{\lambda_I} g_i^{IM}(\theta) + K_{II}^n r^{\lambda_{II}} g_i^{IIM}(\theta) \qquad (22)$$

and before normalization,

$$
\begin{aligned}
f_{i1}^{IM}(\theta) &= -\sum_{\alpha=1}^{2}\left[p_\alpha^M \left(\mathbf{b}_\alpha^M\right)_i \xi_\alpha^M(\theta)^{\lambda_I-1} q_\alpha^{IM} + p_{\alpha+3}^M \left(\mathbf{b}_{\alpha+3}^M\right)_i \xi_{\alpha+3}^M(\theta)^{\lambda_I-1} h_\alpha^{IM} \right] \\
f_{i2}^{IM}(\theta) &= \sum_{\alpha=1}^{2}\left[\left(\mathbf{b}_\alpha^M\right)_i \xi_\alpha^M(\theta)^{\lambda_I-1} q_\alpha^{IM} + \left(\mathbf{b}_{\alpha+3}^M\right)_i \xi_{\alpha+3}^M(\theta)^{\lambda_I-1} h_\alpha^{IM} \right] \\
g_i^{IM}(\theta) &= \frac{1}{\lambda_I}\sum_{\alpha=1}^{2}\left[\left(\mathbf{a}_\alpha^M\right)_i \xi_\alpha^M(\theta)^{\lambda_I} q_\alpha^{IM} + \left(\mathbf{a}_{\alpha+3}^M\right)_i \xi_{\alpha+3}^M(\theta)^{\lambda_I} h_\alpha^{IM} \right] \\
f_{i1}^{IIM}(\theta) &= -\sum_{\alpha=1}^{2}\left[p_\alpha^M \left(\mathbf{b}_\alpha^M\right)_i \xi_\alpha^M(\theta)^{\lambda_{II}-1} q_\alpha^{IIM} + p_{\alpha+3}^M \left(\mathbf{b}_{\alpha+3}^M\right)_i \xi_{\alpha+3}^M(\theta)^{\lambda_{II}-1} h_\alpha^{IIM} \right] \\
f_{i2}^{IIM}(\theta) &= \sum_{\alpha=1}^{2}\left[\left(\mathbf{b}_\alpha^M\right)_i \xi_\alpha^M(\theta)^{\lambda_{II}-1} q_\alpha^{IIM} + \left(\mathbf{b}_{\alpha+3}^M\right)_i \xi_{\alpha+3}^M(\theta)^{\lambda_{II}-1} h_\alpha^{IIM} \right] \\
g_i^{IIM}(\theta) &= \frac{1}{\lambda_{II}}\sum_{\alpha=1}^{2}\left[\left(\mathbf{a}_\alpha^M\right)_i \xi_\alpha^M(\theta)^{\lambda_{II}} q_\alpha^{IIM} + \left(\mathbf{a}_{\alpha+3}^M\right)_i \xi_{\alpha+3}^M(\theta)^{\lambda_{II}} h_\alpha^{IIM} \right]
\end{aligned}
\tag{23}
$$

Here the superscript M indicates material A or B, $K_{\mathrm{m}}^{\mathrm{n}}$ are notch stress intensity factors where m corresponds to deformation mode I or II that are analogous to the opening and sliding modes in a homogeneous notched solid, $\lambda_{\mathrm{n}}-1$ are the stress singularities, and f_{ij}^{mM} and g_i^{mM} are functions depending on angle θ and material stiffnesses. In Eq. (22), only the stress intensity factors $K_{\mathrm{I}}^{\mathrm{n}}$ and $K_{\mathrm{II}}^{\mathrm{n}}$ cannot be determined from the asymptotic analysis. They depend on the geometry of the notched body, material elastic constants, and the far-field loading.

The path independent H-integral is based on the application of Betti's reciprocal work theorem which suppose two sets of elastic fields: the actual and the complementary. If λ is a root of Eq. (21), so is $\lambda^* = -\lambda$ (Wu and Chang, 1993). Hence, the chosen complementary solution is given by Eq. (24) and Eq. (25).

$$
\begin{aligned}
f_\alpha^*(z_\alpha) &= \frac{1}{\lambda^*} z_\alpha^{\lambda^*} q_\alpha^* \\
f_{\alpha+3}^*(\bar{z}_\alpha) &= \frac{1}{\lambda^*} \bar{z}_\alpha^{\lambda^*} h_\alpha^*
\end{aligned}
\tag{24}
$$

$$
\begin{aligned}
\sigma_{ij}^{M*}(r,\theta) &= K_I^{n*} r^{-\lambda_I-1} f_{ij}^{IM*}(\theta) + K_{II}^{n*} r^{-\lambda_{II}-1} f_{ij}^{IIM*}(\theta) \\
u_i^{M*}(r,\theta) &= K_I^{n*} r^{-\lambda_I} g_i^{IM*}(\theta) + K_{II}^{n*} r^{-\lambda_{II}} g_i^{IIM*}(\theta)
\end{aligned}
\tag{25}
$$

In the absence of body forces and singularities, the H-integral takes the form:

$$
H = \int_\Gamma \left(\sigma_{ij} u_i^* - \sigma_{ij}^* u_i\right) n_j ds = 0
\tag{26}
$$

where Γ is a closed contour around the notch tip, n_j is the unit outward normal to Γ, σ_{ij}, u_i and σ_{ij}^*, u_i^* are the actual and complementary stresses and displacements that satisfy the equilibrium and constitutive relations, respectively.

Taking a counter-clockwise contour around the notch tip from the lower face to upper face, in polar coordinates, the above equation is expressed as

$$
H = \int_{-\beta}^{\alpha} \left(\sigma_{rr} u_r^* + \sigma_{r\theta} u_\theta^* - \sigma_{rr}^* u_r - \sigma_{r\theta}^* u_\theta\right) r d\theta
\tag{27}
$$

and in Cartesian coordinates, it is given by

$$H = \int_y \left(\sigma_x u_x^* + \sigma_{xy} u_y^* - \sigma_x^* u_x - \sigma_{xy}^* u_y \right) dy + \int_x \left(\sigma_y u_y^* + \sigma_{xy} u_x^* - \sigma_y^* u_y - \sigma_{xy}^* u_x \right) dx \tag{28}$$

Taking advantage of Eq. (26), we obtain an explicit expression for the mode I scaling factor K_I^{n*} by setting $H = H_I = K_I^n$ and similarly the mode II scaling factor K_{II}^{n*} by setting $H = H_{II} = K_{II}^n$.

Dimensionless considerations illustrate that the stress intensity factor K^n takes the form:

$$K^n = \sigma_0 (length)^{1-\lambda} Y(geometry) \tag{29}$$

where σ_0 is a nominal stress and Y is a non-dimensional function of geometry.

4. Application to Si-Glass-Si triple stacks

4.1 Specification of Si-Glass-Si triple stacks with mixed-mode I and II loading

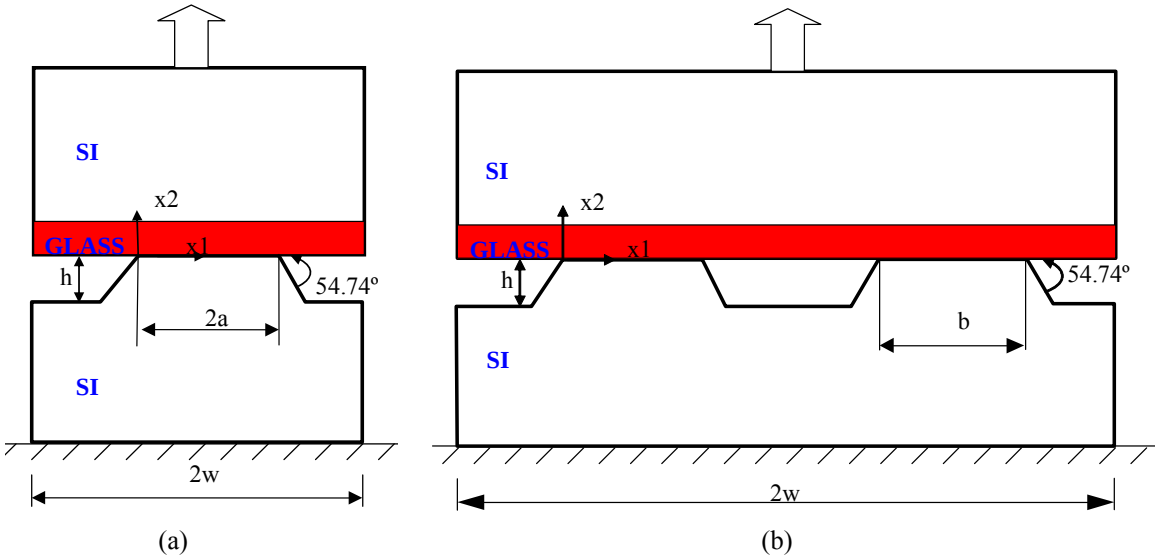

Fig. 2. 54.74° Notched (a) MESA and (b) FRAME triple-stacks specimens

In this work, triple stacks are composed of Si-Glass-Si multimaterials. Two types of specimens, MESA and FRAME, Fig. 2, have been studied. The overall width of the specimen ($2w$) is $3500\mu m$, the etching depth (the height of bond pad, h) is $18\mu m$. Five bond lengths ($2a$), 700, 1000, 1414, 1700 and $2000\mu m$, and four glass thicknesses (t), 3, 3.6, 5 and $10\mu m$, have been considered for the MESA specimens. For the FRAME specimens, five bond lengths ($2b$), 400, 800, 1200, 1600 and $1900\mu m$, and five glass thicknesses, 3, 3.6, 5, 10 and $18\mu m$, have been analyzed. A remote tensile nominal stress $\sigma_0 = F / 2wt_1$ is applied to all the specimens, where t_1 is the thickness of the specimen in x_3 direction. Brittle fracture initiated at the interface corner. It should be noted that even though the specimens have remote tension, they are subjected to mixed-mode I and II loading at notch tip. The interface corner is $\gamma = 54.74^\circ$ which is a result of etching process. Silicon is an elastic brittle material and its elastic stiffness matrix corresponding to the $x_1 - x_2$ axes in Fig. 2 is given by Eq. (30). Corning #7740 PYREX glass is

used here with elastic modulus $E = 63GPa$ and Poisson's ratio $\nu = 0.2$. Making use of symmetry, we only take account of a half-model in the plane strain finite element analysis for both specimens. ABAQUS was used in the analysis.

$$C_{ij} = \begin{bmatrix} 194.36 & 63.9 & 35.24 & 0 & 0 & 0 \\ 63.9 & 165.7 & 63.9 & 0 & 0 & 0 \\ 35.24 & 63.9 & 194.36 & 0 & 0 & 0 \\ 0 & 0 & 0 & 79.56 & 0 & 0 \\ 0 & 0 & 0 & 0 & 50.9 & 0 \\ 0 & 0 & 0 & 0 & 0 & 79.56 \end{bmatrix} GPa \tag{30}$$

For the materials considered, using the asymptotic singularity analysis described in Section 2, we obtain the eigenvalues $\lambda_I = 0.5078$, $\lambda_{II} = 0.6199$. The angular variation of the stress and displacement fields $f_{ij}^{I}(\theta)$, $g_i^{I}(\theta)$, $f_{ij}^{I*}(\theta)$ and $g_i^{I*}(\theta)$ are shown in Fig. 3 (a), and $f_{ij}^{II}(\theta)$, $g_i^{II}(\theta)$, $f_{ij}^{II*}(\theta)$ and $g_i^{II*}(\theta)$ are shown in Fig. 3 (b) where $i, j = r, \theta$.

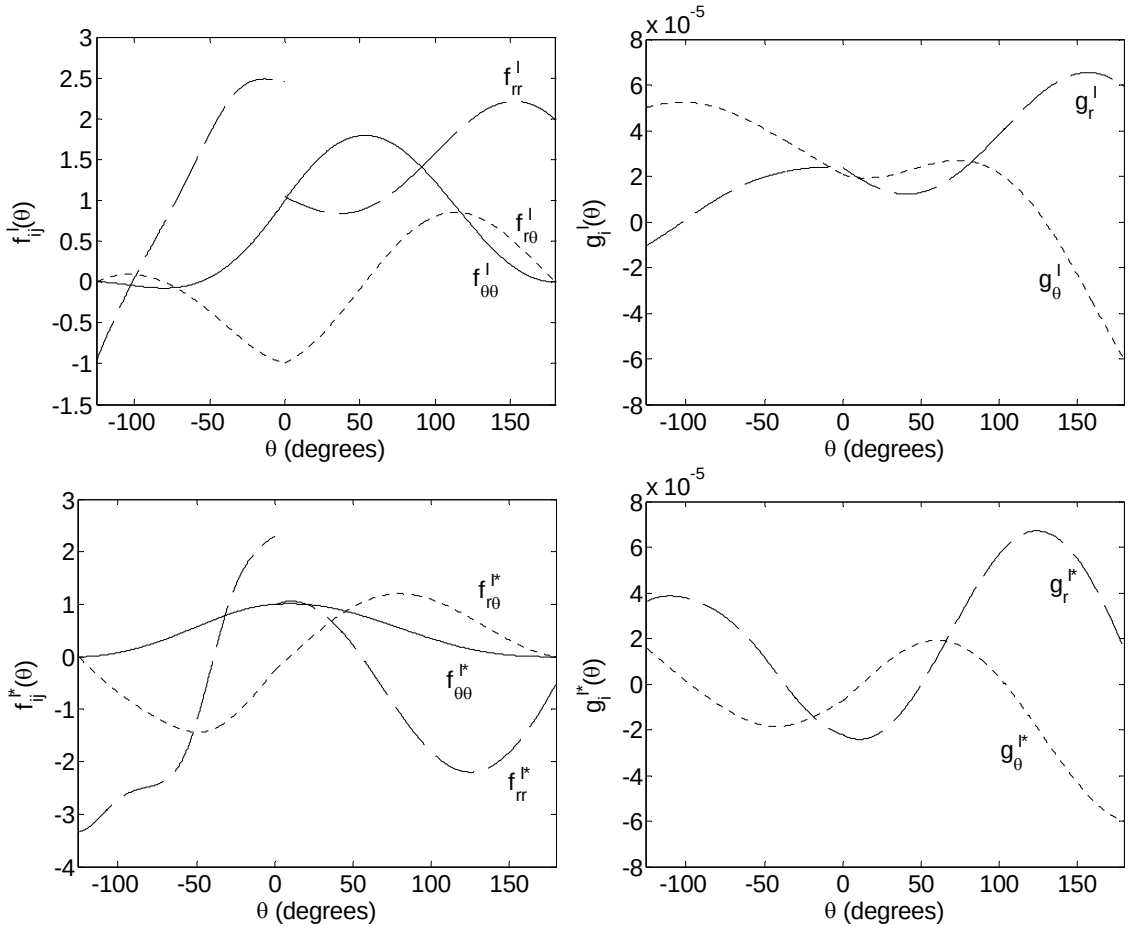

(a)

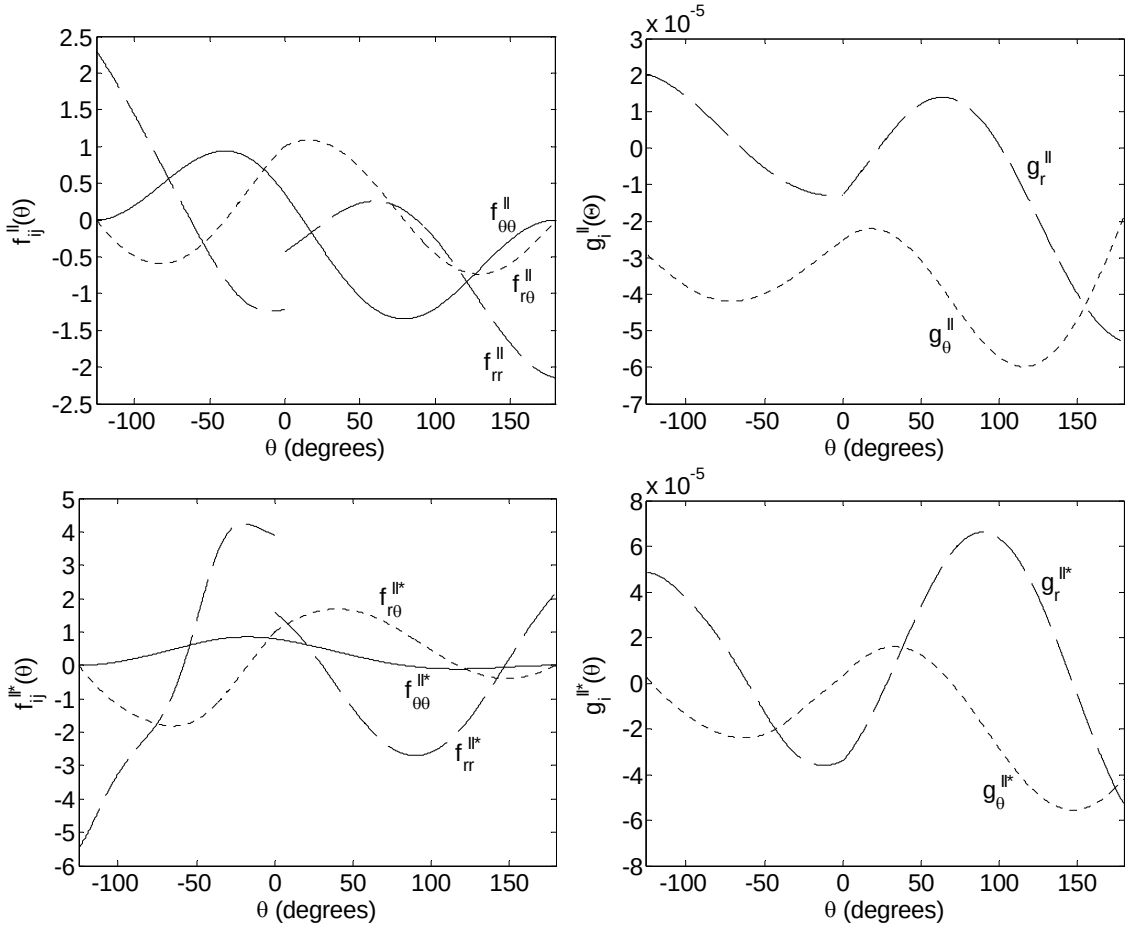

(b)

Fig. 3. Angular variation of the stress and displacement fields (a) $f_{ij}^{I}(\theta)$, $g_i^{I}(\theta)$, $f_{ij}^{I*}(\theta)$, $g_i^{I*}(\theta)$ and (b) $f_{ij}^{II}(\theta)$, $g_i^{II}(\theta)$, $f_{ij}^{II*}(\theta)$, $g_i^{II*}(\theta)$ for Si-Glass-Si triple stacks with notch angle $\gamma = 54.74^{\circ}$

In order to study the effect of glass thickness and bond area on the fracture behavior, dimensional considerations of K_m^n yield the following form:

$$K_m^n = \sigma_0 w^{1-\lambda_m} Y_m^n\left(\tfrac{a}{w}, \tfrac{h}{w}, \tfrac{t}{h}\right) \tag{31}$$

where $Y_m^n\left(\tfrac{a}{w}, \tfrac{h}{w}, \tfrac{t}{h}\right)\left(m = I, II\right)$ is a dimensionless calibration function and is specific for the geometry, the thickness of glass layer, boundary conditions, and elastic constants. In this study, we only take a fixed value of $\tfrac{h}{w} = 0.0103$; consequently, $Y_m^n\left(\tfrac{a}{w}, \tfrac{h}{w}, \tfrac{t}{h}\right)$ reduces to $Y_m^n\left(\tfrac{a}{w}, \tfrac{t}{h}\right)$. Furthermore, we can write

$$\begin{aligned} Y_m^n\left(\tfrac{a}{w}, \tfrac{t}{h}\right) &= Y_{ref1} \cdot f_1(\tfrac{a}{w}) \cdot g_1(\tfrac{t}{h}) \quad \text{for MESA} \\ Y_m^n\left(\tfrac{b}{w}, \tfrac{t}{h}\right) &= Y_{ref2} \cdot f_2(\tfrac{b}{w}) \cdot g_2(\tfrac{t}{h}) \quad \text{for FRAME} \end{aligned} \tag{32}$$

where

$$f_1(\tfrac{a}{w}) = \frac{Y_m^n\left(\tfrac{a}{w}, \tfrac{t}{h} = 0.2\right)}{Y_{ref1}}, \; g_1(\tfrac{t}{h}) = \frac{Y_m^n\left(\tfrac{a}{w} = 0.286, \tfrac{t}{h}\right)}{Y_{ref1}}, \; Y_{ref1} = Y_m^n\left(\tfrac{a}{w} = 0.286, \tfrac{t}{h} = 0.2\right)$$

$$f_2(\tfrac{b}{w}) = \frac{Y_m^n\left(\tfrac{b}{w}, \tfrac{t}{h} = 0.2\right)}{Y_{ref2}}, \; g_2(\tfrac{t}{h}) = \frac{Y_m^n\left(\tfrac{b}{w} = 0.114, \tfrac{t}{h}\right)}{Y_{ref2}}, \; Y_{ref2} = Y_m^n\left(\tfrac{b}{w} = 0.114, \tfrac{t}{h} = 0.2\right)$$

4.2 Results

4.2.1 Validation of the H-integral approach

Before it can be conveniently applied to study the fracture problem, the accuracy of the H-integral should be quantified for the Si-Glass-Si triple stack problem. It is found that for the MESA and FRAME specimens, the stress intensity factors calculated from the H-integral agree very well with asymptotic solutions obtained directly by finite element computations of displacements along the notch flanks or of the stress along the interface. The variations are within 5% for all calculations.

Table 1 – Table 4 (Y_{ref} in boldface) show the dimensionless stress intensity factors Y_I^n and Y_{II}^n obtained from H-integral and asymptotic analysis with different bond length and glass thickness for both MESA and FRAME specimens.

Table 1

Y_I^n and Y_{II}^n obtained from H-integral and asymptotic analysis with $\frac{a}{w} = 0.286$ for MESA specimens.

t/h	$Y^I_{H\text{-integral}}$	$Y^I_{u0\text{-asymptotic}}$	$Y^I_{s00\text{-asymptotic}}$	$Y^{II}_{H\text{-integral}}$	$Y^{II}_{u0\text{-asymptotic}}$	$Y^{II}_{s00\text{-asymptotic}}$
0.167	0.477	0.461	0.488	0.986	0.942	0.972
0.200	**0.479**	0.464	0.488	0.978	0.937	0.966
0.278	0.483	0.469	0.489	0.964	0.928	0.955
0.556	0.491	0.479	0.492	0.935	0.910	0.932

Table 2

Y_I^n and Y_{II}^n obtained from H-integral and asymptotic analysis with $\frac{t}{h} = 0.2$ for MESA specimens

a/w	$Y^I_{H\text{-integral}}$	$Y^I_{u0\text{-asymptotic}}$	$Y^I_{s00\text{-asymptotic}}$	$Y^{II}_{H\text{-integral}}$	$Y^{II}_{u0\text{-asymptotic}}$	$Y^{II}_{s00\text{-asymptotic}}$
0.200	0.579	0.561	0.589	1.177	1.128	1.163
0.286	**0.479**	0.464	0.488	0.978	0.937	0.966
0.404	0.394	0.381	0.401	0.806	0.776	0.797
0.486	0.350	0.339	0.357	0.719	0.695	0.711
0.571	0.311	0.302	0.317	0.640	0.612	0.633

Table 3

Y_I^n and Y_{II}^n obtained from H-integral and asymptotic analysis with $\frac{b}{w} = 0.114$ for FRAME specimens.

t/h	$Y^I_{H\text{-integral}}$	$Y^I_{u0\text{-asymptotic}}$	$Y^I_{s00\text{-asymptotic}}$	$Y^{II}_{H\text{-integral}}$	$Y^{II}_{u0\text{-asymptotic}}$	$Y^{II}_{s00\text{-asymptotic}}$
0.167	0.494	0.478	0.506	1.020	0.980	1.010
0.200	**0.497**	0.481	0.506	1.018	0.979	1.005
0.278	0.503	0.488	0.509	1.007	0.973	0.998
0.556	0.518	0.506	0.520	0.991	0.970	0.986
1.000	0.536	0.524	0.536	0.983	0.963	0.982

Table 4

Y_I^n and Y_{II}^n obtained from H-integral and asymptotic analysis with $\frac{t}{h}=0.2$ for FRAME specimens.

b/w	$Y^I_{H\text{-integral}}$	$Y^I_{u\theta\text{-asymptotic}}$	$Y^I_{s0\theta\text{-asymptotic}}$	$Y^{II}_{H\text{-integral}}$	$Y^{II}_{u\theta\text{-asymptotic}}$	$Y^{II}_{s0\theta\text{-asymptotic}}$
0.114	**0.497**	0.481	0.506	1.018	0.979	1.005
0.229	0.335	0.325	0.341	0.693	0.668	0.685
0.343	0.275	0.266	0.280	0.571	0.546	0.564
0.457	0.246	0.238	0.250	0.511	0.492	0.505
0.543	0.234	0.227	0.238	0.486	0.466	0.480

4.2.2 Empirical solutions of Y_I^n and Y_{II}^n for MESA and FRAME specimens

To facilitate engineering application, we established empirical solutions of Y_I^n for MESA and FRAME specimens. The following geometrical ranges are considered: the solutions are applicable over the range $0.2 \le \frac{a}{w} \le 0.571,\ 0.167 \le \frac{t}{h} \le 0.556$ for MESA specimens, and over the range $0.114 \le \frac{b}{w} \le 0.543,\ 0.167 \le \frac{t}{h} \le 1$ for FRAME specimens, respectively. According to Eq. (32), the normalized results obtained from H-integral approach are accurately fitted by the power function $f_i\left(geometry\right) = j\left(geometry\right)^k$ and $g_i\left(geometry\right) = l\left(geometry\right)^s$, $i = 1, 2$. The best-fit values of the parameters j, k, l and s are shown in Fig. 4 and Fig. 5 for MESA and FRAME, respectively.

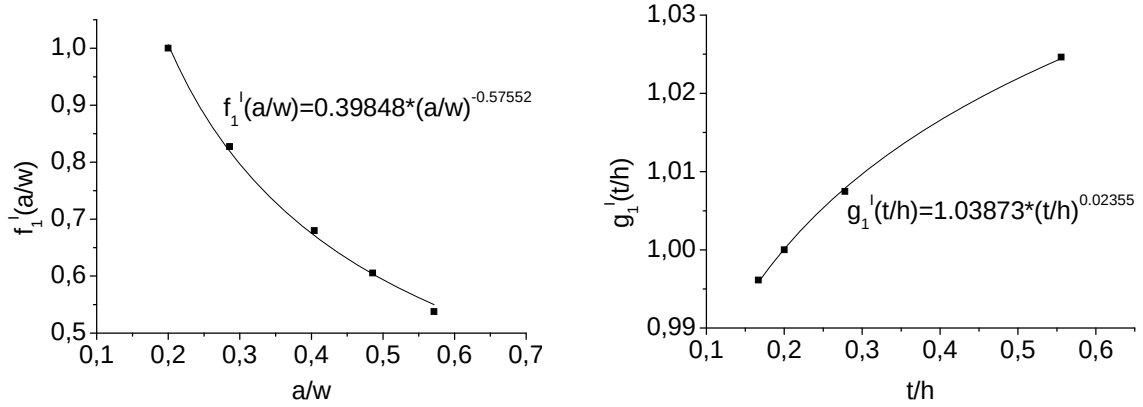

Fig. 4. $f_1^I(\frac{a}{w})$ and $g_1^I(\frac{t}{h})$ for MESA specimens $(0.2 \le \frac{a}{w} \le 0.571,\ 0.167 \le \frac{t}{h} \le 0.556)$

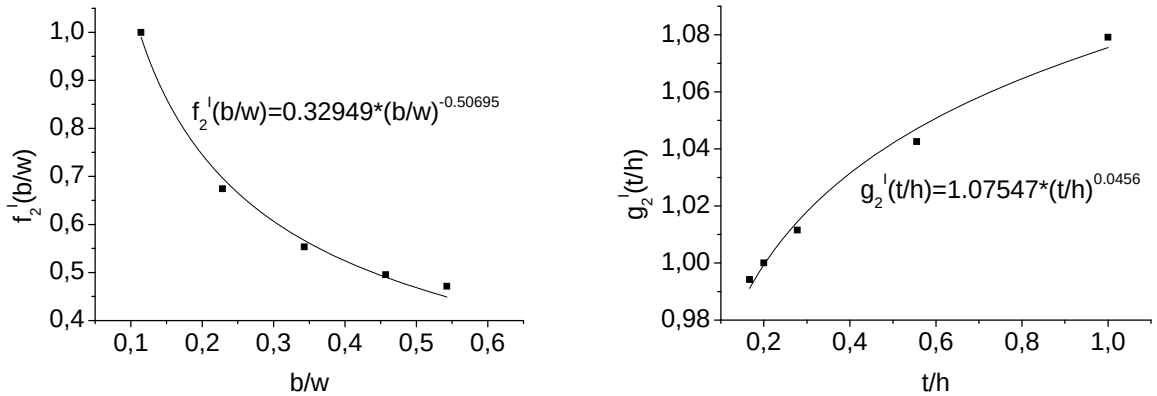

Fig. 5. $f_2^I(\frac{b}{w})$ and $g_2^I(\frac{t}{h})$ for FRAME specimens $(0.114 \le \frac{b}{w} \le 0.543,\ 0.167 \le \frac{t}{h} \le 1)$

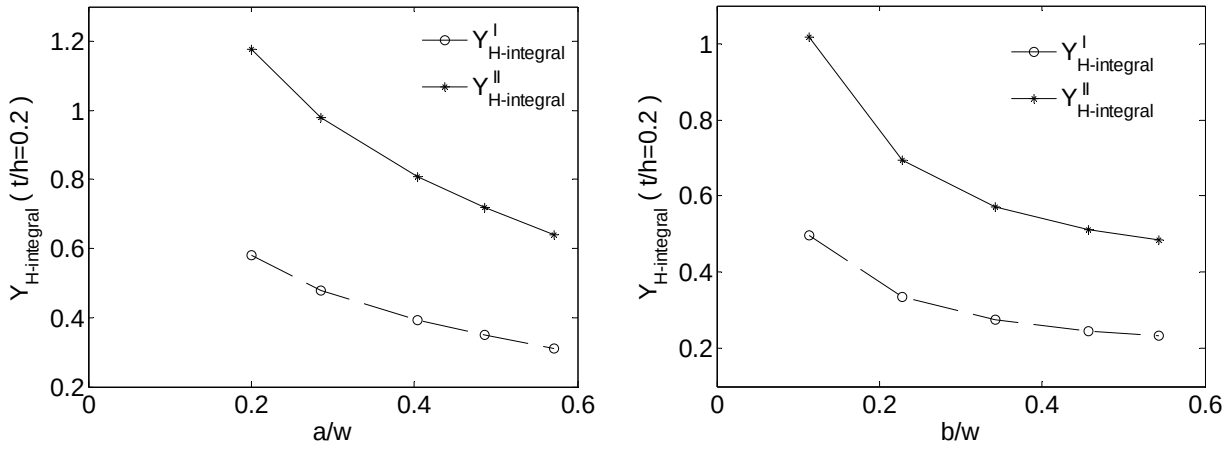

Fig. 6. $Y^{I}_{H-\mathrm{int}egral}$ and $Y^{II}_{H-\mathrm{int}egral}$ for (a) MESA specimens and (b) FRAME specimens

From Eqs. (4.2) and (4.3), the dimensionless stress intensity factor Y^{n}_{I} obtained from the H-integral can be fitted by the following functions:

$$Y^{I}_{H\text{-}\mathrm{int}egral}\left(\tfrac{a}{w},\tfrac{t}{h}\right)=Y^{I}_{ref\,1}\times 0.39848\left(\tfrac{a}{w}\right)^{-0.57552}\times 1.03873\left(\tfrac{t}{h}\right)^{0.02355} \tag{33}$$

where

$$Y^{I}_{ref\,1}=Y^{I}_{\left(\frac{a}{w}=0.286,\frac{t}{h}=0.2\right)}=0.479 \quad \text{and} \quad 0.2\le\tfrac{a}{w}\le 0.571,\ 0.167\le\tfrac{t}{h}\le 0.556.$$

for the MESA specimens, and

$$Y^{I}_{H\text{-}\mathrm{int}egral}\left(\tfrac{b}{w},\tfrac{t}{h}\right)=Y^{I}_{ref\,2}\times 0.32949\left(\tfrac{b}{w}\right)^{-0.50695}\times 1.07547\left(\tfrac{t}{h}\right)^{0.0456} \tag{34}$$

where

$$Y^{I}_{ref\,2}=Y^{I}_{\left(\frac{b}{w}=0.114,\frac{t}{h}=0.2\right)}=0.497 \text{ and } 0.114\le\tfrac{b}{w}\le 0.543,\ 0.167\le\tfrac{t}{h}\le 1.$$

for the FRAME specimens.

Fig. 6 compares the $Y^{I}_{H-\mathrm{int}egral}$ and $Y^{II}_{H-\mathrm{int}egral}$. It can be observed from Fig. 6 that both $Y^{I}_{H-\mathrm{int}egral}$ and $Y^{II}_{H-\mathrm{int}egral}$ decrease with increasing bond area.

4.2.3 Effect of glass thickness

In order to understand the effect of glass thickness on the stress intensity factor, we have artificially extended glass thickness to $t=1750\mu m$. Fig. 7 compares the thin-film MESA specimen with glass thickness $t=3\mu m$ and the extreme bimaterial MESA specimen with glass thickness $t=1750\mu m$. It can be observed that the thicker the glass layer, the higher the $Y^{I}_{H-\mathrm{int}egral}$.

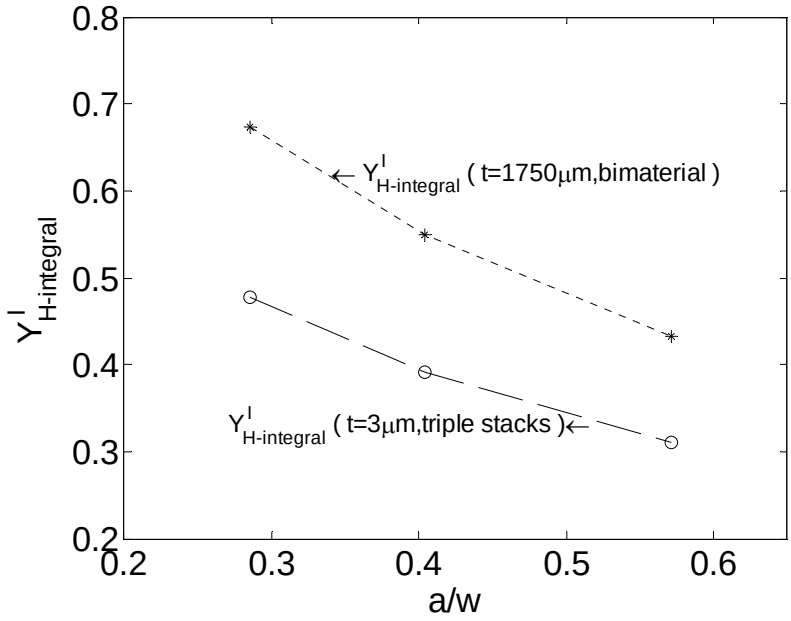

Fig. 7. The dimensionless stress intensity factors for two glass thicknesses.

It also has been found from Fig. 8 that the Y_I^n increases with glass thickness while basically decreases for mode II loading as the glass thickness increases. Furthermore, for thin-film MESA and FRAME specimens, Fig. 9, it can be observed that varying thickness of glass does not affect Y_I^n and Y_{II}^n significantly. Nevertheless, for the other MESA specimens with thicker glass layer, the stress intensity factors differ greatly. Hence, it can be concluded that the glass thickness is an important geometrical quantity affecting the stress intensity factors for triple stacks with thick glass layer.

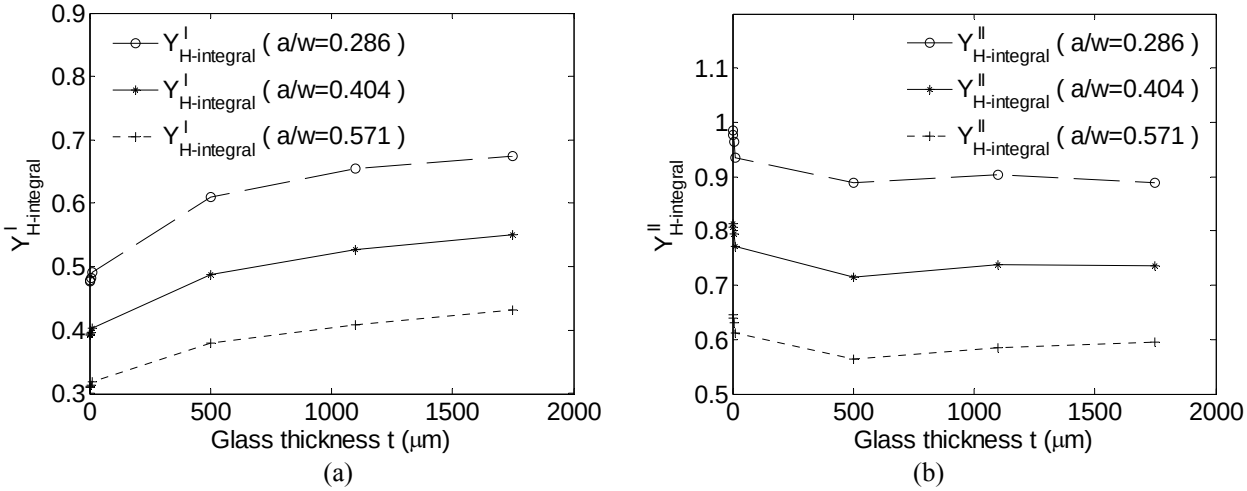

Fig. 8. (a) $Y^{I}_{H-\text{integral}}$ and (b) $Y^{II}_{H-\text{integral}}$ for MESA specimens with glass thickness over the range $3-1750\mu m$

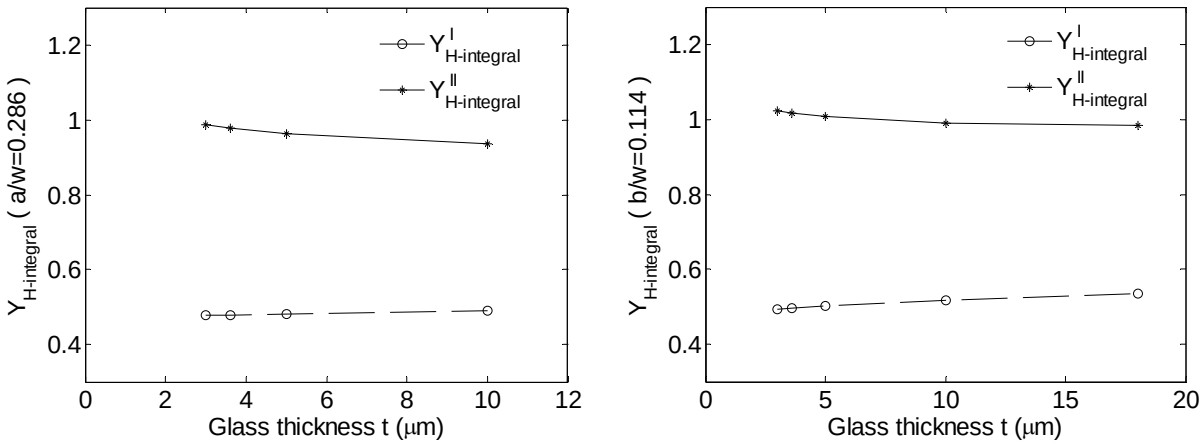

Fig. 9. $Y^{I}_{H-integral}$ and $Y^{II}_{H-integral}$ for thin-film (a) MESA and (b) FRAME triple stacks

4.2.4 Failure criterion

Fracture resistance of structural components with stress concentration at sharp notches can be evaluated by different failure criteria. As discussed earlier, the notch tip in both MESA and FRAME specimens is subjected to mixed-mode loading. It is interesting to investigate the failure criterion. In order to assess whether K^{n}_{IC} can be used to predict fracture initiation, various MESA and FRAME specimens were designed for pull tests (Visser, 2002). Ten to twenty different test specimens were used for each specific bond area and the experimental failure strength was fitted to Weibull distributions. Chips were glued onto grinded hexagonal head cap screws with a thin layer of Micro Bond^{TM} III CTCA3-3 or Loctite 420. The dimensions of the test specimen are summarized in Table 5. One wafer in each wafer couple for thin-film anodic bonding experiment was covered with a sputtered layer of PYREX, Corning#7740 glass ($3.6 \pm 0.2 \mu m$ thick) on top of a thin dielectric layer. A thin dielectric layer was always grown or deposited before sputtering of the glass layer so as to reduce the possibility of electrical breakdown during the bonding process. The thin dielectric layer was removed from the backside of the wafers before bonding for electrical contacting.

Table 5

Dimensions of bond areas for test specimens for pull tests (Visser, 2002).

Geometry name	**Outer dimensions (μm×μm)**	**Inner dimensions (μm×μm)**
MESA 1	1000 × 1000	-
MESA 2	1414× 1414	-
MESA 3	2000 × 2000	-
FRAME 1	2700 × 2700	2300 × 2300
FRAME 2	2700 × 2700	1900 × 1900
FRAME 3	2700 × 2700	1100 × 1100
Etch process	500 g KOH : 1 l DIW, 80 °C, 18-20 μm	

It is well known that a traditional yield criterion is not applicable to correlate with failure because typically the failure load measured from tests depends on specimen geometry, size and type of remote loading. Instead, some studies have shown that the critical stress intensity factor K_C^n can be used as a single parameter to correlate fracture initiation at sharp notches, which is possibly independent of some geometry parameters (e.g., Dunn et al., 1997a; 2000; Labossiere and Dunn, 1999; Suwito, 1997).

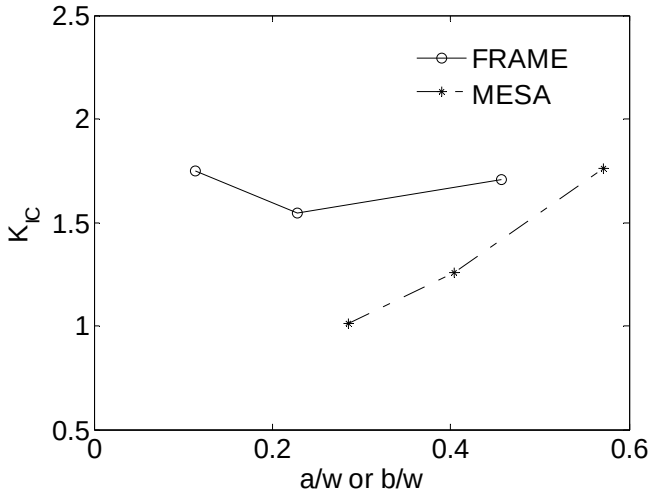

Fig. 10. The critical stress intensity factor for MESA and FRAME specimens

The corner in the present test specimens involves mixed-mode deformation. From the asymptotic analysis, the stress singularity for mode I is strong, but it is weaker for mode II. This is discussed by Dunn et al. (2000). In this case, the critical stress intensity $K_C^n = \left\{K_{IC}^n, K_{IIC}^n\right\}$ is mainly characterized by K_{IC}^n. The critical notch stress intensity factor, K_{IC}^n, can be computed from Eq. (4.2) using $\sigma_0 = \sigma_f$, the nominal failure strength, which is calculated using the measured failure force divided by the overall structure cross-section area in the pull test. According to average fracture strength σ_f (Visser, 2002), the critical stress intensity factors K_{IC}^n based on the test specimens are shown in Fig. 10. For the MESA specimen, the critical stress intensity factor K_{IC}^n obtained for the averaged failure strength for the three specimens of different bond length are 1.01, 1.26 and 1.76 $MPa \cdot mm^{0.4922}$, respectively; while for the FRAME, the corresponding critical stress intensity factors are 1.75, 1.54 and 1.71 $MPa \cdot mm^{0.4922}$. The average value of K_{IC}^n is 1.34$MPa \cdot mm^{0.4922}$ for MESA specimens and 1.67$MPa \cdot mm^{0.4922}$ for FRAME specimens, respectively. The averaged experimental nominal failure strengths and the strengths calculated using the averaged K_{IC}^n for the different bond area are shown in Table 6 and Fig. 11. It can be seen that the averaged K_{IC}^n can be used to predict brittle fracture of the anodic-bonded FRAME specimens. However, for the MESA specimens the agreement is not very satisfactory. The cause of deviations for MESA specimens will be studied subsequently in more detail (Section 5.2).

Table 6

Comparison of the experimental and predicted nominal failure strength σ_f

Specimen	Weibull average experimental σ_f (MPa)	Predicted σ_f (MPa)	Specimen	Weibull average experimental σ_f (MPa)	Predicted σ_f (MPa)
MESA1	1.600	2.126	FRAME 1	2.674	2.545
MESA2	2.424	2.587	FRAME 2	3.497	3.775
MESA3	4.286	3.271	FRAME 3	5.257	5.139

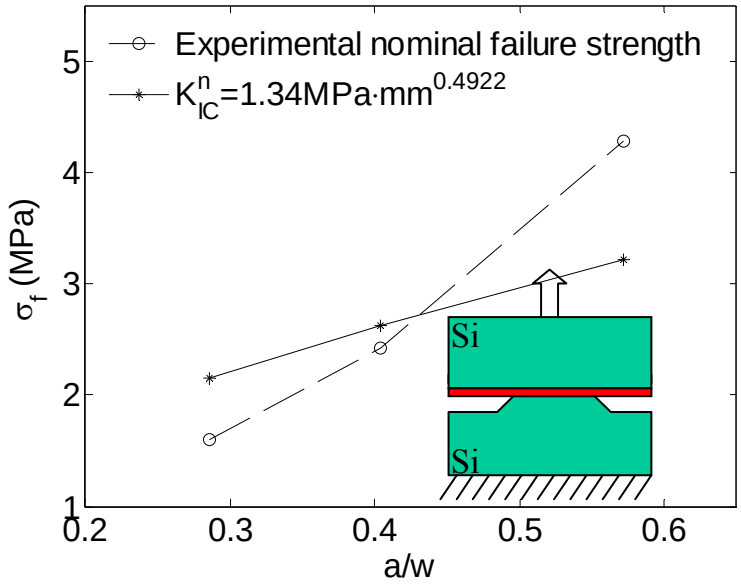

(a)

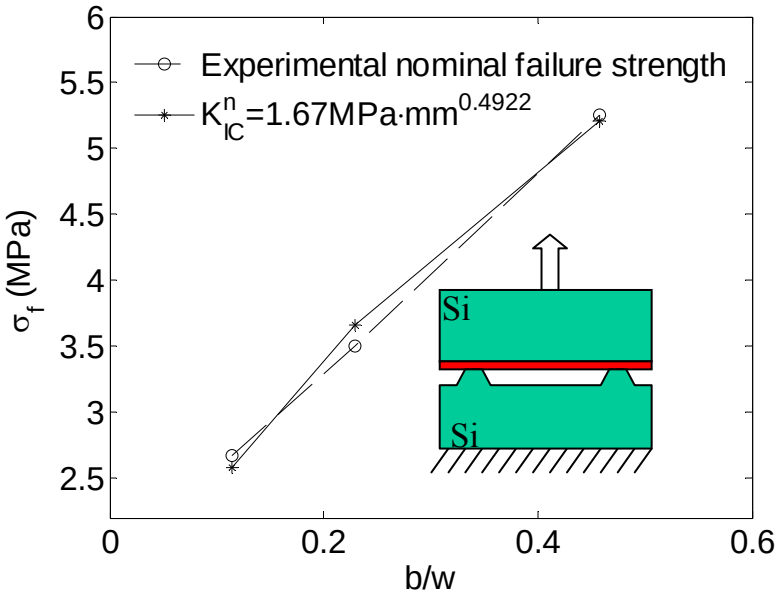

(b)

Fig. 11. The experimental and predicted nominal failure strength σ_f for (a) MESA and (b) FRAME

It should be noted that the failure strength employed in the industry is defined as the measured failure force divided by the overall bonded area, i.e., the net-section bond strength σ_N (see Fig. 12). The bond strength for MESA and FRAME specimens are shown in Fig. 13. It can be seen from Fig. 13 that a distinct geometry dependence is not observed for MESA specimens, but for FRAME specimens a significant geometry effect can be seen. With respect to the bond area, a large bond strength of the thinnest FRAME was observed, but increasing the bond area for the FRAME specimen does not necessarily lead to a proportionally higher resistance against an externally applied force.

The failure criterion applied here is based on the assumption that K-dominated annulus exists around the interface corner. The elastic fields can neither be very close to notch tip which is disturbed by material nonlinearities and geometric irregularities nor be far away from the interface corner which is affected by far-field loading and boundaries. To qualify this K-dominated annulus, finite element analysis is performed at failure loads. The accuracy of the failure criterion is further depicted in Fig. 14 which shows a logarithmic diagram of the interface normal and shear stresses near the notch tip with $\frac{b}{w} = 0.229$ and $\frac{t}{h} = 0.2$. The normal stress $\sigma_{\theta\theta}$ obtained from two methods agrees to 5% within a distance of $2.5\,\mu m$ while the shear stress $\sigma_{r\theta}$ agrees to 10% within a distance of $0.7\,\mu m$. Similar results are obtained for other specimens.

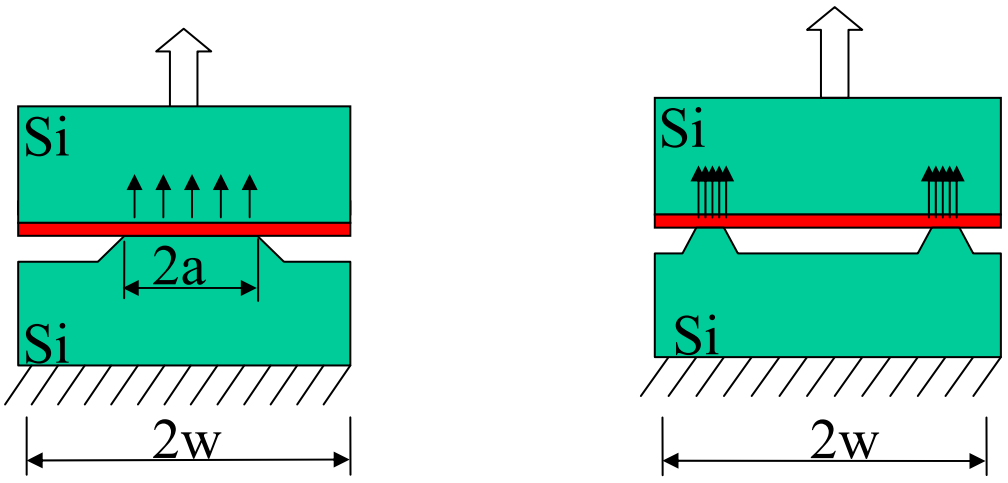

(a) (b)

Fig. 12. Schematic definition of net-section bond strength σ_N for (a) MESA and (b) FRAME

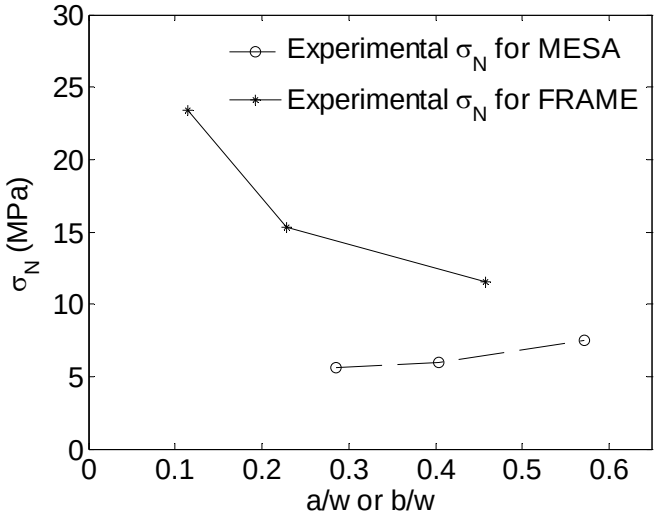

Fig. 13. Net-section bond strength σ_N for MESA and FRAME specimens

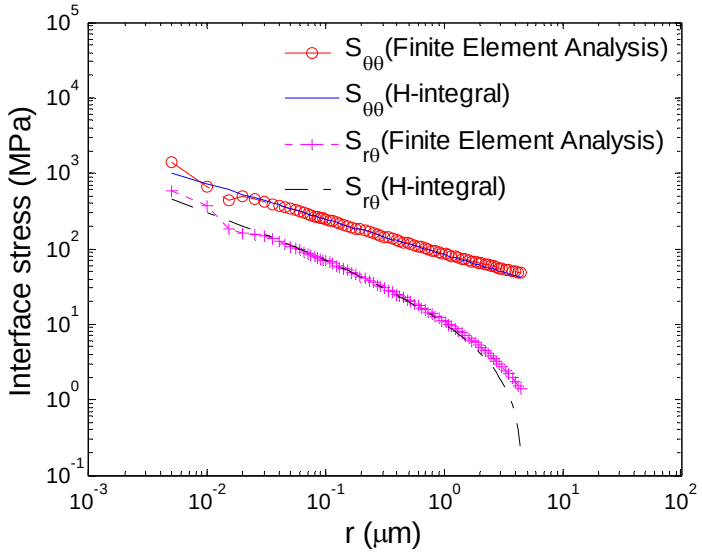

Fig. 14. Interface stress near the notch tip with $\frac{b}{w} = 0.229$ and $\frac{t}{h} = 0.2$ for FRAME specimens

5. Discussion

5.1 Mesh effect

The important feature of H-integral approach is that a relatively coarse mesh can be used for the finite element analysis (e.g., Labossiere and Dunn, 1999; Zhang and Mikkola, 1992). For example, for MESA specimen with $\frac{a}{w} = 0.286$ and $\frac{t}{h} = 0.278$, a fine and coarse mesh near the notch tip are depicted in Fig. 15. Through the glass layer, only five elements are created for the coarse mesh model while 39 elements are used for the fine mesh model. The smallest element size for the fine and coarse mesh is 0.01 and 1 μm, respectively. It should be pointed out that the smallest mesh size is restricted by geometric conditions around the notch tip, such as glass thickness, etching depth and so on. Furthermore, four integral contours around the notch tip are tested with the coarse meshes and the values of stress intensity factors are 2.154, 2.137, 2.155, and

2.145 $MPa \cdot mm^{0.4922}$, respectively. As a result, the deviation of stress intensity from 2.137 $MPa \cdot mm^{0.4922}$ obtained from fine mesh is less than 1%.

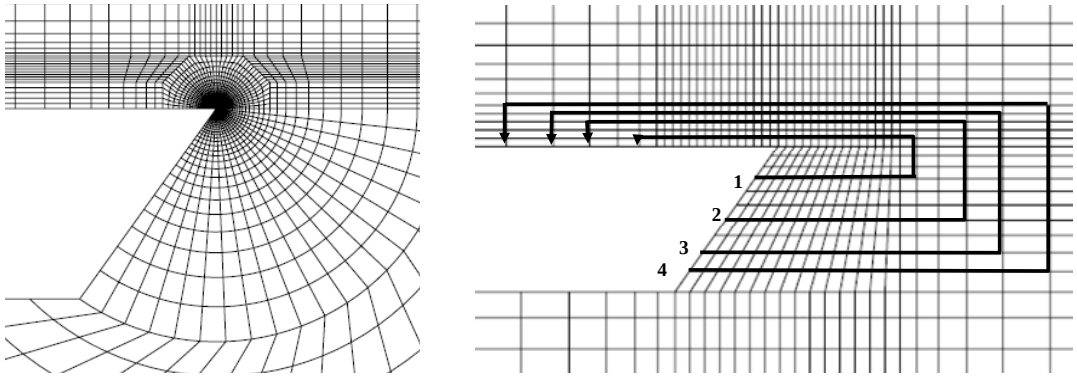

Fig. 15. (a) Fine mesh and (b) coarse mesh at a close look near the notch tip

For MESA Specimen with $\frac{a}{w} = 0.286$ and $\frac{t}{h} = 0.278$

5.2 Uncertainties

In this section, we further interpret the reasons resulting in deviation for MESA specimens and discuss the applicability of a critical stress intensity factor.

For the MESA specimens, the predicted nominal failure strength did not match very well with experimental values. We believe this is mainly due to the difficult control of the loading alignment. The effect of misalignment has been further studied, Fig. 16. Several misalignment values have been tried. It has been found that a loading misalignment of $D = 300\mu m$ will result in a much better agreement. The FRAME specimens are less sensitive to loading misalignment due to large redundancy.

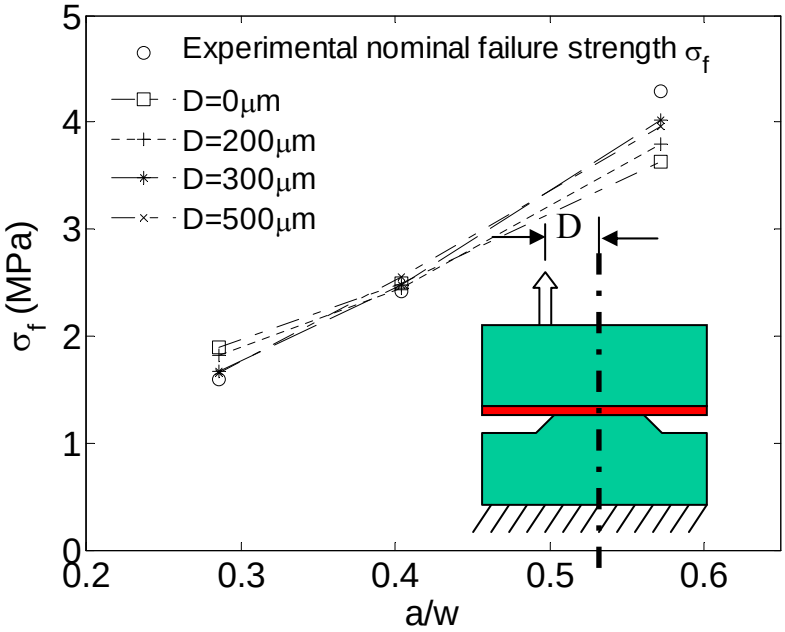

Fig. 16. The effect of loading misalignment on the predicted nominal failure strength σ_f

An important issue for notch mechanics is to understand the applicability of the critical stress intensity factor K_{IC}^{n} for interface corners. Actually, K_{IC}^{n} can no longer be simply treated as a size-independent material parameter like that in the linear elastic fracture mechanics. It depends not only on interface corner geometry and material elastic constants, but also on interface strength resulting in diverse failure modes. For instance, Dunn et al. (2000) and Labossiere et al. (2002) carried out similar tests with a weaker interface and obtained smaller critical stress intensity factor than that with a strong interface. For the test specimens employed herein, we have a strongly bonded interface and it was also observed that fracture initiated from the notch tip and propagated into the glass or partly along the bonded interface.

In addition, residual stress can possibly influence the results and it deserves attention in the future work. It may be one of the reasons for the scatter of failure strength in the tests.

Furthermore, it is observed from finite element analyses that the thickness of Si-wafers also affects the dimensionless stress intensity factor. For thin Si-wafers, for example, 0.35-1.75mm thick, the values of stress intensity can apparently vary with thickness of Si-wafers. However, when Si-wafers are thick enough, for instance, larger than 1.75mm, the thickness dependence will disappear. This effect will be investigated more in the future.

Finally, the critical stress intensity factor K_{IC}^{n} derived here did not yield the same value for both MESA and FRAME specimens with the same notch angle. The exact reasons are not apparent. Apart from the discussions above, the possible reasons leading to the differences are as follows: the simplified use of a single parameter K_{IC}^{n} in mixed-mode loading, the control of loading alignment, different failure modes and the effect of residual stress.

6. Conclusions

For the triple stacks interface corner problem considered in this paper, the stress intensity factors obtained from the H-integral approach show excellent agreement with those obtained from the asymptotic solutions by finite element calculations of displacements along the notch flanks or of stresses along the interface. The deviation of the displacement approach and the stress approach from the H-integral approach is less than 5%.

The effect of glass thickness on the stress intensity factor has been studied. It has been found that the mode I stress intensity factor increases with glass thickness while basically decreases for mode II loading as the glass thickness increases. Moreover, the stress intensity factors vary significantly with a thicker glass layer but are not affected greatly for thin-film anodic-bonded triple stacks. Hence, it turns out that the glass thickness is an important geometrical quantity affecting the stress intensity factors for triple stacks with a thick glass layer.

In order to facilitate engineering application, empirical solutions of stress intensity factors for MESA and FRAME specimens have been proposed. It should be pointed out that the critical stress intensity factor K_{IC}^{n} depends on the interface corner geometry, material elastic constants, failure modes and residual stress. In this paper, $K_{IC}^{n}=1.34MPa\cdot mm^{0.4922}$ and $K_{IC}^{n}=1.67MPa\cdot mm^{0.4922}$ have been used to characterize MESA and FRAME specimens, respectively. Loading alignment has been found to play a significant role in fracture behavior of MESA specimens.

Reference List

Bogy, D. B., Wang, K. C., (1971). Stress Singularities at Interface Corners in Bonded Dissimilar Materials. International Journal of Solids and Structures 7**,** 993-1005.

Brooks, A. D., Hardesty, C. A., Donovan, R. P., (1972). Low-Temperature Electrostatic Silicon-To-Silicon Seals Using Sputtered Borosilicate Glass. Journal of the Electrochemical Society 119**,** 545-546.

Cho, S. B., Lee, K. R., Choy, Y. S., Yuuki, R., (1992). Determination of Stress Intensity Factors and Boundary Element Analysis for Interface Cracks in Dissimilar Anisotropic Materials. Engineering Fracture Mechanics 43**,** 603-614.

Choi, W. B., Ju, B. K., Lee, Y. H., Jeong, J. W., Haskard, M. R., Lee, N. Y., Sung, M. Y., Oh, M. H., (1997). Experimental analysis on the anodic bonding with an evaporated glass layer. Journal of Micromechanics and Microengineering 7**,** 316-322.

Dempsey, J. P., Sinclair, G. B., (1979). On the Stress Singularities in the Plane Elasticity of the Composite Wedge. Journal of Elasticity 9**,** 373-391.

Dempsey, J. P., Sinclair, G. B., (1981). On the Singular Behavior at the Vertex of a Bimaterial Wedge. Journal of Elasticity 11**,** 317-327.

Dunn, M. L., Cunningham, S. J., Labossiere, P. E. W., (2000). Initiation toughness of silicon/glass anodic bonds. Acta Materialia 48**,** 735-744.

Dunn, M. L., Suwito, W., Cunningham, S., (1997a). Fracture initiation at sharp notches: Correlation using critical stress intensities. International Journal of Solids and Structures 34**,** 3873-3883.

Dunn, M. L., Suwito, W., Cunningham, S., May, C. W., (1997b). Fracture initiation at sharp notches under mode I, mode II, and mild mixed mode loading. International Journal of Fracture 84**,** 367-381.

Eshelby, J. D., Read, W. T., Shockley, W., (1953). Anisotropic Elasticity with Applications to Dislocation Theory. Acta Metallurgica 1**,** 251-259.

Hein, V. L., Erdogan, F., (1971). Stress Singularities in a Two Material Wedge. International Journal of Fracture Mechanics 7**,** 317-330.

Hutchinson, J. W., Suo, Z., (1992). Mixed-Mode Cracking in Layered Materials. Advances in Applied Mechanics, Vol 29 29**,** 63-191.

Labossiere, P. E. W., Dunn, M. L., (1999). Stress intensities at interface corners in anisotropic bimaterials. Engineering Fracture Mechanics 62**,** 555-575.

Labossiere, P. E. W., Dunn, M. L., Cunningham, S. J., (2002). Application of bimaterial interface corner failure mechanics to silicon/glass anodic bonds. Journal of the Mechanics and Physics of Solids 50**,** 405-433.

Mason, W. P., (1958). Physical Acoustics and the Properties of Solids. Van Nostrand, New York.

Pageau, S. S., Joseph, P. F., Biggers, S. B., (1995). Finite-Element Analysis of Anisotropic Materials with Singular Inplane Stress-Fields. International Journal of Solids and Structures 32**,** 571-591.

Quenzer, H. J., Schulz, A. V., Kinkopf, T., Helm, T., (2001). Anodic-bonding on glass layers prepared by a

spin-on glass process: preparation process and experimental results. Transducers'01, Eurosensors XV (The 11th International Conference on Solid-State Sensors and Actuators).

Stroh, A. N., (1958). Dislocations and Cracks in Anisotropic Elasticity. Philosophical Magazine 3**,** 625-646.

Suwito, W., (1997). Fracture of notched silicon microstructures. Ph.D thesis, University of Colorado.

Suwito, W., Dunn, M. L., Cunningham, S. J., (1998). Fracture initiation at sharp notches in single crystal silicon. Journal of Applied Physics 83**,** 3574-3582.

Suwito, W., Dunn, M. L., Cunningham, S. J., Read, D. T., (1999). Elastic moduli, strength, and fracture initiation at sharp notches in etched single crystal silicon microstructures. Journal of Applied Physics 85**,** 3519-3534.

Ting, T. C. T., (1996). Anisotropic Elasticity: Theory and Applications. Oxford University Press, New York.

Ting, T. C. T., (1997). Stress Singularities at the Tip of Interfaces in Polycrystals. Damage and Failure of Interfaces, Rossmanith (ed.) 75-82.

Ting, T. C. T., Chou, S. C., (1981). Edge Singularities in Anisotropic Composites. International Journal of Solids and Structures 17**,** 1057-1068.

Visser, M. M., (2002). Wafer bonding for MEMS. Ph.D Thesis, University of Oslo.

Wallis, G., Pomerantz, D. I., (1969). Field Assisted Glass-Metal Sealing. Journal of Applied Physics 40**,** 3946-3949.

Williams, M. L., (1952). Stress Singularities Resulting from Various Boundary Conditions in Angular Corners of Plates in Extension. Journal of Applied Mechanics-Transactions of the ASME 19**,** 526-528.

Wu, K. C., Chang, F. T., (1993). Near-Tip Fields in A Notched Body with Dislocations and Body Forces. Journal of Applied Mechanics-Transactions of the ASME 60**,** 936-941.

Wu, K. C., Chen, C. T., (1996). Stress analysis of anisotropic elastic V-notched bodies. International Journal of Solids and Structures 33**,** 2403-2416.

Zhang, Z. L., Mikkola, T. P. J., (1992). A Simple Path-Independent Integral for Calculating Mixed-Mode Stress Intensity Factors. Fatigue & Fracture of Engineering Materials & Structures 15**,** 1041-1049.

PAPER II

Evaluation of fracture mechanics parameters for free edges in multi-layered structures with weak singularities

Shang LY, Zhang ZL and Skallerud B.

*International Journal of Solids and Structures 2009;**46**(5):1134-48.*

Evaluation of fracture mechanics parameters for free edges in multi-layered structures with weak singularities

L. Y. Shang, Z. L. Zhang and B. Skallerud*

Department of Structural Engineering, Norwegian University of Science and Technology (NTNU), N-7491 Trondheim, Norway

Abstract

This study focuses on the stress intensity factors for free edges in multi-layered structural components. The effects of elastic constants of various material combinations on the weak singularity at free edges are analyzed. Using the H-integral approach, the effects of elastic mismatch parameters, the bond area and the thickness of the thin metal layer on the stress intensity factor are quantified and the results are compared with detailed finite element solutions. A good agreement between numerical predictions obtained from the H-integral and the detailed FE results is achieved, showing the applicability of this approach. Similar to a crack problem, the singular elastic field dominates in an annular region adjacent to the notch tip. The relationship between the valid range of the K -dominated field and the thin-film thickness is then demonstrated. Furthermore, the competition of crack initiation between the free edge interface (180º opening angle) and a 90º notch interface in a generic specimen is investigated, in order to find out which is the prevailing failure mode. Comparison between isotropic Si and anisotropic Si substrate is also illustrated. Anisotropy of the Si substrate has a significant influence on the stress intensity factor when combined with an Au or Al metal layer but not with a Cu layer. Additionally, standardized numerical formulae of the dimensionless stress intensity factor have been derived to guide the engineering application.

Keywords: weak singularity, fracture mechanics, free edge, multi-layer, stress intensity factor

1. Introduction

Multi-layered thin films on silicon substrates are often used in micro-electro-mechanical systems (MEMS) because they provide certain advantages over mechanical connectors. By virtue of elastic mismatch and/or notch angle, stress concentrations may develop at the notch corner (Fig. 1) and a weak singularity (λ>0.9) may exist at free edges (Fig. 2). Weak singularities can cause malfunctions and result in mechanical failures. An interface edge and a notch are critical positions for crack initiation. Subjected to the remote mechanical loading, the interface stress field around the notch corner is proportional to $K_m^n r^{\lambda_m - 1} \left(m = 1, 2, \cdots N\right)$ where N is the number of eigenvalues available from the characteristic equation. Superscript n indicates the notch for the sake of distinction from the stress intensity factor K_m in classical fracture mechanics, r is the radial distance from the notch corner and $\lambda_m - 1$ is the order of the stress singularity. The stress field is singular for $0 < \mathrm{Re}(\lambda_m) < 1$ where $\mathrm{Re}(\lambda_m)$ is the real part of λ_m. Here K_m^n is the intensity of notch stress field with respect to eigenvalue λ_m. The dependence of the order of notch stress singularity on the material properties and on the notch geometry is well understood (e.g., Williams, 1952; Carpenter, 1984a; 1984b; Hutchinson and Suo, 1992; Chen and Nisitani, 1993; Yang and Munz, 1997; Labossiere and Dunn, 1999; Paggi and Carpinteri, 2008). The magnitude of critical K_m^n depends not only on joint geometry, material properties and applied load, but also on failure mode, residual stress, mode mixity and loading alignment, see Shang et al. (2008). The

knowledge of both K_m^n and λ_m is needed to fully describe the stress and displacement fields near the interface corner. Therefore, the motivation for our work is to properly characterize the singular stresses and associated displacements so that joint geometries and material combinations can be appropriately chosen to minimize risk of failure. In addition, if more than one critical position exists to render failure in a structure, for instance, interface X and interface Y shown in Fig. 3, the evaluation of interface strength becomes an important issue. As far as we know, very few studies have concerned the competition between different notches in MEMS components. Carpinteri and Paggi (2007) discussed the competition between different failure modes for the problem of crack propagation from the fracture mechanism's point of view. In comparison, we herein focus on various notch angles and from the mechanical perspective address the competition between different crack initiation sites to find out which is the prevailing failure mode in multi-layered structures. In addition, one dielectric layer SiO_2 (Fig. 3) often is grown or deposited on the silicon substrate during the bonding process. However, Kitamura et al. (2007) reported that the effect of this thin interlayer on the stress distributions along the interface is negligible. Hence, in the current study we omit this layer.

The failure initiation criterion at interface corners has been discussed in many studies (e.g., Stern et al., 1976; Sinclair, 1985; Carpenter and Byers, 1987; Munz and Yang, 1993; Carpenter, 1995; Yang and Munz, 1997; Labossiere and Dunn, 1998; Dunn et al., 2000; Reedy and Guess, 2002; Qian, 2001; Wang et al., 2002). Mainly two different failure criteria have been proposed to predict the failure initiation at sharp notches (Fig. 1) or wedge corners (e.g., Luo and Subbarayan, 2007). One is based on the assumption of "small scale yielding" near the corner. The failure occurs when the dominating stress intensity factor reaches a critical value (e.g., Hutchinson, 1990; Reedy and Guess, 1993; Yin, 1999). Alternatively, failure occurs when the function of comparable stress intensity factors, for example in the $K_I - K_{II}$ space in case of mixed-mode deformation, reaches a critical value (e.g., Labossiere et al., 2002). In the other approach, failure starts at the notch corner when the strain energy density at a point ahead of the notch reaches a critical value (e.g., Sih and Ho, 1991). Our paper addresses methods for crack initiation analysis at free edges and the stress intensity factor-based approach will be employed. A convenient computational procedure using the path independent H-integral approach is utilized. With this, the stress intensity factor for a general notch problem is obtained. The H-integral approach for cracked isotropic solids, pioneered by Stern et al. (e.g., Stern et al., 1976; Stern and Soni, 1975; 1976; Hong and Stern, 1978; Stern, 1979) and Snyder and Cruse (1975), was extended by Carpenter (1984a), Sinclair et al. (1984; 1985) and Babuska and Miller (1984) to notched solids in isotropic media where both mode I and mode II loading were taken into account. This was further extended to an isotropic bimaterial notched body by Carpenter and Byers (1987) and Banks-Sills (1997), and applied by Labossiere and Dunn (1999) to a general sharp notch with anisotropic materials. The effect of higher order terms $(\lambda_m > 1)$ on the stress state near the interface corner of a bi-material joint is demonstrated by Qian and Akisanya (1999). For the last decades, there has been much development of special hybrid and displacement-based finite elements in order to improve the accuracy of the solution. Nonetheless, the H-integral approach differs from the other methods in that a path independent contour integral combining finite element results with an asymptotic analysis is evaluated. With this, no special elements are required, relatively coarse finite element meshes can be used and complicated loading and boundary condition can be easily handled, thus avoiding time-consuming mesh refinement near the singularity.

This paper is organized as follows. First, the theoretical free edge singularity is calculated for a bi-material system and the actual stress fields in the multi-layer system are then analyzed by detailed finite element simulations. Second, some standardized numerical formulae are provided,

that are useful for engineering applications. Furthermore, using the H-integral approach, the effects of the elastic mismatch parameters, the bond area and the thickness of the thin metal layer on the stress intensity factor are investigated and quantified. Fourth, the competition of crack initiation between a free edge interface (180º opening angle) and a 90º notch interface in a generic MEMS specimen (Fig. 3) is discussed. Finally, numerical predictions obtained from the H-integral approach are shown to be in agreement with the detailed finite element solutions, demonstrating that the former is applicable for multi-layered structures with weak singularities. The relationship between the K-dominated field and the thin-film thickness is provided.

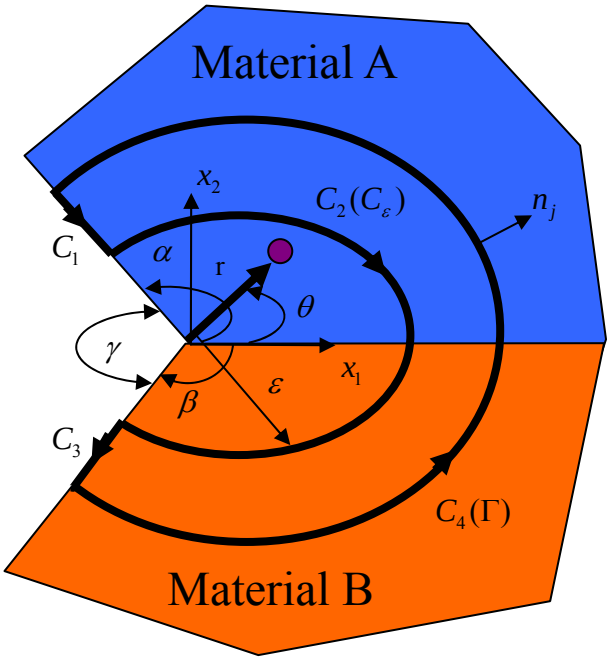

Fig. 1 Schematic plot of a closed integration contour around a general corner in dissimilar materials where $C = C_1 + C_2 + C_3 + C_4, C_2 = C_\varepsilon, C_4 = \Gamma$

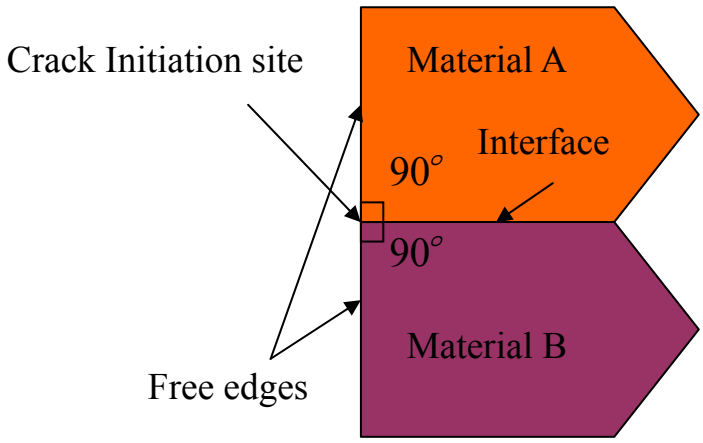

Fig. 2 Schematic plot of an edge-bonded interface in a bi-material system.

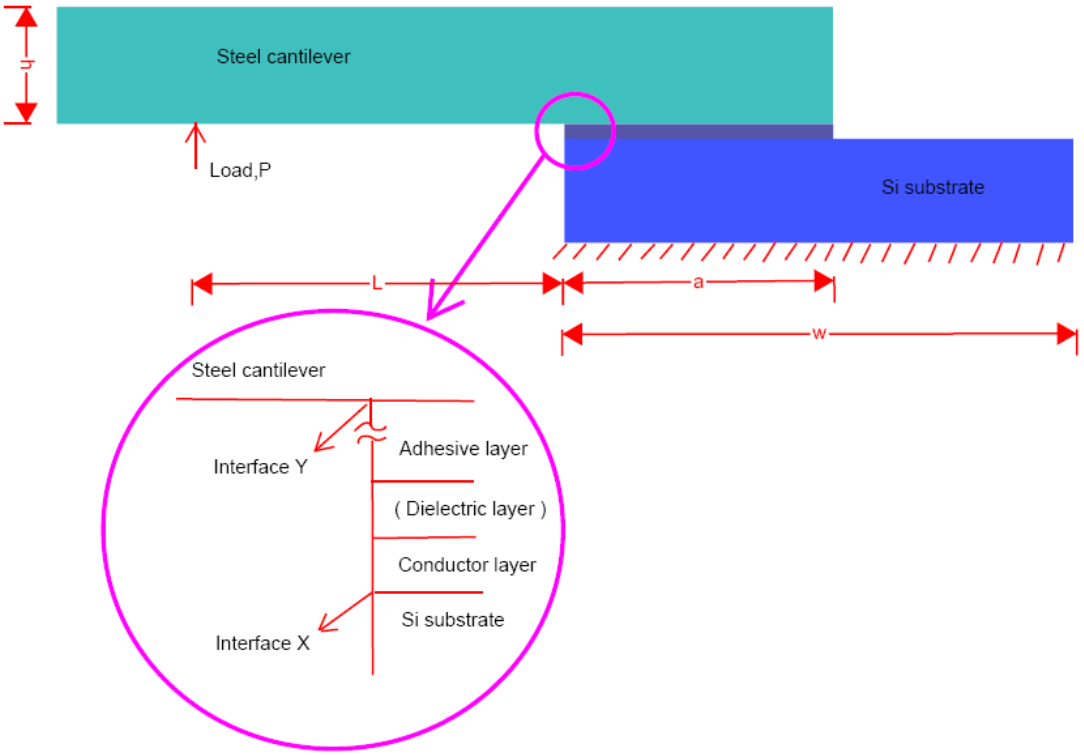

Fig. 3 Schematic plot of the generic specimen and loading conditions.

2. Asymptotic analysis

In order to obtain the order of stress singularity, which depends both on the notch angle and on the elastic parameters, a preliminary asymptotic analysis of the stress field has to be carried out first. Asymptotic analysis of the singular stress field at the vertex of re-entrant corners involves two eigenvalue problems. One is material related and the other is geometry related. The theory is briefly summarized in this section.

It is well known from Williams (1952) that the eigen-equation in a notched/cracked body for an isotropic material (i.e. $\alpha = \beta$ in Fig. 1) can be represented by eq. (1) where plus sign and minus sign are associated with the opening mode and sliding mode, respectively

$$\lambda \sin(2\pi - \gamma) \pm \sin(\lambda(2\pi - \gamma)) = 0 \tag{1}$$

The stress singularity depends only on the notch angle γ regardless of material. For a crack, $\alpha = \beta = \pi$, Eq. (1) simplifies to $\sin 2\pi\lambda^{I} = \sin 2\pi\lambda^{II} = 0$ and the stress singularity is $-½$; for an edge, $\alpha = \beta = 90^{\circ}$, the stress singularity disappears. Furthermore, the characteristic equation of the stress singularity for a general re-entrant corner with two arbitrarily oriented traction free surfaces at $\theta = \alpha$ and $\theta = -\beta$ is expressed by Carpenter (1984a)

$$\det\begin{vmatrix} \cos(2\lambda\beta)-\cos(2\lambda\alpha) & -\sin(2\lambda\beta)-\sin(2\lambda\alpha) \\ +\lambda\cos(2\beta)-\lambda\cos(2\alpha) & +\lambda\sin(2\beta)+\lambda\sin(2\alpha) \\ \sin(2\lambda\beta)+\sin(2\lambda\alpha) & \cos(2\lambda\beta)-\cos(2\lambda\alpha) \\ +\lambda\sin(2\beta)+\lambda\sin(2\alpha) & -\lambda\cos(2\beta)+\lambda\cos(2\alpha) \end{vmatrix}=0 \tag{2}$$

The general configuration for a notch/wedge/crack geometry in dissimilar anisotropic materials is addressed here, see Fig. 1. Such a situation usually results in mixed-mode deformations and the stress fields are no longer symmetric and/or anti-symmetric.

In general, the stresses and displacements in the vicinity of the interface corner are obtained using complex variable methods or the Airy's stress function approach. Using either of these methods, it can be shown that the asymptotic fields near the interface corner can be expressed as

$$\begin{aligned} \sigma_{ij}^{M} &= \sum_{m=1}^{N} K_m^n r^{\lambda_m-1} f_{ij}^{mM}(\theta,\lambda_m)+\sigma_{ij0}^{M}(\theta) \\ u_i^{M} &= \sum_{m=1}^{N} K_m^n r^{\lambda_m} g_i^{mM}(\theta,\lambda_m)+u_{i0}^{M}(\theta) \end{aligned} \tag{3}$$

where $\lambda_m\,(m=1,2,\cdots N)$ are the eigenvalues of the problem. Superscript M indicates material A or B which is elastic, homogeneous, isotropic or anisotropic. $\sigma_{ij0}^{M}(\theta)$ is the constant stress field ($\mathrm{Re}(\lambda_m)=1$) independent of the radial distance from the notch corner and $u_{i0}^{M}(\theta)$ is the associated displacement field near the interface corner. These terms can be determined analytically and are finite for thermal loading and/or surface tractions on the notch flanks but vanish for remote mechanical loading. The remaining stress term is comprised of several stress fields of the form $K_m^n r^{\lambda_m-1}$. When two or more stress fields of the form $K_m^n r^{\lambda_m-1}$ exist near the notch corner, one pair of K_m^n and λ_m-1 describes one stress field, and the total stresses are determined by superposing contributions from all stress fields. There are an infinite number of values λ_m which satisfy the eigenvalue equations. Both the stress intensity factor and the stress singularity may be real positive, real negative or complex, but in most circumstances, they are real constants (e.g., Qian and Akisanya, 1999; Banks-Sills and Sherer, 2002). Although not explicitly shown in Eq. (3), there are certain special combinations of elastic properties and notch angles that can also generate logarithmic singularities (e.g., Bogy, 1971; Dempsey and Sinclair, 1979; Dempsey and Sinclair, 1981; Dempsey, 1995; Chen, 1996; Sinclair, 1999). In this study, the power-logarithmic singularity is not considered. Moreover, only positive λ_m are admissible in order to ensure finite displacements at the notch tip. $f_{ij}^{mM}(\theta,\lambda_m)$ is a function describing the angular profile of the stress field in conjunction with material elastic properties and the opening angle. Note that $f_{ij}^{mM}(\theta,\lambda_m)$ is non-dimensional but $g_i^{mM}(\theta,\lambda_m)$ has the unit of $(\text{length})^2(\text{force})^{-1}$. They are determined analytically while the eigenvalues $\lambda_m\,(m=1,2,\cdots,N)$ for a given notch geometry are obtained by solving a characteristic equation. The closed-form expression for these functions will be briefly described below. More details can be found in references such as Stroh (1958); Ting (1996); Labossiere and Dunn (1999); Shang et al. (2008).

Consider a linear elastic body with a re-entrant corner subjected to remote in-plane mechanical loading, see Fig. 1. Without loss of generality, we focus on two singular terms, i.e. $0<\lambda_1\le\lambda_2<1$,

considering the higher order terms ($\lambda_m > 1$) to be insignificant. The singular stress and displacement field around the notch tip can be reduced as follows:

$$\sigma_{ij}^{M}(r,\theta) = K_1^n r^{\lambda_1 - 1} f_{ij}^{1M}(\theta,\lambda_1) + K_2^n r^{\lambda_2 - 1} f_{ij}^{2M}(\theta,\lambda_2)$$
$$u_i^{M}(r,\theta) = K_1^n r^{\lambda_1} g_i^{1M}(\theta,\lambda_1) + K_2^n r^{\lambda_2} g_i^{2M}(\theta,\lambda_2) \tag{4}$$

r and θ are the polar coordinates with an origin at the notch tip. For the homogeneous isotropic case, $\lambda_1 = \lambda_2 = ½$, corresponding to the definition by Williams (1952) and Hong and Stern (1978).

The first eigenvalue problem proceeds as follows. Employing Stroh's sextic formalism (e.g., Stroh, 1958; Ting, 1996), the displacements $\mathbf{u}$ and stress function $\boldsymbol{\phi}$ in the material $M\,(M = A, B)$ around the interface corner can be expressed by

$$\mathbf{u} = \sum_{\alpha=1}^{3} \left[\mathbf{a}_\alpha f_\alpha(z_\alpha) + \overline{\mathbf{a}}_\alpha f_{\alpha+3}(\overline{z}_\alpha) \right] \tag{5}$$

$$\boldsymbol{\phi} = \sum_{\alpha=1}^{3} \left[\mathbf{b}_\alpha f_\alpha(z_\alpha) + \overline{\mathbf{b}}_\alpha f_{\alpha+3}(\overline{z}_\alpha) \right] \tag{6}$$

f_α are arbitrary functions of the arguments z_α, where $z_\alpha = x_1 + p_\alpha x_2$ is the complex variable. f_α depend on the geometry, radial distance from the interface corner and material elastic parameters. The six complex eigenvalues p_α satisfy $p_{\alpha+3} = \overline{p}_\alpha$ and are the solutions of a quadratic eigenvalue problem (7). In addition, $\mathbf{a}$ and $\mathbf{b}$ are the Stroh eigenvectors, satisfy $\mathbf{a}_{\alpha+3} = \overline{\mathbf{a}}_\alpha$ and $\mathbf{b}_{\alpha+3} = \overline{\mathbf{b}}_\alpha$, related through the matrices $\mathbf{Q}$, $\mathbf{R}$ and $\mathbf{T}$ described in the following. p_α, $\mathbf{a}_\alpha$ and $\mathbf{b}_\alpha$ depend only on the elastic stiffnesses C_{ijkl}. Without loss of generality, the imaginary part of p_α is taken to be positive. Overbars of p_α, z_α, $\mathbf{a}$, $\mathbf{b}$ denote the complex conjugates.

Using the stress-strain law $\sigma_{ij} = C_{ijkl} u_{k,l}$ and the static equilibrium equations $C_{ijkl} u_{k,lj} = 0$ with eq. (5), the resulting eigenvalue equations can be written in matrix form as:

$$\left\{ \mathbf{Q} + p(\mathbf{R} + \mathbf{R}^{\mathrm{T}}) + p^2 \mathbf{T} \right\} \mathbf{a} = \mathbf{0} \tag{7}$$

where $Q_{ik} = C_{i1k1}$, $R_{ik} = C_{i1k2}$ and $T_{ik} = C_{i2k2}$. For a non-trivial solution of $\mathbf{a}$, the characteristic equation must be zero, i.e. $\det\left| \mathbf{Q} + p(\mathbf{R} + \mathbf{R}^{\mathrm{T}}) + p^2 \mathbf{T} \right| = 0$, which results in six roots for the eigenvalue *p*. In matrix form and with Voigt's notation, we have

$$\mathbf{Q} = \begin{bmatrix} C_{11} & C_{16} & C_{15} \\ C_{16} & C_{66} & C_{56} \\ C_{15} & C_{56} & C_{55} \end{bmatrix},\ \mathbf{T} = \begin{bmatrix} C_{66} & C_{26} & C_{46} \\ C_{26} & C_{22} & C_{24} \\ C_{46} & C_{24} & C_{44} \end{bmatrix} \text{ and } \mathbf{R} = \begin{bmatrix} C_{16} & C_{12} & C_{14} \\ C_{66} & C_{26} & C_{46} \\ C_{56} & C_{25} & C_{45} \end{bmatrix} \tag{8}$$

In the special case of isotropic elasticity

$$\mathbf{Q} = \begin{bmatrix} \chi + 2\mu & 0 & 0 \\ 0 & \mu & 0 \\ 0 & 0 & \mu \end{bmatrix},\ \mathbf{T} = \begin{bmatrix} \mu & 0 & 0 \\ 0 & \chi + 2\mu & 0 \\ 0 & 0 & \mu \end{bmatrix},\ \mathbf{R} = \begin{bmatrix} 0 & \chi & 0 \\ \mu & 0 & 0 \\ 0 & 0 & 0 \end{bmatrix} \tag{9}$$

where the Lamé constants are expressed by $\chi = \dfrac{E\nu}{(1+\nu)(1-2\nu)}$ and $\mu = \dfrac{E}{2(1+\nu)}$ with E being

Young's modulus and ν being Poisson's ratio for material A or B. Making use of the constitutive equation and Eq. (6), the relation between **a** and **b** can be written:

$$\mathbf{b} = \left(\mathbf{R}^{\mathrm{T}} + p\mathbf{T}\right)\mathbf{a} = -\frac{1}{p}\left(\mathbf{Q} + p\mathbf{R}\right)\mathbf{a} \tag{10}$$

With this, the above quadratic eigenvalue problem can be recast as a conventional six-dimensional linear eigenvalue problem

$$\begin{bmatrix} \mathbf{N}_1 & \mathbf{N}_2 \\ \mathbf{N}_3 & \mathbf{N}_1^T \end{bmatrix} \begin{Bmatrix} \mathbf{a} \\ \mathbf{b} \end{Bmatrix} = p \begin{Bmatrix} \mathbf{a} \\ \mathbf{b} \end{Bmatrix}$$

$$\Rightarrow \mathbf{N}\boldsymbol{\eta} = p\boldsymbol{\eta}, \quad \boldsymbol{\eta} = \begin{Bmatrix} \mathbf{a} \\ \mathbf{b} \end{Bmatrix} \tag{11}$$

where $\mathbf{N}_1 = -\mathbf{T}^{-1}\mathbf{R}^{\mathrm{T}}$, $\mathbf{N}_2 = \mathbf{T}^{-1}$ and $\mathbf{N}_3 = -\mathbf{Q} + \mathbf{R}\mathbf{T}^{-1}\mathbf{R}^{\mathrm{T}}$. Eshelby et al. (1953) stated that since p cannot be real if the strain energy is to be positive, we have three pairs of complex conjugates for p as well as for $\boldsymbol{\eta}$. If p_α and $\boldsymbol{\eta}_\alpha \left(\alpha = 1, 2, \cdots, 6\right)$ are the eigenvalues and eigenvectors, we let

$$\left.\begin{aligned} p_{\alpha+3} &= \overline{p}_\alpha, \ \ \mathrm{Im}\, p_\alpha > 0 \\ \boldsymbol{\eta}_{\alpha+3} &= \overline{\boldsymbol{\eta}}_\alpha \end{aligned}\right\} \ \alpha = 1, 2, 3 \tag{12}$$

where Im denotes the imaginary part.

The Stroh eigenvectors are determined up to an arbitrary constant. They are normalized as

$$\mathbf{a}_\alpha = \frac{\hat{\mathbf{a}}_\alpha}{\sqrt{2\hat{\mathbf{a}}_\alpha^{\mathrm{T}}\hat{\mathbf{b}}_\alpha}} \ \text{ and } \ \mathbf{b}_\alpha = \frac{\hat{\mathbf{b}}_\alpha}{\sqrt{2\hat{\mathbf{a}}_\alpha^{\mathrm{T}}\hat{\mathbf{b}}_\alpha}}, \ \alpha = 1, 2, 3 \tag{13}$$

where $\hat{\mathbf{a}}_\alpha$ and $\hat{\mathbf{b}}_\alpha$ are the non-normalized eigenvectors, i.e. those that would be produced by a standard eigensolver; $\mathbf{a}_\alpha$ and $\mathbf{b}_\alpha$ represent the direction of the displacement $\mathbf{u}_\alpha$ and traction $\mathbf{t}_\alpha$, respectively .

Now we turn to the second eigenvalue problem, i.e. finding the stress singularity governed by λ_m. As suggested by Ting (1996; 1997); Labossiere and Dunn (1999), we choose $f\left(z_\alpha\right)$ as

$$f_\alpha\left(z_\alpha\right) = \frac{1}{\lambda} z_\alpha^\lambda q_\alpha \ \text{ and } \ f_{\alpha+3}\left(\overline{z}_\alpha\right) = \frac{1}{\lambda}\overline{z}_\alpha^\lambda h_\alpha \tag{14}$$

where q_α and h_α are the unknown complex constants and will be determined by Eq. (19) once λ is obtained. Using the expression $z_\alpha = x_1 + p_\alpha x_2 = r\xi_\alpha(\theta) = r(\cos\theta + p_\alpha \sin\theta)$, the displacements and tractions in a plane polar coordinate system originated at the notch tip are derived

$$\mathbf{u}^M = \frac{1}{\lambda} r^\lambda \sum_{\alpha=1}^{3} \left[\xi_\alpha^M \left(\theta\right)^\lambda \mathbf{a}_\alpha q_\alpha + \overline{\xi}_\alpha^M \left(\theta\right)^\lambda \overline{\mathbf{a}}_\alpha h_\alpha \right]$$

$$\mathbf{t}^M = \frac{\lambda}{r}\varphi = r^{\lambda-1} \sum_{\alpha=1}^{3} \left[\xi_\alpha^M \left(\theta\right)^\lambda \mathbf{b}_\alpha q_\alpha + \overline{\xi}_\alpha^M \left(\theta\right)^\lambda \overline{\mathbf{b}}_\alpha h_\alpha \right] \tag{15}$$

where superscript M indicates material A or B. The second eigenvalue problem can be solved using the boundary conditions for the interface notch problem, see Fig. 1.

The traction-free boundary conditions on the notch flanks ($\theta = \alpha, \ \theta = -\beta$) and the continuity conditions of the stresses and displacements along the interface ($\theta = 0$) result in the following

boundary condition equations

$$\mathbf{t}^A(\alpha)=0,\ \mathbf{t}^B(-\beta)=0,\ \mathbf{t}^A(0)=\mathbf{t}^B(0),\ \mathbf{u}^A(0)=\mathbf{u}^B(0) \tag{16}$$

Substituting eq. (15) into eq. (16), a group of 12 linear equations in the 12 unknown coefficients q_α^M, h_α^M $(M=A,B;\alpha=1,2,3)$ is deduced.

$$\begin{aligned}
&\sum_{\alpha=1}^{3}\xi_\alpha^A(\alpha)^\lambda\,\mathbf{b}_\alpha^A q_\alpha^A+\sum_{\alpha=1}^{3}\bar{\xi}_\alpha^A(\alpha)^\lambda\,\bar{\mathbf{b}}_\alpha^A h_\alpha^A=0\\
&\sum_{\alpha=1}^{3}\xi_\alpha^B(-\beta)^\lambda\,\mathbf{b}_\alpha^B q_\alpha^B+\sum_{\alpha=1}^{3}\bar{\xi}_\alpha^B(-\beta)^\lambda\,\bar{\mathbf{b}}_\alpha^B h_\alpha^B=0\\
&\sum_{\alpha=1}^{3}\xi_\alpha^A(0)^\lambda\,\mathbf{b}_\alpha^A q_\alpha^A+\sum_{\alpha=1}^{3}\bar{\xi}_\alpha^A(0)^\lambda\,\bar{\mathbf{b}}_\alpha^A h_\alpha^A-\sum_{\alpha=1}^{3}\xi_\alpha^B(0)^\lambda\,\mathbf{b}_\alpha^B q_\alpha^B-\sum_{\alpha=1}^{3}\bar{\xi}_\alpha^B(0)^\lambda\,\bar{\mathbf{b}}_\alpha^B h_\alpha^B=0\\
&\sum_{\alpha=1}^{3}\xi_\alpha^A(0)^\lambda\,\mathbf{a}_\alpha^A q_\alpha^A+\sum_{\alpha=1}^{3}\bar{\xi}_\alpha^A(0)^\lambda\,\bar{\mathbf{a}}_\alpha^A h_\alpha^A-\sum_{\alpha=1}^{3}\xi_\alpha^B(0)^\lambda\,\mathbf{a}_\alpha^B q_\alpha^B-\sum_{\alpha=1}^{3}\bar{\xi}_\alpha^B(0)^\lambda\,\bar{\mathbf{a}}_\alpha^B h_\alpha^B=0
\end{aligned} \tag{17}$$

Using eq. $(17)_1$ and $(17)_2$, we express $\mathbf{h}^A$ in terms of $\mathbf{q}^A$ and $\mathbf{q}^B$ in terms of $\mathbf{h}^B$, respectively. A non-trivial solution exists only if the determinant of the coefficient matrix vanishes. This occurs when the eigenvalue, λ, satisfies the following equation which is dependent on the stiffness matrix, C_{ijkl}:

$$\begin{bmatrix}
\mathbf{b}^A\left(\mathbf{B}^A\right)^{-1}-\bar{\mathbf{b}}^A\left(\bar{\mathbf{B}}^A\right)^{-1} & \left(\mathbf{b}^B\left(\mathbf{B}^B\right)^{-1}-\bar{\mathbf{b}}^B\left(\bar{\mathbf{B}}^B\right)^{-1}\right)\\
\mathbf{a}^A\left(\mathbf{B}^A\right)^{-1}-\bar{\mathbf{a}}^A\left(\bar{\mathbf{B}}^A\right)^{-1} & \left(\mathbf{a}^B\left(\mathbf{B}^B\right)^{-1}-\bar{\mathbf{a}}^B\left(\bar{\mathbf{B}}^B\right)^{-1}\right)
\end{bmatrix}
\begin{Bmatrix}\mathbf{B}^A\mathbf{q}^A\\ \bar{\mathbf{B}}^B\mathbf{h}^B\end{Bmatrix}=\mathbf{0} \tag{18}$$

which results in six simultaneous eigenvalue equations with six unknowns $q_\alpha^A,\ h_\alpha^B(\alpha=1,2,3)$

$$\mathbf{K}(\lambda)\ \ \mathbf{D}(\lambda)=\mathbf{0},\ \ \det\mathbf{K}(\lambda)=0 \tag{19}$$

In the above equations, $\mathbf{B}^A=\left[\xi_1^A(\alpha)^\lambda\,\mathbf{b}_1^A,\ \ \xi_2^A(\alpha)^\lambda\,\mathbf{b}_2^A,\ \ \xi_3^A(\alpha)^\lambda\,\mathbf{b}_3^A\right]$, $\mathbf{B}^B=\left[\xi_1^B(-\beta)^\lambda\,\mathbf{b}_1^B,\ \ \xi_2^B(-\beta)^\lambda\,\mathbf{b}_2^B,\ \ \xi_3^B(-\beta)^\lambda\,\mathbf{b}_3^B\right]$, $\mathbf{D}=\left[\mathbf{B}^A\mathbf{q}^A,\ \bar{\mathbf{B}}^B\mathbf{h}^B\right]^{\mathrm{T}}$, $\mathbf{a}^M=\left[\mathbf{a}_1^M,\mathbf{a}_2^M,\mathbf{a}_3^M\right]$, $\mathbf{b}^M=\left[\mathbf{b}_1^M,\mathbf{b}_2^M,\mathbf{b}_3^M\right]$, $\mathbf{q}^M=\left[q_1^M,q_2^M,q_3^M\right]^{\mathrm{T}}$, $\mathbf{h}^M=\left[h_1^M,h_2^M,h_3^M\right]^{\mathrm{T}}$ $(M=A,B)$

Eventually, in the particular case of a crack $(\gamma=0^\circ)$ with an isotropic or anisotropic uni-material, the well-known result, $\lambda=½$ is obtained. In the case of an edge notch $\left(\gamma=180^\circ,\alpha=90^\circ\right)$ with a homogeneous isotropic or anisotropic material, we obtain $\lambda=1$ and the stress singularity disappears. Once the value of λ has been computed from the characteristic equation (19), the eigenvectors $\mathbf{q}^M$, $\mathbf{h}^M$ can be calculated.

3. Computation of stress intensity factors by the H-integral approach

To complete the knowledge of the stress and displacement fields in the neighbourhood of a notch tip, the stress intensity factors are required. Once the order of the stress singularity is obtained from the asymptotic analysis above, the stress intensity factor for a sharp notch, wedge corner or a crack can be computed using the path independent H-integral approach (e.g., Shang et

al., 2008; Labossiere and Dunn, 1999). Based on Betti's reciprocal work theorem (Rogers and Causey, 1962), the concept of this contour integral method is to combine the numerical stress and displacement solutions with an appropriate complementary field so that the value of the integral gives the magnitude of the notch stress intensity. This simple procedure comes with significant savings in computational time compared to the other approaches and also with the possibility to easily perform parametric analyses.

Consider for example a closed contour C excluding the stress singularity in a planar linear elastic body, as shown in Fig. 1. The Betti's reciprocal law in the absence of any body force can be stated as

$$\oint_C \left(\sigma_{ij}u_i^* - \sigma_{ij}^* u_i\right) n_j ds = 0 \quad where\ C = C_1 + C_2 + C_3 + C_4 \tag{20}$$

and where $(i, j) = (r, \theta)$ are the plane polar coordinates centered at the interface corner, n_j is the outward unit normal to the counterclockwise closed contour C, ds is an infinitesimal line segment of C. σ_{ij}, u_i are the notch corner stress and displacement fields in terms of eigenvalue $\lambda_m (\lambda_m \neq 1)$ and stress intensity factor K_m^n, σ_{ij}^*, u_i^* are complementary singular stresses and displacements satisfying the same boundary conditions as (σ_{ij}, u_i) but with respect to an associated eigenvalue λ_m^* and stress intensity factor K_m^{n*}. Note that the employed complementary field has no physical significance here.

Szabo and Babuska (1988) and Wu and Chang (1993) showed that if λ_m is an eigenvalue for the given material properties and notch geometry, $\lambda_m^* = -\lambda_m$ is also the eigenvalue for the same problem. Hence, the near-tip stress and displacement fields corresponding to the eigenvalue λ_m^* can be taken as the complementary fields. According to eq. (4), they are described by

$$\begin{aligned}
\sigma_{ij}^{M^*}(r,\theta) &= K_1^{n^*} r^{-\lambda_1 - 1} f_{ij}^{1M^*}\left(\theta, -\lambda_1\right) + K_2^{n^*} r^{-\lambda_2 - 1} f_{ij}^{2M^*}\left(\theta, -\lambda_2\right) \\
u_i^{M^*}(r,\theta) &= K_1^{n^*} r^{-\lambda_1} g_i^{1M^*}\left(\theta, -\lambda_1\right) + K_2^{n^*} r^{-\lambda_2} g_i^{2M^*}\left(\theta, -\lambda_2\right)
\end{aligned} \tag{21}$$

Since the integration in (20) vanishes along the traction free surfaces C_1 and C_3. i.e. $\sigma_{ij} n_j = \sigma_{ij}^* n_j = 0$, see Fig. 1, it reduces to

$$-\int_{C_2} \left(\sigma_{ij}u_i^* - \sigma_{ij}^* u_i\right) n_j ds = \int_{C_4} \left(\sigma_{ij}u_i^* - \sigma_{ij}^* u_i\right) n_j ds \tag{22}$$

On the left-hand side of Eq. (22), the contour integral is simplified to either one coefficient proportional to the stress intensity factor or a linear combination of K_1^n and K_2^n for an arbitrarily small radius ε (e.g., Stern et al., 1976)

$$I_\varepsilon = -\int_{C_2} \left(\sigma_{ij}u_i^* - \sigma_{ij}^* u_i\right) n_j ds = e_1 K_1^n + e_2 K_2^n \tag{23}$$

where e_1, e_2 are constants. The unstarred stresses and displacements along C_2 were taken from the asymptotic analysis, eq. (4), while the starred stresses and displacements were employed from the complementary singular field, eq. (21).

Accordingly, only the outer contour C_4 is involved in the numerical integration for determining the desired stress intensity factors. The H-integral is defined as

$$H = \int_{C_4} \left(\sigma_{ij}u_i^* - \sigma_{ij}^* u_i\right) n_j ds = \int_{\Gamma} \left(\sigma_{ij}u_i^* - \sigma_{ij}^* u_i\right) n_j ds \tag{24}$$

and in polar coordinates, the above equation becomes

$$H = \int_{-\beta}^{\alpha} \left(\sigma_{rr} u_r^* + \sigma_{r\theta} u_\theta^* - \sigma_{rr}^* u_r - \sigma_{r\theta}^* u_\theta \right) r d\theta \tag{25}$$

In eq. (24), Γ can be any contour within the planar linear elastic body commencing on the lower notch flank and terminating on the upper. The unstarred fields (σ_{ij}, u_i) are obtained from the finite element calculations while the starred fields (σ_{ij}^*, u_i^*) are taken from the complementary singular field satisfying the same boundary conditions as those for (σ_{ij}, u_i)

For a general corner (Fig. 1), we can define the respective stress intensity factors by

$$K_1^n = \lim_{\theta=0, r\to 0} \frac{\sigma_{\theta\theta}(r,\theta)}{r^{\lambda_1 - 1}},\ K_2^n = \lim_{\theta=0, r\to 0} \frac{\tau_{r\theta}(r,\theta)}{r^{\lambda_2 - 1}} \tag{26}$$

where $\sigma_{\theta\theta}$, $\tau_{r\theta}$ are the normal and shear component in the θ direction of the stress field, respectively. λ_1, λ_2 are the eigenvalues stemming from the corresponding eigen-equation (19).

The different stress intensity factors K_1^n and K_2^n corresponding to the individual eigenvalues λ_1 and λ_2 can be evaluated simultaneously (e.g., Carpenter and Byers, 1987). Alternatively, it can be attained independently as described here. Since the eigenvectors $\mathbf{q}^M$, $\mathbf{h}^M$ in eq. (18) for each eigenvalue are determined only up to an arbitrary constant, we normalize the stress fields such that $\sigma_{\theta\theta}(r, \theta = 0) = K_1^n r^{\lambda_1 - 1}, \tau_{r\theta}(r, \theta = 0) = K_2^n r^{\lambda_2 - 1}$. Similarly, for the complementary field: $\sigma_{\theta\theta}^*(r, \theta = 0) = K_1^{n*} r^{-\lambda_1 - 1}$, $\tau_{r\theta}^*(r, \theta = 0) = K_2^{n*} r^{-\lambda_2 - 1}$. Note that the complementary field must satisfy the equilibrium equations and traction-free conditions on the notch flanks so that the integral along the inner contour C_ε yields the desired stress intensity factor. Moreover, the complementary solution is chosen with eigenvalue $\lambda_m^* = -\lambda_m$ to eliminate the dependence of the integrand on the r-coordinate. With all these conditions, the magnitudes of $K_m^{n*}(m = 1, 2)$ are determined so that the resulting inner contour integral identically produces K^n, either $K_1^n(e_1 = 1,\ e_2 = 0)$ or $K_2^n(e_1 = 0,\ e_2 = 1)$. The choice of $K_m^{n*}(m = 1, 2)$ is also described by Banks-Sills and Sherer (2002) and Zhang and Mikkola (1992).

4. Results and discussion

In this section, we apply the path independent H-integral approach to an edge notch and a 90° notch in multi-layered structures as depicted in Fig. 4. Finite element analyses are performed with ABAQUS. Eight-noded quadrilateral, reduced integration elements were used. Plane strain conditions are assumed in all simulations and three dimensional effects are not considered. We also assume that the materials are perfectly bonded along the interface. The loading system proposed by Kitamura et al. (2002; 2003; 2007) has been chosen for the study. Typical material combinations in microelectronic devices are taken into consideration. The elastic properties of the materials are listed in Table 1. Beam span L, height h and width of silicon substrate w are 10, 1 and 3.4mm, respectively. A $350\,\mu m$ thick [100] silicon substrate and $8\,\mu m$ thick adhesive layer is employed for all specimens.

4.1. Order of singularity results

The eigenvalues describing the order of the stress singularity for different material combinations are listed in Table 2. These can be obtained analytically from eq. (19). It can be seen that the orders of the stress singularities at interface X vary from -0.07 to 0. Hence, interface X displays a typical weak singularity problem. Combined with commonly used metal layer, the isotropic silicon has slightly higher singularity compared to the anisotropic silicon. For the cases such as Si/Cu, Ta/Si and TiN/Si, λ is almost equal to 1, i.e., vanishing singularity. Additionally, for all the material combinations studied here, Au and Al have stronger singularities than the rest. interface Y shows a higher singularity than interface X.

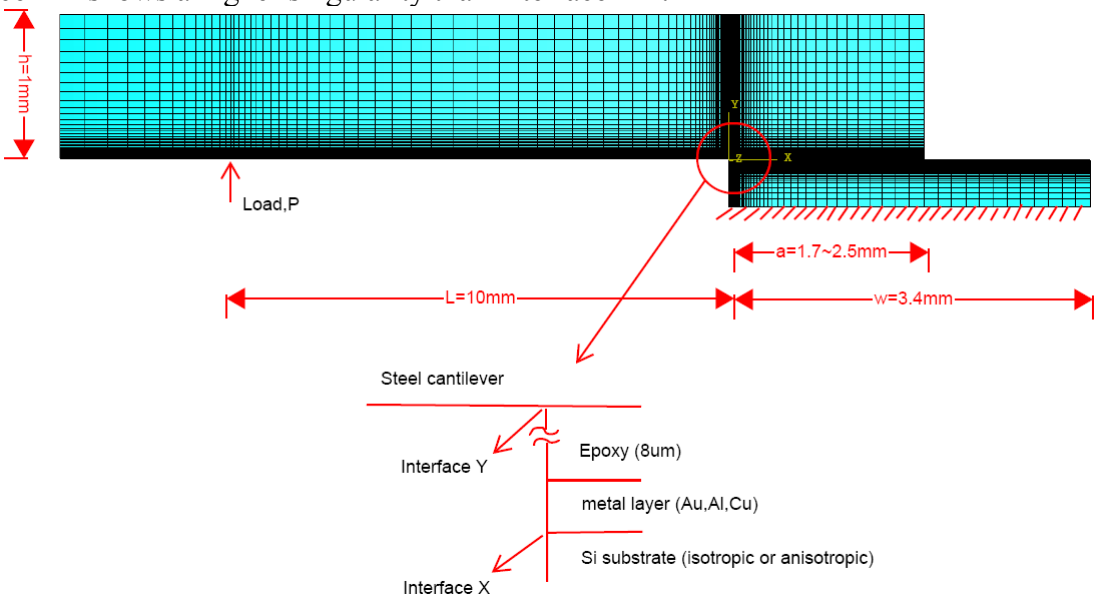

Fig. 4 Finite Element mesh and dimensions.

Table 1

Elastic properties used in Finite Element Analysis

	Isotropic Materials					
Materials Elasticity	**Au**	**Cu**	**Al**	**Si**	**Steel**	**Epoxy**
Young's Modulus (GPa)	83	129	70	167	200	2.50
Poisson's Ratio	0.44	0.34	0.35	0.30	0.30	0.30
Materials Elasticity	**SiO2**	**Ta**	**TiN**	**TaN**	**Glass**	**SiN**
Young's Modulus (GPa)	92	186	195	350	63	304
Poisson's Ratio	0.30	0.34	0.3	0.35	0.20	0.27
	Anisotropic Silicon [100]					
Elastic Stiffness Matrix	$\mathbf{S} = \begin{bmatrix} S_{11} & S_{12} & S_{12} & 0 & 0 & 0 \\ S_{12} & S_{11} & S_{12} & 0 & 0 & 0 \\ S_{12} & S_{12} & S_{11} & 0 & 0 & 0 \\ 0 & 0 & 0 & S_{44} & 0 & 0 \\ 0 & 0 & 0 & 0 & S_{44} & 0 \\ 0 & 0 & 0 & 0 & 0 & S_{44} \end{bmatrix} GPa$ where $S_{11} = 165.7GPa,\ S_{12} = 63.9GPa,\ S_{44} = 79.56GPa$ (Mason, 1958)					

Table 2

The eigenvalues describing the order of stress singularity with the varying material properties and the corner geometry

	Material A	**Material B**	λ_1	**Material A**	**Material B**	λ_1
Interface X (free edge)	Au	Isotropic silicon	0.9332	Au	Anisotropic silicon	0.9522
	Al		0.9304	Al		0.9481
	Cu		0.9912	Cu		0.9967
	Glass		0.9710	Glass		0.9825
	SiO2		0.9718	SiO2		0.983
	Ta		1	Ta		0.9981
	TiN		0.9979	TiN		0.9946
	SiN		0.9689	SiN		0.9624
	TaN		0.9637	TaN		0.9556
Interface Y (90° notch)	Steel	Epoxy	0.7049			

4.2. The influence of elastic properties of bi-materials on the stress singularity

Various researchers have studied material mismatch parameters and the stress singularities at interface corners/wedges/cracks since the pioneering work described by Williams (1952; 1959). By contrast, our study focuses on the evaluation of the weak singularity for a free edge interface (Fig. 2). A wide range of elastic moduli and Poisson's ratios has been taken into account, covering most material combinations of interest in the electronic industry. The influence of elastic constants in various material combinations on the free edge singularity is displayed in the following.

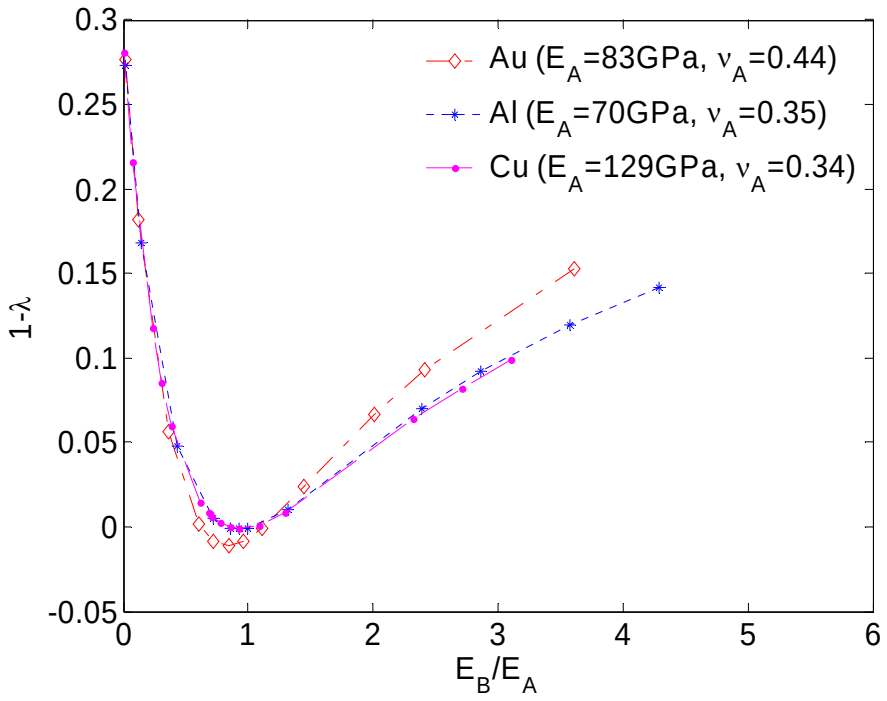

Fig. 5 The effect of Young's modulus ratio ($\nu_B = 0.30$) on weak singularity.

First, the orders of stress singularities are illustrated for the free edge with conventional metal material, i.e., Au, Al, Cu as upper material A together with a wide range of values for $\frac{E_B}{E_A}$. Varying E_B, it can be observed from Fig. 5 that the stress singularity decreases first with modulus ratio $\frac{E_B}{E_A}$ and then increases with $\frac{E_B}{E_A}$ when the material A is more compliant than the substrate material B. Note that if both $\frac{E_B}{E_A}=1$ and the Poisson's ratio $\nu_A=\nu_B$ are met, the stress singularity $1-\lambda$ is zero in just one point on the abscissa, which is equivalent to the case for edge-bonded homogeneous isotropic material. The reason why we get a region of vanishing singularity instead of one point, see Fig. 5, is due to the different value of Poisson's ratio for material A and B here. Moreover, the effect of Poisson's ratio on stress singularity is further depicted in Fig. 6. The more the Poisson's ratio of material A deviates from 0.3, the wider is the range of the no-singularity zone ($\lambda \geq 1$). For example, no stress singularity occurs when the Poisson's ratio of material A equals 0.45 and its Young's modulus ranges from 140 to 230 GPa. Similarly, the singularity vanishes when the Poisson's ratio of material A equals 0.2 and its Young's modulus varies from 90 to 160 GPa. When the Poisson's ratio of material A equals 0.3, the range of its Young's modulus to reach no-singularity shrinks to around 150 GPa.

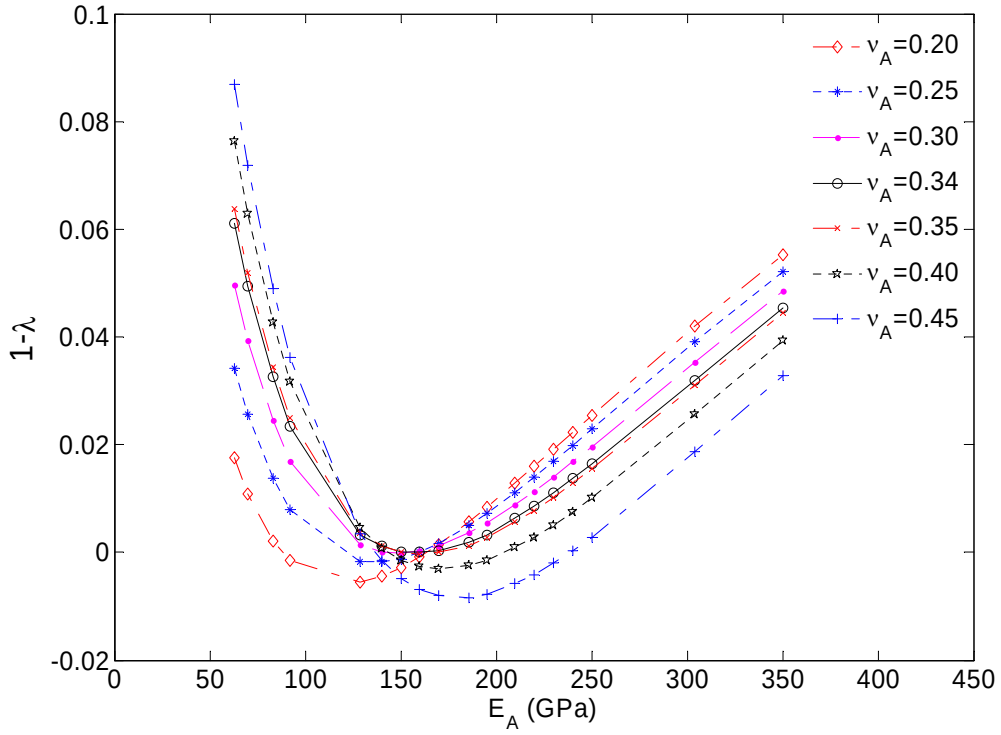

Fig. 6 The effect of Poisson's ratio on weak singularity when material B is [100] silicon.

4.3. Standardized numerical formulae for the stress intensity factor

For a practical application of the H-integral, standardized numerical formulae for calculating the stress intensity factor for the specimens considered in this study can be derived. Since K_m^n has the dimension of $(stress)(length)^{1-\lambda_m}$, it is impossible to compare the magnitude of the stress intensity factor for different material combinations even if the notch geometry is the same. With the aim of a quantitative measure of the stress intensity factor for various materials and applied loads, the following non-dimensional stress intensity factor (e.g., Labossiere and Dunn, 1999; Carpinteri et al., 2006) can be used

$$Y_m^n\left(\frac{a}{w},\frac{t}{t_0}\right)=\frac{K_m^n}{\frac{6PL}{bh^2}w^{1-\lambda}} \tag{27}$$

where a, w, t, t_0, P, L, b, and h denote, respectively, the bond length, substrate width, conductor layer thickness, nominal/characteristic thickness, concentrated force, and span, width and height of the steel beam (Fig. 4), whereas Y is a shape function depending on the geometry of the structure by means of the ratios $\frac{a}{w}$, $\frac{t}{t_0}$. Furthermore, we can write

$$Y_m^n\left(\frac{a}{w},\frac{t}{t_0}\right)=Y_{ref}^n\cdot f\left(\frac{a}{w}\right)\cdot g\left(\frac{t}{t_0}\right) \tag{28}$$

where

$$f\left(\frac{a}{w}\right)=\frac{Y_m^n\left(\frac{a}{w},\frac{t}{t_0}=0.2\right)}{Y_{ref}^n},\ g\left(\frac{t}{t_0}\right)=\frac{Y_m^n\left(\frac{a}{w}=0.5,\frac{t}{t_0}\right)}{Y_{ref}^n},\ Y_{ref}^n=Y_m^n\left(\frac{a}{w}=0.5,\frac{t}{t_0}=0.2\right)$$

According to Eq. (28), the results obtained from the H-integral approach can be fitted to the power function $f(geometry)=j(geometry)^k$ and $g(geometry)=l(geometry)^s$. The best-fit values of the parameters j, k, l and s are shown in Fig. 7 for the isotropic Au/Si multi-layered structure. The detailed values obtained from H-integral approach and mathematical fit are given in Table 3. Moreover, the reference geometry we chose here is representative for practical applications.

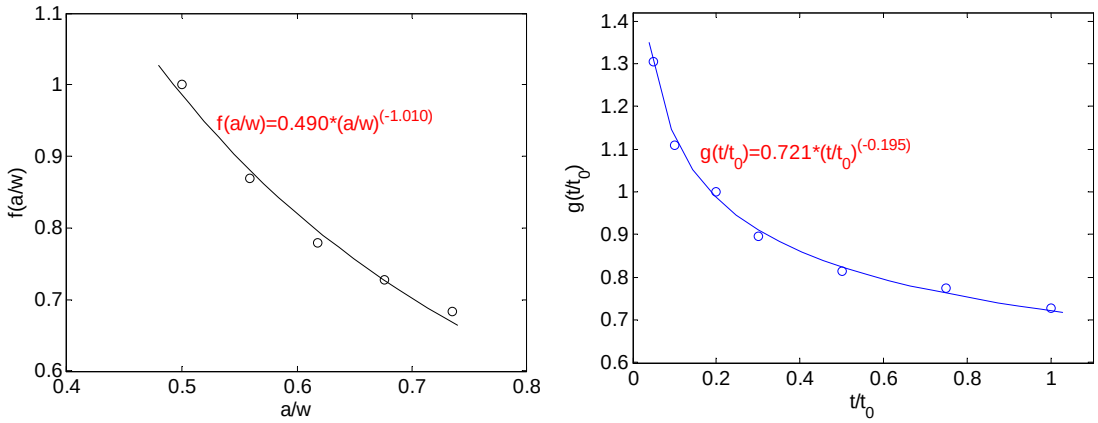

Fig. 7 The power function $f\left(\frac{a}{w}\right)$ and $g\left(\frac{t}{t_0}\right)$ for isotropic Au/Si multi-layered structure

Table 3

Fitting of the H-integral solutions for isotropic Au/Si multi-layered structure

$\frac{a}{w}$	$\frac{Y_m^n\left(\frac{a}{w},\frac{t}{t_0}=0.2\right)}{Y_{ref}^n}$	$f\left(\frac{a}{w}\right)$	$\frac{t}{t_0}$	$\frac{Y_m^n\left(\frac{a}{w}=0.5,\frac{t}{t_0}\right)}{Y_{ref}^n}$	$g\left(\frac{t}{t_0}\right)$
0.5	1	0.989	0.05	1.304	1.292
0.56	0.869	0.881	0.1	1.109	1.128
0.62	0.779	0.797	0.2	1	0.986
0.68	0.727	0.727	0.3	0.895	0.911
0.74	0.683	0.668	0.5	0.815	0.825
			0.75	0.773	0.773
			1	0.729	0.721

Consequently, a standardized numerical formula for the engineering design reads

$$Y^n_{H\text{-integral}}\left(\tfrac{a}{w},\tfrac{t}{t_0}\right)=1.464\times 0.490\left(\tfrac{a}{w}\right)^{-1.010}\times 0.721\left(\tfrac{t}{t_0}\right)^{-0.195} \tag{29}$$

where

$$Y^n_{ref}=Y^n_{\left(\frac{a}{w}=0.5,\frac{t}{t_0}=0.2\right)}=1.464,\ t_0=1000nm \text{ and } 0.5\le\tfrac{a}{w}\le 0.74,\ 0.05\le\tfrac{t}{t_0}\le 1.$$

Such relationships can be derived for other material combinations as well.

4.4. Effects of material mismatch, conductor layer thickness, and bond area on the dimensionless stress intensity factor Y

The aim of this section is to present a parametric study including the effect of material mismatch, thin film thickness, and bond area on the singular stress field.

Using the geometry, loading and mesh illustrated in Fig. 4 as a basis, material combinations are chosen relevant to the integrated circuits industry. The effect of the elastic mismatch on stress intensity factor is investigated here. Alternative conductor layers of copper (Cu), gold (Au) or aluminium (Al) are employed for material A, see Fig. 2. For the free edge interface (interface X), it can be observed from Fig. 8 that the structure with a Cu layer yields the highest dimensionless stress intensity factor Y_1^n, followed by that with Au and Al layer. Comparison between isotropic Si and anisotropic Si substrate is also included. Anisotropy of the Si substrate has a significant influence on the stress intensity factor when combined with an Au or Al metal layer but not with a Cu layer. Unlike the response of the structure with a Cu layer, the stress intensity factor for an isotropic Si substrate is lower than that for an anisotropic Si substrate with the other two metal materials. We believe this is due to the copper and isotropic silicon having similar elastic constants and single crystal silicon being only slightly elastically anisotropic (Suwito, 1997). Besides, Au and Al have similar performance owing to $\frac{E_{Au}}{E_{Al}}\approx 1$. It is not surprising that the influence of the metal material properties and the anisotropy of silicon substrate on the stress intensity factor for the 90° sharp notch (interface Y) is insignificant.

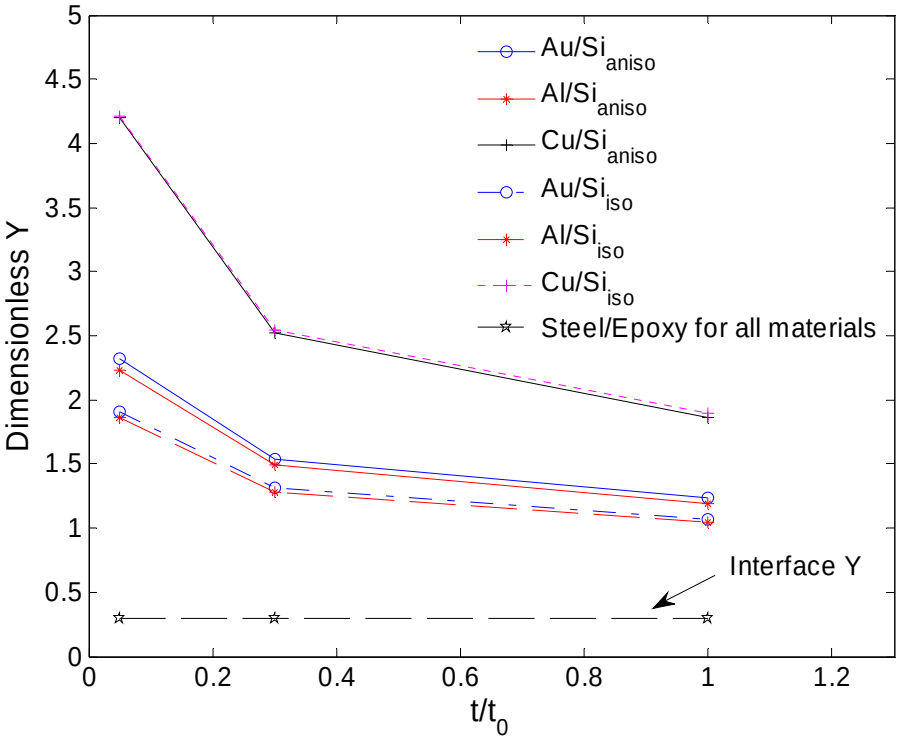

Fig. 8 The effect of material properties and thickness of metal layer on the dimensionless stress intensity factor ($t_0 = 1000nm$)

Fig. 8 also shows the effect of thin-film thickness on the dimensionless stress intensity factor. In these simulations, the bond area is kept constant ($a = 1.7$ mm), the thin film thickness equal to 50, 100, 200, 300, 500, 750 and 1000 nm are analyzed. It turns out that the magnitude of stress intensity factor for interface X approaches a constant value with increasing the thickness of metal layer. It is clearly shown that the contribution of thin-film thickness needs to be considered in order to accurately describe the singular stress state in the vicinity of free edge interface when the metal layer is less than 300 nm thick. That is to say, the stress intensity factor is sensitive to thin-film thickness in some cases whereas the thickness component can be ignored in considering the dimensionless stress intensity factor when metal layer is above a certain thickness. On the other hand, the stress intensity factor decreases with the increasing conductor layer thickness but the variation of metal layer thickness has no contribution to the change of singular stress field for interface Y.

In addition, the effect of the bond width is depicted in Fig. 9. In this case, the metal layer (Au) remains 200 nm thick ($\frac{t}{t_0} = 0.2$), the isotropic silicon substrate thickness is 3.4 mm whereas the bond width is varied from 1.7 to 2.5 mm. The stress intensity factor for interface X clearly decreases with the bond area but change insignificantly for interface Y.

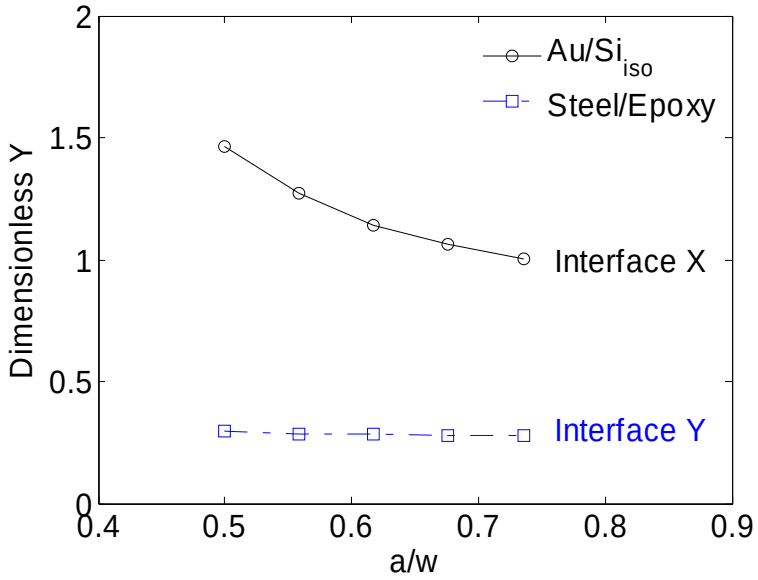

Fig. 9 The effect of bond area for an isotropic Si substrate

4.5. The competition between the 90° notch interface and the free edge interface

It is of interest to discuss the competition of crack initiation between the free edge interface (interface X) and the 90º notch interface (interface Y) in the chosen specimens. The dimensionless stress intensity factor Y is higher for the former than for the latter as shown in Fig. 8. But the stress field is governed by the combination of Y and λ, i.e., the stress is proportional to $\frac{Y}{r^{1-\lambda}}$. In the competition between notch X and Y this has to be considered. For notch Y, λ is 0.7049, and for notch X, λ is an order of magnitude less. In addition, the fracture resistance for the material at notch X and Y will differ. Hence, the fracture competition is governed by the set (K or Y, λ, fracture resistance) of notch X and Y, respectively.

4.6. Applicability of the H-integral and existence of the K-dominated field

The proposed H-integral approach is based on the assumption of anisotropic elasticity with the dominance of a K-field. The asymptotic solution has poor approximation very close to and far away from the interface corner. Stress singularity at the notch tip is only theoretically possible as the notch root radius will be finite, the material can be non-linear and inhomogeneous. Provided that the inelastic zone is much smaller than the K-dominated field, the stress obtained from the asymptotic analysis can reflect the actual stress state. The plastic region is controlled by the yield stress. Following the work of Irwin (1960), the plastic zone size is estimated by Banks-Sills and Sherer (2002) for dissimilar isotropic bi-material and by Suwito (1997) for anisotropic silicon. In our investigation, since the analyses are for linear elastic materials, it is assumed that the plastic zone size is very small, i.e., small scale yielding conditions hold at the interface corner.

Far away from the notch tip, the solution is perturbed by finite boundaries and loading so that K_m^n can no longer characterize the actual stress state and then higher order terms are required to describe the behaviour. As a result, the asymptotic solution has a limited domain of validity.

To quantify the extent of the region dominated by the K-field and validate the applicability of

the H-integral approach, finite element calculations were performed for diverse material combinations, illustrated in Fig. 10. The stress component $\sigma_{\theta\theta}$ along the interface X is employed. Subjected to the remote load of 200 μN, the results obtained from the H-integral approach and the detailed FE solutions agree satisfactorily, e.g., the normal stress $\sigma_{\theta\theta}$ obtained from two methods agrees to 10% within a distance of 52.5 nm for Al (200 nm)/Si case with 2100 μm bond width. Similar results are obtained for the other material systems.

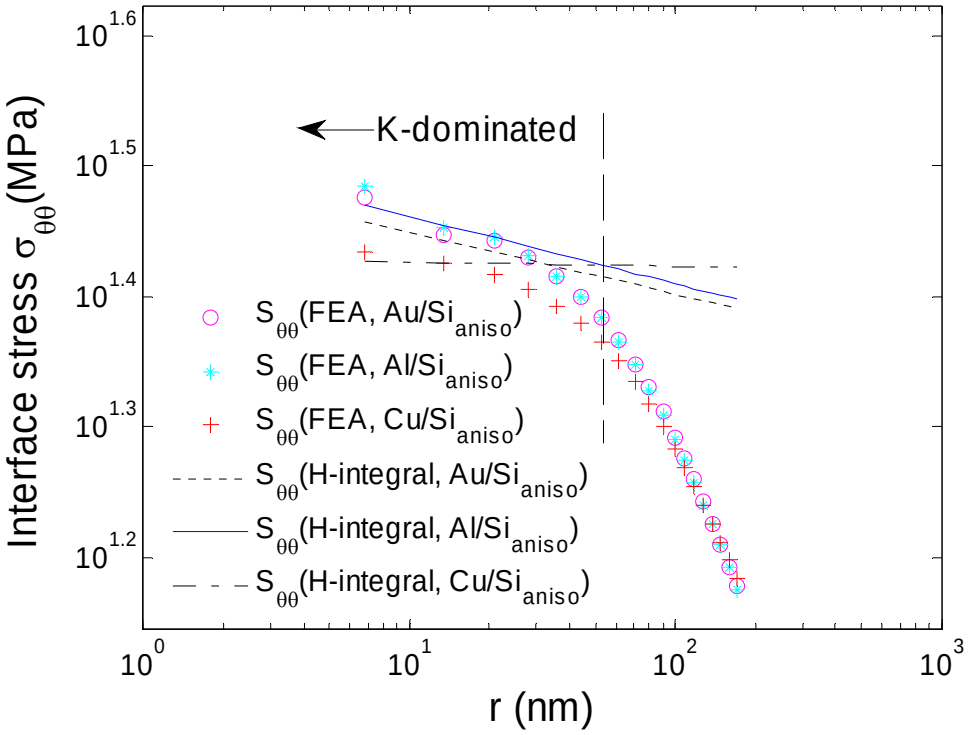

Fig. 10 Comparison of interface stress from asymptotic solutions associated with λ_1 and the detailed finite element results for different material combinations

Furthermore, a full singular stress field can be developed in an infinite bi-material system. Crack initiation is clearly governed by this *K*-dominated field. However, this is not always the case for a multi-layered thin film system. The extent of the singular field is strongly influenced by finite geometry, such as the thin film thickness. It is possible to evaluate the size of *K*-field by comparing the asymptotic solution to a detailed FE numerical analysis. Consider an Au layer bonded with a 1.7 mm wide isotropic silicon substrate. Fig. 11 shows the interface stress $\sigma_{\theta\theta}$ from detailed finite element analysis with varying metal layer thickness subjected to remote load of 200 μN. Regarding a 5% deviation of predicted $\sigma_{\theta\theta}$ calculated from the H-integral approach from the detailed FE results, Fig. 12 further shows the relationship between the valid range of *K*-field and the thin-film thickness for the free edge interface. The thicker the metal layer, the more extensive is the valid range of *K*-field for interface X. In contrast to Fig. 10, the valid *K*-field is much larger for interface Y displayed in Fig. 13. It should be also pointed out that even though the metal layer thickness reaches nanometer scale, the stress intensity factor K_m^n can still characterize the singular stress field. The H-integral approach is a sufficient and effective way to evaluate the

interface failure for multi-layered thin film structures, remembering that the selection of the outer contour should be neither very close to nor far away from the notch tip. It should also be noted that inaccuracy of the stress intensity factor can be induced by the numerical approximations made in the finite element calculation and by the numerical integration scheme adopted to calculate the H-integral. It can be improved by generating a reasonable finite element mesh and choosing a contour with a reasonable number of integration points, sufficiently far from the notch tip (e.g., Stern et al., 1976; Carpenter, 1984a; 1984b; Banks-Sills, 1997; Labossiere and Dunn, 1998; 1999; Banks-Sills and Sherer, 2002). It has also been observed that the choice of the integration path is less significant for interface Y than that for interface X.

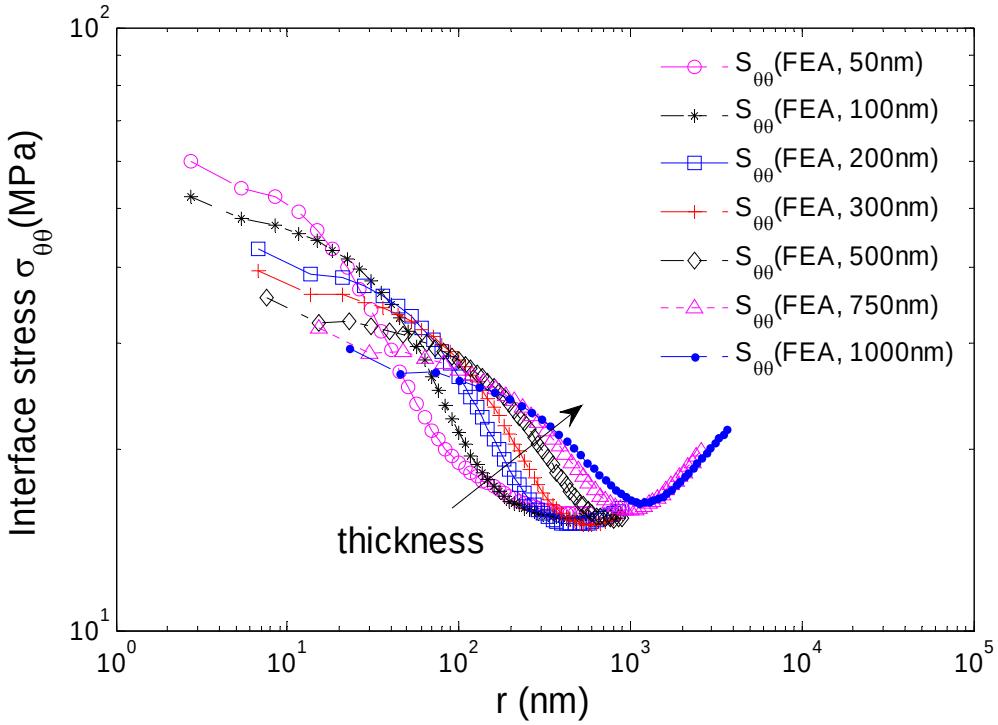

Fig. 11 The interface stresses obtained from detailed finite element solution with varying metal layer thickness

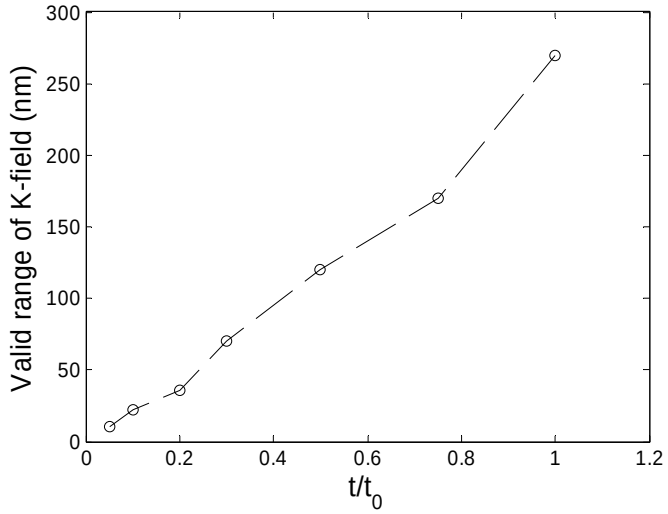

Fig. 12 The relationship of K-dominated field and thin-film thickness.

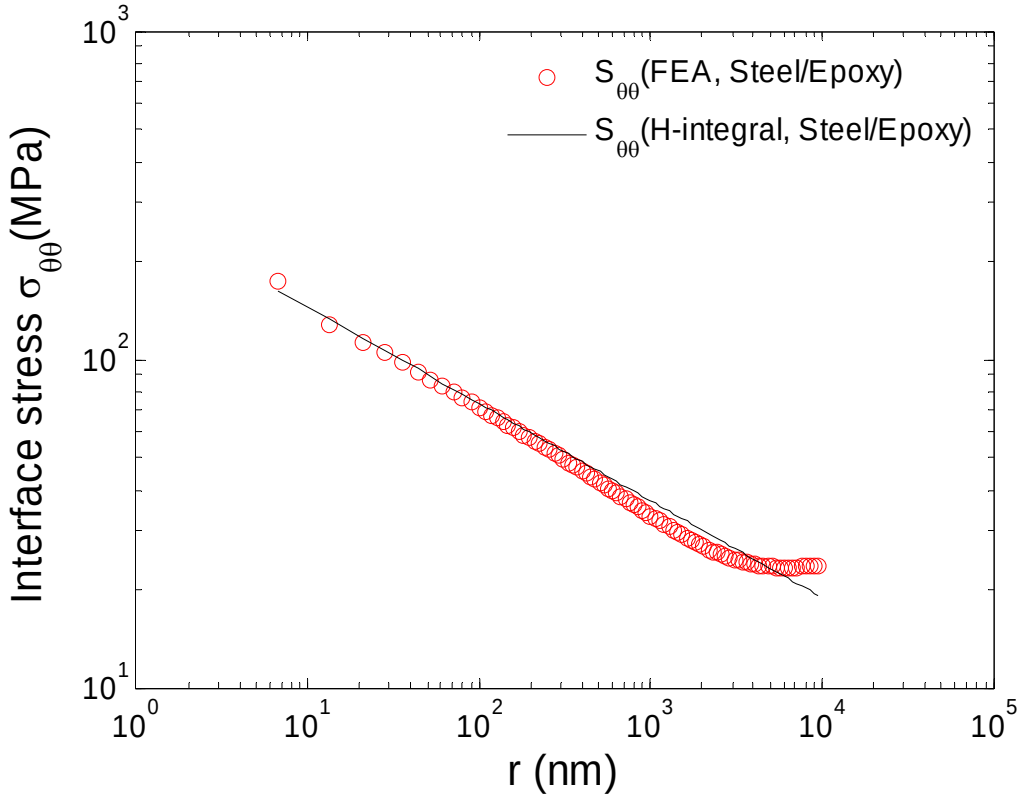

Fig. 13 Interface stress for interface Y with 200nm thick metal layer

A failure criterion based on the critical concentrated stress σ_{fc} (Kitamura et al., 2007) has been proposed to characterize the crack initiation. It was shown that the slope of interface stress is very moderate and the stress near the edge is almost constant in the nanometer (or atomic) range among the specimens with metal layer (200nm thick) in the region of $r < 500$ nm . However, our study found that an observable stress gradient exists for both interface X and interface Y shown in Fig. 11 and Fig. 14. Besides, from the magnified view of stress distributions near the free edge interface, see Fig. 15, it indicates that the stress gradient is significant for the specimens with metal layers thinner than 100 nm . As a consequence, we believe that the critical stress intensity factor is a feasible and alternative method to correlate crack initiation compared with critical failure strength for the problem shown in

Fig. *3*. However, when the thin-film thickness is very low and the elastic singularity may not dominate a region compared to the inelastic zone, it may be possible that K_m^n no longer is feasible for fracture initiation prediction. Note that from Table 2, the slope of the stress versus r curves for this material combination should ideally be -0.0668. Some deviation from this value appears in the slopes in Fig. 15. This is due to the influence of the layer thickness and some inaccuracies, and the finite element meshes employed to get these very detailed stress results close to the notch tip.

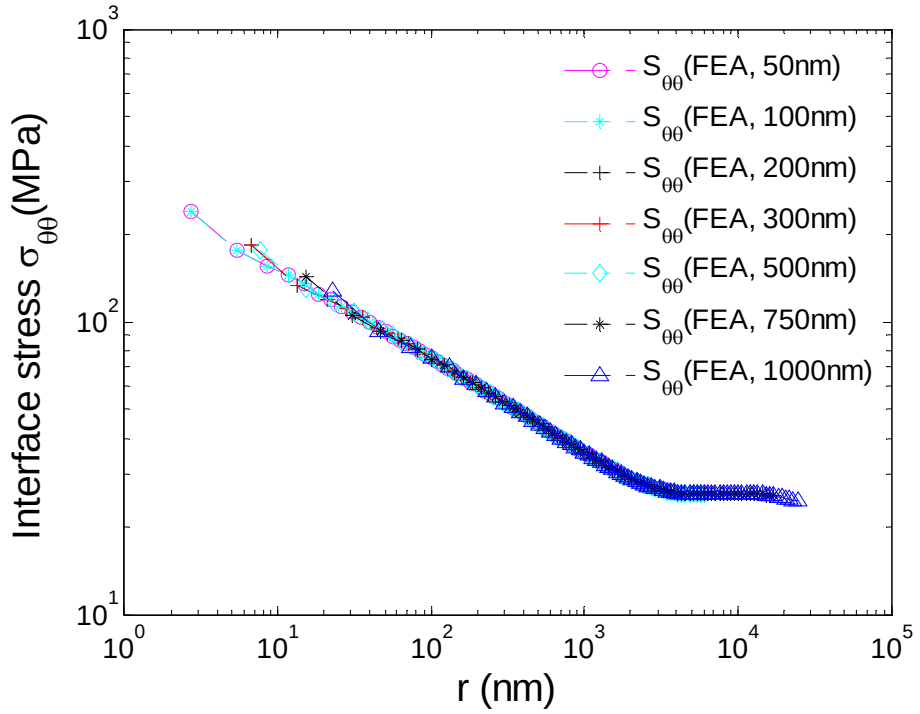

Fig. 14 The stress distributions along the interface Y.

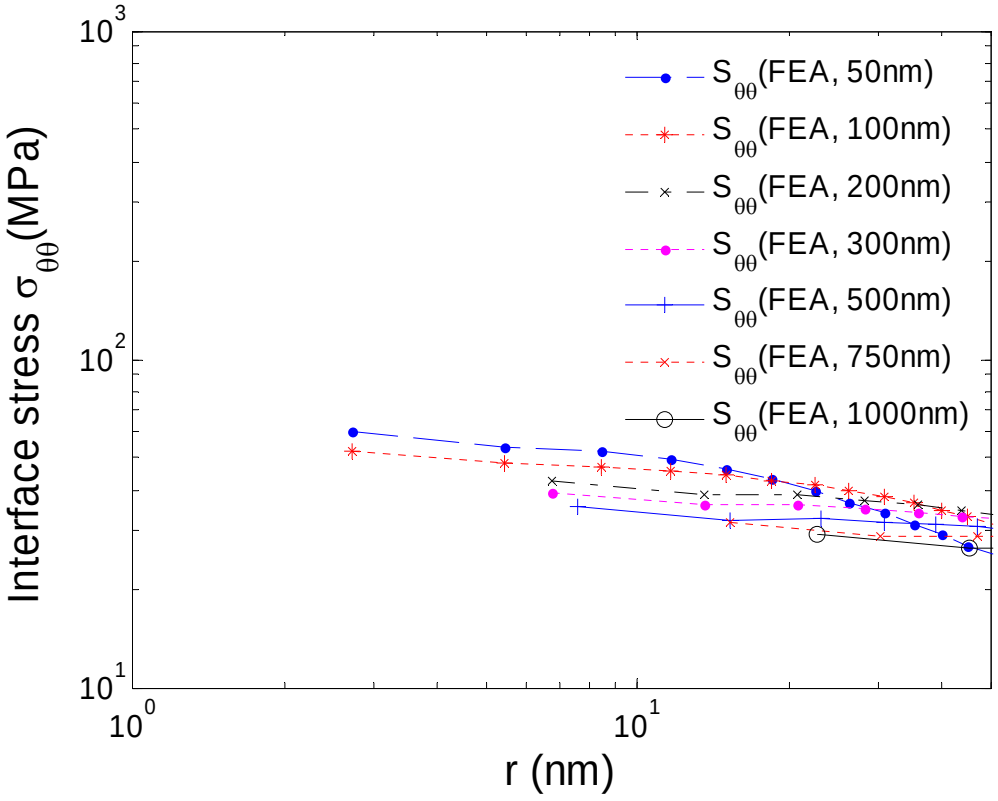

Fig. 15 The magnified view (log–log plot) of the stress distributions near the interface edge for the Au/Si specimens.

It is also worth noting that the deformation is actually mixed-mode for an interfacial notch with dissimilar materials. Interface shear stress and normal stress for Au (200 nm)/Si case with 2100 μm versus the distance from the interface corner are plotted in Fig. 16. Note that the shear stress along the interface is much lower than the normal stress. Mode I deformation is dominating in the cases analyzed here. Again, one typical case of Au(200 nm)/Si was chosen for comparison, as depicted in Fig. 4. Finite element calculations were performed with the applied load equal to the failure load 0.6 N (Kitamura et al., 2007). The free edge fracture toughness attained from H-integral approach is $5.8\ \text{MPa m}^{0.067}$, which matches well with $5.3 \pm 0.5\ \text{MPa m}^{0.067}$ from the literature (Kitamura et al., 2007). Therefore, this comparison suggests that the critical mode I stress intensity factor can be used to correlate the onset of fracture at the interface corner.

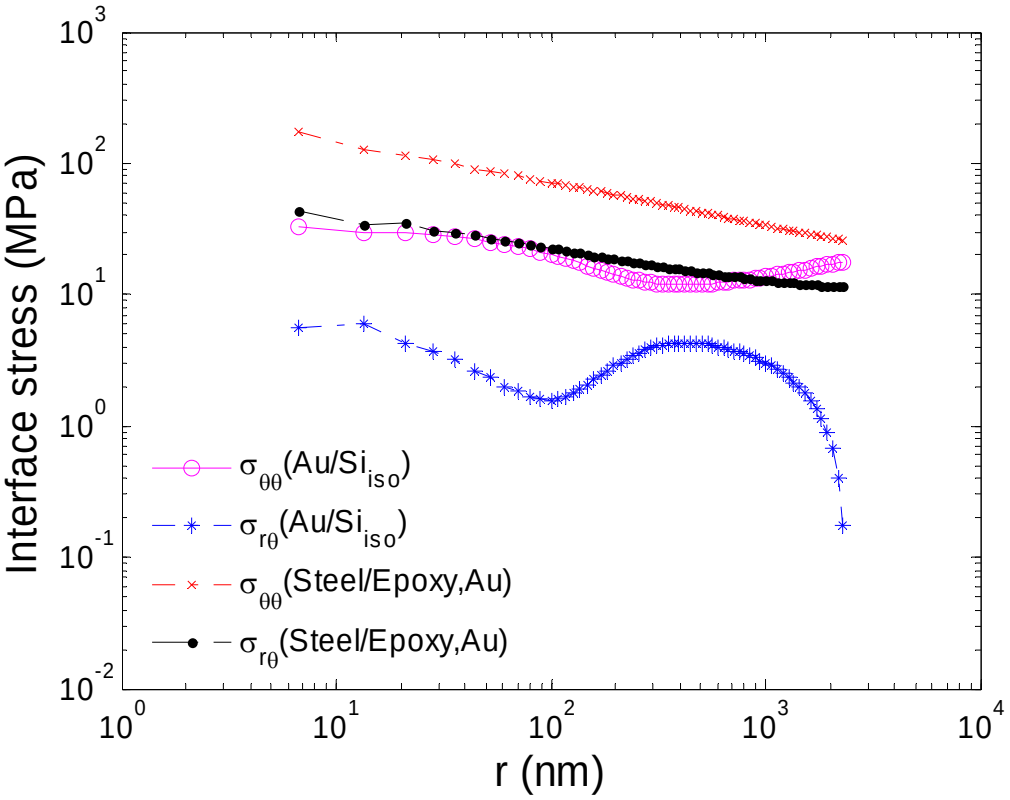

Fig. 16 Interface normal stress and shear stress

A possible criticism of H-integral approach arises in that we have disregarded the possibility of plastic deformation in ductile metal layer. To check the validity of this approximation, elastic-plastic analysis was executed to allow plastic deformation in the metal layer. Taking Au (200 nm)/Si as an example and assuming the elastic–linear hardening model with a yield stress of 160 MPa and a hardening modulus of 8.3 GPa . Applying the critical delamination load $P_c = 0.6$ N from (Kitamura et al., 2007) to the specimen, it is observed that no plastic strain occurred in the finite element analysis. An explanation for this is that the relatively stiff silicon substrate and the steel cantilever compared with the compliant gold film restrain the plastic deformation of the metal layer. On the other hand, given that silicon exhibits no observable plasticity at room temperature (Lawn, 1995), it is reasonable to assume the K-field is relatively

large compared to the plastic zone at the notch tip. This is further supported by Sinclair and Lawn's (1972) calculation, which shows that strong crack tip non-linearities extend only a few atomic spacings from the crack tip.

5. Conclusions

Our study shows that the H-integral is a feasible and a reliable approach to compute the edge stress intensity factor in multi-layered structural components with weak singularities. The asymptotic analysis provides the basis for a proper modelling of the singular stress field and illustrates the dependence of stress singularity on elastic mismatch parameters. The stress intensity factors are obtained for a wide range of material and geometry parameters.

A wide range of material combinations which commonly appear in the integrated circuits industry is considered. The effects of elastic mismatch, bond area and metal layer thickness on the stress intensity factor have been quantified. The proposed approach is favourable from an engineering point of view, due to the fact that such situations are occurring very frequently in composite structural elements and it can be used as a supplement for a preliminary design of new components.

Furthermore, the analysis of the competition for crack initiation between a free edge interface and a 90º notch interface in the chosen specimen has been presented and the question of prevailing failure mode in multi-layered structural components is addressed. Due to the possibility to shift the crack initiation site between two different notch interfaces, sufficient attention should be paid to this issue.

The applicability of the H-integral approach and existence of the K-dominated field has been studied. The extent of the singular field is assessed by comparing the asymptotic solution to the detailed Finite Element analysis of the stress fields. It is observed that the valid range of the K-field is strongly influenced by thin-film thickness. The relation between the K-field and thin-film thickness is depicted as well. Again, to demonstrate the accuracy of this contour integral approach, example problems are considered and results are in good agreement with those from the literature.

In addition, plastic deformation in the ductile material, anisotropy of the silicon substrate and different failure criterions have been explored. Standardized numerical formulae have also been provided to for practical application of the H-integral.

Note that the grown of thin interlayers between the Silicon substrate and the steel cantilever is not considered in the present study. This hypothesis results in perfectly bonded interfaces, assuming no relative displacements between each other. The validity of this hypothesis deserves further discussion (e.g., Sinclair, 1996; Carpinteri and Paggi, 2008).

Reference List

Babuska, I., Miller, A., (1984). The Post-Processing Approach in the Finite-Element Method .2. the Calculation of Stress Intensity Factors. International Journal for Numerical Methods in Engineering 20**,** 1111-1129.

Banks-Sills, L., (1997). A conservative integral for determining stress intensity factors of a bimaterial strip. International Journal of Fracture 86**,** 385-398.

Banks-Sills, L., Sherer, A., (2002). A conservative integral for determining stress intensity factors of a bimaterial notch. International Journal of Fracture 115**,** 1-26.

Bogy, D. B., (1971). Two edge-bonded elastic wedges of different materials and wedge angles under surface tractions. Journal of Applied Mechanics 38**,** 377-386.

Carpenter, W. C., (1984a). Calculation of Fracture-Mechanics Parameters for A General Corner. International Journal of Fracture 24**,** 45-58.

Carpenter, W. C., (1984b). Mode I and Mode II stress intensity factors for plates with cracks of finite opening. International Journal of Fracture 26**,** 201-214.

Carpenter, W. C., (1995). Insensitivity of the reciprocal work contour integral method to higher order eigenvectors. International Journal of Fracture 73**,** 93-108.

Carpenter, W. C., Byers, C., (1987). A Path Independent Integral for Computing Stress Intensities for V-Notched Cracks in A Bi-Material. International Journal of Fracture 35**,** 245-268.

Carpinteri, A., Paggi, M., (2007). Numerical analysis of fracture mechanisms and failure modes in bi-layered structural components. Finite Elements in Analysis and Design 43**,** 941-953.

Carpinteri, A., Paggi, M., (2008). Thermo-elastic mismatch in nonhomogeneous beams. Journal of Engineering Mathematics 61**,** 371-384.

Carpinteri, A., Paggi, M., Pugno, N., (2006). Numerical evaluation of generalized stress-intensity factors in multi-layered composites. International Journal of Solids and Structures 43**,** 627-641.

Chen, D. H., (1996). Logarithmic singular stress field in a semi-infinite plate consisting of two edge-bonded wedges subjected to surface tractions. International Journal of Fracture 75**,** 357-378.

Chen, D. H., Nisitani, H., (1993). Singular Stress-Field Near the Corner of Jointed Dissimilar Materials. Journal of Applied Mechanics-Transactions of the ASME 60**,** 607-613.

Dempsey, J. P., (1995). Power-Logarithmic Stress Singularities at Bi-Material Corners and Interface Cracks. Journal of Adhesion Science and Technology 9**,** 253-265.

Dempsey, J. P., Sinclair, G. B., (1979). On the Stress Singularities in the Plane Elasticity of the Composite Wedge. Journal of Elasticity 9**,** 373-391.

Dempsey, J. P., Sinclair, G. B., (1981). On the Singular Behavior at the Vertex of a Bimaterial Wedge. Journal of Elasticity 11**,** 317-327.

Dunn, M. L., Cunningham, S. J., Labossiere, P. E. W., (2000). Initiation toughness of silicon/glass anodic bonds. Acta Materialia 48**,** 735-744.

Eshelby, J. D., Read, W. T., Shockley, W., (1953). Anisotropic Elasticity with Applications to Dislocation Theory. Acta Metallurgica 1**,** 251-259.

Hong, C. C., Stern, M., (1978). Computation of Stress Intensity Factors in Dissimilar Materials. Journal of Elasticity 8**,** 21-34.

Hutchinson, J. W., (1990). Mixed mode fracture mechanics of interfaces. Metal-Ceramic Interfaces, Acta-Scripta Metalurgica Proceedings Series 4**,** 295-306.

Hutchinson, J. W., Suo, Z., (1992). Mixed-Mode Cracking in Layered Materials. Advances in Applied Mechanics, Vol 29 29**,** 63-191.

Irwin, G. R., (1960). Plastic zone near a crack tip and fracture toughness. Seventh Sagamore Ordinance Materials Research Conference 6**,** 63-79.

Kitamura, T., Hirakata, H., Itsuji, T., (2003). Effect of residual stress on delamination from interface edge between nano-films. Engineering Fracture Mechanics 70**,** 2089-2101.

Kitamura, T., Hirakata, H., Van Truong, D., (2007). Initiation of interface crack at free edge between thin films with weak stress singularity. Thin Solid Films 515**,** 3005-3010.

Kitamura, T., Shibutani, T., Ueno, T., (2002). Crack initiation at free edge of interface between thin films in advanced LSI. Engineering Fracture Mechanics 69**,** 1289-1299.

Labossiere, P. E. W., Dunn, M. L., (1998). Calculation of stress intensities at sharp notches in anisotropic media. Engineering Fracture Mechanics 61**,** 635-654.

Labossiere, P. E. W., Dunn, M. L., (1999). Stress intensities at interface corners in anisotropic bimaterials. Engineering Fracture Mechanics 62**,** 555-575.

Labossiere, P. E. W., Dunn, M. L., Cunningham, S. J., (2002). Application of bimaterial interface corner failure mechanics to silicon/glass anodic bonds. Journal of the Mechanics and Physics of Solids 50**,** 405-433.

Lawn, B., (1995). Fracture of Brittle Solids. University Press, Cambridge.

Luo, Y. P., Subbarayan, G., (2007). A study of multiple singularities in multi-material wedges and their use in analysis of microelectronic interconnect structures. Engineering Fracture Mechanics 74**,** 416-430.

Mason, W. P., (1958). Physical Acoustics and the Properties of Solids. Van Nostrand, New York.

Munz, D., Yang, Y. Y., (1993). Stresses Near the Edge of Bonded Dissimilar Materials Described by 2 Stress Intensity Factors. International Journal of Fracture 60**,** 169-177.

Paggi, M., Carpinteri, A., (2008). On the stress-singularities at multi-material interfaces and related analogies with fluid dynamics and diffusion. ASME Applied Mechanics Reviews 61**,** 1-22.

Qian, Z. Q., (2001). On the evaluation of wedge corner stress intensity factors of bi-material joints with surface tractions. Computers & Structures 79**,** 53-64.

Qian, Z. Q., Akisanya, A. R., (1999). Wedge corner stress behaviour of bonded dissimilar materials. Theoretical and Applied Fracture Mechanics 32**,** 209-222.

Reedy, E. D., Guess, T. R., (1993). Comparison of Butt Tensile-Strength Data with Interface Corner Stress Intensity Factor Prediction. International Journal of Solids and Structures 30**,** 2929-2936.

Reedy, E. D., Guess, T. R., (2002). Nucleation and propagation of an edge crack in a uniformly cooled epoxy/glass bimaterial. International Journal of Solids and Structures 39**,** 325-340.

Rogers, G. L., Causey, M. L., (1962). Mechanics of engineering structures. John Wiley and Sons, New York.

Shang, L. Y., Zhang, Z. L., Skallerud, B., (2008). Fracture of anodic-bonded silicon-thin film glass-silicon triple stacks. Engineering Fracture Mechanics 75**,** 1064-1082.

Sih, G. C., Ho, J. W., (1991). Sharp Notch Fracture Strength Characterized by Critical Energy Density. Theoretical and Applied Fracture Mechanics 16**,** 179-214.

Sinclair, G. B., (1985). A Remark on the Determination of Mode-I and Mode-Ii Stress Intensity Factors for Sharp Re-Entrant Corners. International Journal of Fracture 27**,** R81-R85.

Sinclair, G. B., (1996). On the influence of cohesive stress-separation laws on elastic stress singularities. International Journal of Elasticity 44**,** 203-221.

Sinclair, G. B., (1999). Logarithmic stress singularities resulting from various boundary conditions in angular corners of plates in extension. Journal of Applied Mechanics-Transactions of the ASME 66**,** 556-560.

Sinclair, G. B., Okajima, M., Griffin, J. H., (1984). Path Independent Integrals for Computing Stress Intensity Factors at Sharp Notches in Elastic Plates. International Journal for Numerical Methods in Engineering 20**,** 999-1008.

Sinclair, J. E., Lawn, B. R., (1972). Atomistic Study of Cracks in Diamond-Structure Crystals. Proceedings of the Royal Society of London Series A-Mathematical and Physical Sciences 329**,** 83-&.

Snyder, M. D., Cruse, T. A., (1975). Boundary-Integral Equation Analysis of Cracked Anisotropic Plates. International Journal of Fracture 11**,** 315-328.

Stern, M., (1979). Numerical-Calculation of Thermally Induced Stress Intensity Factors. Journal of Elasticity 9**,** 91-95.

Stern, M., Becker, E. B., Dunham, R. S., (1976). Contour Integral Computation of Mixed-Mode Stress Intensity Factors. International Journal of Fracture 12**,** 359-368.

Stern, M., Soni, M. L., (1975). The calculation of stress intensity factors in anisotropic materials by a contour integral method. Computational Fracture Mechanics, ASME 2nd National Congress on Pressure Vessels and Piping, San Francisco.

Stern, M., Soni, M. L., (1976). On the Computation of Stress Intensities at Fixed-Free Corners. International Journal of Solids and Structures 12**,** 331-337.

Stroh, A. N., (1958). Dislocations and Cracks in Anisotropic Elasticity. Philosophical Magazine 3**,** 625-646.

Suwito, W., (1997). Fracture of notched silicon microstructures. Ph.D thesis, University of Colorado.

Szabo, B. A., Babuska, I., (1988). Computation of the amplitude of stress singular terms for cracks and re-entrant corners. San Antonio, TX, United States.

Ting, T. C. T., (1996). Anisotropic Elasticity: Theory and Applications. Oxford University Press, New York.

Ting, T. C. T., (1997). Stress Singularities at the Tip of Interfaces in Polycrystals. Damage and Failure of Interfaces, Rossmanith (ed.) 75-82.

Wang, X. S., Deng, Y. H., Li, Y. Q., (2002). An experimental investigation of failure behavior of conducting polythiophene coating films. Journal of Materials Science 37**,** 4743-4748.

Williams, M. L., (1952). Stress Singularities Resulting from Various Boundary Conditions in Angular Corners of Plates in Extension. Journal of Applied Mechanics-Transactions of the ASME 19**,** 526-528.

Williams, M. L., (1959). The stresses around a fault or crack in dissimilar media. Bulletin of the Seismological Society of America 49**,** 199-204.

Wu, K. C., Chang, F. T., (1993). Near-Tip Fields in A Notched Body with Dislocations and Body Forces. Journal of Applied Mechanics-Transactions of the ASME 60**,** 936-941.

Yang, Y. Y., Munz, D., (1997). Stress singularities in a dissimilar materials joint with edge tractions under mechanical and thermal loadings. International Journal of Solids and Structures 34**,** 1199-1216.

Yin, W. L., (1999). Mixed mode stress singularities in anisotropic composites. Thick Composites for Load Bearing Structures, ASME, AMD 235**,** 33-45.

Zhang, Z. L., Mikkola, T. P. J., (1992). A Simple Path-Independent Integral for Calculating Mixed-Mode Stress Intensity Factors. Fatigue & Fracture of Engineering Materials & Structures 15**,** 1041-1049.

PAPER III

Comments on the evaluation of the stress intensity factor for a general re-entrant corner in anisotropic bi-materials

Shang LY, Zhang ZL and Skallerud B.

Engineering Fracture Mechanics, accepted, DOI: 10.1016/j.engfracmech.2009.01.012

Technical note:

Comments on the evaluation of the stress intensity factor for a general re-entrant corner in anisotropic bi-materials

L. Y. Shang, Z. L. Zhang and B. Skallerud

Department of Structural Engineering, Norwegian University of Science and Technology (NTNU), N-7491 Trondheim, Norway

Abstract

This paper illustrates an efficient contour integral procedure to obtain stress intensity factors in combination of the asymptotic analysis with finite element analysis. Note that this set-up is very general: the material can be anisotropic elastic, and the specimen can be built as a bi-material system, notches of arbitrary opening angle can be analyzed (γ=0 → crack, γ=180° → free edge). The purpose of this technical note is to comment on three issues in the notch mechanics: the interpretation of the eigenvalue equation, the definition of stress intensity factors, and the effect of the outer contour location on H-integral evaluations.

Keywords: stress intensity factor, contour location, notch mechanics, eigenvalue equation

1. Introduction

It is well known that the failure of many bonded joints often initiates at the interface corner (Fig. 1) due to the stress concentration. The singular stress fields around the corner play an important role in assessing the reliability of the joints and can be characterized by eigenvalues λ_m and notch stress intensity factors K_m^n. An efficient contour integral procedure to obtain stress intensity factors in combination of the asymptotic analysis with finite element analysis is briefly illustrated in Fig. 2. Note that this set-up is very general: the material can be anisotropic elastic, and the specimen can be built as a bi-material system, notches of arbitrary opening angle can be analyzed (γ=0 → crack, γ=180° → free edge). The detailed descriptions can be found elsewhere (Shang et al., 2008; 2009).

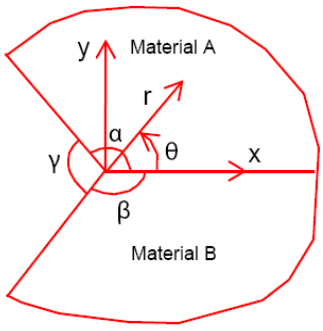

Fig. 1 Schematic plot of a re-entrant corner in a bi-material system

The purpose of this technical note is to comment on three issues in the notch mechanics: the interpretation of the eigenvalue equation, the definition of stress intensity factors, and the effect of the outer contour location on H-integral evaluations.

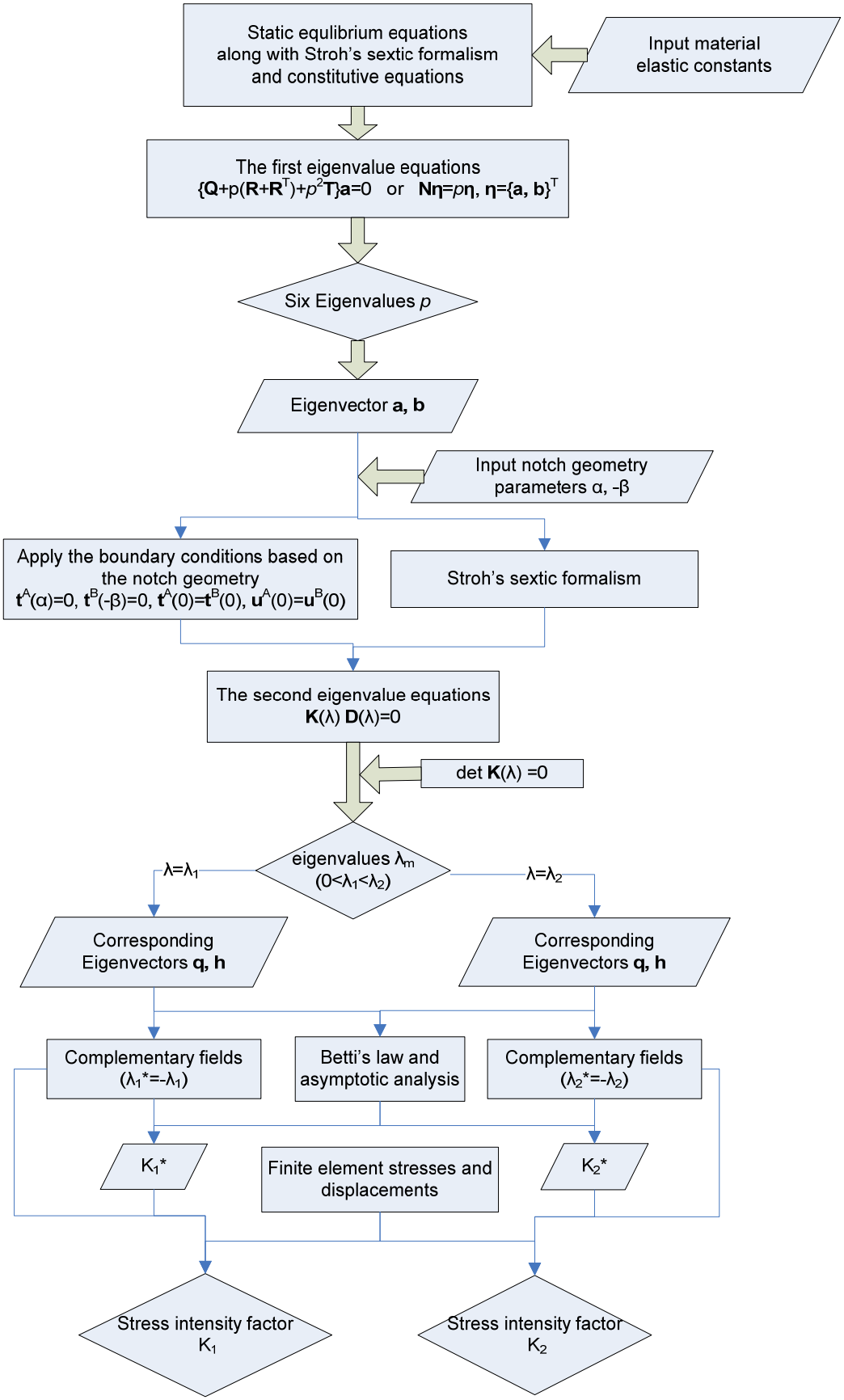

Fig. 2 flow chart illustrating the procedure to obtain the stress intensity factor

2. Interpretation of the eigenvalue equation

Utilizing the traction-free boundary conditions (1) on the notch flanks ($\theta=\alpha,\ \theta=-\beta$) and continuity along the interface,

$$\mathbf{t}^A(\alpha)=0,\ \mathbf{t}^B(-\beta)=0,\ \mathbf{t}^A(0)=\mathbf{t}^B(0),\ \mathbf{u}^A(0)=\mathbf{u}^B(0) \tag{1}$$

six simultaneous eigenvalue equations with six unknowns $q_\alpha^A,\ h_\alpha^B\ (\alpha=1,2,3)$ are deduced as:

$$\begin{bmatrix} \mathbf{b}^A\left(\mathbf{B}^A\right)^{-1}-\bar{\mathbf{b}}^A\left(\bar{\mathbf{B}}^A\right)^{-1} & \left(\mathbf{b}^B\left(\mathbf{B}^B\right)^{-1}-\bar{\mathbf{b}}^B\left(\bar{\mathbf{B}}^B\right)^{-1}\right) \\ \mathbf{a}^A\left(\mathbf{B}^A\right)^{-1}-\bar{\mathbf{a}}^A\left(\bar{\mathbf{B}}^A\right)^{-1} & \left(\mathbf{a}^B\left(\mathbf{B}^B\right)^{-1}-\bar{\mathbf{a}}^B\left(\bar{\mathbf{B}}^B\right)^{-1}\right) \end{bmatrix} \begin{Bmatrix} \mathbf{B}^A\mathbf{q}^A \\ \bar{\mathbf{B}}^B\mathbf{h}^B \end{Bmatrix} = \mathbf{0} \tag{2}$$

The above equation can be simplified to

$$\mathbf{K}_1(\lambda)\ \mathbf{D}(\lambda)=\mathbf{0},\ \det\mathbf{K}_1(\lambda)=0 \tag{3}$$

where $\xi_\alpha(\theta)=(\cos\theta+p_\alpha\sin\theta)$, $\mathbf{B}^A=\left[\xi_1^A(\alpha)^\lambda\mathbf{b}_1^A,\ \xi_2^B(\alpha)^\lambda\mathbf{b}_2^A,\ \xi_3^B(\alpha)^\lambda\mathbf{b}_3^A\right]$, $\mathbf{B}^B=\left[\xi_1^B(-\beta)^\lambda\mathbf{b}_1^B,\ \xi_2^B(-\beta)^\lambda\mathbf{b}_2^B,\ \xi_3^B(-\beta)^\lambda\mathbf{b}_3^B\right]$, $\mathbf{D}=\left[\mathbf{B}^A\mathbf{q}^A,\ \bar{\mathbf{B}}^B\mathbf{h}^B\right]^{\mathrm{T}}$, $\mathbf{a}^M=\left[\mathbf{a}_1^M,\mathbf{a}_2^M,\mathbf{a}_3^M\right]$, $\mathbf{b}^M=\left[\mathbf{b}_1^M,\mathbf{b}_2^M,\mathbf{b}_3^M\right]$, $\mathbf{q}^M=\left[q_1^M,q_2^M,q_3^M\right]^{\mathrm{T}}$, $\mathbf{h}^M=\left[h_1^M,h_2^M,h_3^M\right]^{\mathrm{T}}$. $M=A,\ B$ corresponds to material system *A* or *B*. With this, the eigenvalues $\lambda_m(1,2,...)$ can be obtained.

One aspect that is not clearly shown in the literature is why the determinant of the matrix $\mathbf{K}_1(\lambda)$ is sufficient for a non-trival solution of (3) regardless of the matrix $\mathbf{D}(\lambda)$, noting that the matrix $\mathbf{D}$ is also a function of λ. The reason for it is stated below.

Equation (2) can be rewritten as

$$\underbrace{\underbrace{\begin{bmatrix} \mathbf{b}^A\left(\mathbf{B}^A\right)^{-1}-\bar{\mathbf{b}}^A\left(\bar{\mathbf{B}}^A\right)^{-1} & \left(\mathbf{b}^B\left(\mathbf{B}^B\right)^{-1}-\bar{\mathbf{b}}^B\left(\bar{\mathbf{B}}^B\right)^{-1}\right) \\ \mathbf{a}^A\left(\mathbf{B}^A\right)^{-1}-\bar{\mathbf{a}}^A\left(\bar{\mathbf{B}}^A\right)^{-1} & \left(\mathbf{a}^B\left(\mathbf{B}^B\right)^{-1}-\bar{\mathbf{a}}^B\left(\bar{\mathbf{B}}^B\right)^{-1}\right) \end{bmatrix}}_{\mathbf{K}_1} \underbrace{\begin{bmatrix} \mathbf{B}^A & \mathbf{0} \\ \mathbf{0} & \bar{\mathbf{B}}^B \end{bmatrix}}_{\mathbf{K}_2} \begin{Bmatrix} \mathbf{q}^A \\ \mathbf{h}^B \end{Bmatrix}}_{\mathbf{K}} = \mathbf{0} \tag{4}$$

That is,

$$\mathbf{K}(\lambda)\ \mathbf{q}=\mathbf{0} \tag{5}$$

A non-trivial solution exists only if the determinant of the coefficient matrix vanishes, i.e.:

$$\det\mathbf{K}(\lambda)=0\Leftrightarrow\det\left(\mathbf{K}_1(\lambda)\mathbf{K}_2(\lambda)\right)=0\Leftrightarrow\det\mathbf{K}_1(\lambda)\cdot\det\mathbf{K}_2(\lambda)=0 \tag{6}$$

Furthermore,

$$
\begin{aligned}
&\det \mathbf{K}_2(\lambda) = \det \mathbf{B}^A \bullet \det \bar{\mathbf{B}}^B \\
&= \det\left[\xi_1^A(\alpha)^\lambda \mathbf{b}_1^A,\quad \xi_2^A(\alpha)^\lambda \mathbf{b}_2^A,\quad \xi_3^A(\alpha)^\lambda \mathbf{b}_3^A\right] \bullet \det\left[\xi_1^B(-\beta)^\lambda \mathbf{b}_1^B,\quad \xi_2^B(-\beta)^\lambda \mathbf{b}_2^B,\quad \xi_3^B(-\beta)^\lambda \mathbf{b}_3^B\right] \\
&= \det\left(\xi_1^A(\alpha)^\lambda \cdot \xi_2^A(\alpha)^\lambda \cdot \xi_3^A(\alpha)^\lambda\right) \cdot \det\left[\mathbf{b}_1^A,\quad \mathbf{b}_2^A,\quad \mathbf{b}_3^A\right] \\
&\quad \bullet \det\left(\xi_1^B(-\beta)^\lambda \cdot \xi_2^B(-\beta)^\lambda \cdot \xi_3^B(-\beta)^\lambda\right) \cdot \det\left[\mathbf{b}_1^B,\quad \mathbf{b}_2^B,\quad \mathbf{b}_3^B\right] \\
&= \underbrace{\det\left(\xi_1^A(\alpha)^\lambda \cdot \xi_2^A(\alpha)^\lambda \cdot \xi_3^A(\alpha)^\lambda\right)}_{\neq 0} \cdot \underbrace{\det\begin{bmatrix} b_{11}^A & b_{12}^A & b_{13}^A \\ b_{21}^A & b_{22}^A & b_{23}^A \\ b_{31}^A & b_{32}^A & b_{33}^A \end{bmatrix}}_{\neq 0} \\
&\quad \bullet \underbrace{\det\left(\xi_1^B(-\beta)^\lambda \cdot \xi_2^B(-\beta)^\lambda \cdot \xi_3^B(-\beta)^\lambda\right)}_{\neq 0} \cdot \underbrace{\det\begin{bmatrix} b_{11}^B & b_{12}^B & b_{13}^B \\ b_{21}^B & b_{22}^B & b_{23}^B \\ b_{31}^B & b_{32}^B & b_{33}^B \end{bmatrix}}_{\neq 0}
\end{aligned}
\tag{7}
$$

$\mathrm{Det}\mathbf{K}_2(\boldsymbol{\lambda}) \neq 0$, and consequently Eq. (6) reduces to $\det \mathbf{K}_1(\lambda) = 0$.

3. Definition of stress intensity factors

Another issue in the notch mechanics relates to the definition of stress intensity factors. The concept of K_1^n, K_2^n and K_3^n in notch mechanics is quite different from the three deformation modes in traditional fracture mechanics. As we know, an interface edge and a notch are critical positions for crack initiation. Subjected to the remote mechanical loading, the interface stress field around the notch corner is proportional to $K_m^n r^{\lambda_m - 1}\left(m = 1, 2, \cdots N\right)$ where N is the number of eigenvalues available from the characteristic equation. Superscript n indicates the notch for the sake of distinction from the stress intensity factor K_m in classical fracture mechanics, r is the radial distance from the notch corner and $\lambda_m - 1$ is the order of the stress singularity. The stress field is singular for $0 < \mathrm{Re}(\lambda_m) < 1$ where $\mathrm{Re}(\lambda_m)$ is the real part of λ_m.

For a re-entrant corner (Fig. 1), we can define the two first stress intensity factors in terms of the opening and shear stress along either the interface for bi-materials or the bisector of homogeneous isotropic or anisotropic material, by using λ_1 and λ_2. Note that this is not the same as the Mode I and Mode II stress intensity factors employed in classical fracture mechanics

$$
K_1^n = \lim_{\theta=0, r\to 0} \frac{\sigma_{\theta\theta}(r,\theta)}{r^{\lambda_1 - 1}},\ K_2^n = \lim_{\theta=0, r\to 0} \frac{\tau_{r\theta}(r,\theta)}{r^{\lambda_2 - 1}}
\tag{8}
$$

where $\sigma_{\theta\theta}$, $\tau_{r\theta}$ are the normal and shear component of the stress field, respectively. Note that the definition of the stress intensity factor for a general corner problem is somewhat arbitrary. Nevertheless, some authors gave a different definition from (8). For instance, Stern and Soni (1976) used the following definition

$$
K_1^n = \lim_{\theta=0, r\to 0} \frac{\sigma_{\theta\theta}(r,\theta)}{r^{\lambda_1 - 1}},\ K_2^n = \lim_{\theta=0, r\to 0} \frac{\tau_{r\theta}(r,\theta)}{r^{\lambda_1 - 1}}
\tag{9}
$$

where the value of λ_1 is the smallest non-negative root of the characteristic equation (Stern and Soni, 1976; Carpenter, 1984a) and the principal part of the elastic state (near-tip displacements and stresses) is then precisely the eigenstate in terms of the value of λ_1. Carpenter (1984a) also followed this notation but changed back to (8) for all his subsequent studies. It is noted that there is two alternative ways of defining K_2^n. Hence, we focus on the shear stress term in eqs. (8) and (9) subsequently.

In a historical perspective, the former definition (8) seems more reasonable. This definition is supported by Suwito's (Dunn et al., 1997) experimental work. In his investigation, the notched flexure specimen (isotropic acrylic) were subjected to pure mode II loading and the eigenvalue describing the stress singularity of 90° notch was $\lambda_2 = 0.9085$ ($\lambda_1 = 0.5445$). Displacement components along the notch flanks were used to extract K_2^n. The critical stress intensity factor K_2^n was used to correlate fracture initiation. Meanwhile, it was illustrated that a better fit to detailed finite element results could be achieved if the constant term ($\lambda = 1$) was also considered.

As a matter of fact, the slope of $\log r$ versus $\log \tau_{r\theta}$ curve is no other than the order of the stress singularity $\lambda - 1$ for a single deformation mode. As for mixed-mode, usually the sum of the different singular fields, such as $K_1^n + K_2^n$ terms, will match the detailed finite element results in a wider range than that with any individual stress intensity factor K_1^n or K_2^n. However, the dominating stress intensity factor can be in good agreement with the detailed FE solutions.

The definition (8) is further explored in the following example. Consider a 90° notched specimen having the dimensions: height $H = 42$ mm, width $w = 17.2$ mm and notch depth $d = 1.78$ mm, see Fig. 3. The Young's modulus and Poisson's ratio for the specimen are 72.6 GPa and 0.2, respectively. The specimen is subjected to an asymmetrical displacement. This provides an antisymmetric field of deformation for pure mode II loading. ABAQUS is used in the numerical modelling work. The total structure is meshed using standard eight-noded isoparametric elements. These elements perform well for elastic analysis. The plane strain conditions are assumed. Half a model with mesh refinement is also displayed in Fig. 3. Consequently, the logarithmic plot of shear stress at $\theta = 0$ versus the distance from the notch tip is depicted in Fig. 4. It is noted that the predicted values with regard to the definition (8) match the finite elements solutions satisfactorily, but a poor match is obtained with the results in terms of the definition (9). Similar conclusions are found for a 60º notched specimen.

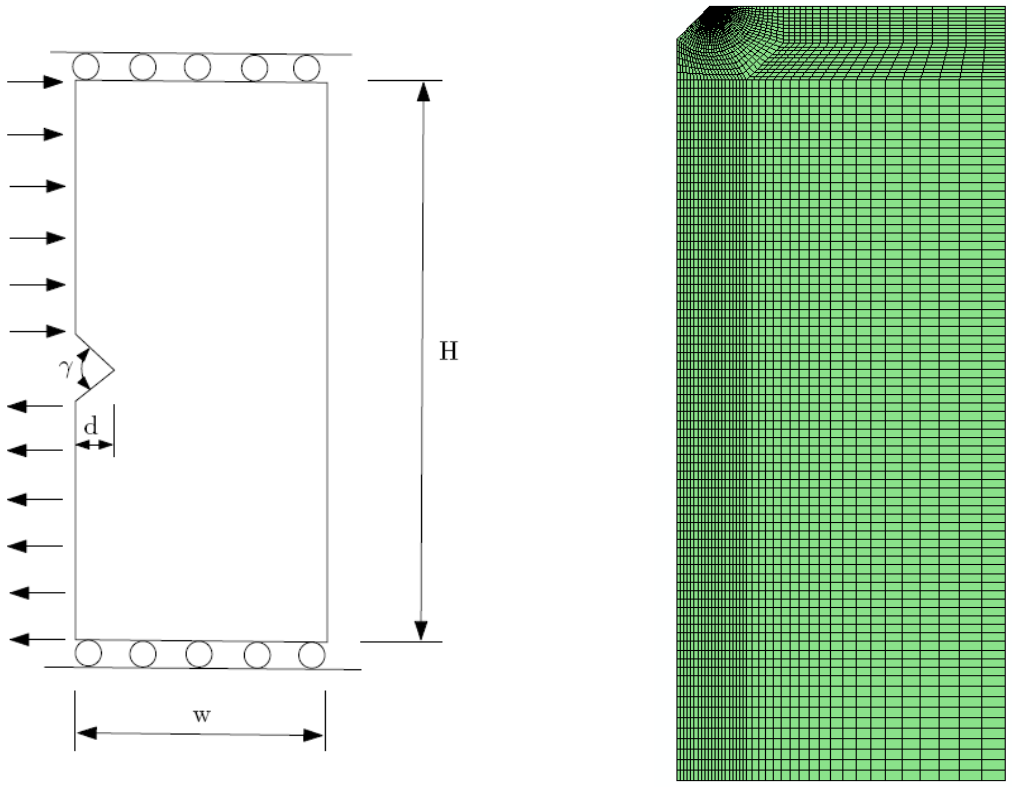

Fig. 3 Model subjected to pure mode II loading.

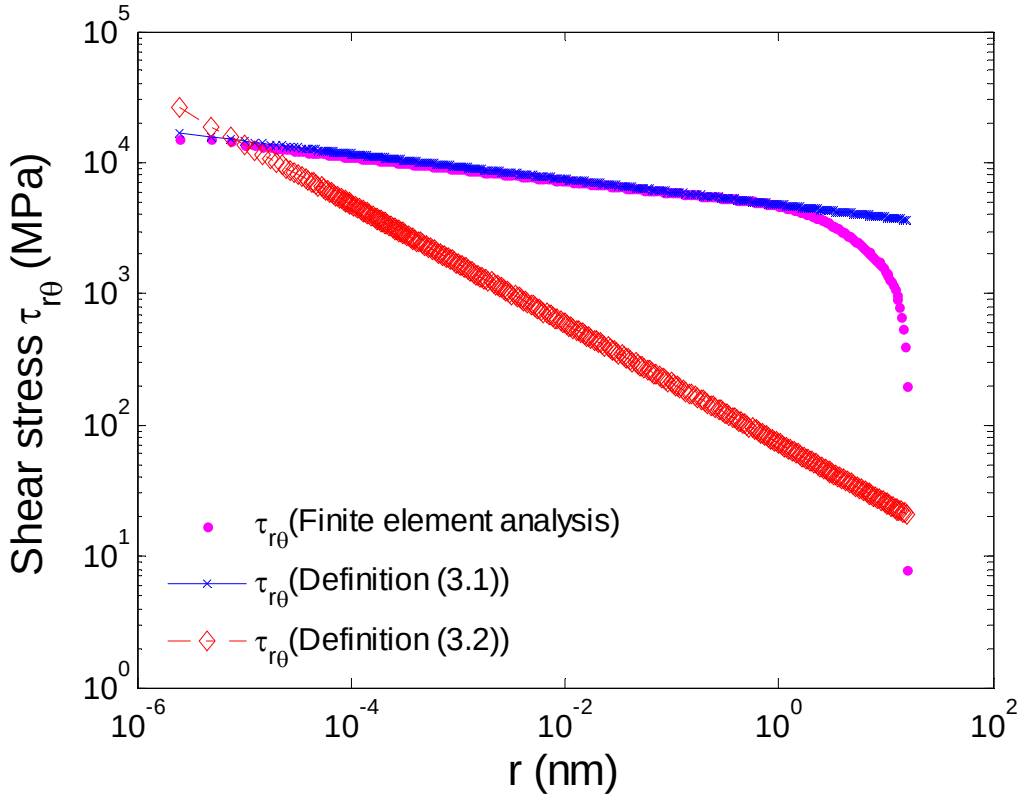

Fig. 4 Comparison of FE results and asymptotic prediction obtained from two different definitions.

Additionally, the in-plane and anti-plane deformation, in general, may be coupled for anisotropic solids, e.g., in-plane loading gives rise to anti-plane displacements and vice-versa. In certain cases, however, the in-plane and anti-plane deformation can decouple. This situation occurs when the elastic components in the 6×6 stiffness matrix

$$C_{14} = C_{15} = C_{24} = C_{25} = C_{46} = C_{56} = 0, \tag{10}$$

as described by Ting (1996). The asymptotic analysis mentioned above assumes that the in-plane and anti-plane deformation is decoupled. Then, the method to solve anti-plane problem is separated and described in other literature (e.g., Ting, 1996; Dunn et al., 2001).

4. Selection of the outer integration path

The H-integral approach, as a tool to derive stress intensity factors for notches and cracks, is based on a combination of finite element results, Betti's law, and asymptotic analysis with a complementary field (Shang et al., 2008; 2009). The H-integral approach differs from the other methods in that it utilizes the finite element data remote from the notch tip. As a result, there is no need to employ extensive mesh refinement and special singular elements near the corner. Theoretically, this contour integral is path-independent. Carpenter (1984a) studied a 90° corner problem for a homogeneous material with plane stress analysis, Stern and Soni (1976) explored the computation of stress intensities at fixed-free corners. Both of them stated that results are relatively insensitive to which outer contour is chosen.

Nonetheless, this is not always true. Stern et al. (1976)analyzed crack and tilt crack problems and found that the accuracy and stability of the results are exceptional with the worst error for any contour studied being 2.4% for K_I and 5.3% for K_{II}. While this accuracy is typical, more deviation is usually found between the various contours. The innermost contour (very close to the crack tip) usually gives less accuracy than the contours more remote from the crack tip. Carpenter (Carpenter, 1984b) performed plane stress analysis and showed that the further the contour lies from the notch tip, the greater the number of nodes had to be considered for a given accuracy of results, particularly for K_2^n. Moreover, Carpenter and Byers (1987) investigated a 90° corner problem and indicated that prediction of the stress intensity factor, in general, is better with the smaller radii than with the larger radii but there were some exceptions. Stern et al. (1976) also pointed out that results from the exterior contour (very close to finite boundaries) are not likely to be satisfactory in the presence of discontinuities in the boundary data. The reason for this variation of results with radii and deformation mode was unclear.

In our investigation, the selection of outer contour location should be neither very close to nor far away from the notch tip (e.g., Shang et al., 2008; 2009; Labossiere and Dunn, 1998; 1999). Far away from the notch tip, the solution is perturbed by finite boundaries and loading, such as a thin-film interlayer in a multi-layered structure (e.g., Shang et al., 2008) and a traction surface. As a result, K_m^n can no longer characterize the actual stress state and then higher order terms are required to describe the behaviour. The accuracy of H-integral approach can be evaluated by comparing with asymptotic solutions obtained directly by finite element computations of displacements along the notch flanks or of the stresses along the interface or bisection line ($\theta = 0$). The worst deviations for any contour studied (Shang et al., 2008) are typically 3% for K_1^n and 5% for K_2^n.

As indicated in some other studies (e.g., Carpenter, 1984a; 1984b; Stern et al., 1976;

Labossiere and Dunn, 1998; 1999; Banks-Sills, 1997; Banks-Sills and Sherer, 2002), inaccuracy of the stress intensity factor can be induced by the numerical approximations (Gauss points or nodes, idealization) made in the finite element calculations and by the numerical integration schemes (programming details) adopted to calculate the H-integral. It can be improved by generating a reasonable finite element mesh, averaging results obtained along various contours and choosing a contour with a reasonable number of integration points, sufficiently far from the notch tip where the numerical results are generally smooth. Furthermore, the acquisition of complementary stress intensity factors K_m^{n*} on actual integration paths may also provide an alternative check for accuracy of computational procedures.

5. Conclusions

Since the notch mechanics is a quite new field, some unsolved problems still exist. It is essential to clear up any confusion about this subject matter. This technical note mainly addresses three issues. Eigen-equation with regard to the stress singularity is interpreted from a mathematical viewpoint and the detailed calculation of eigenvalues for the corner problem has been presented. The different definitions of stress intensity factors is explained in a historical perspective and the stress intensity factor with respect to the shear stress component has been addressed by means of example calculation. The analysis shows that the definition according to (8) provides the most accurate results. The effect of contour selection is further discussed and some suggestions are made for improving accuracy of results.

Reference List

Banks-Sills, L., (1997). A conservative integral for determining stress intensity factors of a bimaterial strip. International Journal of Fracture 86**,** 385-398.

Banks-Sills, L., Sherer, A., (2002). A conservative integral for determining stress intensity factors of a bimaterial notch. International Journal of Fracture 115**,** 1-26.

Carpenter, W. C., (1984a). Calculation of Fracture-Mechanics Parameters for A General Corner. International Journal of Fracture 24**,** 45-58.

Carpenter, W. C., (1984b). Mode I and Mode II stress intensity factors for plates with cracks of finite opening. International Journal of Fracture 26**,** 201-214.

Carpenter, W. C., Byers, C., (1987). A Path Independent Integral for Computing Stress Intensities for V-Notched Cracks in A Bi-Material. International Journal of Fracture 35**,** 245-268.

Dunn, M. L., Hui, C. Y., Labossiere, P. E. W., Lin, Y. Y., (2001). Small scale geometric and material features at geometric discontinuities and their role in fracture analysis. International Journal of Fracture 110**,** 101-121.

Dunn, M. L., Suwito, W., Cunningham, S., May, C. W., (1997). Fracture initiation at sharp notches under mode I, mode II, and mild mixed mode loading. International Journal of Fracture 84**,** 367-381.

Labossiere, P. E. W., Dunn, M. L., (1998). Calculation of stress intensities at sharp notches in anisotropic media. Engineering Fracture Mechanics 61**,** 635-654.

Labossiere, P. E. W., Dunn, M. L., (1999). Stress intensities at interface corners in anisotropic bimaterials. Engineering Fracture Mechanics 62**,** 555-575.

Shang, L. Y., Zhang, Z. L., Skallerud, B., (2008). Fracture of anodic-bonded silicon-thin film glass-silicon triple stacks. Engineering Fracture Mechanics 75**,** 1064-1082.

Shang, L. Y., Zhang, Z. L., Skallerud, B., (2009). Evaluation of fracture mechanics parameters for free edges in multi-layered structures with weak singularities. International Journal of Solids and Structures 46**,** 1134-1148.

Stern, M., Becker, E. B., Dunham, R. S., (1976). Contour Integral Computation of Mixed-Mode Stress Intensity Factors. International Journal of Fracture 12**,** 359-368.

Stern, M., Soni, M. L., (1976). On the Computation of Stress Intensities at Fixed-Free Corners. International Journal of Solids and Structures 12**,** 331-337.

Ting, T. C. T., (1996). Anisotropic Elasticity: Theory and Applications. Oxford University Press, New York.

APPENDIX

Extension study in crack initiation at free edges with weak singularity

APPENDIX Extension study in crack initiation at free edges with weak singularity 123

With the development of micromachining techniques, multi-layered thin films on silicon substrates have a wide variety of applications in electronics packaging and integrated circuits. Due to the elastic mismatch, stress concentrations may develop and a weak singularity (λ>0.9) may exist at free edges (Fig. 1). The initiation of failure at free edges in multi-material systems often occurs.

This appendix is used as a supplement to Paper II. Free-edge in multi-layered structural components with weak singularities is further examined. Standardized numerical formulae for varying material combinations are proposed from a design engineer's perspective. It has also been shown that the material dependence can be normalized. The extent of the K-dominated field is assessed by comparing the asymptotic solution to the detailed finite element analysis. It is observed that the valid range of the K-field is strongly influenced by thin-film thickness but not by bond width.

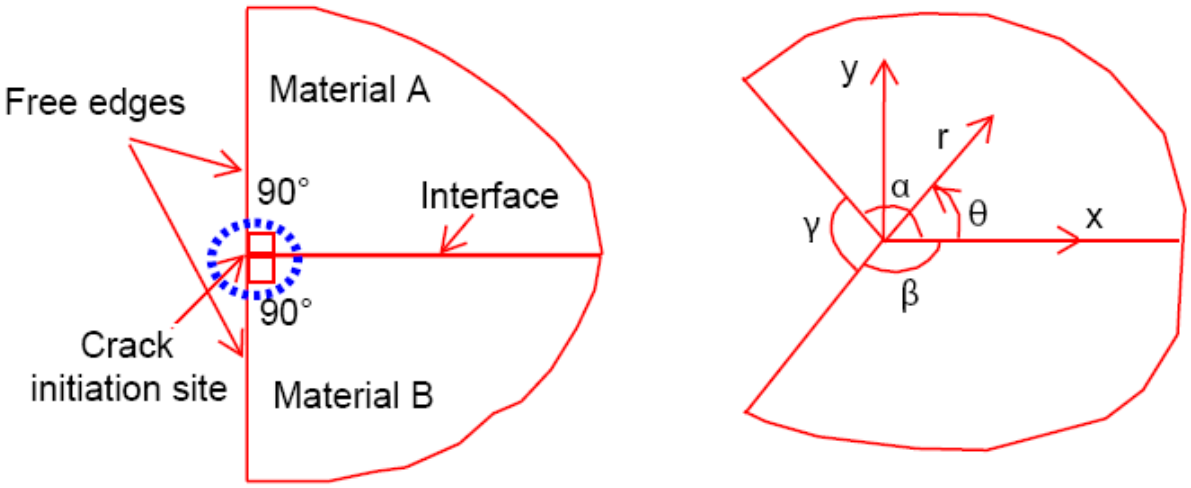

Fig. 1 An edge geometry with dissimilar materials

The multi-layered structures considered in our study are shown again in Fig. 2. Typical material combinations in microelectronic devices are taken into account. The elastic properties of the materials and the evaluation of λ for various joint geometries and material combinations are listed in Table 1. Plane strain conditions are assumed in all modelling. Finite element analyses are performed with ABAQUS. Eight-noded isoparametric elements were used. We also assume that the materials are perfectly bonded along the interface. The mesh refinement, dimensions and loading conditions are depicted in Fig. 2. Beam span L, height h and width w of silicon substrate are 10, 1 and 3.4 mm, respectively. The anisotropic silicon substrate employed here is 350 μm thick oriented in [100] crystal direction with elastic constants of $C_{11}=165.7\text{GPa}$, $C_{12}=63.9\text{GPa}$ and $C_{44}=79.56\text{GPa}$ (Mason, 1958).

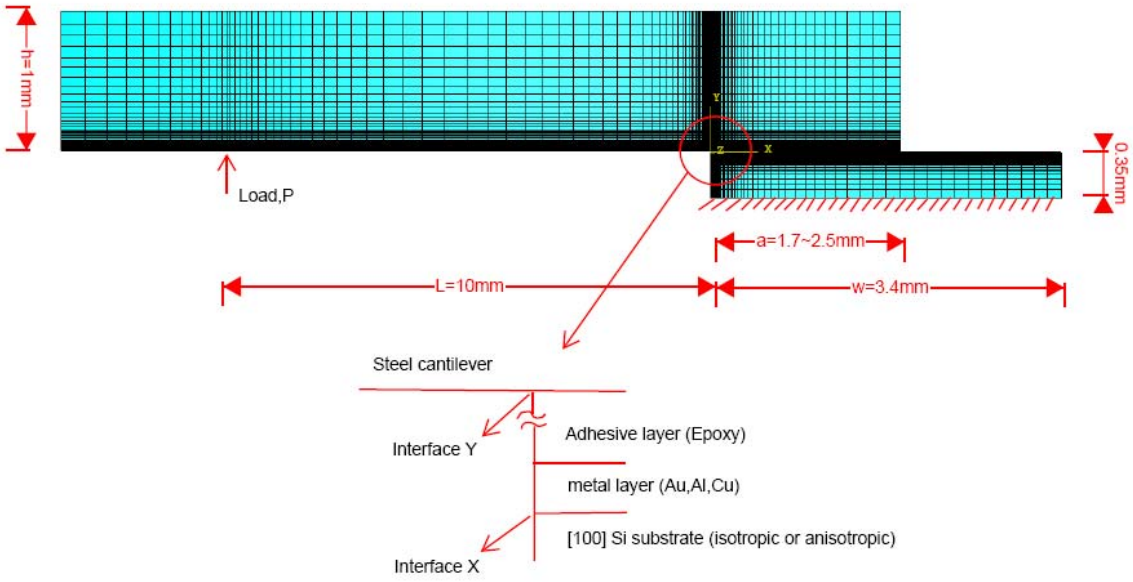

Fig. 2 Specimen geometry, finite element mesh and loading conditions.

Table 1

Material elastic properties and the orders of stress singularities with varying material combinations and joint geometries

	Isotropic Materials					
Materials Elasticity	**Au**	**Cu**	**Al**	**Si**	**Steel**	**Epoxy**
Young's Modulus (GPa)	83	129	70	167	200	2.50
Poisson's Ratio	0.44	0.34	0.35	0.30	0.30	0.30

Interface X	**Material A**	**Material B**	λ_1	**Material A**	**Material B**	λ_1
	Au	Isotropic silicon	0.9332	Au	Anisotropic silicon	0.9522
	Al		0.9304	Al		0.9481
	Cu		0.9912	Cu		0.9967
Interface Y	Steel	Epoxy	0.7049			

Non-dimensional stress intensity factor

A combination of the finite element results and a path independent contour integral is used to evaluate the stress intensity factor. Since K_m^n has the unit of $(stress)(length)^{1-\lambda_m}$, dimensional considerations dictate that

$$Y_m^n\left(\frac{a}{w},\frac{t}{t_0}\right)=\frac{K_m^n}{\frac{6PL}{bh^2}w^{1-\lambda}}, \tag{1}$$

where a, w, t, t_0, P, L, b, and h denote, respectively, the bond length, substrate width, conductor layer thickness, nominal thickness, concentrated force, and span, width and height of the steel beam (Fig. 2), whereas Y is a shape function depending on the notch geometry and material

elastic constants. Furthermore, we can write

$$Y_m^n\left(\tfrac{a}{w},\tfrac{t}{t_0}\right)=Y_{ref}^n\cdot f\left(\tfrac{a}{w}\right)\cdot g\left(\tfrac{t}{t_0}\right), \tag{2}$$

where

$$f\left(\tfrac{a}{w}\right)=\frac{Y_m^n\left(\tfrac{a}{w},\tfrac{t}{t_0}=0.2\right)}{Y_{ref}^n},\ g\left(\tfrac{t}{t_0}\right)=\frac{Y_m^n\left(\tfrac{a}{w}=0.5,\tfrac{t}{t_0}\right)}{Y_{ref}^n},\ Y_{ref}^n=Y_m^n\left(\tfrac{a}{w}=0.5,\tfrac{t}{t_0}=0.2\right).$$

The results obtained from the H-integral approach can be fitted to the power function $f\left(geometry\right)=j\left(geometry\right)^k$ and $g\left(geometry\right)=l\left(geometry\right)^s$. The best-fit values for the isotropic Cu/Si and Au/Si cases are shown in Fig. 3.

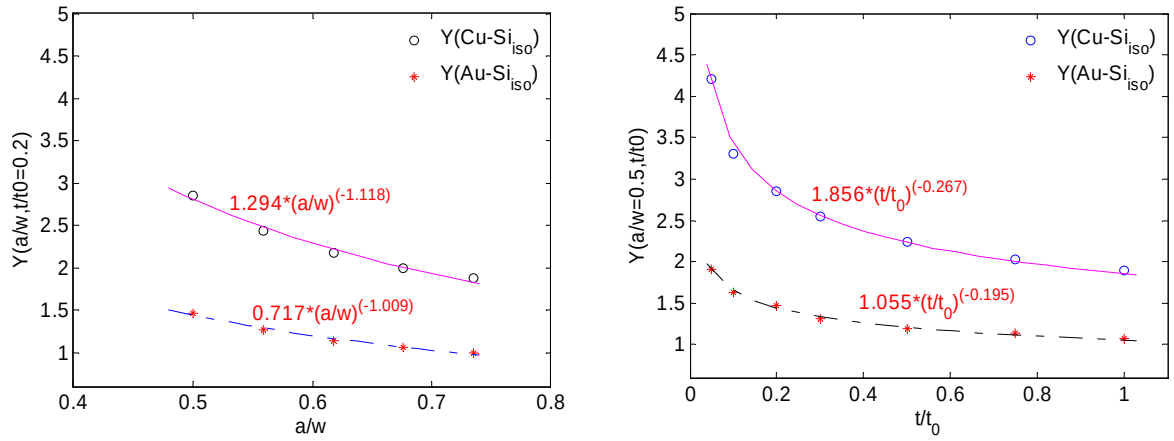

Fig. 3 Non-normalized fitting functions (Cu/Si and Au/Si)

Consequently, standardized numerical formulae for two individual cases read for the isotropic Cu/Si case:

$$Y_{H\text{-integral}}^n\left(\tfrac{a}{w},\tfrac{t}{t_0}\right)=2.854\times0.454\left(\tfrac{a}{w}\right)^{-1.118}\times0.651\left(\tfrac{t}{t_0}\right)^{-0.267},\ \text{where}\ t_0=1000nm \tag{3}$$

and for the isotropic Au/Si case:

$$Y_{H\text{-integral}}^n\left(\tfrac{a}{w},\tfrac{t}{t_0}\right)=1.464\times0.490\left(\tfrac{a}{w}\right)^{-1.009}\times0.721\left(\tfrac{t}{t_0}\right)^{-0.195},\ \text{where}\ t_0=1000nm \tag{4}$$

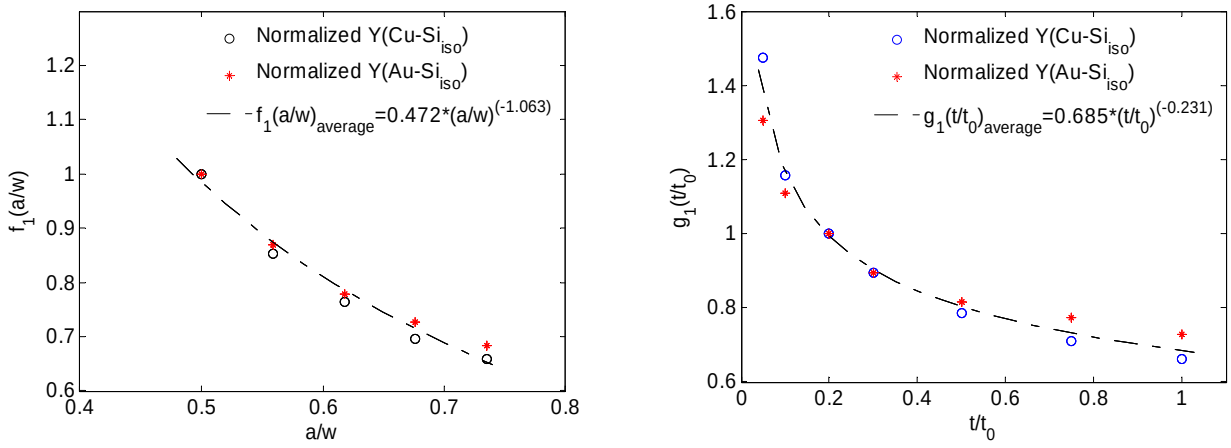

Fig. 4 The power function $f\left(\tfrac{a}{w}\right)$ and $g\left(\tfrac{t}{t_0}\right)$ for different material combinations

Furthermore, if we normalize the dimensionless stress intensity factor by dividing with the corresponding reference value, the respective power function for different material combinations amazingly falls very close to one curve, see Fig. 4. The greatest scatters of two individual cases from the average fitting are 7.8% and 5.6% for Cu/Si and Au/Si case, respectively. It is still appreciable from the engineering's perspective. Hence, the average solution proposed here may be a favorable alternative.

Discussion: Applicability of H-integral approach

The proposed H-integral approach is based on the assumption of elasticity with the dominance of a K-field. Consider a typical case for an Au layer bonded with an isotropic silicon substrate. The interface stress component $\sigma_{\theta\theta}$ is plotted against the distance from the free edges with varying metal layer thickness (Fig. 5a) and various bond width (Fig. 5b). The extent of the K-dominated region is estimated by comparing finite element results with asymptotic analysis. The two solutions are in good agreement for all the cases. It matches up to a radial distance of 70 nm for the specimen with a 1.7 mm wide and 300 nm thick metal layer regarding a 5% deviation. It matches up to 45 nm for the specimen with a 200 nm thick and 2.5 mm wide metal layer considering a 10% difference. As expected, the thicker the thin-film layer, the greater is the valid K-dominated region. Within the bond range we investigated here, the difference of K-field has not a significant dependence on the bond width. It seems that the deviation is slightly larger with increasing bond width but tends to stabilize for the specimens with a bond width larger than 2.3 mm. Moreover, the use of the critical stress intensity factor as a failure initiation parameter requires that the size of inelastic zone (process zone) should be much smaller than the extent of the K-field under the failure load. Taking Au(200 nm)/Si as an example and assuming the elastic–linear hardening model with a yield stress of 160 MPa and a hardening modulus of 8.3 GPa. Applying the critical delamination load $P_c = 0.6$ N (Kitamura et al., 2007) to the specimen, it was observed that no plastic strain occurred in the finite element analysis.

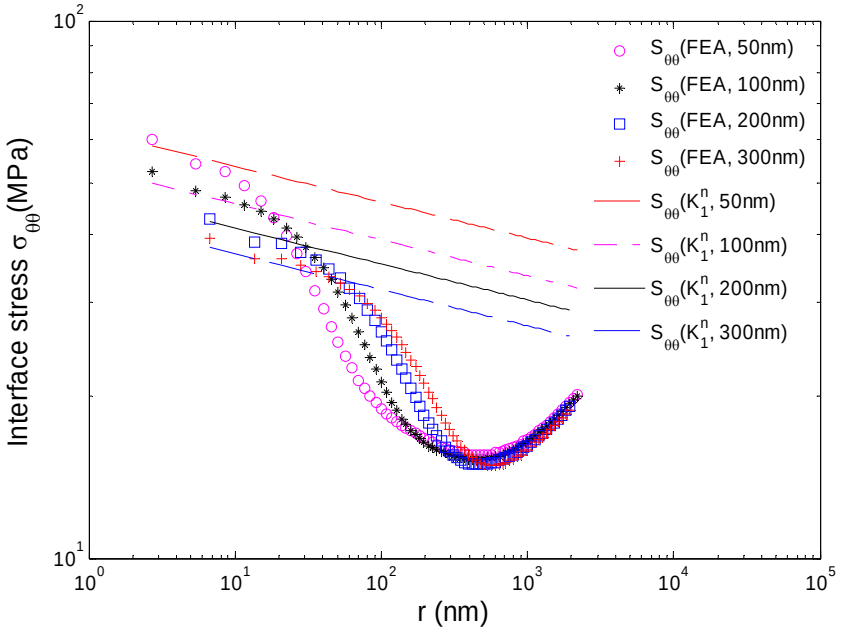

(a)

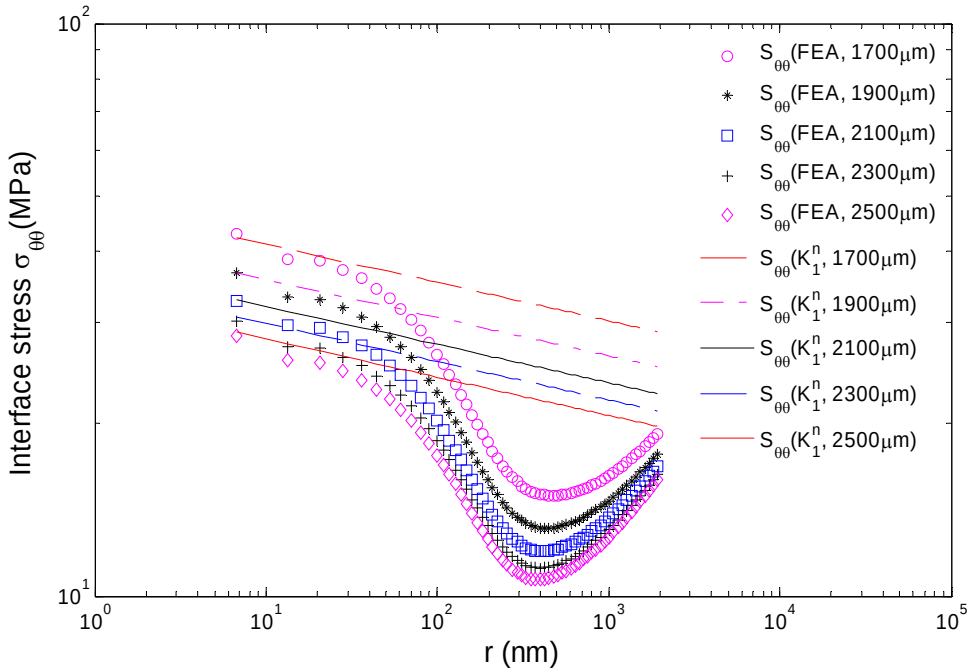

(b)

Fig. 5 K -dominated field for specimens with (a) an Au layer thickness from 50 to 300 nm and (b) an Au layer bond width from 1.7 to 2.5 mm

Summary

To provide application guidance for engineers, standardized numerical formulae for normalized stress intensity factors are summarized corresponding to different material combinations. It has also been shown that the material dependence can be normalized. The average solution proposed here may be a favorable alternative to provide application guidance for engineers. Furthermore, the extent of the K -dominated field is assessed by comparing the asymptotic solution to the detailed finite element analysis. It is observed that the valid range of the K -field is strongly influenced by thin-film thickness but not by bond width.

Reference List

Kitamura, T., Hirakata, H., Van Truong, D., (2007). Initiation of interface crack at free edge between thin films with weak stress singularity. Thin Solid Films 515**,** 3005-3010.

Mason, W. P., (1958). Physical Acoustics and the Properties of Solids. Van Nostrand, New York.

DEPARTMENT OF STRUCTURAL ENGINEERING
NORWEGIAN UNIVERSITY OF SCIENCE AND TECHNOLOGY

N–7491 TRONDHEIM, NORWAY
Telephone: +47 73 59 47 00 Telefax: +47 73 59 47 01

"Reliability Analysis of Structural Systems using Nonlinear Finite Element Methods",
C. A. Holm, 1990:23, ISBN 82-7119-178-0.

"Uniform Stratified Flow Interaction with a Submerged Horizontal Cylinder",
Ø. Arntsen, 1990:32, ISBN 82-7119-188-8.

"Large Displacement Analysis of Flexible and Rigid Systems Considering Displacement-Dependent Loads and Nonlinear Constraints", K. M. Mathisen, 1990:33, ISBN 82-7119-189-6.

"Solid Mechanics and Material Models including Large Deformations",
E. Levold, 1990:56, ISBN 82-7119-214-0, ISSN 0802-3271.

"Inelastic Deformation Capacity of Flexurally-Loaded Aluminium Alloy Structures",
T. Welo, 1990:62, ISBN 82-7119-220-5, ISSN 0802-3271.

"Visualization of Results from Mechanical Engineering Analysis",
K. Aamnes, 1990:63, ISBN 82-7119-221-3, ISSN 0802-3271.

"Object-Oriented Product Modeling for Structural Design",
S. I. Dale, 1991:6, ISBN 82-7119-258-2, ISSN 0802-3271.

"Parallel Techniques for Solving Finite Element Problems on Transputer Networks",
T. H. Hansen, 1991:19, ISBN 82-7119-273-6, ISSN 0802-3271.

"Statistical Description and Estimation of Ocean Drift Ice Environments",
R. Korsnes, 1991:24, ISBN 82-7119-278-7, ISSN 0802-3271.

“Properties of concrete related to fatigue damage: with emphasis on high strength concrete”,
G. Petkovic, 1991:35, ISBN 82-7119-290-6, ISSN 0802-3271.

"Turbidity Current Modelling",
B. Brørs, 1991:38, ISBN 82-7119-293-0, ISSN 0802-3271.

"Zero-Slump Concrete: Rheology, Degree of Compaction and Strength. Effects of Fillers as Part Cement-Replacement", C. Sørensen, 1992:8, ISBN 82-7119-357-0, ISSN 0802-3271.

"Nonlinear Analysis of Reinforced Concrete Structures Exposed to Transient Loading",
K. V. Høiseth, 1992:15, ISBN 82-7119-364-3, ISSN 0802-3271.

"Finite Element Formulations and Solution Algorithms for Buckling and Collapse Analysis of Thin

Shells", R. O. Bjærum, 1992:30, ISBN 82-7119-380-5, ISSN 0802-3271.

"Response Statistics of Nonlinear Dynamic Systems",
J. M. Johnsen, 1992:42, ISBN 82-7119-393-7, ISSN 0802-3271.

"Digital Models in Engineering. A Study on why and how engineers build and operate digital models for decisison support", J. Høyte, 1992:75, ISBN 82-7119-429-1, ISSN 0802-3271.

"Sparse Solution of Finite Element Equations",
A. C. Damhaug, 1992:76, ISBN 82-7119-430-5, ISSN 0802-3271.

"Some Aspects of Floating Ice Related to Sea Surface Operations in the Barents Sea",
S. Løset, 1992:95, ISBN 82-7119-452-6, ISSN 0802-3271.

"Modelling of Cyclic Plasticity with Application to Steel and Aluminium Structures",
O. S. Hopperstad, 1993:7, ISBN 82-7119-461-5, ISSN 0802-3271.

"The Free Formulation: Linear Theory and Extensions with Applications to Tetrahedral Elements with Rotational Freedoms", G. Skeie, 1993:17, ISBN 82-7119-472-0, ISSN 0802-3271.

"Høyfast betongs motstand mot piggdekkslitasje. Analyse av resultater fra prøving i Veisliter'n",
T. Tveter, 1993:62, ISBN 82-7119-522-0, ISSN 0802-3271.

"A Nonlinear Finite Element Based on Free Formulation Theory for Analysis of Sandwich Structures", O. Aamlid, 1993:72, ISBN 82-7119-534-4, ISSN 0802-3271.

"The Effect of Curing Temperature and Silica Fume on Chloride Migration and Pore Structure of High Strength Concrete", C. J. Hauck, 1993:90, ISBN 82-7119-553-0, ISSN 0802-3271.

"Failure of Concrete under Compressive Strain Gradients",
G. Markeset, 1993:110, ISBN 82-7119-575-1, ISSN 0802-3271.

"An experimental study of internal tidal amphidromes in Vestfjorden",
J. H. Nilsen, 1994:39, ISBN 82-7119-640-5, ISSN 0802-3271.

"Structural analysis of oil wells with emphasis on conductor design",
H. Larsen, 1994:46, ISBN 82-7119-648-0, ISSN 0802-3271.

"Adaptive methods for non-linear finite element analysis of shell structures",
K. M. Okstad, 1994:66, ISBN 82-7119-670-7, ISSN 0802-3271.

"On constitutive modelling in nonlinear analysis of concrete structures",
O. Fyrileiv, 1994:115, ISBN 82-7119-725-8, ISSN 0802-3271.

"Fluctuating wind load and response of a line-like engineering structure with emphasis on motion-induced wind forces",
J. Bogunovic Jakobsen, 1995:62, ISBN 82-7119-809-2, ISSN 0802-3271.

"An experimental study of beam-columns subjected to combined torsion, bending and axial actions",
A. Aalberg, 1995:66, ISBN 82-7119-813-0, ISSN 0802-3271.

"Scaling and cracking in unsealed freeze/thaw testing of Portland cement and silica fume concretes",
S. Jacobsen, 1995:101, ISBN 82-7119-851-3, ISSN 0802-3271.

"Damping of water waves by submerged vegetation. A case study of laminaria hyperborea",

A. M. Dubi, 1995:108, ISBN 82-7119-859-9, ISSN 0802-3271.

"The dynamics of a slope current in the Barents Sea",
Sheng Li, 1995:109, ISBN 82-7119-860-2, ISSN 0802-3271.

"Modellering av delmaterialenes betydning for betongens konsistens",
Ernst Mørtsell, 1996:12, ISBN 82-7119-894-7, ISSN 0802-3271.

"Bending of thin-walled aluminium extrusions",
Birgit Søvik Opheim, 1996:60, ISBN 82-7119-947-1, ISSN 0802-3271.

"Material modelling of aluminium for crashworthiness analysis",
Torodd Berstad, 1996:89, ISBN 82-7119-980-3, ISSN 0802-3271.

"Estimation of structural parameters from response measurements on submerged floating tunnels",
Rolf Magne Larssen, 1996:119, ISBN 82-471-0014-2, ISSN 0802-3271.

“Numerical modelling of plain and reinforced concrete by damage mechanics”,
Mario A. Polanco-Loria, 1997:20, ISBN 82-471-0049-5, ISSN 0802-3271.

“Nonlinear random vibrations - numerical analysis by path integration methods”,
Vibeke Moe, 1997:26, ISBN 82-471-0056-8, ISSN 0802-3271.

“Numerical prediction of vortex-induced vibration by the finite element method”,
Joar Martin Dalheim, 1997:63, ISBN 82-471-0096-7, ISSN 0802-3271.

“Time domain calculations of buffeting response for wind sensitive structures”,
Ketil Aas-Jakobsen, 1997:148, ISBN 82-471-0189-0, ISSN 0802-3271.

"A numerical study of flow about fixed and flexibly mounted circular cylinders",
Trond Stokka Meling, 1998:48, ISBN 82-471-0244-7, ISSN 0802-3271.

“Estimation of chloride penetration into concrete bridges in coastal areas”,
Per Egil Steen, 1998:89, ISBN 82-471-0290-0, ISSN 0802-3271.

“Stress-resultant material models for reinforced concrete plates and shells”,
Jan Arve Øverli, 1998:95, ISBN 82-471-0297-8, ISSN 0802-3271.

“Chloride binding in concrete. Effect of surrounding environment and concrete composition”,
Claus Kenneth Larsen, 1998:101, ISBN 82-471-0337-0, ISSN 0802-3271.

“Rotational capacity of aluminium alloy beams”,
Lars A. Moen, 1999:1, ISBN 82-471-0365-6, ISSN 0802-3271.

“Stretch Bending of Aluminium Extrusions”,
Arild H. Clausen, 1999:29, ISBN 82-471-0396-6, ISSN 0802-3271.

“Aluminium and Steel Beams under Concentrated Loading”,
Tore Tryland, 1999:30, ISBN 82-471-0397-4, ISSN 0802-3271.

"Engineering Models of Elastoplasticity and Fracture for Aluminium Alloys",
Odd-Geir Lademo, 1999:39, ISBN 82-471-0406-7, ISSN 0802-3271.

"Kapasitet og duktilitet av dybelforbindelser i trekonstruksjoner",
Jan Siem, 1999:46, ISBN 82-471-0414-8, ISSN 0802-3271.

“Etablering av distribuert ingeniørarbeid; Teknologiske og organisatoriske erfaringer fra en norsk ingeniørbedrift”, Lars Line, 1999:52, ISBN 82-471-0420-2, ISSN 0802-3271.

“Estimation of Earthquake-Induced Response”,
Símon Ólafsson, 1999:73, ISBN 82-471-0443-1, ISSN 0802-3271.

“Coastal Concrete Bridges: Moisture State, Chloride Permeability and Aging Effects”
Ragnhild Holen Relling, 1999:74, ISBN 82-471-0445-8, ISSN 0802-3271.

”Capacity Assessment of Titanium Pipes Subjected to Bending and External Pressure”,
Arve Bjørset, 1999:100, ISBN 82-471-0473-3, ISSN 0802-3271.

“Validation of Numerical Collapse Behaviour of Thin-Walled Corrugated Panels”,
Håvar Ilstad, 1999:101, ISBN 82-471-0474-1, ISSN 0802-3271.

“Strength and Ductility of Welded Structures in Aluminium Alloys”,
Miroslaw Matusiak, 1999:113, ISBN 82-471-0487-3, ISSN 0802-3271.

“Thermal Dilation and Autogenous Deformation as Driving Forces to Self-Induced Stresses in High Performance Concrete”,
Øyvind Bjøntegaard, 1999:121, ISBN 82-7984-002-8, ISSN 0802-3271.

“Some Aspects of Ski Base Sliding Friction and Ski Base Structure”,
Dag Anders Moldestad, 1999:137, ISBN 82-7984-019-2, ISSN 0802-3271.

"Electrode reactions and corrosion resistance for steel in mortar and concrete",
Roy Antonsen, 2000:10, ISBN 82-7984-030-3, ISSN 0802-3271.

"Hydro-Physical Conditions in Kelp Forests and the Effect on Wave Damping and Dune Erosion. A case study on Laminaria Hyperborea",
Stig Magnar Løvås, 2000:28, ISBN 82-7984-050-8, ISSN 0802-3271.

"Random Vibration and the Path Integral Method",
Christian Skaug, 2000:39, ISBN 82-7984-061-3, ISSN 0802-3271.

"Buckling and geometrical nonlinear beam-type analyses of timber structures",
Trond Even Eggen, 2000:56, ISBN 82-7984-081-8, ISSN 0802-3271.

”Structural Crashworthiness of Aluminium Foam-Based Components”,
Arve Grønsund Hanssen, 2000:76, ISBN 82-7984-102-4, ISSN 0809-103X.

“Measurements and simulations of the consolidation in first-year sea ice ridges, and some aspects of mechanical behaviour”, Knut V. Høyland, 2000:94, ISBN 82-7984-121-0, ISSN 0809-103X.

”Kinematics in Regular and Irregular Waves based on a Lagrangian Formulation”,
Svein Helge Gjøsund, 2000-86, ISBN 82-7984-112-1, ISSN 0809-103X.

”Self-Induced Cracking Problems in Hardening Concrete Structures”,
Daniela Bosnjak, 2000-121, ISBN 82-7984-151-2, ISSN 0809-103X.

"Ballistic Penetration and Perforation of Steel Plates",
Tore Børvik, 2000:124, ISBN 82-7984-154-7, ISSN 0809-103X.

"Freeze-Thaw resistance of Concrete. Effect of: Curing Conditions, Moisture Exchange and

Materials", Terje Finnerup Rønning, 2001:14, ISBN 82-7984-165-2, ISSN 0809-103X

Structural behaviour of post tensioned concrete structures. Flat slab. Slabs on ground", Steinar Trygstad, 2001:52, ISBN 82-471-5314-9, ISSN 0809-103X.

"Slipforming of Vertical Concrete Structures. Friction between concrete and slipform panel", Kjell Tore Fosså, 2001:61, ISBN 82-471-5325-4, ISSN 0809-103X.

"Some numerical methods for the simulation of laminar and turbulent incompressible flows", Jens Holmen, 2002:6, ISBN 82-471-5396-3, ISSN 0809-103X.

“Improved Fatigue Performance of Threaded Drillstring Connections by Cold Rolling”, Steinar Kristoffersen, 2002:11, ISBN: 82-421-5402-1, ISSN 0809-103X.

"Deformations in Concrete Cantilever Bridges: Observations and Theoretical Modelling", Peter F. Takâcs, 2002:23, ISBN 82-471-5415-3, ISSN 0809-103X.

"Stiffened aluminium plates subjected to impact loading", Hilde Giæver Hildrum, 2002:69, ISBN 82-471-5467-6, ISSN 0809-103X.

"Full- and model scale study of wind effects on a medium-rise building in a built up area", Jónas Thór Snæbjørnsson, 2002:95, ISBN82-471-5495-1, ISSN 0809-103X.

“Evaluation of Concepts for Loading of Hydrocarbons in Ice-infested water”, Arnor Jensen, 2002:114, ISBN 82-417-5506-0, ISSN 0809-103X.

”Numerical and Physical Modelling of Oil Spreading in Broken Ice”, Janne K. Økland Gjøsteen, 2002:130, ISBN 82-471-5523-0, ISSN 0809-103X.

”Diagnosis and protection of corroding steel in concrete”, Franz Pruckner, 20002:140, ISBN 82-471-5555-4, ISSN 0809-103X.

“Tensile and Compressive Creep of Young Concrete: Testing and Modelling”, Dawood Atrushi, 2003:17, ISBN 82-471-5565-6, ISSN 0809-103X.

“Rheology of Particle Suspensions. Fresh Concrete, Mortar and Cement Paste with Various Types of Lignosulfonates”, Jon Elvar Wallevik, 2003:18, ISBN 82-471-5566-4, ISSN 0809-103X.

“Oblique Loading of Aluminium Crash Components”, Aase Reyes, 2003:15, ISBN 82-471-5562-1, ISSN 0809-103X.

“Utilization of Ethiopian Natural Pozzolans”, Surafel Ketema Desta, 2003:26, ISSN 82-471-5574-5, ISSN:0809-103X.

“Behaviour and strength prediction of reinforced concrete structures with discontinuity regions”, Helge Brå, 2004:11, ISBN 82-471-6222-9, ISSN 1503-8181.

“High-strength steel plates subjected to projectile impact. An experimental and numerical study”, Sumita Dey, 2004:38, ISBN 82-471-6281-4 (elektr. Utg.), ISBN 82-471-6282-2 (trykt utg.), ISSN 1503-8181.

“Alkali-reactive and inert fillers in concrete. Rheology of fresh mixtures and expansive reactions.” Bård M. Pedersen, 2004:92, ISBN 82-471-6401-9 (trykt utg.), ISBN 82-471-6400-0 (elektr. utg.), ISSN 1503-8181.

“On the Shear Capacity of Steel Girders with Large Web Openings”. Nils Christian Hagen, 2005:9 ISBN 82-471-6878-2 (trykt utg.), ISBN 82-471-6877-4 (elektr. utg.), ISSN 1503-8181.

”Behaviour of aluminium extrusions subjected to axial loading”. Østen Jensen, 2005:7, ISBN 82-471-6872-3 (elektr. utg.) , ISBN 82-471-6873-1 (trykt utg.), ISSN 1503-8181.

”Thermal Aspects of corrosion of Steel in Concrete”. Jan-Magnus Østvik, 2005:5, ISBN 82-471-6869-3 (trykt utg.) ISBN 82-471-6868 (elektr.utg), ISSN 1503-8181.

”Mechanical and adaptive behaviour of bone in relation to hip replacement.” A study of bone remodelling and bone grafting. Sébastien Muller, 2005:34, ISBN 82-471-6933-9 (trykt utg.) (ISBN 82-471-6932-0 (elektr.utg), ISSN 1503-8181.

“Analysis of geometrical nonlinearities with applications to timber structures”. Lars Wollebæk, 2005:74, ISBN 82-471-7050-5 (trykt utg.), ISBN 82-471-7019-1 (elektr. Utg.), ISSN 1503-8181.

“Pedestrian induced lateral vibrations of slender footbridges”, Anders Rönnquist, 2005:102, ISBN 82-471-7082-5 (trykt utg.), ISBN 82-471-7081-7 (elektr.utg.), ISSN 1503-8181.

“Initial Strength Development of Fly Ash and Limestone Blended Cements at Various Temperatures Predicted by Ultrasonic Pulse Velocity”, Tom Ivar Fredvik, 2005:112, ISBN 82-471-7105-8 (trykt utg.), ISBN 82-471-7103-1 (elektr.utg.), ISSN 1503-8181.

“Behaviour and modelling of thin-walled cast components”, Cato Dørum, 2005:128, ISBN 82-471-7140-6 (trykt utg.), ISBN 82-471-7139-2 (elektr. utg.), ISSN 1503-8181.

“Behaviour and modelling of selfpiercing riveted connections”, Raffaele Porcaro, 2005:165, ISBN 82-471-7219-4 (trykt utg.), ISBN 82-471-7218-6 (elektr.utg.), ISSN 1503-8181.

”Behaviour and Modelling og Aluminium Plates subjected to Compressive Load”, Lars Rønning, 2005:154, ISBN 82-471-7169-1 (trykt utg.), ISBN 82-471-7195-3 (elektr.utg.), ISSN 1503-8181

”Bumper beam-longitudinal system subjected to offset impact loading”, Satyanarayana Kokkula, 2005:193, ISBN 82-471-7280-1 (trykt utg.), ISBN 82-471-7279-8 (elektr.utg.), ISSN 1503-8181.

“Control of Chloride Penetration into Concrete Structures at Early Age”, Guofei Liu, 2006:46, ISBN 82-471-7838-9 (trykt utg.), ISBN 82-471-7837-0 (elektr. utgave), ISSN 1503-8181.

“Modelling of Welded Thin-Walled Aluminium Structures”, Ting Wang, 2006:78, ISBN 82-471-7907-5 (trykt utg.), ISBN 82-471-7906-7 (elektr.utg.), ISSN 1503-8181.

”Time-variant reliability of dynamic systems by importance sampling and probabilistic analysis of ice loads”, Anna Ivanova Olsen, 2006:139, ISBN 82-471-8041-3 (trykt utg.), ISBN 82-471-8040-5 (elektr.utg.), ISSN 1503-8181.

“Fatigue life prediction of an aluminium alloy automotive component using finite element analysis of surface topography”. Sigmund Kyrre Ås, 2006:25, ISBN 82-471-7791-9 (trykt utg.), ISBN 82-471-7791-9 (elektr.utg.), ISSN 1503-8181.

”Constitutive models of elastoplasticity and fracture for aluminium alloys under strain path change”, Dasharatha Achani, 2006:76, ISBN 82-471-7903-2 (trykt utg.), ISBN 82-471-7902-4 (elektr.utg.), ISSN 1503-8181.

"Simulations of 2D dynamic brittle fracture by the Element-free Galerkin method and linear fracture mechanics", Tommy Karlsson, 2006:125, ISBN 82-471-8011-1 (trykt utg.), ISBN 82-471-8010-3 (elektr.utg.), ISSN 1503-8181.

"Penetration and Perforation of Granite Targets by Hard Projectiles", Chong Chiang Seah, 2006:188, ISBN 82-471-8150-9 (printed ver.), ISBN 82-471-8149-5 (electronic ver.) ISSN 1503-8181.

"Deformations, strain capacity and cracking of concrete in plastic and early hardening phases", Tor Arne Hammer, 2007:234, ISBN 978-82-471-5191-4 (trykt utg.), ISBN 978-82-471-5207-2 (elektr.utg.) ISSN 1503-8181.

"Crashworthiness of dual-phase high-strength steel: Material and Component behaviour", Venkatapathi Tarigopula, 2007:230, ISBN 82-471-5076-4 (trykt utg.) ISBN 82-471-5093-1 (elektr.utg.) ISSN 1503-8181.

"Fibre reinforcement in load carrying concrete structures", Åse Lyslo Døssland, 2008:50, ISBN 978-82-471-6910-0 (trykt utg.), ISBN 978-82-471-6924-7 (elektr.utg.), ISSN 1503-8181.

"Low-velocity penetration of aluminium plates", Frode Grytten, 2008:46, ISBN 978-82-471-6826-4 (trykt utg.) ISBN 978-82-471-6843-1 (elektr. Utg.) ISSN 1503-8181.

"Robustness studies of structures subjected to large deformations", Ørjan Fylling, 2008:24, ISBN 978-82-471-6339-9 (trykt utg.) ISBN 978-82-471-6342-9 (elektro.utg.) ISSN 1503-8181.

"Constitutive modelling of morsellised bone",Knut Birger Lunde, 2008:92, ISBN 978-82-471-7829-4 (trykt utg.) ISBN 978-82-471-7832-4 (elektro.utg.) ISSN 1503-8181.

"Experimental Investigations of Wind Loading on a Suspension Bridge Girder", Bjørn Isaksen, 2008:131, ISBN 978-82-471-8656-5 (trykt utg.) ISBN 978-82-471-8673-2 (elektro.utg.) ISSN 1503-8181.

"Cracking Risk of Concrete Structures in The Hardening Phase", Guomin Ji, 2008:198, ISBN 978-82-471-1079-9 (printed ver.), ISBN 978-82-471-1080-5 (electronic ver.) ISSN 1503-8181.

"Modelling and numerical analysis of the porcine and human mitral apparatus", Victorien Emile Prot, 2008:249, ISBN 978-82-471-1192-5 (printed ver.), ISBN 978-82-471-1193-2 (electronic ver.), ISSN 1503-8181.

"Strength analysis of net structures", Heidi Moe, 2009:48, ISBN 978-82-471-1468-1 (printed ver.), ISBN 978-82-471-1469-8 (electronic ver.) ISSN1503-8181.

"Numerical analysis of ductile fracture in surface cracked shells", Espen Berg, 2009:80, ISBN 978-82-471-1537-4 (printed ver.), ISBN 978-82-471-1538-1 (electronic ver.) ISSN 1503-8181.

"Subject specific finite element analysis of bone - for evaluation of the healing of a leg lengthening and evaluation of femoral stem design", Sune Hansborg Pettersen, 2009:99, ISBN 978-82-471-1579-4 (printed ver.), ISBN 978-82-471-1580-0 (electronic ver.), ISSN 1503-8181.